

**Identification and characterisation
of drug-tolerant persister cells
arising in response to targeted
CHK1 inhibition**

LeAnne Carmichael

The Institute of Cancer Research

University of London



This thesis is submitted for the degree of PhD

Declaration

I confirm that the work presented in this thesis is my own. The use of materials and support from other sources has been fully acknowledged throughout the text.



LeAnne Carmichael

Abstract

Drug-tolerant persisters (DTPs) are a subpopulation of slow-cycling cells that have been identified in several cancer cell lines following lethal exposure to targeted and cytotoxic therapeutics and shown to precede acquisition of diverse and clinically relevant drug resistance mechanisms. To date, much of the data comes from studies using tyrosine kinase inhibitors and it is unclear if this persister phenotype is broadly observed in response to drugs that act by various anti-tumour mechanisms. Herein, a subpopulation of slow-cycling SK-N-AS cells survived treatment with lethal concentrations of SRA737; a clinically relevant CHK1 inhibitor. Surviving cells represent a large proportion of the starting population and have increased global histone H3 lysine 27 trimethylation (H3K27_{me3}). Continued lethal SRA737 exposure leads to the emergence of a drug-tolerant expanded persister (DTEP) population, marked by resumed proliferation and cross-resistance to other small molecule CHK1/CHK2 and DNA damage response (DDR) inhibitors. H3K27_{me3} remains elevated in DTEPs but is diminished after drug release, suggesting a role for epigenetic regulation/reprogramming in both DTP formation and progression. Inhibition of the H3K27 methyltransferase EZH2 using tazemetostat inhibits DTP-to-DTEP transition but fails to abrogate DTP formation or DTEP survival, confirming the requirement of epigenetic plasticity for persister cell progression. Comparison to SRA737 resistant populations generated by dose-escalation revealed differential responses to further CHK1 inhibition and specific enrichment of genes associated with JAK-STAT signalling in persister-derived populations. Interestingly, exogenous IFN γ , but not JAK inhibition, delayed the emergence of a drug resistant population from an SRA737-induced DTP bottleneck, suggesting that overactivation of the IFN γ signalling pathway is detrimental to DTP progression. In conclusion, I have characterised DTPs arising within a novel and clinically relevant therapeutic context, defined differences between pathways to drug resistance through DTPs and dose escalation, and uncovered EZH2 activity and IFN γ signalling as potential intervention points to eradicate this persistent population.

Acknowledgements

Firstly, I would like to thank the Institute of Cancer Research for funding and supporting my PhD studies.

Deepest thanks to my primary supervisor, Dr Olivia Rossanese, for giving me the opportunity to work on this exciting project and guiding me through my scientific and academic development in my journey from Scientific Officer to PhD candidate. I hope I've done you proud. Thank you for carving out time in your insanely busy diary to share your valuable feedback and expertise during the preparation of many presentations, reports, and this thesis. I must also thank you for being an inspiration to me, as a woman in STEM; I'm not sure I would've pursued this course without it.

A very special thank you to my associate supervisor, Dr Michael Bright, for your support and encouragement through this, at times difficult, process. There have been ups and downs on this project, and you've always listened with compassion and kindness, and helped me to overcome any obstacles. Thank you for all your scientific insight and discussions that have helped me generate new ideas and ways of thinking – it's hard to do that as a team of one. Now we can get back to securing funding for the CCRC, having our research-based sitcom commissioned, and many more DTPika's!

Huge thanks to Qiong Gao (Alice) and Dr Konstantinos Mitsopoulos for analysing the RNA sequencing data, meeting with me to talk through the things I didn't understand, and dealing with all my requests for the preparation of figures for this thesis. Thanks also to everyone at the ICR who has trained me on equipment, given me advice, provided feedback on presentations, and helped me develop my skills as a researcher. Thank you all for being so friendly and open with your expertise.

Another special thank you to all the past and present members of the Target Evaluation and Molecular Therapeutics team. You have been my second family

and nurtured me along this journey. To Rebecca Rogers, Caitlin McCarthy, Fiona Want, and Sam Hutchinson-Cook, you inspire me every day to be a better scientist and are the greatest support network a person could wish for. You have been my cheerleaders on the darkest days and my closest companions throughout this experience. Thanks for laughing and crying with me. I treasure you all.

Honourable mentions to Yorkshire Tea, Cherry Coke Zero, and Giant 'Really Cheesy' Wotsits for getting me through writing this thesis.

Last, but by no means least, an enormous thank you to my family and friends for always supporting, encouraging, and believing in me. Thanks to my parents for letting me be me and for always being there, and to my siblings for being my best friends. And finally, the biggest thank you of them all goes to my husband, James. I simply could not have done any of this without you. You are my rock - thank you for everything. And thank you for Mr Pip. Both of you have been a lifeline to me and I am eternally grateful to have you in my life.

I'd like to dedicate this thesis to LeAnne Carmichael, circa 2009-2015.
You are good enough. You can do it.

Table of contents

Abstract	3
List of figures	12
List of tables	15
Abbreviations	17
Chapter 1 Introduction	24
1.1. Knowledge is power	24
1.2. Drug resistance in cancer – inspired by bacteria	26
1.3. Identification and characterisation of drug-tolerant persisters in cancer.....	28
1.4. Mechanisms of drug-tolerance in cancer.....	30
1.4.1. Epigenetic alterations	30
1.4.2. Cellular reprogramming	32
1.5. Clinical evidence for DTP emergence in cancer	34
1.6. The role of drug-tolerance in the evolution of cancer resistance.....	36
1.7. A view on drug-tolerance in cancer	37
1.8. Targeting monopolar spindle 1 kinase (MPS1) in cancer.....	38
1.9. Targeting checkpoint kinase 1 (CHK1) in cancer.....	39
1.9.1. CHK1 is a key effector of the DNA damage response (DDR) signalling pathway.....	39
1.9.2. CHK1 in cancer	41
1.9.3. Targeted inhibition of CHK1 using small molecules	42
1.9.4. Mechanisms of CHK1 inhibitor resistance	44
Chapter 2 Materials and methods	48
2.1. Cell lines and culture	48
2.1.1. Cell lines.....	48
2.1.2. Culture conditions and passage	48
2.1.3. Cryopreservation and recovery.....	49

2.1.4.	Population doubling time (PDT).....	49
2.2.	Compounds and recombinant human proteins	49
2.3.	Cell viability assay for compound GI ₅₀ determination.....	51
2.3.1.	CellTiter-Glo® assay	51
2.3.2.	Seeding density optimisation	51
2.3.3.	Compound GI ₅₀ determination	52
2.4.	Acute and long-term lethal drug exposure	53
2.4.1.	15-day time course	53
2.4.2.	50-day time course	54
2.5.	Drug-tolerant persister (DTP) and expanded persister (DTEP) cells.....	54
2.5.1.	Generation	54
2.5.2.	mKate2-SK-N-AS stable cell line	55
2.5.3.	DTP quantification	55
2.5.4.	DTP-to-DTEP transition	56
2.6.	Dose-escalation	56
2.7.	Dilutive proliferation assay	57
2.8.	β-galactosidase activity assay	57
2.9.	Apoptosis and Cytotoxicity assay	58
2.10.	Cell lysis and Western blotting	59
2.10.1.	Cell lysis	59
2.10.2.	Protein quantification	60
2.10.3.	Western blotting	60
2.10.4.	Detection	61
2.10.5.	Quantification	62
2.11.	RNA sequencing	64
2.11.1.	RNA extraction and sequencing	64
2.11.2.	Alignment and gene read count.....	64
2.11.3.	Differential expression and pathway enrichment analysis	64

2.11.4. Gene signature scores	65
2.12. Colony forming assay.....	66
2.13. Cytokine array.....	66
Chapter 3 Drug-tolerant persister cells arise following lethal exposure to a targeted CHK1 inhibitor.....	69
3.1. Introduction	69
3.2. Identification of a persister cell model.....	72
3.2.1. Determining lethal compound concentrations for persister cell studies	72
3.2.2. A subpopulation of cells survive acute lethal compound exposure.....	75
3.2.3. Response to lethal drug exposure is context specific.....	79
3.2.4. Investigating progression of putative DTP populations	81
3.3. Confirming persister cell identity in response to lethal SRA737 exposure in SK-N-AS cells	84
3.3.1. Surviving SK-N-AS cells harbour persister cell hallmarks	84
3.3.2. SK-N-AS DTPs are a heterogeneous population	89
3.4. Discussion.....	91
Chapter 4 SRA737 resistant populations derived through the persister cell bottleneck or dose-escalation employ different mechanisms to overcome therapeutic challenge	96
4.1. Introduction	96
4.2. Characterising SK-N-AS populations emerging from the persister cell bottleneck	97
4.2.1. DTEP and drug-released cell populations are less sensitive to further challenge with SRA737	97
4.2.2. SRA737-derived DTEP and released cells are cross-resistant to alternative small molecule inhibitors of CHK1 and CHK2.....	100
4.2.3. DTEP and drug-released cells are cross-resistant to additional DDR inhibitors.....	102
4.3. Acute lethal SRA737 exposure has long-term effects following drug release	104

4.3.1. Drug-released populations show variation in recovering SRA737 sensitivity	104
4.3.2. Resensitisation to SRA737 is accompanied by resensitisation to additional DDR inhibitors	107
4.4. Gene expression profiles are altered in SK-N-AS persister cell populations ..	108
4.4.1. Persister cell populations harbour distinct gene expression profiles	109
4.4.2. GSEA reveals common transcriptional alterations in different persister cell populations	113
4.4.3. Persister cells express gene signatures related to senescence, diapause, and quiescence	115
4.5. Characterising dose-escalated SRA737 resistant populations	117
4.5.1. Dose-escalated populations are insensitive to further challenge with SRA737	117
4.6. Dose-escalated cells are also cross-resistant to additional small molecule DDR inhibitors	120
4.7. Gene expression profiles are altered in dose-escalated SRA737-resistant populations	122
4.7.1. Dose-escalated SRA737-resistant cells harbour transcriptional changes	122
4.7.2. GSEA reveals common transcriptional alterations in dose-escalated populations	126
4.7.3. Gene signatures related to senescence and quiescence are elevated in dose-escalated populations	127
4.8. Comparison of persister and dose-escalated populations reveals persister-specific mechanisms of SRA737 drug-resistance	129
4.8.1. The ATR-CHK1 DDR signalling axis is differentially altered in persister-derived and dose-escalated SRA737 resistant populations	129
4.8.2. Dose-escalated cells are more sensitive to WEE1/CHK1 inhibitor combination treatment than DTEPs	133
4.8.3. Epigenetic alteration is a persister cell specific strategy	135

4.8.4. Identifying persister-specific mechanisms by comparison of RNAseq data..	136
4.9. Discussion.....	139
Chapter 5 EZH2-mediated hypermethylation of histone H3 lysine 27 (H3K27) is required for persister cell progression	145
5.1. Introduction	145
5.2. Investigating the requirement of EZH2 for persister cell formation and survival	147
5.2.1. SRA737-induced DTEPs are not sensitive to EZH2 inhibition.....	147
5.2.2. EZH2 activity is not required for DTP formation	149
5.2.3. Tazemetostat induces senescence in SRA737-induced DTPs	151
5.3. Investigating the requirement of EZH2 activity for DTP progression.....	154
5.3.1. Tazemetostat abrogates DTP-to-DTEP transition under continued SRA737 exposure	154
5.3.2. Populations emerging from a combination-induced DTP bottleneck are more resistant to SRA737.....	157
5.4. Discussion.....	160
Chapter 6 IFNγ activation hinders DTEP emergence under lethal SRA737 exposure.....	163
6.1. Introduction	163
6.2. Investigating the role of IFN γ -JAK1/2-STAT1 signalling in DTP formation in response to lethal SRA737 exposure	166
6.2.1. Cytokine secretion is upregulated in SRA737-induced DTPs.....	166
6.2.2. Optimising conditions for persister cell studies using exogenous IFN γ and JAK/STAT inhibitors	167
6.2.3. DTP formation is unaffected by inhibition or activation of IFN γ -JAK1/2-STAT1 signalling	170
6.2.4. Inhibition or activation of IFN γ signalling does not alter composition of the SRA737-induced DTP population at day 7	171
6.2.5. SRA737-induced DTPs have an IFN γ -like secretory cytokine profile	173

6.3.	Investigating the requirement of IFN γ -JAK1/2-STAT1 signalling for persister cell progression	175
6.3.1.	Ruxolitinib fails to abrogate DTP-to-DTEP transition under SRA737 exposure	175
6.3.2.	Exogenous IFN γ treatment hinders DTP-to-DTEP transition under continued SRA737 exposure	178
6.4.	Characterising populations emerging from a combination-induced DTP bottleneck.....	181
6.4.1.	Populations emerging under SRA737 alone and in combination with ruxolitinib or IFN γ respond similarly to further challenge with SRA737...	181
6.5.	Discussion.....	185
Chapter 7	General Discussion	189
7.1.	Introduction	189
7.2.	DTPs mediate resistance to SRA737	190
7.3.	DTPs are more prevalent in response to SRA737 exposure.....	192
7.4.	Persistence and dormancy are interlinked.....	195
7.5.	Distinct drug-resistance mechanisms emerge from the DTP bottleneck	199
7.6.	Entry into the DTP state has long-term consequences.....	204
7.7.	EZH2 activity is required for DTEP emergence from the DTP bottleneck	206
7.8.	IFN γ signalling – master regulator of DTP cell fate?.....	208
7.9.	Concluding remarks	212
References	213
Appendix	229

List of figures

Figure 1-1: Persister cell mechanisms.	34
Figure 1-2: DTP formation and contribution to the evolution of drug-resistance in cancer.	37
Figure 1-3: DNA damage response signalling through the ATR-CHK1 and ATM-CHK2 axes.....	41
Figure 3-1: GI ₅₀ determination of selected compounds in MDA-MB-231, SK-N-AS, and A549 cells.....	74
Figure 3-2: Putative persister subpopulations are detected in MDA-MB-231, SK-N-AS, and A549 cells following acute lethal compound exposure.	78
Figure 3-3: Response to lethal compound exposure is dependent on cellular and therapeutic contexts.....	80
Figure 3-4: SK-N-AS cells undergo DTP-to-DTEP transition with prolonged exposure to lethal concentrations of SRA737.....	83
Figure 3-5: SK-N-AS cells remaining after lethal SRA737 exposure exhibit persister cell characteristics.....	88
Figure 3-6: SRA737-induced SK-N-AS DTPs are a heterogeneous population.....	90
Figure 4-1: SK-N-AS DTEP and drug-released cells are insensitive to further pharmacological inhibition of CHK1.	99
Figure 4-2: SK-N-AS DTEP and drug-released populations are cross-resistant to alternative small molecule inhibitors of CHK1 and CHK2.	101
Figure 4-3: SK-N-AS DTEP and drug-released cells are similarly cross-resistant to additional DDR pathway inhibitors.	104
Figure 4-4: Drug-released populations regain SRA737 sensitivity via different routes.	106
Figure 4-5: Transcriptional alterations in DTP and DTEPs are partially reversed after SRA737 withdrawal.	110
Figure 4-6: Persister cell populations adopt distinct gene expression profiles.	112
Figure 4-7: Persister cells express dormancy-related gene signatures.	116

Figure 4-8: Dose-escalated SK-N-AS populations have a distinct resistance phenotype.	119
Figure 4-9: SRA737 resistant populations derived through the persister cell bottleneck or dose-escalation are similarly cross-resistant to additional DDR inhibitors.	121
Figure 4-10: Transcriptional profiles are altered in dose-escalated SRA737-resistant populations.	123
Figure 4-11: Dose-escalated SRA737-resistant populations have altered transcriptional profiles.	125
Figure 4-12: Dose-escalated SRA737-resistant cells express senescence and quiescence-related gene signatures.	128
Figure 4-13: Persister-derived and dose-escalated SRA737 resistant populations harbour distinct alterations in the ATR-CHK1 DDR signalling axis.	132
Figure 4-14: Dose-escalated cells are more sensitive to WEE1 and CHK1 inhibitor combination.	134
Figure 4-15: Epigenetic alterations are specific to persister-derived populations.	135
Figure 4-16: Persister populations harbour unique transcriptional alterations.	138
Figure 5-1: SRA737-induced DTEPs are not sensitive to EZH2 inhibition using tazemetostat.	148
Figure 5-2: EZH2 histone methyltransferase activity is not required for SRA737-induced DTP formation.	151
Figure 5-3: EZH2 inhibition induces β -galactosidase activity in SRA737-induced DTPs.	153
Figure 5-4: EZH2 activity is required for DTP progression under continued SRA737 exposure.	156
Figure 5-5: Biomarker modulation in SRA737 and tazemetostat combination studies.	157
Figure 5-6: Persister-derived populations emerging from SRA737 and tazemetostat combination treatment appear to be more resistant to SRA737.	158
Figure 6-1: IL-2, IL-6, and IFN γ signalling through the JAK-STAT pathway.	164
Figure 6-2: SRA737-induced DTPs upregulate cytokine secretion.	167

Figure 6-3: SRA737-induced DTP formation is unaffected by inhibition or activation of the IFN γ -JAK1/2-STAT1 pathway.	169
Figure 6-4: The SRA737-induced DTP population is unperturbed by combination treatment with ruxolitinib or exogenous IFN γ	172
Figure 6-5: Cytokine secretion in SRA737-induced DTPs phenocopies direct IFN γ stimulation.	174
Figure 6-6: DTP-to-DTEP transition under lethal SRA737 exposure is unaffected by ruxolitinib-mediated inhibition of JAK1/2.	177
Figure 6-7: Exogenous IFN γ treatment abrogates DTP-to-DTEP transition under lethal SRA737 exposure.....	180
Figure 6-8: SRA737 potency is unchanged in populations emerging from the SRA737 and ruxolitinib or SRA737 and IFN γ combination DTP bottlenecks.	183
Appendix Figure 1: mKate2-SK-N-AS cells are a suitable model for persister cell studies.	231
Appendix Figure 2: Potency of WEE1i AZD1775 in parental SK-N-AS cells.....	232
Appendix Figure 3: Gene expression changes in additional cytokine signalling pathways.	233
Appendix Figure 4: ATR-CHK1 signalling in independently generated DTEP populations.	234
Appendix Figure 5: ATR-CHK1 signalling in independently generated dose-escalated populations.	235
Appendix Figure 6: ATR-CHK1 signalling in independently generated drug-released populations.	236
Appendix Figure 7: Optimising recombinant human cytokine and small molecule JAK inhibitor doses for use in persister cell studies.	237

List of tables

Table 1-1: <i>In vitro</i> biochemical and cellular potency values of CHK1 inhibitors.	44
Table 2-1: Source, stock, and storage information for compounds and human recombinant proteins.	50
Table 2-2: Optimal conditions for cell viability (GI_{50}) assay.....	51
Table 2-3: Conditions for 15- and 50-day persister cell time course experiments.....	54
Table 2-4: Formulation of NP-40 and RIPA cell lysis buffers.....	59
Table 2-5: Primary and secondary antibodies used for Western blotting.....	63
Table 3-1: <i>In vitro</i> biochemical and cellular potency values of CHK1 and MPS1 inhibitors in on-going clinical trial.....	71
Table 3-2: Summary of cellular potency values (GI_{50}) and approximate 100X GI_{50} compound concentrations used in DTP experiments.	75
Table 4-1: Summary of cellular potency values (GI_{50}) for indicated compounds in drug-naïve, DTEP, and drug-released populations at day 50.	102
Table 4-2: Summary of cellular potency values (GI_{50}) for indicated compounds in drug-naïve cells and replicate drug-released populations at day 274.	108
Table 4-3: Commonly enriched Hallmark gene sets from the MSigDB database in DTP and DTEP populations.....	114
Table 4-4: Summary of cellular potency values (GI_{50}) for indicated compounds in drug-naïve and 10 μ M dose-escalated populations at day 71.	121
Table 4-5: Commonly enriched Hallmark gene sets from the MSigDB database in dose-escalated populations.	127
Table 5-1: Summary of cellular potency values (GI_{50}) for SRA737 in indicated persister-derived and control populations.	159
Table 6-1: <i>In vitro</i> biochemical and cellular potency values of JAK or STAT inhibitors.	165
Table 6-2: Potency of JAK/STAT inhibitors in SK-N-AS cells as measured by pY701-STAT1 modulation (IC_{50}) and cell viability (GI_{50}).	170

Table 6-3: Summary of cellular potency (GI_{50}) values for SRA737 or ruxolitinib in indicated persister-derived and control populations.	184
Appendix Table 1: <i>In vitro</i> biochemical kinase screen for SRA737.....	229
Appendix Table 2: <i>In vitro</i> biochemical selectivity of SRA737 against selected kinases.	230

Abbreviations

A

A3A/A3A ^{WT}	Apolipoprotein B messenger RNA editing catalytic polypeptide-like 3-A (wild-type)
Abs	Absolute
ac	Acetylated
AKT	RAC-alpha serine/threonine-protein kinase
ALK	Anaplastic lymphoma kinase
APOBEC	Apolipoprotein B messenger RNA editing catalytic polypeptide-like
AML	Acute myeloid leukaemia
ATACseq	Assay for Transposase-Accessible Chromatin with sequencing
ATM(i)	Ataxia telangiectasia mutated protein (inhibitor/inhibition)
ATR(i)	Ataxia telangiectasia and Rad3 related (inhibitor/inhibition)

B

BCA	Bicinchoninic acid
β-gal	Beta-galactosidase
BRAF	B-Raf Proto-Oncogene, serine/threonine kinase
BSA	Bovine serum albumin

C

CCL1/I-309	C-C motif chemokine ligand 1
CCL2/MCP-1	C-C motif chemokine ligand 2
CCL5/RANTES	C-C motif chemokine ligand 5
CD4	Cluster of differentiation 4
CD8	Cluster of differentiation 8
CDK1(i)	Cyclin dependant kinase 1 (inhibitor/inhibition)
pY15-CDK1	Phosphorylated tyrosine-15 CDK1
CDK4/6	Cyclin dependant kinase 4/6
ChIPseq	Chromatin immunoprecipitation with sequencing
CHK1(i)	Checkpoint kinase 1 (inhibitor/inhibition)
pS296-CHK1	Phosphorylated serine-296 CHK1
CHK2(i)	Checkpoint kinase 2 (inhibitor/inhibition)
CO ₂	Carbon dioxide
CSCs	Cancer Stem Cells
CUT&Tag	Cleavage Under Targets and Tagmentation
CXCL1/GROα	C-X-C motif chemokine ligand 1
CXCL10/IP-10	C-X-C motif chemokine ligand 10
CXCL11/I-TAC	C-X-C motif chemokine ligand 11
CXCL12/SDF-1	C-X-C motif chemokine ligand 12

D

D7-DTP	Day 7 DTPs
ddH ₂ O	Double distilled water

dim	Dimension
DDR(i)	DNA damage response (inhibitors/inhibition)
DMEM	Dulbecco's Modified Eagle Medium
DMSO	Dimethyl sulfoxide
DNA	Deoxyribonucleic acid
DRP	Drug-released persisters
dsDNA	Double-stranded DNA
DTEPs	Drug-tolerant expanded persisters/persister cells
DTPs	Drug-tolerant persisters/persister cells
E	
EDTA	Ethylenediaminetetraacetic acid
EED	Embryonic ectoderm development
EGFR(i)	Epidermal growth factor receptor (inhibitor/inhibition)
EHMT2/G9a	Euchromatic histone lysine methyltransferase 2
EMT	Epithelial-to-mesenchymal transition
EF1 α	Elongation factor 1 alpha
ESC-1 μ M	Escalated to 1 μ M (dose-escalated)
ESC-10 μ M	Escalated to 10 μ M (dose-escalated)
Ex/Em	Excitation/Emission
ETOP	Etoposide
EZH2	Enhancer of zeste homolog 2
F	
FAO	Fatty acid oxidation
FBS	Foetal bovine serum
FDA	Food and Drug Administration (U.S.)
FDR	False discovery rate
G	
G-CSF	Granulocyte-colony stimulating factor
GEM	Gemcitabine
GI ₅₀	Half-maximum growth inhibitory concentration
GM-CSF	Granulocyte-macrophage colony-stimulating factor
GS	Gene signature score
GSEA	Gene set enrichment analysis
H	
H2AX	H2A.X variant histone
γ H2AX	Phosphorylated serine-139 H2A.X
H3/HH3	Histone H3
H3K4	Histone H3 lysine 4
H3K9	Histone H3 lysine 9
H3K18	Histone H3 lysine 18
H3K27	Histone H3 lysine 27
HDAC	Histone deacetylase

HER2	Human epidermal growth factor receptor 2
HR	Homologous recombination
HCl	Hydrochloric acid

I

IC ₅₀	Half-maximum inhibitory concentration
ICAM1/CD54	Intercellular adhesion molecule 1
ICR	Institute of Cancer Research
IFN γ	Interferon gamma
IL-1 α	Interleukin-1 alpha
IL-1 β	Interleukin-1 beta
IL-1ra	Interleukin-1 receptor antagonist protein
IL-2	Interleukin-2
IL-4	Interleukin-4
IL-10	Interleukin-10
IL-12 p70	Interleukin-12 subunit p70
IL-13	Interleukin-13
IL-16	Interleukin-16
IL-17A	Interleukin-17A
IL-17E	Interleukin-17E
IL-18/IL-1F4	Interleukin-18
IL-21	Interleukin-21
IL-27	Interleukin-27
IL-32 α	Interleukin-32 alpha

J

JAK1/JAK2/JAK3	Janus kinase 1/2/3
JAKi	Janus kinase inhibitor/inhibition

K

K	Lysine
KDM	Histone lysine demethylase

L

LOF	Loss-of-function
Log ₂ FC	Fold-change, on a log ₂ scale

M

m ⁶ A	N ⁶ -Methyladenosine
MAPK	Mitogen activated protein kinase
MDS	Multi-dimensional scaling
me ^{1/2/3}	Mono/di/tri-methylated or methylation
MET	MET Proto-Oncogene, receptor tyrosine kinase
MET	Mesenchymal-to-epithelial transition
MHC Class I/I	Major histocompatibility complex class I/II
MIF	Macrophage migration inhibitory factor

MIP-1 α /MIP-1 β	Macrophage inflammatory protein 1-alpha/Macrophage inflammatory protein 1-beta
MMR	Mismatch repair
MPS1(i)	Monopolar spindle kinase 1 (inhibitor/inhibition)
MRD	Minimal residual disease
mRNA	Messenger RNA
mTOR	Mechanistic target of rapamycin kinase
Myc	MYC Proto-Oncogene, BHLH transcription factor
N	
N/A	Not applicable
NB	Neuroblastoma
NF κ B	Nuclear factor NF-kappa-B p105 subunit
NIR	Near infrared
NSCLC	Non-small cell lung cancer
O	
OXPHOS	Oxidative phosphorylation
P	
p	Probability value
PAC	Paclitaxel
PALB	Palbociclib
PBS	Phosphate-buffered saline
PD-1	Programmed cell death protein 1
PDGFR(i)	Platelet derived growth factor receptor (inhibitor/inhibition)
PDL-1	Programmed death ligand 1
PDX	Patient-derived xenograft
PI3K	Phosphoinositide 3-kinase
PIK3CA	Phosphatidylinositol-4,5-Bisphosphate 3-Kinase Catalytic Subunit Alpha
PRC2	Polycomb repressive complex 2
PTM(s)	Post-translational modification(s)
PVDF	Polyvinylidene fluoride
R	
RAD51	DNA repair protein RAD51 homolog 1
RAS	"Rat sarcoma" GTPase
REL	Released
rh	Recombinant human
RNA	Ribonucleic acid
RNAi	RNA interference
RNAseq	RNA sequencing
RPA	Replication protein A
RPMI-1640	Roswell Park Memorial Institute (RPMI) 1640 medium
RT	Room temperature
(R)TKi	(Receptor) tyrosine kinase inhibitor/inhibition
RUX	Ruxolitinib

S

SAC	Spindle assembly checkpoint
SCLC	Small cell lung cancer
SD	Standard deviation
SDS	Sodium dodecyl sulphate
Serpin E1/PAI-1	Serpin family E member 1/Plasminogen activator inhibitor 1
shRNA	Short-hairpin RNA interference
ssDNA	Single-stranded DNA
SRA	SRA737
STAT1/3/5	Signal transducer and activator of transcription 1/3/5
STR	Short tandem repeat
SUZ12	Suppressor of zeste 12 protein homolog

T

T ₀	Time zero, time of treatment
T-25/T-75/T-175	Tissue culture flask with 25/75/175 cm ² growth area
TAZ	Tazemetostat
TCR	T-cell receptor
TEAD	TEA domain transcription factor
TNBC	Triple negative breast cancer
TNF α	Tumour necrosis factor-alpha
TP53	Tumour protein p53
TREM-1	Triggering receptor expressed on myeloid cells 1

U

Un	Undetermined
USP1	Ubiquitin carboxyl-terminal hydrolase 1
UTR	Untranslated region

W

WEE1(i)	Wee1-like protein kinase (inhibitor/inhibition)
WT	Wild-type

Y

YAP	Yes-associated protein
-----	------------------------

Units & Symbols

°C	Degrees Celsius
cm ²	Squared centimetres
d	Days
g	Gravity (gravitational constant)
h	Hours
μ g	Microgram
μ L	Microlitre
μ M	Micromolar

μm	Micrometre
mL	Millilitre
mM	Millimolar
mm	Millimetre
ng	Nanogram
nm	Nanometre
pH	Potential of hydrogen
®	Registered trademark
T _{End}	Test sample at end point
™	Trademark
%	Percent
V	Volts
V _{End}	Vehicle sample at end point
X/x	Times (multiple)
> or ≥	Greater than, or Equal to or greater than
< or ≤	Less than, or Equal to or less than
±	Plus or minus
~	Approximately

Chapter 1

Introduction

Chapter 1 Introduction

1.1. Knowledge is power

Advances in molecular profiling have helped identify differences between cancerous and “normal” cells and improved our understanding of cancer pathogenesis. This has led to the discovery of driver gene alterations that promote tumorigenesis, dawning a new era of molecularly targeted therapies that have shown considerable clinical efficacy in defined patient populations. By specifically effecting cancer cells, targeted agents can also ameliorate side effects caused by general cytotoxic chemotherapies providing patients with not only better, but kinder treatments.

A well-known example is the use of herceptin (trastuzumab) to treat human epidermal growth receptor 2 (HER2) positive breast cancer; a subtype that harbours genetic amplification of the *ERBB2* gene, resulting in overexpression of HER2 receptors at the cell surface (Berger et al. 1988). This induces constitutive HER2 receptor tyrosine kinase activity and downstream signalling through the RAS/MAPK and PI3K/AKT pathways to promote cancer cell survival, proliferation, and metastasis (reviewed in (Moasser 2007)). HER2 overexpression is observed in ~20% of primary breast cancers and is associated with disease relapse and poorer overall survival (Slamon et al. 1987; Berger et al. 1988). Herceptin is a humanised recombinant monoclonal antibody directed against the extracellular domain of the HER2 receptor (Hudziak et al. 1989) to inhibit its activation and subsequent oncogenic signalling. Herceptin treatment was shown to effectively inhibit the growth of HER2 overexpressing breast cancer cells and, furthermore, sensitise them to tumour necrosis factor (TNF)-induced cell death (Hudziak et al. 1989). Subsequent clinical investigations reported improved response rates, increased time to progression, and better overall survival in HER2 positive breast cancer patients receiving herceptin as first-line and adjuvant chemotherapy (Cobleigh et al. 1999; Vogel et al. 2002; Slamon et al. 2001). Importantly, the addition of herceptin was not clinically beneficial in patients without *ERBB2* amplification or HER2 protein overexpression

(Fehrenbacher et al. 2020), demonstrating the importance of appropriate patient stratification. The success of these clinical studies culminated in the approval of herceptin as the first antibody-targeted therapy for the treatment of HER2 positive metastatic breast cancer in 1998 (Siegel 1998).

Beyond focussing on individual cellular processes, targeted therapies are now being developed to alter multi-cellular interactions. This is exemplified by immunotherapies such as avelumab and nivolumab, that act as checkpoint inhibitors to promote anti-cancer immune responses. Cancer cells display a variety of tumour-specific antigens on their surface via MHC class I/II receptors (Segal et al. 2008). Some of these are neoantigens, produced as a result of irregular protein production caused by increased genetic mutation, dysregulated RNA splicing, and irregular post-translational modification in cancer cells (reviewed in (Smith et al. 2019; Minati, Perreault, and Thibault 2020)). During the course of normal immune surveillance, such “non-self” antigens are detected by cognate T-cell receptors (TCR) on circulating CD4 and CD8 positive T-cells, triggering T-cell activation and subsequent induction of an adaptive immune response to kill the cell (Townsend et al. 1986). However, cancer cells have developed a way of subverting this process by, amongst other mechanisms, overexpressing the programmed death ligand-1 (PDL-1) protein at the cell surface (Nakanishi et al. 2007; Inman et al. 2007). PDL-1 plays a key role in the immune checkpoint. Simultaneous binding of PDL-1 to the programmed cell death protein 1 (PD-1) receptor on T-cells at the time of antigen recognition halts immune activation to ensure immune responses are executed appropriately (Freeman et al. 2000). This failsafe mechanism, in place to ensure only “non-self” cells are destroyed, is exploited by cancer cells to avoid immune-mediated death (Iwai et al. 2002; Yang et al. 2008). As such, PDL-1 overexpression correlates with poorer prognosis in several cancer types (Ohigashi et al. 2005; Thompson and Kwon 2006; Nakanishi et al. 2007). Avelumab and nivolumab are therapeutic antibodies targeted against PDL-1 and PD-1, respectively, whose binding block the PD-1-PDL-1 interaction to relieve negative regulation on T-cell activity and promote immune-mediated cell killing (Boyerinas et al. 2015). Both these agents demonstrated efficacy in clinical trial (Kaufman et al. 2016; Wolchok

et al. 2013), resulting in their FDA approval for use in the treatment of Merkel cell carcinoma (avelumab) and advanced melanoma (nivolumab) in 2017 and 2014, respectively.

Subsequent drug discovery efforts have resulted in FDA approval of >150 targeted therapies for the treatment of multiple cancers (NCI 2023). However, as observed with general cytotoxic chemotherapies, this initial success has been undermined by the eventual emergence of resistance. Given that recurrence rates can be as high as 85% (Corrado et al. 2017) and refractory disease is associated with poorer survival outcomes (Morris et al. 2014; Crump et al. 2017; Chihara et al. 2017), drug resistance represents a major limitation to effective, long-term anti-cancer treatment. Overcoming drug resistance mechanisms represents an attractive approach to anti-cancer therapy and, as such, is a key area in cancer research.

1.2. Drug resistance in cancer – inspired by bacteria

Various paths to resistance have been identified in cancer and are broadly characterised as mutational or non-mutational mechanisms. Some of the most well characterised include genetic mutation of drug targets (Yun et al. 2008), upregulation of drug efflux pumps and metabolic enzymes (Bell et al. 1985; Michael and Doherty 2005), and engagement of compensatory signalling pathways (Villanueva et al. 2010; Serra et al. 2011). Whether these are pre-existing and selected for (intrinsic) or acquired under therapeutic pressure is under investigation in the field of cancer evolution. Nonetheless, rather than being mutually exclusive, it is likely that a combination of these mechanisms occur simultaneously within a heterogeneous tumour population to drive the emergence of drug resistance (Salgia and Kulkarni 2018; Bell and Gilan 2020).

This is exemplified in the treatment of non-small cell lung cancers (NSCLC) with small molecule receptor tyrosine kinase inhibitors ((R)TKi) targeted against the epidermal growth factor receptor (EGFR). *EGFR* amplification or mutations are detected in up to 89% of patients with NSCLC (Gupta et al. 2009), resulting in

increased or constitutive activation of the EGFR receptor and downstream signalling through the PI3K/AKT, RAS/MAPK, and JAK/STAT pathways that promote cancer cell proliferation, survival, and metastasis (reviewed in (Gerber 2008)). As such, increased EGFR activity is associated with poorer clinical outcome (Hirsch et al. 2003). Approximately 60% of patients that progress on first- and second-generation EGFR inhibitors (EGFRi), such as erlotinib and afatinib, harbour the *EGFR*^{T790M} gatekeeper mutation (Pao et al. 2005; Yu et al. 2013) that prevents drug binding to the EGFR active site (Yun et al. 2008). Subsequent molecular profiling revealed additional genomic aberrations in tumours from EGFRi resistant patients, including amplification of the bypass signalling genes *MET* (Bean et al. 2007) and *HER2* (Yu et al. 2013), and mutations in genes encoding downstream signalling proteins, such as *PIK3CA* and *BRAF* (Sequist et al. 2011; Ohashi et al. 2012; Chafft et al. 2012). These mutations were identified in both the presence and absence of *EGFR*^{T790M}, providing evidence for the simultaneous emergence of diverse drug resistance mechanisms from a heterogenous tumour population. Furthermore, several patient studies reported histological alterations in up to 10% of EGFRi resistant tumours, including transformation to small cell lung cancer (SCLC) (Yu et al. 2013; Marcoux et al. 2019) and epithelial-to-mesenchymal transition (EMT) (Sequist et al. 2011), demonstrating the role of cellular plasticity in promoting drug resistance.

Aside from mutational strategies, there has been accumulating evidence supporting the role of non-mutational mechanisms in the emergence of drug resistance. The observation that some patients benefited from a “drug holiday”, in which their non-responsive tumours regained drug sensitivity following a period of withdrawal (Kurata et al. 2004; Cara and Tannock 2001), implicated engagement of a reversible, non-heritable resistance mechanism and suggested the existence of a “drug-tolerant” cellular phenotype that had not yet progressed to *bona fide* genetic resistance. Such cells have, in fact, been reported in bacteria following anti-microbial exposure since the 1940s, however have only recently been characterised in human cancer (Sharma et al. 2010).

Joseph W. Bigger was the first to describe bacterial persistence following the observation that penicillin treatment failed to completely eradicate all *Staphylococcus pyogenes* bacterium (Bigger 1944a; Bigger 1944b). These persistent cells are slow-growing and harbour no resistance-conferring genetic mutations, as progeny that emerge from this population are sensitive to antibiotic exposure (Keren et al. 2004; Lechner, Lewis, and Bertram 2012). In light of this, they are considered to be regulated by epigenetic processes that alter gene expression in the absence of changes to the underlying genetic code (reviewed in (Riber and Hansen 2021)). Experimental investigations and mathematical modelling showed that bacterial cells stochastically switch between quiescent persister and normal proliferative states within an unperturbed population, with the persistence phenotype becoming increasingly prevalent during the stationary growth phase and in response to antibiotic challenge (Balaban et al. 2004). Moreover, persister production increases if antibiotic exposure occurs during the mid-exponential and stationary growth phases (Keren et al. 2004; Lechner, Lewis, and Bertram 2012), when the population is a mix of slow-growing and proliferating cells. This relationship was fully described in subsequent reports concluding that persistence is linked to pre-existing heterogeneity, providing bacterial populations with a bet-hedging strategy to ensure their survival in the event of environmental challenges (Balaban et al. 2004; Kussell et al. 2005). Persisters have been observed in a number of bacterial species in response to different antimicrobial agents, indicating that they represent a conserved response to therapy-induced stress. The clinical relevance of this phenotype was revealed by studies showing that bacterial persisters promote the emergence of antibiotic resistance by increasing their mutational rate (Windels et al. 2019) and, as such, providing a reservoir of viable cells for the evolution of drug resistance.

1.3. Identification and characterisation of drug-tolerant persisters in cancer

The emergence of non-mutationally “drug-tolerant” cancer cell populations was reported in early drug resistance studies. Initial isolates of doxorubicin-resistant murine neuroblastoma reverted to a drug sensitive state after doxorubicin

removal but developed stable resistance with prolonged drug exposure (Baskin, Rosenberg, and Dev 1981). Unstable drug tolerance was associated with the appearance of double minute chromosomes, extrachromosomal circular DNA fragments that can contain resistance conferring or oncogenic gene amplifications (reviewed in (Gebhart 2005)), that diminished with the acquisition of stable resistance. These results suggested the emergence of a transiently drug tolerant population, regulated by non-mutational mechanisms that preceded overt genetic resistance.

Such cells, termed drug-tolerant persisters (DTPs), were first characterised in response to a targeted agent by Sharma and colleagues in an *in vitro* model of NSCLC following 9 days lethal exposure (~100X GI₅₀ value) to the EGFRi erlotinib (Sharma et al. 2010). DTPs accounted for 0.27% of the starting population and were largely quiescent, indicating that they represent a rare subpopulation of cells that can withstand toxic drug concentrations by adopting a slow-cycling state. In the same study, DTPs were also isolated from other cancer cell lines using additional agents, suggesting that their emergence is a common response to therapeutic challenge. This quiescent, drug-tolerant phenotype was reversed within 9 population doublings following erlotinib withdrawal, mirroring a clinical “drug-holiday”. DTPs were also able to resume proliferation under continued lethal erlotinib exposure. These drug-tolerant expanded persisters (DTEPs) were up to 500-fold less sensitive to EGFRi compared to drug-naïve controls but did not contain known genetic resistance mechanisms, such as *EGFR*^{T790M} mutation (Yun et al. 2008; Pao et al. 2005) or *MET* amplification (Bean et al. 2007; Engelman et al. 2007). Consistent with this, DTEPs also regained erlotinib sensitivity following culture in drug-free media; although this took ~30 passages to achieve. Considering day 9 DTPs resensitised at a quicker rate, these observations suggest that reversibility of the persister cell state is related to duration of therapeutic challenge. This seminal report revealed the transient, reversible, and non-mutational characteristics of drug-tolerant persister cell populations in cancer and defined the rules for isolation and identification of DTPs in the field.

1.4. Mechanisms of drug-tolerance in cancer

Drug-tolerant persisters have been identified in a number of cancer cell models, including melanoma (Roesch et al. 2010), breast (Al Emran et al. 2018), and colon cancer (Rehman et al. 2021), suggesting they may represent a common cellular response to therapeutic challenges. This is further supported by recent reports of DTP emergence in response to alternative chemotherapies with different mechanisms of action, including anti-microtubule agents and anti-metabolites (Rehman et al. 2021; Dhimolea et al. 2021). Characterisation of persister cell populations can improve our understanding of the mechanisms involved in regulating their formation, progression, and survival and help to identify potential therapeutic targets to mitigate the development of drug-resistance through the persister-cell bottleneck.

1.4.1. Epigenetic alterations

In the absence of genetic resistance, persister cells are characterised by global changes to post-translational epigenetic modifications that regulate gene expression by altering chromatin architecture and the accessibility of DNA to transcriptional machinery. Such changes were described by Sharma and colleagues (2010), who reported differential nuclease digestion of chromatin extracts from EGFRi-induced DTEPs compared to parental PC9 cells. Further analysis of DTP and DTEP transcriptional profiles by RNA-sequencing revealed a specific upregulation in expression of *KDM5A*; a histone demethylase that catalyses the removal of methyl groups from histone H3 lysine 4 residues (H3K4) (Christensen et al. 2007). Accordingly, this was accompanied by a reduction in the levels of tri- and di-methylated H3K4 in PC9-DTPs generated with gefitinib (Sharma et al. 2010). Subsequent knockdown of *KDM5A* expression using short-hairpin RNA interference (shRNA) effectively reduced emergence of gefitinib-induced DTP and DTEP populations. Consistent with the requirement of *KDM5A* activity for persister cell formation, the number of DTPs was increased by overexpression of exogenous *KDM5A*. Together, these results demonstrate an

important role for epigenetic mechanisms in the formation and progression of drug-tolerant cancer cell populations.

Further comprehensive profiling using mass spectrometry revealed extensive changes to additional epigenetic modifications on histone H3 (Guler et al. 2017). In particular, modifications associated with repressive heterochromatin, such as H3 lysine 27 tri-methylation (H3K27_{me3}), were globally increased in PC9-DTPs generated with erlotinib. Concomitantly, modifications associated with permissive euchromatin were decreased. Interestingly, these alterations were absent in PC9-DTEPs and PC9-DTPs that had been recovered in drug free medium, suggesting that epigenetic mechanisms may be required for maintaining drug-tolerance in slow-cycling, but not proliferating, persister cell populations. An RNAi screen of 298 epigenetic genes identified a requirement for the histone H3 lysine 9 methyltransferase EHMT2/G9a for DTP formation in PC9 cells treated with erlotinib. This effect was confirmed upon genetic (CRISPR knockout) and pharmacological inhibition of EHMT2/G9a, that resulted in a significant reduction in the number of DTPs generated following erlotinib exposure. In addition, EHMT2/G9a knockout substantially abrogated the emergence of DTEP populations after 30 days exposure to erlotinib when compared to parental control. This study demonstrates the diversity of epigenetic alterations in drug-tolerant persister cell populations and provides further evidence for their pivotal role in drug-induced DTP formation and progression.

In addition to changes in post-translational modifications on chromatin, a novel epitranscriptomic mechanism has also been reported. Using an *in vitro* model of BRAF^{V600E} mutant melanoma (A375 cells), persister cells generated with lethal concentrations of BRAFi and MEKi in combination (PLX4032 and cobimetinib, respectively) showed a reduction in nascent protein production and polysome-bound mRNAs, indicating a downregulation of translational activity (Shen et al. 2019). Despite this, genome-wide polysome profiling, wherein polysome-bound mRNAs are sequenced and analysed by Gene Ontology, revealed that 178 genetic transcripts were actually translated with greater efficiency. Further STRING network analysis showed that these were enriched for genes associated

with chromatin remodelling such as ARID5B; a component of the PHF2-ARID5B histone H3K9 demethylase complex (Baba et al. 2011). Characterisation of polysome-bound mRNAs found an increase in N6-methyladenosine (m⁶A) at the 5'-untranslated region (UTR), where post-translational modifications can regulate translation (Shen et al. 2019). Importantly, all of these alterations were reversed following drug withdrawal, demonstrating their transient induction in the DTP state. shRNA-mediated knockdown of METTL3 and WTAP, two members of the m⁶A methylation complex, significantly inhibited the emergence of persister-derived drug-resistant colonies in A375 cells under long-term exposure to lethal doses of PLX4032 and cobimetinib. Importantly, these data reveal that epigenetic control of gene expression is exerted at the translational and transcriptional level in DTP populations.

Others have reported similar alterations to epigenetic profiles and expression of chromatin-modifying genes in additional *in vitro* DTP models generated with alternative chemotherapies (Liau et al. 2017; Al Emran et al. 2018; Roesch et al. 2010; Vinogradova et al. 2016), consolidating epigenetic mechanisms as a key strategy employed by cancer cells to adopt the persister cell state. Perhaps more importantly, these studies have led to the identification of several epigenetic enzymes as potential targets to abrogate DTP emergence and progression. While targeting these enzymes using genetic or pharmacological tools has shown some efficacy, they have, at most, only delayed the emergence of persister-derived drug-resistant populations. Failure to completely eradicate DTPs in this context suggests that additional mechanisms are involved in regulating their formation and progression under therapeutic stress.

1.4.2. Cellular reprogramming

In line with changes to the epigenetic landscape and chromatin architecture, gene expression profiles are altered in persister cell populations. Consistent with the slow-cycling DTP state, cell cycle and proliferation related genes are downregulated in persisters generated with TKi (Liau et al. 2017; Shen et al.

2019), Perhaps related to this, enriched genes include those associated with dormancy, quiescence, and stemness.

Gene set enrichment analysis (GSEA) of RNA sequencing data from dasatinib-induced DTPs generated in an *in vitro* model of glioblastoma revealed an enrichment of gene signatures derived from models of quiescent neural stem cell and stem-like medulloblastoma (Liau et al. 2017). Consistent with this, expression of classic cancer stem cell markers CD133 (Singh et al. 2004) and CD15 (Son et al. 2009) were upregulated at the transcript and protein level in DTPs. In addition, expression of *SOX2*, *SOX4*, and *NOTCH1* were increased (Liau et al. 2017) and notch signalling was upregulated. As master transcriptional regulators of pluripotent, differentiation and developmental gene expression, these data suggest that engagement of developmental processes is important for DTP formation, perhaps by promoting cellular plasticity as a mechanism to overcome therapeutic challenge.

More recently, induction of stress responses has been reported in persisters. Persisters generated with irinotecan in a patient-derived xenograft (PDX) model of colorectal cancer were enriched for a gene signature derived from *in vitro* diapaused mammalian embryos (Rehman et al. 2021). Embryonic diapause is a reversible state of arrested embryonic development that is triggered in response to unfavourable environmental conditions, such as nutrient deprivation (reviewed in (Fenelon, Banerjee, and Murphy 2014)). Interestingly, the diapause signature was not upregulated in tumours that had regrown following removal of chemotherapy (Rehman et al. 2021), demonstrating transient and reversible engagement of this mechanism in DTPs. As such, this data suggests that persister cells adopt a diapause-like state as a stress response strategy to promote their survival under the unfavourable environmental conditions caused by therapeutic challenge.

Additional mechanisms reported in DTP models include metabolic rewiring (Hangauer et al. 2017; Echeverria et al. 2019), endoplasmic reticulum (ER) stress

(Terai et al. 2018), and inflammatory responses (Guler et al. 2017), illustrating the breadth of cellular reprogramming undertaken by persister cells (Figure 1-1).

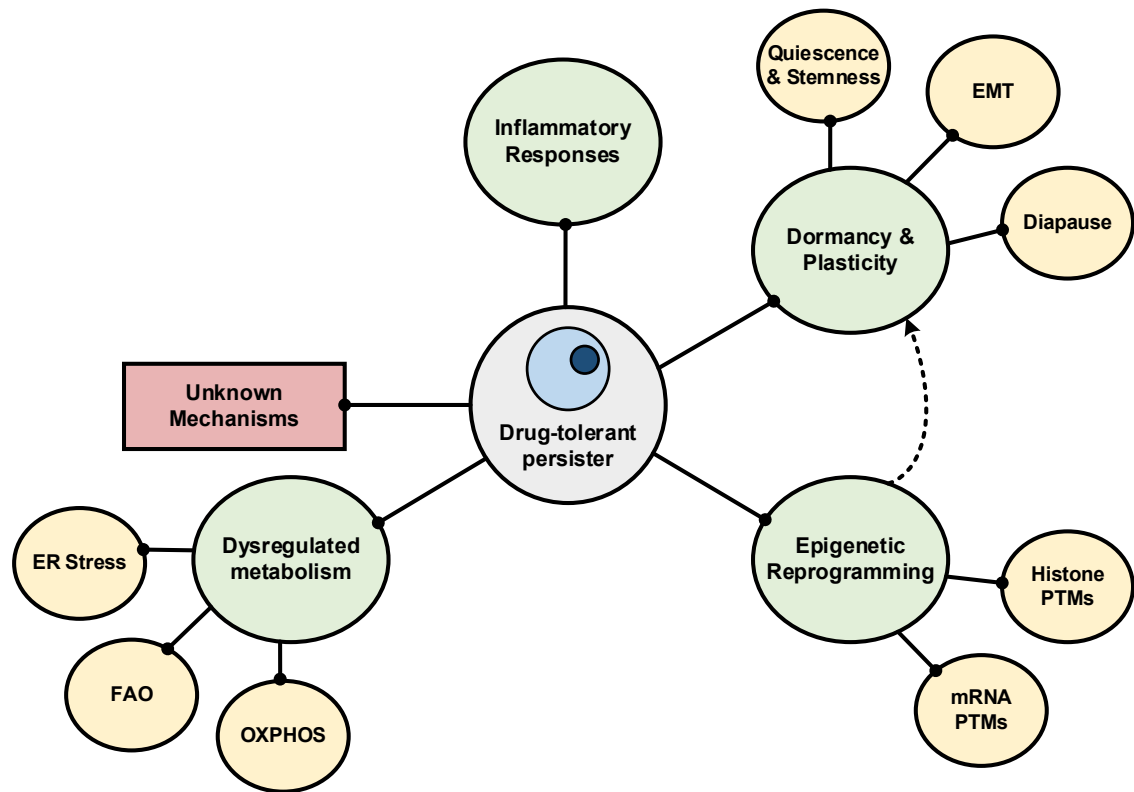


Figure 1-1: Persister cell mechanisms.

Drug-tolerant persisters employ various mechanisms to promote their survival and adaption to overcome therapeutic challenge. Different mechanisms may act concurrently; for example, epigenetic reprogramming can promote expression of quiescence-related genes. The mechanisms outlined here are not exhaustive but represent what has been discussed herein. For further reading, please refer to an excellent review article by (Cabanos and Hata 2021). FAO: fatty acid oxidation; OXPHOS: oxidative phosphorylation; PTMs: post-translational modifications.

1.5. Clinical evidence for DTP emergence in cancer

The observation that up to 50% of patients with EGFRi resistant tumours do not harbour a validated resistance mutation (Leonetti et al. 2019) suggests that a considerable proportion of refractory disease could be attributed to non-mutational mechanisms, such as persistence. However, clinical evidence for the emergence of a drug-tolerant persister population in patients receiving

chemotherapy is limited, in part, due to the lack of a *bona fide* persister cell 'marker' or molecular profile that can be used to detect or isolate this rare population. Aside from the "drug holiday" phenomenon (Kurata et al. 2004; Cara and Tannock 2001), arguably the most clinically relevant comparison is to minimal residual disease (MRD) occurring in patients receiving continuous systemic targeted chemotherapy. MRD can remain clinically silent for several years but then re-emerge as treatment refractory disease, suggesting the presence of lingering viable tumour cells at the point of remission. Given these parallels with DTPs, PDX models of MRD have been used to investigate persister cell responses to chemotherapy *in vivo*.

Using a PDX model of colorectal cancer, tumours driven to MRD with standard of care irinotecan treatment regrew after drug withdrawal (Rehman et al. 2021). Immunohistochemical analysis of MRD and regrowth tumours revealed a reduction in proliferative Ki67 staining in MRD samples, mirroring the slow-cycling DTP state. Ki67 staining returned to control levels following regrowth in the absence of chemotherapy. Moreover, regrowth tumours showed sensitivity to further irinotecan treatment after re-implantation into new mice. These results are consistent with cancer cells entering a transient and reversible drug-tolerant state. Similar observations were reported using a PDX model of TNBC, in which MRD was generated with doxorubicin treatment (Echeverria et al. 2019). An alternative explanation for these results is that chemotherapy enriches for cancer stem cells that subsequently drive tumour repopulation. However, MRD tumours were not enriched for CD44^{high}/CD24^{low} expression (Echeverria et al. 2019); a specific phenotype associated with cancer stem-like cells (Hurt et al. 2008; Ghuwalewala et al. 2016), nor did they display increased tumour-initiation (Rehman et al. 2021; Echeverria et al. 2019). These results support the identity of MRD tumours as a drug-tolerant persister population and demonstrates their emergence in response to drug treatment *in vivo*. With advances in technologies such as single-cell RNA sequencing, detection and de-coding of rare persisters in patients could be on the horizon.

1.6. The role of drug-tolerance in the evolution of cancer resistance

The discovery that genetic resistance mechanisms can arise *de novo* from DTPs has revealed the potential impact of the drug tolerant state in anti-cancer therapy. PC9 cells harbouring the *EGFR*^{T790M} gatekeeper mutation following treatment with the EGFRi gefitinib were found to originate from both pre-existing resistant cells and slow-cycling DTPs (Hata et al. 2016). In contrast to early-resistant clones that arose from pre-existing mutants, late *EGFR*^{T790M}-resistant clones emerged from slow-cycling DTPs after >20 weeks gefitinib treatment. Accordingly, this was accompanied by decreased sensitivity to gefitinib and a concomitant increase in sensitivity to osimertinib; a third generation EGFRi targeted against the *EGFR*^{T790M} mutant protein. Together, these results clearly demonstrate that genetic resistance mutations can be acquired in drug-tolerant populations during prolonged drug exposure. Given that resistance was conferred by pre-existing mutants and the DTP bottleneck, this data also indicates that the two mechanisms occur simultaneously within a heterogeneous tumour population to drive the emergence of therapeutic resistance (Figure 1-2).

Additional genetic aberrations have been identified in persister-derived, EGFRi resistant colonies generated from a clonal PC9 cell line (Ramirez et al. 2016). Clinically relevant mutations, including *BRAF*^{G466A} and *MET* amplification, as well as mutations in *NRAS* and *PIK3CA* genes were detected following ~10 months culture in 2.5 µM erlotinib, demonstrating that acquired resistance mechanisms are not limited by the DTP state. Furthermore, pharmacological screening revealed differential drug sensitivities amongst EGFRi resistant clones. While all were resistant to further challenge with additional EGFRi, several populations demonstrated sensitivity to small molecule inhibitors targeted against MET, MEK, and mTOR that correlated with genetic alteration of the target or pathway related proteins. Importantly, this study shows that diverse drug resistance mechanisms can emerge from clonal populations under the same therapeutic pressure, providing evidence that drug-tolerant persister cells provide a reservoir for cancer evolution. Furthermore, these results indicate that the DTP state can provide

new therapeutic opportunities by targeting activated pathways that may confer collateral drug sensitivity in the persistent population.

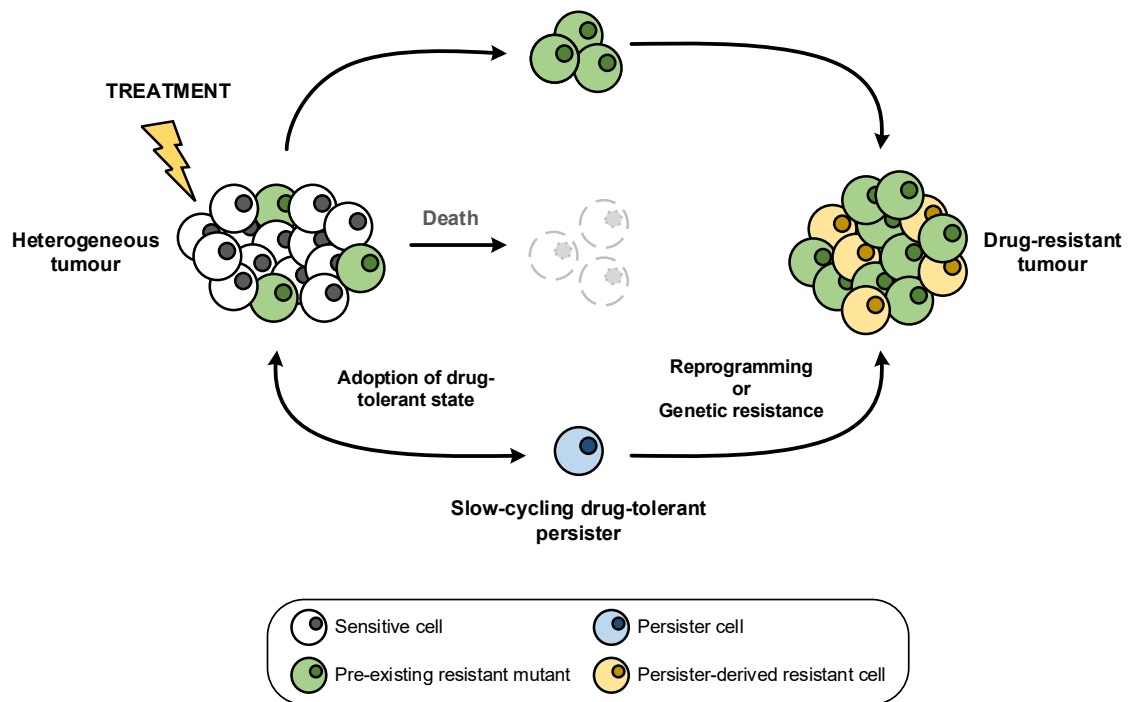


Figure 1-2: DTP formation and contribution to the evolution of drug-resistance in cancer. While most tumour cells will die in response to chemotherapeutic exposure, pre-existing resistant mutants will survive and repopulate a drug-resistant tumour. Alternatively, in response to therapeutic stress, sensitive cells can adopt a slow-cycling drug-tolerant state characterised by alterations to epigenetic landscapes and transcriptional profiles. With continued drug exposure, these persisters can undergo cellular reprogramming or acquire *de novo* resistance mutations to resume growth and contribute to the emergence of a drug-resistant tumour.

1.7. A view on drug-tolerance in cancer

Crucially, the studies described heretofore highlight the potential of drug-tolerant persisters to serve as a heterogeneous reservoir of refractory disease (Figure 1-2). As a potentially reversible precursor to genetic resistance, targeting DTPs presents an attractive approach for mitigating drug resistance in cancer. However, despite our growing understanding of persister cell mechanisms, attempts to eradicate them by targeting epigenetic processes have resulted only in delaying the emergence of drug resistant populations from the DTP bottleneck

(Sharma et al. 2010; Guler et al. 2017; Liau et al. 2017; Shen et al. 2019). As such, it is evident that there is more to uncover. Furthermore, while therapeutic contexts are expanding, the majority of data come from studies using tyrosine kinase inhibitors that suppress oncogenic signalling. Hence, it remains unclear whether the persister cell response is induced by diverse therapeutic agents; particularly those that interfere with DNA integrity, such as targeted inhibitors of monopolar spindle 1 kinase (MPS1) or checkpoint kinase 1 (CHK1) that are currently under clinical investigation (NCT03328494 ; NCT02797964 ; NCT02797977). In anticipation of their approval for use in the clinic, it is prudent to investigate and characterise the contribution of persister cells to the emergence of drug resistance under these novel therapeutic contexts.

1.8. Targeting monopolar spindle 1 kinase (MPS1) in cancer

Also known as TTK, MPS1 is a dual-specificity protein kinase required for correct chromosomal alignment and segregation as part of the mitotic spindle assembly checkpoint (SAC) (Abrieu et al. 2001; Maciejowski et al. 2010; Dou et al. 2015). Preclinical studies have identified MPS1 inhibitor (MPS1i) sensitivity in cancer cells characterised by inadequate SAC regulation, chromosomal instability, and aneuploidy, such as triple-negative breast cancer (TNBC) and glioblastoma (Anderhub et al. 2019; Tannous et al. 2013). In this cellular context, MPS1i also potentiates the effects of microtubule polymerising agents (Tannous et al. 2013; Maia et al. 2015; Anderhub et al. 2019). As such, MPS1i are being tested alone and in combination with paclitaxel in TNBC patients (NCT03328494).

As the majority of the work presented in this thesis was conducted using the small molecule CHK1 inhibitor (CHK1i) SRA737, the biological function of CHK1 and rationale for targeting this protein for anti-cancer treatment will be the focus for the remainder of this introduction.

1.9. Targeting checkpoint kinase 1 (CHK1) in cancer

DNA damage can occur as a result of endogenous factors, such as defective DNA repair mechanisms and high levels of oncogenic signalling, or exogenously induced by, for example, DNA damaging chemotherapeutic agents. Unrepaired DNA damage can be a source of genetic alterations that promote malignant transformation, or genetic instability that results in cell death. Repairing DNA damage is therefore of utmost importance to ensure faithful replication of the genetic code during cell division and cell survival. Various repair mechanisms exist, including homologous recombination (HR) and mismatch repair (MMR), and are differentially employed depending on the type of DNA damage incurred. Herein is an overview of the ATR-CHK1 axis of the DNA damage response (DDR) signalling pathway, its role in cancer, and the development of small molecule CHK1 inhibitors to therapeutically target cancer cells.

1.9.1. CHK1 is a key effector of the DNA damage response (DDR) signalling pathway

Checkpoint kinase 1 (CHK1), encoded by the *CHEK1* gene, is a highly conserved serine/threonine protein kinase that coordinates cell cycle and DNA damage response (DDR) checkpoints to preserve genome integrity (Walworth, Davey, and Beach 1993; Sanchez et al. 1997). Although CHK1 can be activated in response to single- (ssDNA) and double-stranded (dsDNA) DNA breaks, it plays a pivotal role in replication stress caused by replication fork stall during DNA synthesis (Gupta et al. 2018). Stalled forks leave extended regions of unstable single-stranded DNA (ssDNA) exposed to degradation by nucleases and, if unresolved, can lead to irreversible fork collapse and genome instability (Pond et al. 2019). To protect the nucleotide sequence and initiate DNA repair and/or fork recovery, exposed ssDNA is coated by replication protein A (Huemer et al.) to recruit and activate ataxia telangiectasia Rad-3 related protein (ATR) (Zou and Elledge 2003) that goes on to phosphorylate CHK1 at two sites, Ser-317 and Ser-345 (Zhao and Piwnicka-Worms 2001). Subsequent autophosphorylation at Ser-296 completes CHK1 activation (Okita et al. 2012) and triggers DDR signalling,

wherein CHK1 phosphorylates a variety of downstream targets to facilitate fork repair or, in the event of irrecoverable fork collapse, initiate cell death (Figure 1-3).

One such target is the phosphatase cell division cycle 25C (Cdc25C). CHK1 phosphorylates Cdc25C at Ser-216, rendering it inactive and subsequently unable to dephosphorylate and activate cyclin dependant kinase 1 (CDK1) at Tyr-15 (Sanchez et al. 1997). CHK1 can also phosphorylate and activate WEE1, which in turn phosphorylates and inactivates CDK1 at Tyr-15 (O'Connell et al. 1997). These actions work in concert to inhibit CDK1, CDK1-cyclin B complex activation, and entry into mitosis, resulting in coordinated G2/M cell cycle arrest. This provides cells with the opportunity to resolve replication stress through DNA repair or, in the event of irrecoverable fork collapse, trigger apoptosis. CHK1 can additionally phosphorylate DNA repair protein RAD51 homolog 1 (RAD51) (Sørensen et al. 2005) and tumour protein p53 (TP53) (Shieh et al. 2000; Ou et al. 2005) to promote HR repair or p53-dependent gene expression, respectively, illustrating its essential and nuanced functions in DDR signalling.

The ATR-CHK1 axis forms one arm of the DDR pathway. In parallel, a second signalling cascade regulated by ataxia-telangiectasia mutated protein (ATM) and checkpoint kinase 2 (CHK2) is activated by dsDNA breaks to induce TP53-mediated cell cycle arrest and DNA repair (reviewed in (Zannini, Delia, and Buscemi 2014)). The observation that CHK1 was also phosphorylated by ATM in response to ionising radiation-induced dsDNA breaks suggested potential cross-talk between the ATR-CHK1 and ATM-CHK2 signalling pathways (Cuadrado et al. 2006). Similar conclusions from others (Jazayeri et al. 2006; Shiotani and Zou 2009) has helped to confirm the interplay between these axes of the DDR pathway for co-ordinating cellular responses to different DNA insults (Figure 1-3).

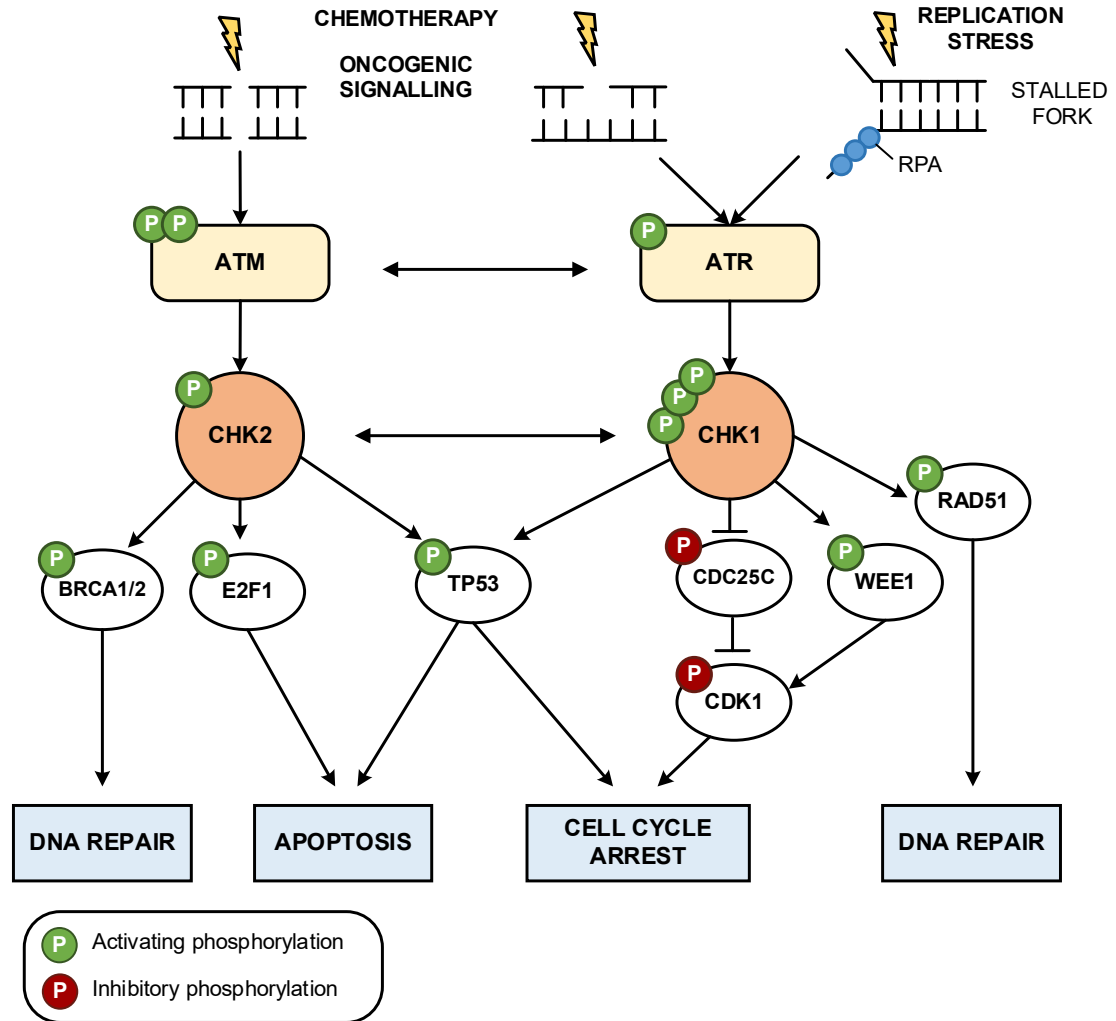


Figure 1-3: DNA damage response signalling through the ATR-CHK1 and ATM-CHK2 axes. In response to DNA damage, CHK1 is phosphorylated and activated by ATR. CHK1 phosphorylates a number of downstream targets to promote cell cycle arrest and DNA repair or, in the event of irrecoverable genomic damage, trigger apoptosis. Cross-talk between the ATR-CHK1 and ATM-CHK2 axes co-ordinates appropriate cellular responses to different DNA insults.

1.9.2. CHK1 in cancer

Cancer cells are characterised by genome instability caused by high levels of replication stress, DNA damage, and dysregulated DNA repair. Due to its fundamental role in maintaining faithful cell division and genome integrity, CHK1 was initially believed to function as a tumour suppressor (Bertoni et al. 1999). This theory has been largely contradicted following the observation that *CHEK1* amplification promotes oncogenic transformation in murine embryonic fibroblasts

(López-Contreras et al. 2012), and CHK1 expression is upregulated in several human cancers including breast (Verlinden et al. 2007), colon (Madoz-Gúrpide et al. 2007) and nasopharyngeal cancer (Sriuranpong et al. 2004). Furthermore, *CHEK1* copy number gain is present in tumour samples from patients with ovarian and small cell lung cancer, osteosarcoma, and diffuse large B-cell lymphoma (TCGA). Numerous studies have reported a requirement for CHK1 in tumorigenesis. Homozygous *CHEK1* deletion in mouse skin reduced carcinogen-induced papilloma formation and inhibited progression to carcinoma (Tho et al. 2012). In another study, CHK1 knockdown induced apoptosis in T-cell acute lymphoblastic leukaemia cells with endogenously high CHK1 expression and activity (Sarmiento et al. 2015). Consistent with the requirement of CHK1 for recovery from replication stress (Gupta et al. 2018) this was accompanied by accumulation of DNA damage caused by increased fork stalling, as measured by enrichment of phosphorylated γ H2AX nuclear foci and RPA, respectively. Furthermore, a genetic screen using RNA interference identified CHK1 as a potentiator of cisplatin response in ovarian cancer cells (Arora et al. 2010). These observations provided evidence for the role of CHK1 as a tumour promoter, and therapeutic rationale for the development of small molecule CHK1 inhibitors (CHK1i).

1.9.3. Targeted inhibition of CHK1 using small molecules

The Institute of Cancer Research (London) and others have developed small molecule CHK1i that are currently under investigation in clinical trials (Table 1-1).

SRA737 is a potent CHK1i with >1000-fold selectivity for CHK1 (IC₅₀ 1.4 nM) over related DDR effector CHK2 (IC₅₀ 2.4 μ M) (Walton et al. 2016) (Appendix Table 1 & 2). SRA737 binds to the ATP binding site of CHK1, preventing ATP hydrolysis and inhibiting CHK1 kinase activity (Osborne et al. 2016). In HT-29 colon cancer cells, SRA737 treatment abrogates gemcitabine-induced CHK1 phosphorylation at Ser-317, Ser-345, and Ser-296 (Walton et al. 2016). Consequently, CHK1-mediated inactivation of CDK1 is diminished and cells continue to progress through the cell cycle without optimal DNA damage repair, culminating in

unrecoverable genomic instability and cell death. Markers of replication stress, including γ H2AX and chromosomal fragmentation, are increased by treatment with the CHK1i prexasertib in HeLa cells (King et al. 2015), showing that pharmacological inhibition of CHK1 activity phenocopies genetic CHK1 knockdown (Sarmiento et al. 2015). Furthermore, administration of SRA737 in combination with gemcitabine or irinotecan significantly delayed growth of HT-29 xenograft tumours *in vivo* compared to either agent alone (Walton et al. 2016), demonstrating the enhanced therapeutic effect of DNA damaging agents upon inhibition of CHK1 activity. Together, these data demonstrate the on-target cellular activity and efficacy of SRA737 treatment in human cancer.

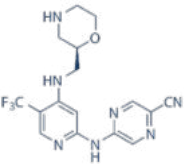
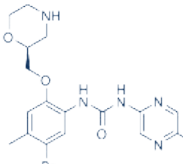
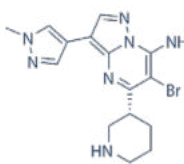
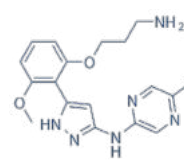
In addition to potentiating the effects of DNA damaging agents, such as gemcitabine and cisplatin (Walton et al. 2016; Barnard et al. 2016), CHK1i have also shown benefit in combination with immunomodulatory drugs. SRA737 treatment in combination with low-dose gemcitabine significantly enhanced the anti-tumour effect of anti-PD-L1 therapy in an *in vivo* model of SCLC (Sen et al. 2019). This was accompanied by a significant increase in the expression of chemotactic cytokines *CXCL10* and *CCL5*, and tumour infiltration of CD8 positive cytotoxic T-cells versus anti-PD-L1 alone. In another study, the CHK1i MK-8776 effectively killed *all-trans* retinoic acid-resistant acute promyelocytic leukaemia cells *in vitro* (Franza et al. 2023), providing evidence that CHK1i can help to overcome resistance to other therapies. Interestingly, this effect was attributed to CHK1i-mediated activation of caspase-1 and subsequent proteasomal degradation of the oncogenic fusion protein PML-RAR α . As the authors failed to robustly confirm CHK1 target engagement, for example by measuring phospho-CHK1 levels, it's possible that this occurred as a result of off-target MK-8776 activity. Regardless, this result provides new insights into potentially novel mechanisms of action of small molecule CHK1i.

Given these results and the observation that CHK1i show single-agent efficacy in cancers with endogenously high levels of DNA damage or dysregulated DDR, such as *MYCN*-amplified neuroblastoma (Cole et al. 2011), SRA737 has been trialled as a monotherapy and in combination with gemcitabine in patients with

genetically predicted sensitivity to CHK1i (NCT02797964 ; NCT02797977). Recent data from a first-in-human human Phase I/II clinical trial showed that treatment with SRA737 in combination with low-dose gemcitabine elicited partial tumour responses in 25% of patients with anogenital cancer, a disease with high un-met clinical need, as well as in those with cervical, ovarian, rectal, and lung cancers (Jones et al. 2023). The use of SRA737 allows for a lower dose of gemcitabine, resulting in reduced incidence of severe toxicities, leading to improved tolerability of the combination compared to standard of care gemcitabine treatment. Altogether, these studies reveal the breadth of potential applications for the use of CHK1i in the clinic.

Table 1-1: *In vitro* biochemical and cellular potency values of CHK1 inhibitors.

[¹] (Osborne et al. 2016); [²] (Walton et al. 2016); [³] (King et al. 2014); [⁴] (Guzi et al. 2011); [⁵] (Montano et al. 2012); [⁶] (King et al. 2015)

Compound	SRA737 (CCT245737)	Rabusertib (LY2603618)	MK-8876 (SCH 900776)	Prexasertib (LY2606368)
Clinical phase	I/II	II	II	II
Structure				
<i>In vitro</i> IC ₅₀ (μM)	0.0013 ^[1]	0.007 ^[3]	0.003 ^[4]	<0.001 ^[6]
Cellular potency				
Cell line	HT29 ^[2]	Calu-6 ^[3]	U2OS ^[5]	HT29 ^[6]
Measure	GI ₅₀ (μM)	pS296 EC ₅₀ (μM)	GI ₅₀ (μM)	GI ₅₀ (μM)
Single-agent	0.70	-	0.55	0.01
Combination	0.09	0.43	-	-
Combo. agent	Gemcitabine	Gemcitabine	-	-

1.9.4. Mechanisms of CHK1 inhibitor resistance

While it's too early to observe mechanisms of resistance in the clinic, pre-clinical evaluation is ongoing to identify CHK1i drug resistance strategies. To date, no mutations to the CHK1 drug binding site have been identified in CHK1i resistant populations generated by dose-escalation (Blosser et al. 2020; Nair et al. 2020; Zhao et al. 2021). In the absence of a “gatekeeper” mutation, studies have

utilised omics technologies to characterise and identify potential mechanisms of CHK1i resistance.

Proteomic analysis showed enrichment of epithelial markers (e.g., E-cadherin and cytokeratin 18) and concomitant depletion of mesenchymal markers (e.g., vimentin) in resistant NCI-H520 cells (squamous lung adenocarcinoma) generated using the CHK1i prexasertib, implicating mesenchymal-epithelial transition (Su et al.) in acquired CHK1i resistance (Blosser et al. 2020). Although NCI-H520 cells are of epithelial origin, only a small proportion stain positive for E-cadherin within bulk populations (Coldren et al. 2006), suggesting that they are heterogenous in nature. As such, it is unclear whether this result reflects true MET or selection of E-cadherin positive cells during drug exposure. Conversely, gene set enrichment analysis (GSEA) revealed upregulation of epithelial-mesenchymal transition (EMT) related genes in prexasertib resistant ovarian and sarcoma cell lines, suggesting that alternative resistance mechanisms may be employed by different cancer types to survive CHK1i exposure.

Genes associated with CHK1 pathway activation were also upregulated in NCI-H520 resistant cells, including *CHEK1*, *WEE1*, and *CDC25A* (Blosser et al. 2020). This is perhaps unsurprising, as overexpression of drug targets and/or components of the target signalling pathway would provide cells with a survival advantage under therapeutic pressure. By contrast, total CHK1 levels were reduced in CHK1i-resistant U2OS cells generated with CCT244747 versus parental controls (Hunter et al. 2022). This was rescued by treatment with the proteasomal inhibitor MG132, suggesting that this reduction is mediated by dysregulated protein degradation. Indeed, further investigation revealed a concomitant downregulation in the expression of ubiquitin-specific peptidase 1 (USP1); a protein deubiquitinase reported to stabilise and protect CHK1 from DNA damage-binding protein 1-dependent degradation during genotoxic stress (Guervilly et al. 2011). Subsequent RNAi-mediated knockdown of USP1 expression in parental U2OS cells reduced total CHK1 protein levels and, accordingly, sensitivity to CCT244747 (Hunter et al. 2022). These results

demonstrate that inhibition of protein stabilising factors to deplete CHK1 is a mechanism by which cells can acquire resistance to small molecule CHK1i.

Downstream CHK1 targets have been implicated in additional models of CHK1i resistance. WEE1 overexpression at the genomic, transcript, and protein level was observed in two prexasertib resistant NSCLC cell lines (Zhao et al. 2021). Subsequent WEE1 inhibition using pharmacological (MK1775) and genomic (RNAi) tools resensitised resistant cells to prexasertib, indicating that increased WEE1 activity is required for CHK1i resistance and providing therapeutic rationale for the combinatorial use of WEE1 and CHK1 inhibitors. In another study, prexasertib resistant *BRCA* wild-type ovarian cancer cell lines demonstrated a sustained cell cycle delay in the G2 phase that was caused by downregulation of cyclin B1 expression and reduced CDK1 activity (Nair et al. 2020). In parental cells, RNAi-mediated gene silencing of cyclin B1 and small molecule inhibition of CDK1 activity promoted resistance to prexasertib. Together, these observations suggest that the primary mechanisms of CHK1i resistance may involve aberrations in the expression and regulation of CHK1 and/or its downstream targets.

While mechanisms of CHK1i resistance continue to be investigated using dose-escalated models, it remains unclear whether the same strategies would emerge via a persister cell bottleneck. In anticipation of CHK1i being approved for clinical use, it is imperative to characterise DTP formation and progression and assess the contribution of DTP-mediated processes to overt drug resistance under this novel therapeutic context.

Chapter 2

Materials and methods

Chapter 2 Materials and methods

2.1. Cell lines and culture

2.1.1. Cell lines

Human NSCLC cell line A549 (CRL-10317) was obtained from the American Type Culture Collection (ATCC) and neuroblastoma cell line SK-N-AS (94092302) from the European Collection of Authenticated Cell Cultures (ECACC). TNBC cell line MDA-MB-231 was kindly provided by Professor S. Linardopoulos (Institute of Cancer Research, UK). All cell lines were authenticated in-house by short tandem repeat (STR) profiling using a *GenePrint*® 10 System (Promega, USA) and confirmed negative for *Mycoplasma* contamination using a Venor®GeM Classic *Mycoplasma* PCR Detection Kit (Minerva Biolabs, Germany) prior to cryostorage in vapour phase liquid nitrogen (see Section 2.1.3). Cell lines were renewed every three months and routinely screened for *Mycoplasma* contamination every 6 - 12 months.

2.1.2. Culture conditions and passage

A549 were maintained in Roswell Park Memorial Institute (RPMI) 1640 medium (Sigma-Aldrich, USA) supplemented with 10% foetal bovine serum (FBS; Gibco, USA). SK-N-AS were maintained in Dulbecco's Modified Eagle Medium (DMEM; Sigma-Aldrich, USA) supplemented with 2 mM L-glutamine (Gibco, USA), 1% non-essential amino acids (Sigma-Aldrich, USA), and 10% FBS. MDA-MB-231 were maintained in DMEM supplemented with 2 mM L-glutamine, 1 mM sodium pyruvate (Sigma-Aldrich, USA), and 10% FBS. All cell lines were incubated at 37 °C in a humidified atmosphere of 5% CO₂ and cultured in Nunc™ tissue-culture flasks or plates (Thermo Fisher Scientific, USA), unless otherwise stated. For passage, cells were washed in phosphate-buffered saline (PBS; Gibco, USA), detached from the tissue culture flask using 0.25% trypsin-ethylenediaminetetraacetic acid (EDTA) solution (Sigma-Aldrich, USA or Gibco, USA), neutralised in medium, and split at an appropriate ratio for each cell line.

2.1.3. Cryopreservation and recovery

Cells grown in T-75 or T-175 tissue culture flasks were detached using trypsin-EDTA and neutralised with addition of medium. Cells were centrifuged for 3 minutes at 450 x g, supernatant aspirated, and pellets resuspended in culture medium supplemented with 50% FBS and 10% dimethyl sulfoxide (DMSO; Sigma-Aldrich, USA). Cell suspensions were aliquoted into Nalgene® Cryo-Tubes (Thermo Fisher Scientific, USA), snap-frozen on dry ice, and stored overnight at -80 °C prior to long-term storage in vapour phase liquid nitrogen. Cells were recovered by incubating cryotubes in a 37 °C water bath until partially thawed, and then thaw completed at room temperature (RT; 21 - 24 °C). Cells were diluted in medium and centrifuged for 5 minutes at 200 x g. Supernatants were aspirated, pellets resuspended in culture medium, and cells transferred to a T-25 or T-75 tissue culture flask containing prewarmed medium.

2.1.4. Population doubling time (PDT)

Cells were seeded in a final volume of 5 mL at 2×10^4 cells/mL into T-25 tissue culture flasks. Cells were detached and counted every 24 - 48 hours for up to 12 days using a Z2 Coulter Particle Count and Size Analyser (Beckman Coulter, USA). PDTs were calculated from log growth phase data using “exponential growth equation” non-linear regression analysis in GraphPad Prism 10.0.

2.2. Compounds and recombinant human proteins

Tazemetostat was kindly gifted by Dr Ben Bellenie (Institute of Cancer Research, UK). All other compounds and human recombinant proteins were sourced, reconstituted, and stored as outlined in Table 2-1. SRA737, BOS-172722, gemcitabine, and paclitaxel were verified by LC-MS after reconstitution by Dr Tatiana McHardy (Institute of Cancer Research, UK). For cell viability (GI_{50}) assay, stock compounds and vehicle controls were loaded into 384-well source plates (Labcyte, USA) in preparation for dispense using an Echo 650 Acoustic Liquid Handler (Labcyte, USA) (see Section 2.3).

Table 2-1: Source, stock, and storage information for compounds and human recombinant proteins.

RT = room temperature (21 - 24 °C); BSA = bovine serum albumin; DMSO = dimethyl sulfoxide; ddH₂O = double-distilled water.

Compound / Protein	Source	Solvent	Stock	Storage
Compounds				
SRA737	Insight Biotechnology, UK	DMSO	10 mM	-80 °C
BOS-172722	Insight Biotechnology, UK	DMSO	10 mM	RT (dark)
Gemcitabine	Insight Biotechnology, UK	DMSO/Saline	1 mM	-80 °C
Paclitaxel	Insight Biotechnology, UK	DMSO	1 mM	-80 °C
AZD1390	Insight Biotechnology, UK	DMSO	10 mM	-80 °C
KU60019	Insight Biotechnology, UK	DMSO	10 mM	-80 °C
AZD6738	Insight Biotechnology, UK	DMSO	10 mM	-80 °C
VE822	Insight Biotechnology, UK	DMSO	10 mM	-80 °C
LY2603618	Insight Biotechnology, UK	DMSO	10 mM	-80 °C
MK8776	Insight Biotechnology, UK	DMSO	10 mM	-80 °C
AZD7762	Insight Biotechnology, UK	DMSO	10 mM	-80 °C
AZD1775	Insight Biotechnology, UK	DMSO	10 mM	-80 °C
Tazemetostat	ICR, UK	DMSO	10 mM	-80 °C
SD-36	Aaron Chemicals, USA	DMSO	10 mM	-80 °C
Tofacitinib	Insight Biotechnology, UK	DMSO	10 mM	-80 °C
Ruxolitinib	Insight Biotechnology, UK	DMSO	10 mM	-80 °C
BMS-911543	Insight Biotechnology, UK	DMSO	10 mM	-80 °C
Palbociclib	Insight Biotechnology, UK	DMSO	10 mM	-80 °C
Etoposide	Sigma-Aldrich, USA	DMSO	1 mM	-80 °C
Puromycin	Sigma-Aldrich, USA	ddH ₂ O	1 mM	-20 °C
Recombinant human proteins				
rh-IL-2	Bio-Techne, USA	100 mM acetic acid + 0.1% BSA	100 µg/mL	-80 °C
rh-IL-6	Bio-Techne, USA	PBS + 0.1% BSA	200 ng/mL	-80 °C
rh-INFγ	Bio-Techne, USA	ddH ₂ O	200 ng/mL	-80 °C

2.3. Cell viability assay for compound GI₅₀ determination

2.3.1. CellTiter-Glo® assay

Briefly, CellTiter-Glo® reagent (Promega, USA) and experimental tissue culture plates were brought to room temperature. CellTiter-Glo® reagent was added 50 µL/well (96-well plates) or 20 µL/well (384-well plates) and plates mixed vigorously for three minutes using a plate shaker. Plates were incubated at RT for 10 minutes and luminescence read using an Envision Multilabel Plate Reader (Perkin Elmer, USA).

2.3.2. Seeding density optimisation

Optimal seeding density and assay end-point were determined for each cell line. Cells were seeded at a range of densities into solid white 96-well or 384-well plates (Corning, USA) in a final volume of 100 µL or 40 µL culture medium, respectively. Luminescence was measured by CellTiter-Glo® assay every 24 hours for a total of 6 days. Optimal seeding density was determined from the linear part of the curve before signal plateau. Increases in luminescence signal were used to calculate the number of expected population doublings for use as an additional control to monitor changes in proliferation rate that can affect GI₅₀ determination (Table 2-2).

Table 2-2: Optimal conditions for cell viability (GI₅₀) assay.

Cell line	Seeding density (cells/well)		End-point (h)	Minimum doublings
	96-well	384-well		
A549	750	N/A	96	3.7
SK-N-AS	1500	800	120	2.2
MDA-MB-231	1500	N/A	120	2.2

2.3.3. Compound GI₅₀ determination

96-well tissue culture plates

Cells were seeded at the optimal density into solid white 96-well plates in a final volume of 100 μ L culture medium and incubated for 24 - 36 hours. BOS-172722, paclitaxel, gemcitabine, and vehicle controls were prepared using an Echo 650 Acoustic Liquid Handler (Labcyte, USA). Stock solutions were dispensed from 384-well source plates (Labcyte, USA) into 96-well U-bottom destination plates (Greiner, Austria), and diluted in vehicle to nine points at 11X final concentration. Dispensed compounds were mixed in 100 μ L culture medium and added 10 μ L/well to assay plates. SRA737 and appropriate vehicle controls were similarly prepared by manual serial dilution of stock compound in vehicle supplemented culture medium and added 10 μ L/well to assay plates. All compound treatments were performed in duplicates at a minimum and vehicle concentration was consistent across the dose range. Plates were gently mixed and incubated at 37 °C, 5% CO₂ for the appropriate time before cell viability was measured by CellTiter-Glo® assay (see Section 2.3.1). A replicate plate was assayed at time zero (T₀). End-point cell viability was calculated relative to the T₀ or vehicle treated control as follows:

$$\% T_0 = \left(\frac{T_{\text{End}}}{T_0} \right) \times 100 \text{ or } \% \text{ Vehicle} = \left(\frac{T_{\text{End}} - T_0}{V_{\text{End}} - T_0} \right) \times 100$$

where T₀ = luminescence at time of treatment, T_{End} = luminescence from compound treated wells at assay end-point, and V_{End} = luminescence from vehicle treated wells at assay end-point. GI₅₀ values were determined using four parameter non-linear regression analysis in GraphPad Prism 10.0. Constraints were applied if appropriate. Both methods of cell viability analysis produce comparable GI₅₀ values.

384-well tissue culture plates

Cells were seeded at the optimal density into solid white 384-well plates in a final volume of 40 μ L culture medium and incubated for 24 - 36 hours. Compounds and vehicle controls were dispensed onto cells using an Echo 650 Acoustic Liquid

Handler (Labcyte, USA) to a 10-point dose-response. All compound treatments were performed in duplicates at a minimum and vehicle concentration was consistent across the dose range. Plates were centrifuged for 1 minute at 200 x g and incubated at 37 °C, 5% CO₂ for 120 hours. Cell viability was measured using the CellTiter-Glo® assay (see Section 2.3.1) and GI₅₀ values determined as previously described (see Section 2.3.3).

GI₅₀ values were used to calculate 100X GI₅₀ compound doses for drug-tolerant persister cell experiments and as a measure of drug sensitivity.

2.4. Acute and long-term lethal drug exposure

2.4.1. 15-day time course

A549, SK-N-AS, or MDA-MB-231 cells were seeded into 6-well tissue culture plates and incubated for 48 hours prior to treatment with the relevant compounds at 100X GI₅₀, or an equivalent concentration of DMSO vehicle as control (Table 2-3). Compound or vehicle supplemented culture medium was renewed every 4 - 5 days and vehicle treated cells were passaged and diluted back to seeding density every 5 days. Cells were counted using a Z2 Coulter Particle Count and Size Analyser (Beckman Coulter, USA) at T₀ and every 24 hours thereafter for a total of 15 days. A replicate plate was loaded onto an IncuCyte® S3 (Sartorius, Germany) and 16 fields of view per well imaged every 12 hours by phase contrast microscopy at 10X magnification. At each time point the surviving proportion was calculated relative to the T₀ using the % T₀ formula in Section 2.3.3. Responses between compound treatments were tested for statistical difference by linear regression using GraphPad Prism 10.0.

Table 2-3: Conditions for 15- and 50-day persister cell time course experiments.

Cell line	Seeding density (cells/well)	Compound	Drug-release (day)
A549	50,000	Gemcitabine	8
SK-N-AS	100,000	SRA737	7
		Gemcitabine	
MDA-MB-231	100,000	BOS-172722	10
		Paclitaxel	

2.4.2. 50-day time course

A549, SK-N-AS, or MDA-MB-231 cells were seeded into 6-well tissue culture plates and treated with compounds as described above (see Section 2.4.1). After 7- (SK-N-AS), 8- (A549), or 10- (MDA-MB-231) days drug exposure, cells were PBS washed and further cultured in compound or vehicle (drug-release) supplemented medium for up to 50 days (Table 2-3). Control cells were cultured and passaged in parallel, and compound supplemented medium was renewed as previously described (see Section 2.4.1). Phase contrast microscopy images from 16 fields/well were captured at 10X magnification every 4 - 5 days using an Incucyte® S3 until end-point.

2.5. Drug-tolerant persister (DTP) and expanded persister (DTEP) cells

2.5.1. Generation

To generate DTPs, SK-N-AS cells were treated with 10 μ M SRA737 (100X GI₅₀) for a total of 7 days, with compound supplemented medium renewed at day 5. After 7 days, DTPs were PBS washed and further cultured for up to 50 days in the presence or absence of SRA737 to generate DTEP or drug-released populations, respectively. Cells exposed to an equivalent DMSO concentration were cultured in parallel as a control and passaged back to seeding density as required. At least three DTP, DTEP, or drug-released populations were

independently generated for RNA sequencing. DTP, DTEP, and drug-released populations were verified by STR profiling and confirmed negative for *Mycoplasma* contamination prior to cryostorage in vapour phase liquid nitrogen.

2.5.2. mKate2-SK-N-AS stable cell line

SK-N-AS cells were seeded in a final volume of 1 mL/well at 9×10^4 cells/mL into a 24-well tissue culture plate (Corning, USA) and incubated for 24 hours. Cells were transduced at a multiplicity of infection of 3 with the Incucyte® Nuclight Red Lentivirus (Sartorius, Germany) reagent diluted in culture medium supplemented with 5 µg/mL Polybrene (Merck, Germany) for 24 hours. The Nuclight Red Lentiviral construct drives expression of a nuclear-restricted mKate2 red fluorescent protein under the control of an EF-1α promoter and harbours a puromycin resistance gene. Transduced cells were therefore propagated under selection with puromycin supplemented culture medium (1 µg/mL; Sigma-Aldrich, USA) and nuclear mKate2 expression confirmed by red fluorescence microscopy using an Incucyte® S3. Population doubling time and SRA737-induced DTP formation were validated against parental SK-N-AS cells prior to experimental use. mKate2-SK-N-AS cells were only maintained in puromycin supplemented medium during routine culture; this was removed for experimental use.

2.5.3. DTP quantification

SK-N-AS cells were seeded in a final volume of 5 mL or 15 mL at 2×10^5 cells/mL into T-25 or T-75 tissue culture flasks, respectively, and incubated for 48 hours prior to DTP generation with SRA737, or treatment with DMSO as control (see section 2.5.1). Cells were counted using a Z2 Coulter Particle Count and Size Analyser at T_0 and day 7. Counts from control treated flasks were multiplied by the day 5 split ratio to calculate total cell number. Day 7 counts were calculated relative to the T_0 using the % T_0 formula in Section 2.3.3. Means from three independent experiments were tested for statistical difference by ordinary one-way ANOVA with Šídák's or Tukey's correction, as indicated, using GraphPad Prism 10.0.

2.5.4. DTP-to-DTEP transition

mKate2-SK-N-AS cells were seeded in a final volume of 1 mL/well at 8.4×10^4 cells/mL into a 24-well tissue culture plate (Corning, USA) and incubated for 48 hours. Prior to compound treatment, plates were imaged by whole-well red fluorescence and phase contrast microscopy at 4X magnification using an Incucyte® SX5 (Sartorius, Germany). Cells were treated with SRA737 to induce DTP formation, or vehicle as control as previously described (see Section 2.5.1). After 7 days, plates were imaged, and DTPs washed in PBS prior to further culture in the presence (DTEP) or absence (drug-release) of compound for up to 50 days. All treatments were performed in duplicate. Compound and vehicle supplemented medium was renewed and vehicle treated cells were passaged and split back to seeding density every 7 days. Whole-well imaging was performed every 7 days until end point. Whole-well cell counts were obtained by Top-Hat segmentation of red fluorescent nuclei using Incucyte software (v2022A) and plotted for each time point. Counts from control treated wells were cumulatively multiplied by split ratios to calculate total cell number. Mean total cell counts at experimental end point from $n \geq 2$ independent experiments were tested for statistical difference by unpaired two-tailed Student's t-test, or ordinary one-way ANOVA with Šídák's correction, as indicated, using GraphPad Prism 10.0. Duplicate samples seeded into T-25 tissue culture flasks were collected for Western blot analysis (see Section 2.10).

2.6. Dose-escalation

Drug-resistant SK-N-AS populations were generated by exposure to increasing SRA737 concentrations over a period of approximately 3 months. SRA737 was increased in 2-fold increments once cells had reached unconstrained proliferation. Thereafter, cells were routinely maintained in 10 μ M SRA737 and resistance confirmed by cell viability (GI_{50}) assay (see Section 2.3). Cells exposed to equivalent DMSO concentrations were cultured in parallel as a control. A total of four pooled dose-escalated populations were independently generated for RNA sequencing. Dose-escalated cells were verified by STR

profiling and confirmed negative for *Mycoplasma* contamination prior to cryostorage in vapour phase liquid nitrogen.

2.7. Dilutive proliferation assay

SK-N-AS cells were seeded in a final volume of 15 mL at 2×10^5 cells/mL into T-75 tissue culture flasks and incubated for 48 hours. Prior to DTP generation with SRA737, cells were stained with 2.5 μ M ViaFluor® 405 SE Cell Proliferation Dye (Biotium, USA) diluted in prewarmed PBS for 15 minutes at 37 °C, 5% CO₂. Dye solution was removed, and cells washed in line with the manufacturer's instructions. DTPs were generated as previously described (see Section 2.5.1) and vehicle treated cells passaged as required. At day 7, cells were collected and resuspended at 0.25 - 1×10^6 cells/mL in PBS, and blue fluorescence signal intensity measured at Ex₄₀₅/Em₄₅₅ nm using a BD LSR II Flow Cytometer (BD Biosciences, USA). A replicate flask was collected and analysed immediately after staining (T₀). Sphero™ Ultra Rainbow standard beads (Spherotech, USA) were run at each time point to control for instrument variability. Mean signal intensity from 10,000 events was determined using BD FACSDiva™ software (BD Biosciences, USA). Means from three independent experiments were tested for statistical difference by ordinary one-way ANOVA with Tukey's correction using GraphPad Prism 10.0.

2.8. β -galactosidase activity assay

Day 7 DTPs and control cells were collected for β -galactosidase activity assay using the CellEvent™ Senescence Green Flow Cytometry Assay kit (Invitrogen, USA) in line with manufacturer's instructions. Briefly, 5×10^5 cells were fixed in 2% paraformaldehyde (Thermo Fisher Scientific, USA) diluted in PBS and then incubated in working solution (Green Probe diluted 1:1000 in Senescence Buffer) for 90 minutes at 37 °C in the absence of CO₂. Cells were washed and pellets resuspended in 500 μ L 1% bovine serum albumin (BSA; Sigma-Aldrich, USA) diluted in PBS. Green fluorescence was measured at Ex₄₉₀/Em₅₂₀ nm using a BD LSR II Flow Cytometer. Cells with a signal intensity $\geq 2 \times 10^4$ relative fluorescence

units, representing >2-fold increase compared to DMSO treated control, were classified as β -galactosidase positive (senescent) and calculated as a percentage of 10,000 total events using BD FACSDiva™ software. Means from three independent experiments were tested for statistical difference by ordinary one-way ANOVA with Dunnett's or Tukey's correction, as indicated, using GraphPad Prism 10.0.

2.9. Apoptosis and Cytotoxicity assay

Apoptosis (caspase 3/7 activity) and cytotoxicity (dead cell protease activity) were measured using the ApoTox-Glo® Triplex assay (Promega, USA). Cells for DTP generation were seeded at high density (1.25×10^4 cells/well) and those for control treatment at low density (1.5×10^3 cells/well) in a final volume of 100 μ L in solid white 96-well plates and incubated for 48 hours. All treatments were performed in triplicate. After 7 days compound or control treatment, plates were assayed in line with the manufacturer's instructions. Briefly, 20 μ L/well Viability/Cytotoxicity Reagent was added to wells, plates mixed and incubated at 37 °C, 5% CO₂ for 90 minutes. Fluorescence intensity was read at two sets of wavelengths to measure cell viability (Ex₄₀₀/Em₅₀₅) and cytotoxicity (Ex₄₈₅/Em₅₂₀) using the PHERAstar FSX Microplate Reader (BMG Labtech, Germany). Caspase-Glo® 3/7 Reagent was then added 100 μ L/well, plates mixed and incubated at RT for 30 minutes. Luminescence was read using a PHERAstar FSX Microplate Reader. Cytotoxicity and apoptosis values were normalised to cell viability and then calculated relative to DMSO treated control. Means from three independent experiments were tested for statistical difference by ordinary one-way ANOVA with Dunnett's or Tukey's correction, as indicated, using GraphPad Prism 10.0.

2.10. Cell lysis and Western blotting

2.10.1. Cell lysis

Plated cells were PBS washed and frozen at -80 °C for a minimum of 24 hours. Lysis buffer was added directly to wells and cells scraped for efficient detachment. Total cell lysates were prepared using either NP-40 or RIPA lysis buffer supplemented with protease (Sigma-Aldrich, USA) and/or phosphatase inhibitors (Thermo Fisher Scientific, USA) (Table 2-4). All lysates were stored at -80 °C and kept at 4 °C during handling.

NP-40 lysates were centrifuged at 4 °C for 10 minutes at 20,000 x g for clarification and protein concentration determined by Bradford assay (see Section 2.10.2). RIPA lysates were sonicated for 10 seconds using an MSE Soniprep 150 followed by 10 minutes incubation on ice and protein concentration determined by bicinchoninic acid (BCA) assay (see Section 2.10.2).

For histone modifications (excluding γ H2AX), 2.5×10^5 total cells were PBS washed, pelleted, and lysed directly in 50 μ L 3X Laemmli sample buffer (200 mM tris-base pH 6.8, 30% glycerol, 8% sodium dodecyl sulphate (SDS), 4% β -mercaptoethanol, and 0.03% bromophenol blue).

Table 2-4: Formulation of NP-40 and RIPA cell lysis buffers.

	NP-40	RIPA
Formulation	250 mM sodium chloride 50 mM HEPES, pH 7.4 0.1% NP-40 substitute 10 mM β -glycerophosphate 1 mM sodium fluoride 1 mM dithiothreitol 0.1 mM sodium orthovanadate	140 mM sodium chloride 10 mM tris-HCl, pH 8.0 0.1% SDS 0.1% sodium deoxycholate 1% Triton X-100
Additive	cOmplete™ mini EDTA-free protease inhibitor 1 tablet per 10 mL	100X Halt™ protease and phosphatase inhibitor cocktail 100 μ L in 10 mL

2.10.2. Protein quantification

Bradford assay

NP-40 lysates were diluted 1:10 - 1:20 in double-distilled water (ddH₂O) and 5 µL added to 200 µL Bradford reagent (Bio-Rad, USA) in a clear 96-well plate. BSA diluted in ddH₂O (0.1 - 2.0 mg/mL) were used as protein standards. All samples were tested in duplicate. Plates were mixed and incubated at RT for 10 minutes. Absorbance was read at 590 nm using a Wallac Victor X4 Multilabel Plate Reader (PerkinElmer, USA), and protein concentrations determined from a standard curve generated using protein standards.

BCA assay

RIPA lysates and protein standards were prepared as described above (see *Bradford assay*) and 10 µL added to 200 µL working BCA reagent (Thermo Fisher Scientific, USA; copper (II) sulphate mixed with BCA 1:50) in a clear 96-well plate. All samples were tested in duplicate. Plates were mixed and incubated at 37 °C for 30 minutes. Absorbance was read at 570 nm using a Wallac Victor X4 Multilabel Plate Reader and protein concentrations determined as previously described (see *Bradford assay*).

2.10.3. Western blotting

Protein lysates were diluted to equal concentration and mixed with 3X Laemmli sample buffer. Lysates were heat denatured at 95 °C for 5 minutes, and 20 - 25 µg separated on Novex™ WedgeWell™ 10% Tris-Glycine gels (Thermo Fisher Scientific, USA) using 1X Tris-Glycine SDS running buffer (Thermo Fisher Scientific, USA) at 150 V for approximately 65 - 80 minutes. SeeBlue™ Plus2 Pre-Stained Protein Standard (Invitrogen, USA) was used as a molecular weight marker. Proteins were transferred onto methanol-activated Immobilon-P polyvinylidene fluoride (PVDF) membranes (Merck, Germany) using 1X Tris-Glycine transfer buffer (Thermo Fisher Scientific, USA) supplemented with 20% methanol (Thermo Fisher Scientific, USA) at 120 V for 90 minutes.

For γ H2AX, the above procedure was applied with the following amendments: 8 - 12 μ g total protein was separated on NuPAGE™ 4 - 12% Bis-Tris gels (Invitrogen, USA) using 1X NuPAGE™ MOPS SDS running buffer (Invitrogen, USA). Proteins were transferred using 1X NuPAGE™ transfer buffer (Invitrogen, USA) supplemented with 20% methanol.

For other histone modifications, the same procedure was applied with the following amendments: 4 - 7 μ L lysate were separated on NuPAGE™ 4 - 12% Bis-Tris gels using 1X NuPAGE™ MOPS SDS running buffer. Proteins were transferred onto methanol-activated Immobilon-FL PVDF membranes (Merck, Germany) using 1X NuPAGE™ transfer buffer supplemented with 20% methanol.

2.10.4. Detection

After transfer, membranes were air dried for 1 hour at RT, reactivated in methanol, and washed in TBS-T (50 mM Tris pH 8.0, 150 mM sodium chloride, 0.1% Tween-20) for 5 minutes. Membranes were incubated in blocking buffer (5% BSA in TBS-T) for 1 hour at RT prior to incubation with primary antibodies overnight at 4 °C (Table 2-5). Membranes were washed four times in TBS-T for 6 minutes and then incubated with HRP- (Bio-Rad, USA) or IRDye- (LI-COR Biosciences, USA) conjugated secondary antibodies for 1 - 2 hours at RT (Table 2-5). Membranes were washed four times in TBS-T for 6 minutes. HRP-conjugated secondary antibodies were detected after membrane incubation in Pierce™ ECL Western Blotting Substrate, SuperSignal™ West Pico PLUS Chemiluminescent Substrate, or SuperSignal™ West Femto Maximum Sensitivity chemiluminescent substrates (Thermo Fisher Scientific, USA) for 3 minutes at RT in the dark. Bound proteins were visualised using the chemiluminescent channel on a LI-COR Odyssey FX Imager (LI-COR Biosciences, USA) for 5 minutes. IRDye-conjugated secondary antibodies were detected by near infrared fluorescence (NIR) using the 700 or 800 channel for 3 minutes.

2.10.5. Quantification

Protein bands were quantified using Image Studio Lite software (v 5.2; LI-COR Biosciences, USA). Signal intensities were normalised to loading control (vinculin or histone H3) and then calculated relative to the indicated control sample. Phosphorylated proteins were similarly normalised, expressed as a ratio over equivalent unphosphorylated (total) protein, and then calculated relative to the indicated control sample.

Table 2-5: Primary and secondary antibodies used for Western blotting.

Antibody	Species	Dilution	Supplier	Product #
Primary antibodies				
Vinculin	Mouse	1:10,000	Sigma	V9264
Wee1	Rabbit	1:1000	CST	4936
Cleaved PARP	Rabbit	1:1000	CST	9541
pS296-Chk1	Rabbit	1:1000	CST	90178
Total Chk1	Mouse	1:1000	CST	2360
pY15-CDK1	Rabbit	1:1000	CST	4539
Total CDK1	Mouse	1:1000	CST	9116
H3K27ac	Rabbit	1:1000	CST	8173
H3K27me3	Rabbit	1:1000	CST	9733
H3K27me2	Rabbit	1:1000	CST	9728
H3K27me1	Rabbit	1:1000	CST	84932
H3K18ac	Rabbit	1:1000	CST	9675
H3K9me3	Rabbit	1:1000	Abcam	ab8898
H3K4me3	Rabbit	1:1000	Diagenode	C15410003
Histone H3	Mouse	1:1000	Active Motif	39763
pS319-H2AX (γ H2AX)	Rabbit	1:2000	Abcam	ab11174
pY701-STAT1	Rabbit	1:1000	CST	7649
STAT1	Rabbit	1:1000	CST	9172
pY705-STAT3	Rabbit	1:1000	CST	9145
STAT3	Rabbit	1:1000	CST	12640
pY694-STAT5	Rabbit	1:1000	CST	4322
STAT5	Rabbit	1:1000	CST	94205
Secondary antibodies				
Anti-rabbit IRDye-680RD	Goat	1:5000	LI-COR Biosciences	926-68071
Anti-mouse IRDye-800CW	Goat	1:5000	LI-COR Biosciences	926-32210
Anti-rabbit HRP	Goat	1:10,000	Bio-Rad	170-6515
Anti-mouse HRP	Goat	1:10,000	Bio-Rad	170-6516

2.11. RNA sequencing

2.11.1. RNA extraction and sequencing

Total RNA was extracted from $0.5 - 2 \times 10^6$ cells using the MagNA Pure 96 Cellular RNA Large Volume Kit and MagNA Pure 96 automated instrument (Roche, Switzerland). RNA was quantified and quality control checked for purity (absorbance 260/280 ~ 2.0 , absorbance 260/230 2.0 - 2.2) using a NanoPhotometer (Implen, Germany). RNA sequencing was performed at Beijing Genomics Institute Inc. (BGI Inc.), Denmark or Hong Kong. Briefly, enriched mRNA was ligated into RNA adaptors to prepare a DNBSEQ™ Eukaryotic mRNA library for sequencing using the DNBSEQ™ Next-Generation Sequencing platform (BGI Inc.). Raw FastQ data were filtered to remove adaptor sequences and low-quality reads using SOAPnuke software (BGI Inc.).

All RNAseq analysis was performed by Qiong Gao with guidance from Dr Konstantinos Mitsopoulos (both Institute of Cancer Research, UK).

2.11.2. Alignment and gene read count

RNAseq paired-end reads (read length 100 base pairs) were aligned to the human GRCh38 reference genome and read counts for each gene were calculated with STAR Aligner (star2.7.6a) (Dobin et al. 2013).

2.11.3. Differential expression and pathway enrichment analysis

The gene read counts were normalized using trimmed mean of M values (TMM) (Robinson and Oshlack 2010) in EdgeR (Robinson, McCarthy, and Smyth 2010). Normalized TMM counts were profiled for differential gene expression using EdgeR's Quasi-likelihood ratio (glmQLFit). Statistically significant differentially expressed genes were selected using an absolute fold change ≥ 2 and false discovery rate (FDR) $< 5\%$, and further filtered to exclude genes in poorly annotated genomic regions, or whose expression was affected by time. The resulting gene lists were functionally annotated using enrichR (Chen et al. 2013;

Kuleshov et al. 2016; Xie et al. 2021) to identify altered pathways due to the corresponding treatments. The pathway enrichment was performed using the following data sources i) the “Hallmark”, “KEGG”, or “GO: Biological Process” gene set databases from MSigDB (Subramanian et al. 2005; Liberzon et al. 2015), and ii) transcription factor databases from ENCODE (ENCODE 2012) and CHEA (Lachmann et al. 2010). For individual pathways, the Benjamini–Hochberg procedure was used to calculate FDR and to adjust for multiple testing. Furthermore, the pathway enrichment was performed with and without proliferation associated genes (Gao et al. 2014) to help identify non-proliferative processes.

RNAseq data from persister and dose-escalated populations could not be directly compared due to batch effects between sequencing runs. Hence, data were interrogated for similarities or differences using comparative plots of Log₂FC in gene expression from DTEP and ESC-10μM populations and Venn diagrams of significantly enriched pathways. Proportional Venn diagrams were constructed using BioVenn (Hulsen, de Vlieg, and Alkema 2008).

2.11.4. Gene signature scores

RNAseq data were interrogated for expression of published gene signatures related to senescence (Fridman and Tainsky 2008), diapause (Rehman et al. 2021), and neural stem cell quiescence (Llorens-Bobadilla et al. 2015). For each sample, a gene signature (GS) score was calculated as a weighted mean of all genes in a signature. This was based on the normalised expression of the gene in the test sample and assignment of a gene-specific weight (1 or -1 according to the direction of their association with the phenotype in the original publication). Means from ≥3 independent experiments were tested for statistical difference by ordinary one-way ANOVA with Šídák’s correction using GraphPad Prism 10.0.

2.12. Colony forming assay

Cells were seeded at low density ($6 - 12 \times 10^3$ cells/well) in a final volume of 2 mLs/well into 6-well tissue culture plates, incubated for 48 hours, and treated with the indicated concentrations of compound or DMSO as vehicle control. DMSO concentration was consistent across the dose range. Compound and vehicle were renewed every 5 days until day 13, when cells were PBS washed and fixed in 10% trichloroacetic acid (Thermo Fisher Scientific, USA) overnight at RT. Colonies were stained with 0.4% sulforhodamine B (Sigma-Aldrich, UK) diluted in 1% acetic acid (Thermo Fisher Scientific, USA) for 90 minutes at RT and visualised using a UV transilluminator following several washes in 1% acetic acid. Duplicate samples were collected for histone Western blot analysis (see Section 2.10).

2.13. Cytokine array

Cytokine secretion in cell supernatants was measured using the Proteome Profiler™ Human Cytokine Array (Bio-Techne, USA). Cell supernatants were collected from DTP and control cells at days 5 and 7. Supernatants were centrifuged at 4 °C for 3 minutes at 450 x g to remove particulates, snap-frozen on dry ice and stored at -80 °C. For analysis, supernatants were thawed on ice and day 5 and 7 samples thoroughly mixed together. The array procedure was performed in line with the manufacturer's instructions. Briefly, 15 µL of reconstituted Human Cytokine Array Detection Antibody Cocktail was added to 700 µL of supernatant from each sample, mixed, and incubated at RT for 1 hour. Sample/antibody mixtures were then incubated with pre-blocked array membranes overnight at 4 °C. Membranes were washed three times for 10 minutes and then incubated with IRDye 800 CW Streptavidin (LI-COR Biosciences, USA) solution (diluted 1:2000 in Array Buffer) at RT for 30 minutes. After further washing, bound proteins were detected by NIR fluorescence using the 800 channel on a LI-COR Odyssey DLx Imager (LI-COR Biosciences, USA). Signal intensities were measured from duplicate capture antibody spots using

Empiria Studio software (v 2.3; LI-COR Biosciences, USA), and calculated relative to DMSO treated control.

Chapter 3

Drug-tolerant persister cells arise following lethal exposure to a targeted CHK1 inhibitor

Chapter 3 Drug-tolerant persister cells arise following lethal exposure to a targeted CHK1 inhibitor

3.1. Introduction

DTPs were first characterised in an *in vitro* model of NSCLC following lethal exposure to small molecule EGFR inhibitors (Sharma et al. 2010) and have since been identified in several cancer cell lines and patient-derived xenografts in response to both targeted and cytotoxic therapeutics (Liau et al. 2017; Al Emran et al. 2018; Rehman et al. 2021; Dhimolea et al. 2021), suggesting that they represent a common tumour response to drug challenge. In the absence of mutational resistance, DTPs are regulated and characterised by global epigenetic changes that alter their transcriptional profiles. In particular, persister cell populations are enriched for epigenetic modifications associated with heterochromatin formation, such as trimethylated histone H3 lysine 9 (H3K9_{me3}) and lysine 27 (H3K27_{me3}), and simultaneously depleted in permissive chromatin modifications, such as H3 lysine 18 acetylation (H3K18_{ac}) (Liau et al. 2017; Guler et al. 2017). However, with prolonged drug exposure DTPs can acquire *de novo* resistance mutations (Hata et al. 2016; Ramirez et al. 2016; Isozaki et al. 2023). As a potentially reversible pre-cursor to genetic resistance, targeting DTPs represents an attractive strategy to mitigate the evolution of drug-resistance in cancer.

While therapeutic contexts are expanding, to date much of the data comes from studies using tyrosine kinase inhibitors (TKi) that abrogate oncogenic signalling. As such, it is unclear if this persister phenotype is also observed in response to drugs that act by alternative anti-tumour mechanisms, for example those targeting monopolar spindle 1 kinase (MPS1) or checkpoint kinase 1 (CHK1) that directly interfere with DNA integrity. The Institute of Cancer Research (ICR) and others have developed small molecule inhibitors of MPS1 (MPS1i) and CHK1 (CHK1i) that are currently under investigation in clinical trials (Table 3-1).

BOS-172722 is small molecule inhibitor of MPS1 (Anderhub et al. 2019), a dual-specificity protein kinase required for correct chromosomal alignment and segregation as part of the mitotic spindle assembly checkpoint (SAC) (Abrieu et al. 2001; Maciejowski et al. 2010; Dou et al. 2015). Preclinical studies identified MPS1i sensitivity in cancer cells characterised by inadequate SAC regulation, chromosomal instability, and aneuploidy, such as triple-negative breast cancer (TNBC). In this cellular context, MPS1i also potentiates the effects of microtubule polymerising agents (Tannous et al. 2013; Maia et al. 2015; Anderhub et al. 2019). As such, BOS-172722 is being tested alone and in combination with paclitaxel in TNBC patients (NCT03328494).

SRA737 is a potent small molecule inhibitor of CHK1 (Walton et al. 2016); a serine/threonine protein kinase that co-ordinates cell cycle and DNA damage repair (DDR) checkpoints in response to genotoxic stress (reviewed in (Zhang and Hunter 2014)). Preclinical studies revealed that CHK1i demonstrated greatest efficacy in combination with DNA damaging agents (Walton et al. 2016) and in cancers with endogenously high levels of DNA damage or dysregulated DDR, such as *MYCN*-amplified neuroblastoma (Cole et al. 2011). Accordingly, SRA737 is being trialled as a monotherapy and in combination with gemcitabine in patients with genetically predicted sensitivity to CHK1i (NCT02797964 ; NCT02797977).

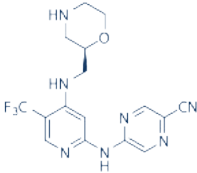
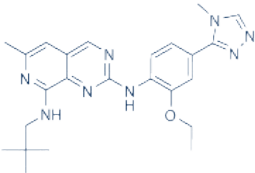
In anticipation of the approval of these agents for clinical use, I reasoned that it is imperative to characterise DTP formation and progression, and to assess the contribution of DTP-mediated processes to overt drug resistance under these new therapeutic contexts.

To maximise the clinical relevance of these experiments, I investigated DTP responses to targeted MPS1 or CHK1 inhibitors within cell line models that reflect the therapeutic context of pre-clinical investigations and on-going current clinical trials. Cell lines were also selected based on single-agent MPS1i or CHK1i sensitivity to minimise overt cytotoxicity caused by excessively high drug concentrations. In addition, I sought to determine whether DTPs also arose in

response to the general chemotherapies being clinically evaluated for use in combination with these targeted agents. In line with these requirements, the CHK1 inhibitor clinical candidate SRA737 and gemcitabine were tested in A549 (NSCLC) and SK-N-AS (neuroblastoma) cell lines, and MPS1 inhibitor BOS-172722 and paclitaxel in TNBC cell line MDA-MB-231.

Table 3-1: *In vitro* biochemical and cellular potency values of CHK1 and MPS1 inhibitors in on-going clinical trial.

^[1] (Osborne et al. 2016); ^[2] (Walton et al. 2016); ^[3] (Woodward et al. 2018); ^[4] (Anderhub et al. 2019)

Target	CHK1	MPS1
Compound	SRA737	BOS-172722
Clinical phase	I/II	I
Structure		
<i>In vitro</i> IC ₅₀ (μM)	0.0013 ^[1]	0.011 ^[3]
Cellular GI ₅₀ (μM)		
<i>Cell line</i>	HT29 ^[2]	MDA-MB-231 ^[4]
<i>Single-agent</i>	0.70	0.094
<i>Combination</i>	0.09 (gemcitabine)	0.035 (paclitaxel)

3.2. Identification of a persister cell model

3.2.1. Determining lethal compound concentrations for persister cell studies

DTP cell populations are commonly generated *in vitro* by exposing tumour cells to compound concentrations ~100-fold the GI_{50} value. To determine GI_{50} values for compounds used in the present study, a cell proliferation assay using CellTiter-Glo® as readout of cell viability was optimised for MDA-MB-231, SK-N-AS, and A549 cells. GI_{50} values were calculated for each compound in the appropriate cell line using non-linear regression analysis of concentration-response data normalised to the number of cells present at the time of treatment (T_0). As well as being useful for calculating the total number of population doublings, cytostatic and cytotoxic drug responses can be differentiated by identifying data points above or below T_0 , respectively; parameters that are often neglected by normalisation to a vehicle control.

Measured GI_{50} values ranged from low micromolar to low nanomolar concentration and agreed with published observations, where available (Table 3-1 & 3-2). Paclitaxel was more potent than BOS-172722 in MDA-MB-231 cells (Figure 3-1A & Table 3-2). Similarly, gemcitabine showed greater potency than SRA737 in both SK-N-AS and A549 cells (Figure 3-1B, 3-1C & Table 3-2) demonstrating a general trend for increased sensitivity to general chemotherapies over targeted agents in these cell lines. SK-N-AS and A549 cells showed comparable sensitivity to gemcitabine (GI_{50} 3 nM & 6 nM, respectively) but differed considerably in sensitivity to SRA737, with SK-N-AS cells being ~20X more sensitive than A549 cells (Table 3-2). This could be attributed to differences in endogenous levels of DNA damage or replication stress, since high levels confer collateral sensitivity to inhibitors of these pathways.

GI_{50} values were used to derive lethal concentrations (~100X GI_{50}) for DTP studies (Table 3-2). In SK-N-AS cells the 100X GI_{50} dose for gemcitabine is situated on the portion of the dose-response curve that falls below T_0 , indicating that such a concentration will induce a cytotoxic response (Figure 3-1A). For

SRA737, this dose falls just above the T_0 , suggesting that this treatment will elicit a cytostatic effect. In A549 cells the dose-response curve indicates that a 100X GI_{50} dose of gemcitabine will have a cytostatic effect as it remains above T_0 (Figure 3-1C). The expected effects of lethal BOS-172722 treatment in MDA-MB-231 cells and SRA737 in A549 cells is uncertain, as the highest doses tested are below the calculated 100X GI_{50} value for these compounds. Interestingly, the 100X GI_{50} doses for any compound failed to reduce cell viability to 0% of the T_0 indicating the presence of a subpopulation of surviving cells at assay endpoint. This is particularly striking in the case of paclitaxel that has low nanomolar potency in MDA-MB-231 cells, and yet fails to completely kill the starting cell population. As similar reports have identified surviving cells as drug-tolerant persisters (Sharma et al. 2010; Liou et al. 2017), these observations suggest the presence of DTP subpopulations under new therapeutic contexts.

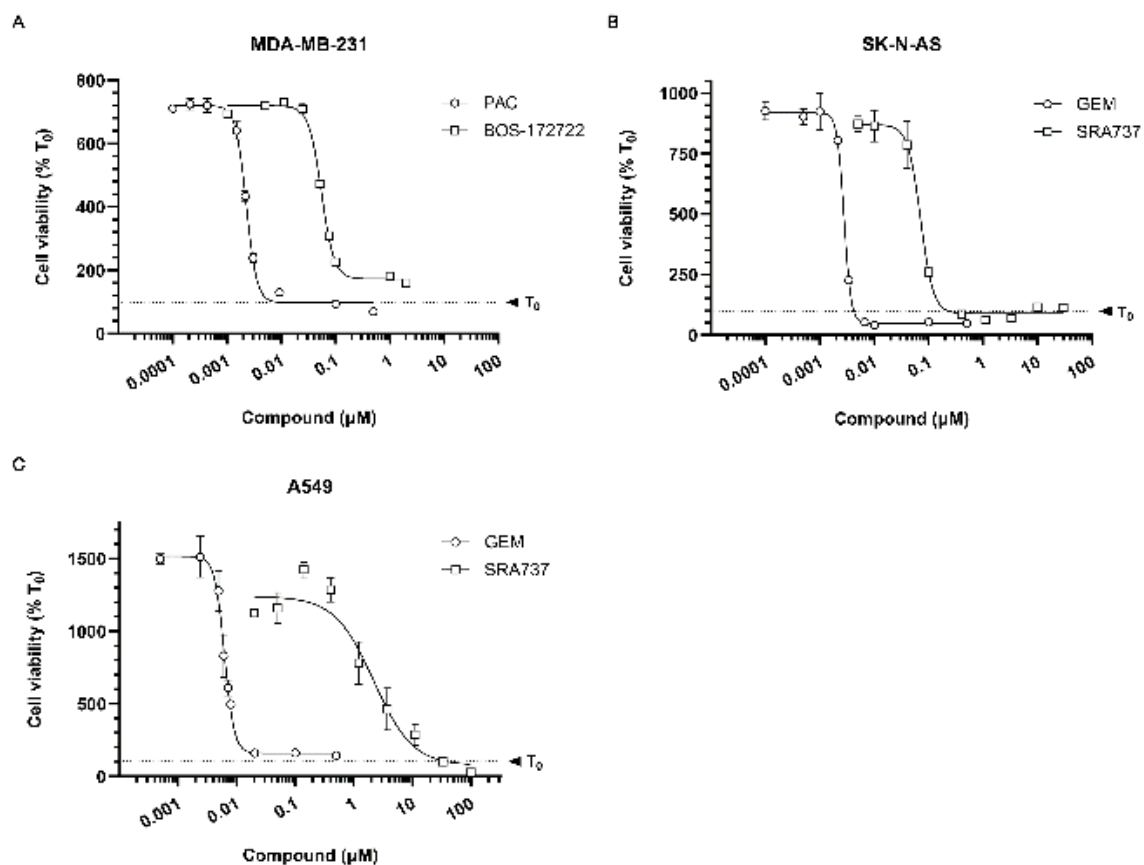


Figure 3-1: GI₅₀ determination of selected compounds in MDA-MB-231, SK-N-AS, and A549 cells.

Non-linear regression analysis of (A) MDA-MB-231, (B) SK-N-AS, and (C) A549 cell viability measured by CellTiter-Glo® assay 120h (A & B) or 96h (C) after compound addition. Graphs show mean±SD of triplicate technical replicates and are representative of n≥3 independent experiments. Dotted line represents T₀. PAC: paclitaxel; GEM: gemcitabine.

Table 3-2: Summary of cellular potency values (GI₅₀) and approximate 100X GI₅₀ compound concentrations used in DTP experiments.GI₅₀ values are mean±SD.

		Concentration (μM)		
		MDA-MB-231	SK-N-AS	A549
Gemcitabine <i>Antimetabolite</i>	GI ₅₀ (n)		0.003 ± 0.000 (3)	0.006 ± 0.001 (3)
	100X GI ₅₀		0.30	0.60
SRA737 <i>CHK1 inhibitor</i>	GI ₅₀ (n)		0.092 ± 0.018 (3)	2.033 ± 0.132 (3)
	100X GI ₅₀		10	200
Paclitaxel <i>Antimicrotubule</i>	GI ₅₀ (n)	0.002 ± 0.001 (4)		
	100X GI ₅₀	0.25		
BOS-172722 <i>MPS1 inhibitor</i>	GI ₅₀ (n)	0.058 ± 0.005 (3)		
	100X GI ₅₀	10		

3.2.2. A subpopulation of cells survive acute lethal compound exposure

To investigate and identify potential DTPs, MDA-MB-231, SK-N-AS, and A549 cells were continuously treated with lethal compound concentrations for 15 days and observed by microscopy at regular intervals. This experiment was not conducted in A549 cells using SRA737 as the high 100X GI₅₀ dose calculated for this agent would likely result in overt cytotoxicity.

Surviving populations were observed in MDA-MB-231 cells after 5-, 10-, and 15-days exposure to 10 μM BOS-172722 or 0.25 μM paclitaxel (Figure 3-2A). Fewer cells appeared to withstand lethal exposure to paclitaxel at day 5 compared to BOS-172722. This trend continued up to day 15, suggesting that different therapeutic assaults may elicit differential persist cell responses in the same cancer cell line. Surviving cells were also observed in SK-N-AS cells treated with 10 μM SRA737 or 0.3 μM gemcitabine (Figure 3-2C). While cell numbers had reduced after 15 days gemcitabine exposure, areas of growth were evident under continued SRA737 treatment. Similarly, a surviving subpopulation of A549 cells were detected after 4 days treatment with 0.6 μM gemcitabine (Figure 3-2E), although these appeared to be greater in number compared to SK-N-AS cells exposed to an equipotent gemcitabine dose (Figure 3-2C). This remained

consistent up to 12 days exposure, indicating differential persister cell responses to the same agent across different cancer cell lines. These microscopic observations demonstrate that there is a subpopulation of cancer cells able to tolerate lethal exposures to DNA damaging agents.

A defining characteristic of persister cell populations is the adoption of global epigenetic changes. To investigate whether the remaining cells observed under microscopy represent a surviving persister cell population, cells were collected and examined for post-translational modifications on histone H3 (H3) by Western blotting.

Slight increases in trimethylated H3 lysine 4 (H3K4_{me3}) and lysine 27 (H3K27_{me3}) were observed at days 5, 10, and 15 in MDA-MB-231 cells treated with 10 μ M BOS-172722 versus T₀ and vehicle treated controls (Figure 3-2B). This coincided with a small decrease in lysine 27 acetylation (H3K27_{ac}). There were no changes in trimethylation at lysine 9 (H3K9_{me3}) or acetylation at lysine 18 (H3K18_{ac}). Contrastingly, the changes observed in SK-N-AS cells were more pronounced. Treatment with 10 μ M SRA737 for 5-, 7-, and 13-days induced a dramatic reduction in H3K27_{ac}, concomitant with a time-dependent increase in H3K27_{me3} and a mild decrease in H3K18_{ac} (Figure 3-2D). SK-N-AS cells also showed no change in H3K9_{me3} levels following SRA737 exposure, however, unlike MDA-MB-231 cells treated with MPS1i, they showed no increase in H3K4_{me3}, indicating that different therapeutic assaults can elicit differential epigenetic alterations. In direct contrast to this, A549 cells treated with 0.6 μ M gemcitabine for 4-, 8-, or 12-days showed a similar pattern of epigenetic alterations to SRA737 treated SK-N-AS cells. No changes were observed in H3K4_{me3} or H3K9_{me3} levels (Figure 3-2F), however there was a clear increase in H3K27_{me3} after 4 days gemcitabine exposure that was maintained to day 12 and accompanied by a time-dependent reduction in H3K27_{ac}.

The global epigenetic alterations observed in SK-N-AS and A549 cells following lethal drug exposures are consistent with persister models published by others (Sharma et al. 2010; Guler et al. 2017; Liau et al. 2017; Al Emran et al. 2018),

providing evidence for the identification of these remaining cells as a drug-tolerant persister population. Furthermore, these results revealed a particular enrichment of hypermethylated H3K27 that was accompanied by H3K27 deacetylation. These marks are strongly associated with the formation of heterochromatin and gene silencing (Heintzman et al. 2009; Wiles and Selker 2017), indicating that epigenetic-mediated downregulation of gene expression may play a key role in DTP emergence under these new therapeutic contexts.

The evidence for positively identifying remaining MDA-MB-231 cells as DTPs is less clear since the observed changes are relatively minor compared to the alterations in SK-N-AS and A549 cells. As only a few epigenetic marks were investigated, expansion using a wider panel of modifications may help to definitively answer this question.

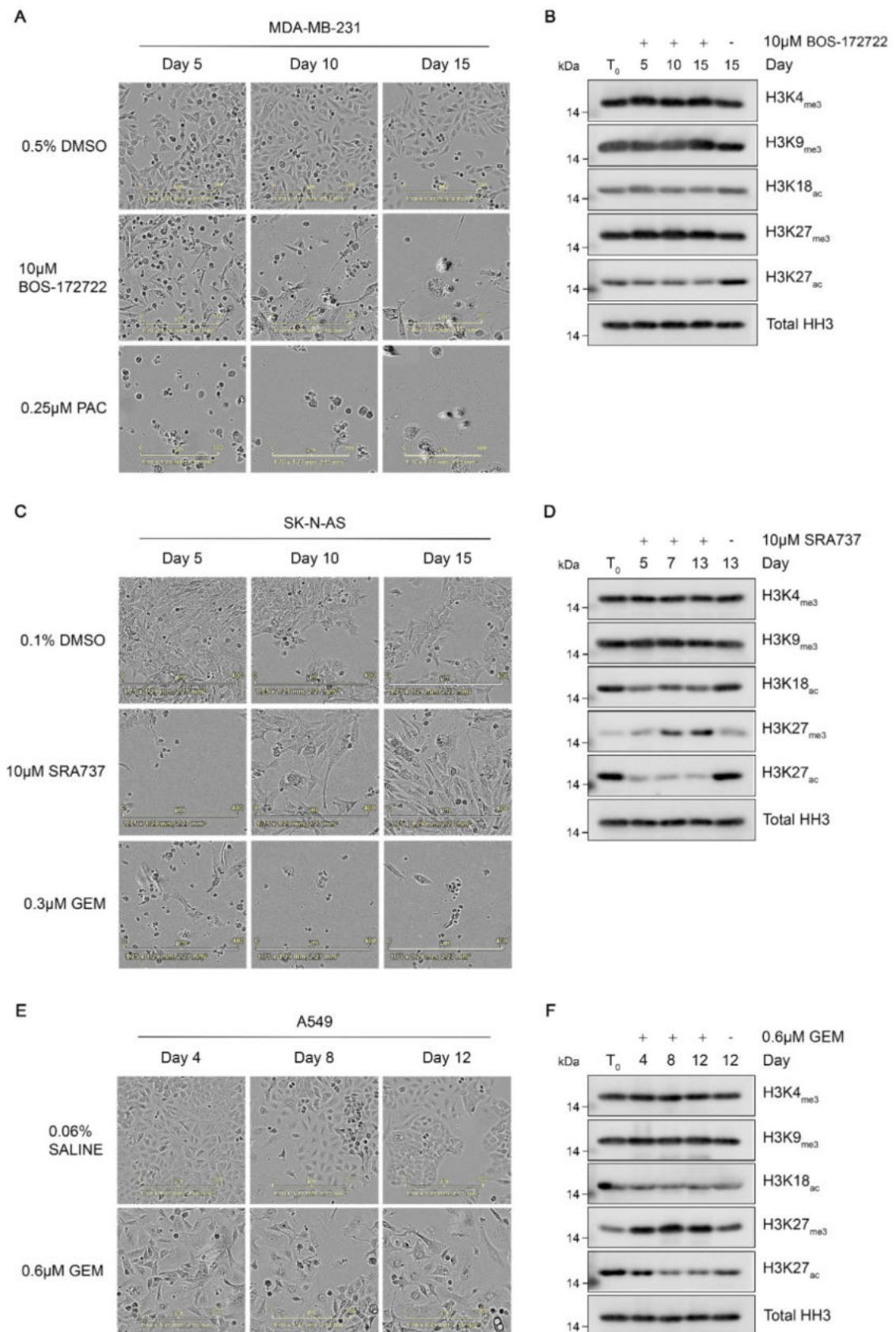


Figure 3-2: Putative persister subpopulations are detected in MDA-MB-231, SK-N-AS, and A549 cells following acute lethal compound exposure.

Continued on next page...

Figure 3-2: continued

Phase-contrast microscopy images of **(A)** MDA-MB-231, **(C)** SK-N-AS, and **(E)** A549 cells during lethal exposure to indicated compounds. **(B, D & F)** Western blot analysis of histone H3 modifications in T₀, compound, and control-treated cells at given time points. Images captured at 10X magnification, scale bar = 300 μm (A & E) or 400 μm (C). Microscopy images are representative of n≥1 independent experiment. Data shown are from a single experiment. PAC: paclitaxel; GEM: gemcitabine.

3.2.3. Response to lethal drug exposure is context specific

Microscopic observations suggested that different anti-cancer agents may induce differential persister cell responses. It is unclear if a given cancer cell line will generate the same number of DTPs in response to diverse drug challenges, or, moreover, if a single therapeutic agent will induce the same number of DTPs in different cancer cell lines. To investigate this, MDA-MB-231, SK-N-AS, and A549 cell numbers were monitored during the course of 15 days continuous lethal drug exposure.

Quantification confirmed microscopic observations in MDA-MB-231 cells treated with BOS-172722 or paclitaxel, with cell numbers remaining consistently higher under 10 μM BOS-172722 (Figure 3-3A). This is consistent with the increased potency of paclitaxel over BOS-172722 in MDA-MB-231 cells (Figure 3-1A & Table 3-2). Linear regression analysis revealed a statistically significant difference in responses to the two compounds (Figure 3-3A) indicating that, in this cellular model, different therapeutic agents may induce a different number of DTPs. Despite showing a 30-fold increase in sensitivity to gemcitabine (Figure 3-1B & Table 3-2), SK-N-AS cells responded similarly to lethal concentrations of SRA737 and gemcitabine (Figure 3-3B). This result is in contrast to microscopic observations, wherein there was a clear difference in cell number between the two treatments (Figure 3-2C). Regardless, this quantification demonstrates that SK-N-AS cells may generate the same number of DTPs in response to different therapeutic agents.

To investigate if the same agent will induce a similar number of DTPs in different cancer cell lines, responses to equipotent concentrations of gemcitabine were

compared between A549 and SK-N-AS cells. Although gemcitabine is similarly potent in A549 and SK-N-As cells (Table 3-2), responses over 15 days lethal exposure were statistically different (Figure 3-3C), confirming that the same therapeutic agent can induce differential persisting cell responses in different cancer cell lines. This is in line with microscopic observations showing more surviving A549 cells after gemcitabine treatment compared to SK-N-AS cells (Figures 3-2C & 3-2E). Taken together, these results indicate that persisting cell responses are likely to be context specific, depending on both the type of therapeutic challenge and cellular context.

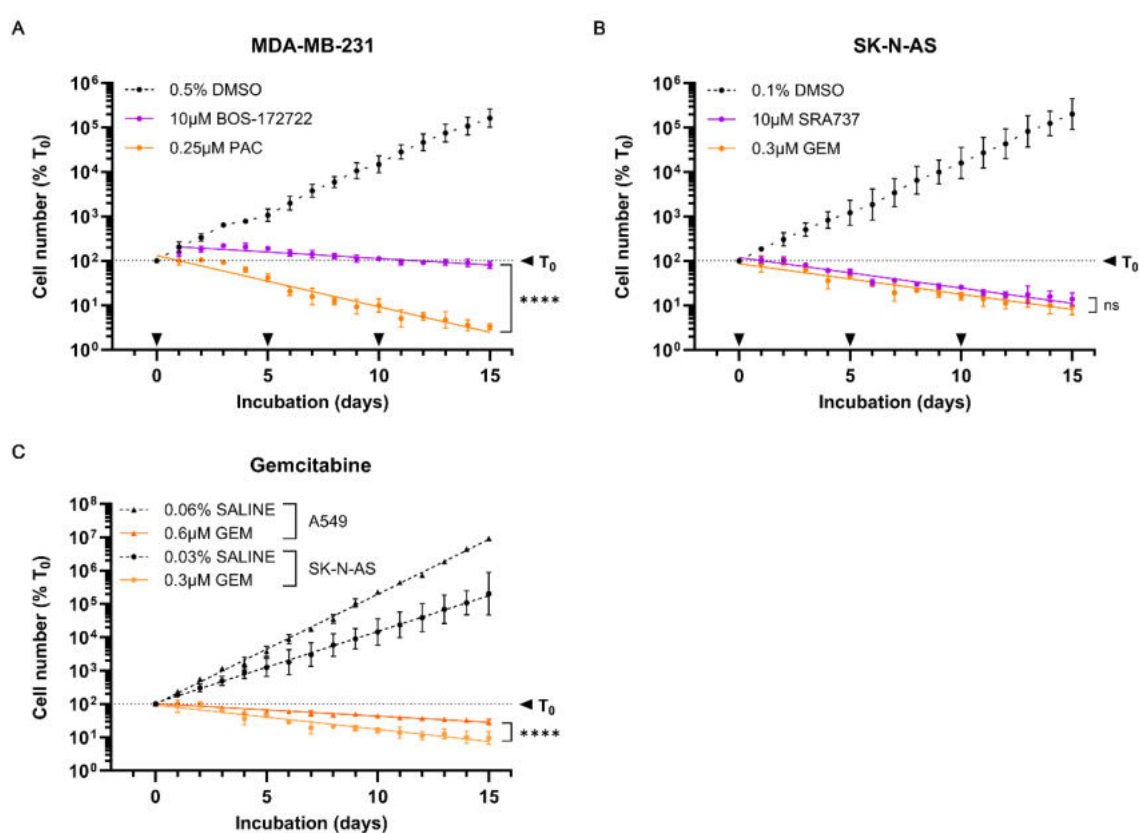


Figure 3-3: Response to lethal compound exposure is dependent on cellular and therapeutic contexts.

Number of (A) MDA-MB-231, (B) SK-N-AS, and (C) A549 and SK-N-AS cells during the course of 15 days continuous lethal exposure to indicated compounds, relative to T_0 (dotted line). Shown in (C) are the number of A549 and SK-N-AS cells over time in response to equipotent concentrations of gemcitabine. Arrowheads indicate compound renewal. Graphs show mean \pm SD of log₁₀ transformed data from three independent experiments. Significance statements refer to comparison of slopes resulting from linear regression analysis. PAC: paclitaxel; GEM: gemcitabine. **** $p < 0.0001$; ns = non-significant.

3.2.4. Investigating progression of putative DTP populations

Another characteristic of persister cells is their ability to resume proliferation with continued drug exposure (DTP-to-DTEP transition) and to recover following removal of therapeutic pressure. However, MDA-MB-231, A549, and SK-N-AS cell numbers had not yet increased by the end of 15 days lethal drug exposure, indicating that a longer incubation time may be necessary to observe this effect. To investigate this phenomenon in the remaining populations after short term lethal exposure, cells were cultured in either the continued presence of 100X GI₅₀ drug concentrations or in vehicle-supplemented medium up to 50 days (Figure 3-4A).

While remaining cells were observed in MDA-MB-231 cells after 10 days lethal exposure to BOS-172722 and paclitaxel (Figure 3-2A), no recovery was observed after a further 40 days culture in the presence of either agent or following drug-release into vehicle-supplemented medium (Figure 3-4B). This suggests that the cell population remaining at day 10 were unfit and unable to resume proliferation, even after removal of therapeutic pressure.

Conversely, a population of proliferating SK-N-AS cells were observed at day 50 after continued culture in the presence and absence of 10 μ M SRA737 (Figure 3-4C; left three panels), demonstrating that the cells surviving 7 days lethal drug exposure are viable. This result is consistent with published reports from other DTP models (Sharma et al. 2010; Liau et al. 2017), providing evidence to support this as a *bona fide* DTEP population. Interestingly, SK-N-AS cells maintained in SRA737 had an altered morphology; appearing larger in size and elongated in comparison to vehicle-treated control (Figure 3-4C). SRA737-released populations were more similar in appearance to vehicle treated cells. Although not measured quantitatively, these microscopic observations suggest that morphological changes may play a role in long-term responses to lethal SRA737 exposure. By contrast, SK-N-AS cells failed to recover after 50 days continuous exposure to 0.6 μ M gemcitabine (Figure 3-4C; right three panels). A small subpopulation of surviving cells were observed following gemcitabine withdrawal;

however, in the absence of cell viability assessments it remains unknown if these cells are viable and/or proliferating.

A similar result was observed in response to gemcitabine in A549 cells (Figure 3-4D). A small number of cells were present after further culture in both the presence and absence of gemcitabine, however there was a general loss of normal morphology when compared to vehicle treated control, with cells appearing flat and spread out. Although these cells survived, it is unclear if they are viable, senescent, or apoptotic.

The data presented in Figures 3-2 to 3-4 demonstrate the presence of a subpopulation of MDA-MB-231, A549, and SK-N-AS cells that are able to survive acute lethal drug exposures. Alterations to epigenetic profiles consistent with other DTP models provides evidence to support their identification as a drug-tolerant population. However, transition to the DTEP state and recovery after drug withdrawal was only observed in SK-N-AS cells treated with the CHK1i SRA737, identifying a putative persister cell response for further investigation.

3.3. Confirming persister cell identity in response to lethal SRA737 exposure in SK-N-AS cells

3.3.1. Surviving SK-N-AS cells harbour persister cell hallmarks

Having identified a putative persister cell response in SK-N-AS cells treated with SRA737, I sought to confirm the identity of remaining cells after lethal drug exposure as DTPs using the hallmarks of persister cells defined by Sharma and colleagues (2010).

DTPs are reported to account for $\leq 5\%$ of the tumour cell population under therapeutic challenge (Sharma et al. 2010), however, in the present study, the remaining cells at day 7 accounted for 24% of the starting population (T_0) (Figure 3-5A & 3-5B). This could be due to differences in the cellular models and targeted agents used for DTP generation. While these cells could represent the starting population, another possibility is that a subpopulation survived initial drug challenge and subsequently proliferated during treatment. To investigate the origin of this surviving fraction, SK-N-AS cells were stained with a dilutive proliferation dye before SRA737 exposure. Since the dye is equally divided between daughter cells, subsequent reductions in signal intensity can be used as a proliferative read-out. After 7 days, signal intensity was reduced by >100 -fold in vehicle treated control compared to freshly stained cells at T_0 (Figure 3-5C), corresponding to 7.5 population doublings. In comparison to vehicle control, cells treated with $10 \mu\text{M}$ SRA737 retained a significantly higher level of signal (Figure 3-5C), representing a 5.6-fold reduction versus T_0 and equating to 2.6 population doublings. Although signal intensity remained relatively high, it was significantly reduced versus the T_0 population (Figure 3-5C) demonstrating that some cell division occurred between days 0 to 7. Nonetheless, consistent with the slow-cycling persister cell hallmark, these data demonstrate that proliferation rate is reduced in the remaining drug-tolerant population. Furthermore, these results indicate that the large proportion of DTPs present at day 7 originate from the starting cell population, rather than a rare group of proliferating cells. This suggests that DTPs are more prevalent within this therapeutic and cellular context

and, as such, implies that the potential for obtaining a drug-tolerant state may not be so rare within bulk tumour cell populations.

The ability to transiently adopt and exit the slow-cycling state is a defining hallmark of DTPs. Data from long-term experiments suggested that surviving cells at day 7 can resume proliferation with continued SRA737 exposure and following SRA737 withdrawal (Figure 3-4C). To further investigate this phenomenon, I generated a stable SK-N-AS cell line expressing a nuclear-localised mKate2 red-fluorescent protein and used them to monitor whole-well cell number during long-term exposure to lethal SRA737 concentration. mKate2-SK-N-AS cells were validated for use as a suitable experimental model by comparison of persister cell responses to parental SK-N-AS cells (Appendix Figure 1). Cells were seeded and treated 48 hours later with 10 μ M SRA737 (Figure 3-5D; black arrow). After 7 days, cells were either maintained in SRA737 or cultured in vehicle-supplemented medium for a further 41 days (Figure 3-5D; purple arrow). Drug-released cells (REL) recovered quickly after SRA737 withdrawal, with cell numbers remaining consistent between days 7 and 13, followed by a steady increase up until day 48. By experimental end-point, drug-released populations were proliferating at the same rate as control treated cells, as demonstrated by a comparable number of population doublings per day (Figure 3-5E). In comparison, cells continuously exposed to SRA737 did not begin to recover until after day 20 (Figure 3-5D). Cell numbers increased more slowly over time, resulting in significantly fewer cells at day 48 compared to drug-released populations (Figures 3-5D & 3-5F). Consistent with this, SRA737 treated cells proliferated at a significantly reduced rate versus vehicle control at day 48 (Figure 3-5E), indicating that transition to a proliferating DTEP population takes longer than recovery following drug withdrawal. In line with long-term microscopy observations, these results demonstrate that slow-cycling SK-N-AS survivors can resume proliferation following removal of SRA737 or progress to DTEPs with continued drug exposure, fulfilling the hallmark of persister cell transience. In addition, these data reveal the kinetics of recovery from the DTP state and progression via DTP-to-DTEP transition under this new therapeutic

context, informing experimental procedures to generate and isolate different persister cell populations for further studies.

DTPs are also characterised by global epigenetic alterations that facilitate transcriptional reprogramming. In line with previous results (Figure 3-2D), there was a global increase in H3K27 tri-methylation (H3K27_{me3}), with concomitant decreases in K27 mono-methylation (H3K27_{me1}) and acetylation (H3K27_{ac}), in drug-tolerant SK-N-AS cells at day 7 (Figure 3-5G). These changes are associated with heterochromatin formation and subsequent gene silencing (Pasini et al. 2010). There was also a mild decrease in H3K18 acetylation (H3K18_{ac}); a modification associated with gene activation (Wang et al. 2008). While no alterations were observed in H3K4_{me3} or H3K9_{me3}, these results remain consistent with reports from other DTP models (Sharma et al. 2010; Guler et al. 2017; Liau et al. 2017; Al Emran et al. 2018), providing further evidence to support the emergence of a DTP population in response to lethal SRA737 exposure in SK-N-AS cells. Furthermore, the enrichment of repressive modifications indicate alteration of the epigenetic landscape and transcriptional profile in SRA737-induced DTPs.

Previous studies report that histone alterations observed in DTP populations are reversed once cells have transitioned to the proliferative DTEP state or recovered following drug release (Sharma et al. 2010; Guler et al. 2017; Liau et al. 2017; Al Emran et al. 2018). Indeed, epigenetic changes returned to control levels in SK-N-AS cells following SRA737 withdrawal (Figure 3-5G). Surprisingly, however, DTEPs maintained high levels of H3K27 methylation and reduced H3K27 acetylation, suggesting that initiation and preservation of these changes may be important for DTP and DTEP cell states, but are superfluous once therapeutic pressure has been removed. Accordingly, the genes regulated by these epigenetic marks may also be required for persister cell formation and progression, suggesting a role for epigenetic regulation in DTP emergence and survival in the context of lethal CHK1 inhibition.

Together, these results satisfy the persister cell hallmarks of drug-tolerance, transient slow-cycling, and epigenetic modulation, confirming the emergence of a *bona fide* DTP population in SK-N-AS cells in response to lethal SRA737 exposure.

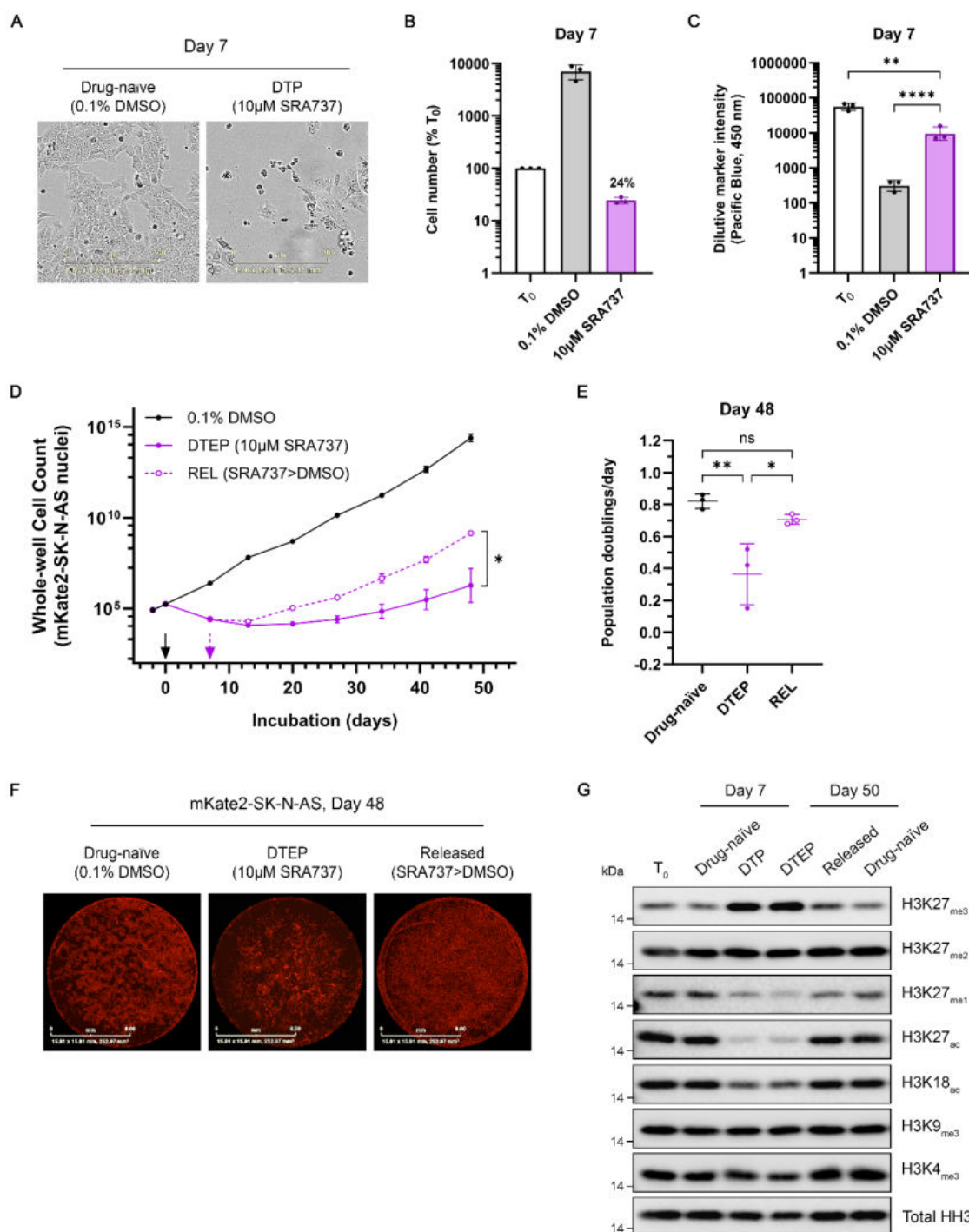


Figure 3-5: SK-N-AS cells remaining after lethal SRA737 exposure exhibit persister cell characteristics.

(A) Phase-contrast microscopy images of SK-N-AS cells treated with vehicle (drug-naïve) or 10 μ M SRA737 (DTP) for 7 days. (B) Number of remaining cells at day 7 relative to the starting population (T₀). (C) Quantification of ViaFluor® proliferative dye in the T₀ population and day 7 vehicle or SRA737 treated cells. (D) Quantification of mKate2-SK-N-AS cells treated with vehicle, SRA737 (DTEP), or SRA737 for 7 days followed by vehicle (REL) at indicated time points. (E) Number of populations doubling/day in indicated cell populations. (F) Whole-well fluorescence microscopy images of mKate2-SK-N-AS cells treated as in (D). (G) Western blot analysis of histone H3 modifications in drug-naïve and different persister cell populations at indicated time points. *Continued on next page...*

Figure 3-5: continued

Images captured at (A) 10X magnification, scale bar = 300 μm and (E) 4X magnification, scale bar = 8 mm. Graphs show mean \pm SD from three independent experiments. Significance statements in (C) result from analysis of log₁₀ transformed data by ordinary one-way ANOVA with Tukey's correction, in (D) from comparison of log₁₀ transformed means at day 48 by unpaired two-tailed Student's t-test, and in (E) from comparison of means by ordinary one-way ANOVA with Tukey's correction. **** $p < 0.0001$; ** $p < 0.01$; * $p < 0.05$; ns = not significant.

3.3.2. SK-N-AS DTPs are a heterogeneous population

SK-N-AS day 7 DTPs account for 24% of the starting population (Figure 3-5B); a figure that exceeds published data for other DTP models by ~5-fold (Sharma et al. 2010). While these cells are slow-cycling and originate from the starting cell population (Figure 3-5C) they could also be accounted for by other cell states, such as apoptosis. To investigate this, day 7 DTPs were assessed for levels of apoptosis and cytotoxicity using the ApoTox-Glo® triplex assay.

As a positive assay control, SK-N-AS cells were treated with 1 μM etoposide for 7 days. Accordingly, caspase 3/7 (apoptosis) and dead cell protease activity (cytotoxicity) were significantly increased by 45- and 12-fold, respectively, relative to DMSO treated control (Figure 3-6A & 3-6B). SK-N-AS DTPs also showed a significant increase caspase 3/7 and dead cell protease activity; however, this corresponded to only a 2-to-3-fold induction versus vehicle control. These data show that a small proportion of remaining cells are apoptotic and/or necrotic but, importantly, these phenotypes do not predominate in the population. This is perhaps consistent with the predicted cytostatic, rather than cytotoxic, effect of lethal SRA737 exposure (Figure 3-1B).

Senescence was also assessed in DTPs using a FACS-based β -galactosidase (β -gal) activity assay and a threshold applied to classify cells as β -gal positive (senescent) or β -gal negative (non-senescent). The CDK4/6 inhibitor palbociclib has been shown to induce senescence in cancer cell models (Perez et al. 2015) and, as such, was used as a positive assay control. Correspondingly, SK-N-AS cells treated with 10 μM palbociclib for 14 days showed a significant 20-fold increase in the proportion of senescent cells relative to DMSO treated control

(Figure 3-6C). Interestingly, the number of β -gal positive cells was also significantly increased in day 7 DTPs, with senescent cells accounting for almost 20% of the total population. This result demonstrates that a considerable proportion of the DTP population is senescent, however the fate of these cells remains unknown.

Together, these data indicate that the day 7 drug-tolerant SK-N-AS population induced by lethal SRA737 exposure is a heterogeneous mix of slow-cycling DTPs, senescent, and apoptotic/necrotic cells. The induction of senescence in a large proportion of cells is of particular interest as it is unclear to what extent they contribute to the emergence, survival, and progression of drug-tolerance.

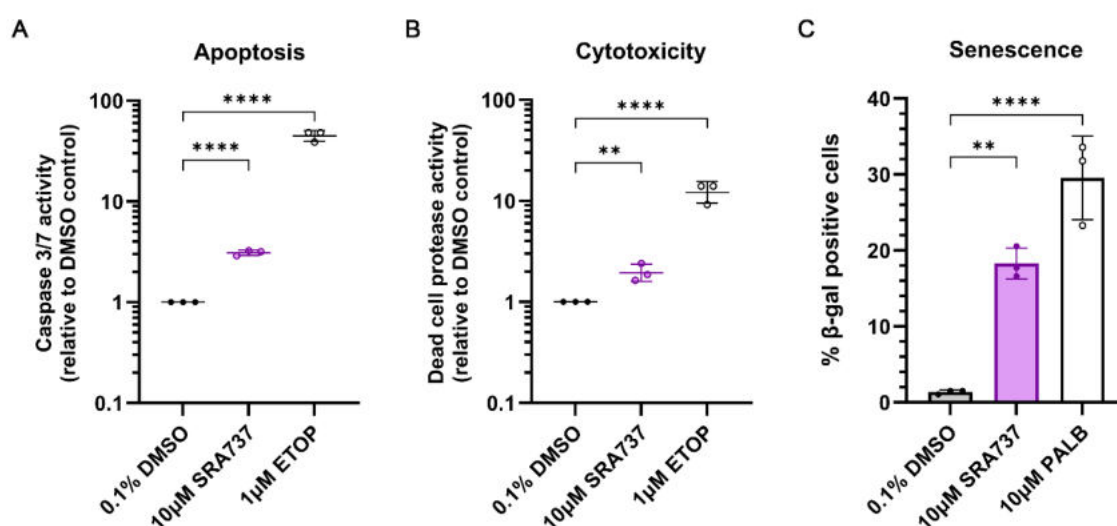


Figure 3-6: SRA737-induced SK-N-AS DTPs are a heterogeneous population.

(A) Caspase 3/7 and (B) dead cell protease activity measured by ApoTox-Glo® in day 7 SRA737-induced DTPs relative to vehicle treated control. Cells treated with 1 μ M etoposide (ETOP) for 7 days served as a positive control. Graphs show mean \pm SD of log₁₀ transformed data from three independent experiments. (C) Proportion of β -galactosidase positive cells in day 7 vehicle treated controls or SRA737-induced DTPs. Cells treated with 10 μ M palbociclib (PALB) for 14 days served as a positive control. Graph shows mean \pm SD from three independent experiments. Significance statements result from comparison of means by ordinary one-way ANOVA with Dunnett's correction. **** $p < 0.0001$; ** $p < 0.001$.

3.4. Discussion

To date, no studies on DTP emergence have been conducted using small molecule inhibitors of MPS1 or CHK1, that exert an anti-cancer effect by interfering with DNA integrity. With MPS1i and CHK1i currently under clinical investigation, it is imperative to characterise DTP formation and progression, and assess the contribution of DTP-mediated processes to overt drug resistance under these new therapeutic contexts. As such, the work here aimed to identify persister cell responses to these targeted inhibitors, and their respective genotoxic combination chemotherapies, using cell line models that reflected the therapeutic context of pre-clinical investigations and on-going clinical trials. The MPS1i BOS-172722 and paclitaxel were tested in TNBC cell line MDA-MB-231, and CHK1i SRA737 and gemcitabine in A549 (NSCLC) and SK-N-AS (neuroblastoma) cell lines.

Drug-tolerant populations were observed in MDA-MB-231, SK-N-AS, and A549 cells following acute lethal exposure to targeted agents and general chemotherapeutics. However, a *bona fide* persister cell response was achieved only in SK-N-AS cells exposed to the CHK1i SRA737, as evidenced by global epigenetic alterations, transient slow-cycling, and transition to a DTEP population with prolonged drug treatment. These observations are in line with recognised persister cell hallmarks and are consistent with reports from others that have identified DTP and DTEP populations using TKi (Sharma et al. 2010; Liau et al. 2017; Al Emran et al. 2018), providing positive confirmation of a persister cell response within this novel therapeutic context.

DTP formation was excluded in the other cellular models based on muted epigenetic changes and failure to progress or recover in the continued presence/absence of drug. However, this could be further investigated using a wider panel of epigenetic marks or alternative experimental procedures for definitive confirmation. For example, while no persister cell response was observed in MDA-MB-231 cells following lethal exposure to paclitaxel, DTPs have been identified and isolated using this agent in MDA-MB-231 3D organoid models

(Dhimolea et al. 2021). This highlights cell growth conditions as another contextual difference that may influence persister cell responses to lethal drug exposure. Although DTP emergence remains unconfirmed in MDA-MB-231 and A549 models, comparison of responses to lethal drug challenges indicate that persister cell generation may be context dependant. SK-N-AS cells respond similarly to lethal concentrations of SRA737 or gemcitabine, indicating that the same number of DTPs are induced by different therapeutic assaults. In direct contrast, MDA-MB-231 cells responded very differently to BOS-172722 or paclitaxel exposure. Furthermore, equipotent doses of gemcitabine induced differential responses in A549 and SK-N-AS cells. Together, this data indicates that adoption of the persister cell state is, to some degree, dependent on both cellular and therapeutic contexts and that certain challenges may be easier to overcome than others.

Previous studies have concluded that DTPs are rare within bulk tumour populations, accounting for $\leq 5\%$ of the cell population under therapeutic challenge (Sharma et al. 2010). In the present study, however, SK-N-AS DTPs surviving 7 days lethal SRA737 exposure account for almost 25% of the starting population (T_0). A potential explanation for this result is that the number of DTPs generated is dependent on the cellular model and therapeutic agent used. Investigations conducted in other cellular models indicate that this is the case. Further studies using a dilutive proliferation dye confirmed that these SRA737-derived persisters originated from the T_0 population, and not from a rare subpopulation of cells that survived initial drug challenge and subsequently proliferated during treatment. This implies that, at least in the context of CHK1i, a considerable proportion of tumour cells can enter a slow cycling DTP state to survive lethal drug exposure.

Interestingly, a substantial proportion ($\sim 20\%$) of SK-N-AS DTPs are senescent, as evidenced by an increase in the number of β -galactosidase positive cells. As the β -galactosidase activity assay was the only method used to quantify senescence, additional read-outs, such as induction of p21 and p16, would be useful to corroborate this result. Drug-induced senescence is a recognised

cellular response to therapeutic stress and several studies indicate that it is reversible (reviewed in (Saleh, Tyutyunyk-Massey, and Gewirtz 2019)). As such, it is possible that these cells could eventually exit the senescent state and re-enter the cell cycle following drug withdrawal or contribute to the emergence of drug-resistance in an analogous mechanism to DTPs. Senescence could even form part of an overall persister cell response. It is likely that persistence and senescence are interlinked, and understanding the nuances of these intertwined mechanisms could be key to addressing drug resistance arising from them.

Epigenetic alterations are frequently reported in persister cells generated using TKi (Sharma et al. 2010; Guler et al. 2017; Liao et al. 2017; Al Emran et al. 2018). Profiling of specific histone H3 modifications revealed similar alterations in SRA737-derived persisters, particularly global H3K27_{me3} enrichment and H3K27_{ac} depletion. These modifications are found within heterochromatic, genetically silent regions of the genome (Wang et al. 2008; Heintzman et al. 2009; Pasini et al. 2010; Wiles and Selker 2017), indicating that SRA737- and TKi-induced DTPs are commonly regulated by epigenetic mechanisms that alter gene expression. These conserved mechanisms could represent pivotal targets to abrogate the emergence of DTP populations in response to different drug challenges. On the other hand, no increases were observed in H3K4_{me3} or H3K9_{me3} in SRA737-induced DTPs indicating that additional, context specific epigenetic reprogramming also occurs. Of note, these data do not exclude the presence of alternative epigenetic changes, such as additional histone modifications or DNA methylation, that may predominate in differentially generated persister populations. In contrast to other reports, epigenetic alterations induced by SRA737 treatment were not reversed following DTEP transition, suggesting that continued epigenetic remodelling is required for DTP progression in this context.

The data presented herein confirm the emergence of a drug-tolerant persister cell population in SK-N-AS cells following lethal exposure to the CHK1i SRA737, identifying the persister cell phenomenon in response to a targeted agent with a diverse mechanism of action. Furthermore, by investigating the kinetics of DTP

progression during long-term SRA737 exposure, I have established protocols for the generation and isolation of DTP, DTEP, and drug-released persister cell populations for further studies. As such, this work represents the foundation for additional characterisation of drug-tolerant populations emerging under this novel therapeutic context.

Chapter 4

SRA737 resistant populations derived through the persister cell bottleneck or dose-escalation employ different mechanisms to overcome therapeutic challenge

Chapter 4 SRA737 resistant populations derived through the persister cell bottleneck or dose-escalation employ different mechanisms to overcome therapeutic challenge

4.1. Introduction

Transition through the DTP bottleneck is one route cancer cells can take to acquire drug resistance. Experimentally, however, most drug resistance models are generated for *in vitro* studies by dose-escalation; where cells are gradually exposed to increasing drug concentration until proliferation is unconstrained at lethal doses. Indeed, several studies have used this approach to identify mechanisms of CHK1i resistance (Blosser et al. 2020; Nair et al. 2020; Lee et al. 2020; Zhao et al. 2021; Hunter et al. 2022). These include altered expression of *CHEK1* (Blosser et al. 2020; Hunter et al. 2022), WEE1 upregulation (Zhao et al. 2021), and engagement of immune signalling pathways (Blosser et al. 2020). Interestingly, these studies have not detected any “gatekeeper” mutations in the CHK1 drug binding site, suggesting that the primary mechanisms of CHK1i resistance may involve aberrations in the expression and regulation of CHK1 and/or its downstream targets. However, it remains unknown whether the same drug resistance strategies would emerge via a persister cell bottleneck.

I hypothesised that persister populations employ distinct mechanisms to overcome therapeutic challenge with SRA737 and that these could represent potential intervention points to abrogate their formation and progression. To test this I generated two experimental SRA737-resistant models in SK-N-AS cells, one derived through the DTP bottleneck and the other via dose-escalation, for comparison of drug sensitivity profiles, ATR-CHK1 signalling activity, and transcriptional alterations to identify persister-specific biological processes for further mechanistic investigation.

4.2. Characterising SK-N-AS populations emerging from the persister cell bottleneck

Having identified a persister cell response in SK-N-AS cells under lethal SRA737 exposure, I sought to further characterise populations emerging from the DTP bottleneck. DTPs were induced by 7 days continuous treatment with 10 μ M SRA737 and subsequently cultured in the presence or absence of drug for a further 43 days to generate drug-tolerant expanded persisters (DTEPs) or drug-released (released) populations, respectively (Figure 4-1A). In parallel, cells were passaged in the presence of 0.1% DMSO as a drug-naïve control.

4.2.1. DTEP and drug-released cell populations are less sensitive to further challenge with SRA737

DTEPs are considerably less sensitive to SRA737, as shown by a ≥ 100 -fold drop-off in GI_{50} potency (Figure 4-1B & Table 4-1). Normalisation of cell viability data to the T_0 revealed that DTEPs proliferate at approximately half the rate of their drug-naïve and drug-released counterparts (Figure 4-1B). These results are consistent with microscopic observations and cell counts during culture in the presence of 10 μ M SRA737 (Figure 3-5). Released populations were also $\sim 2.5X$ less sensitive to SRA737, despite being in drug-free culture for 43 days and recovering their proliferation rate in line with drug-naïve controls (Figure 4-1B & Table 4-1). High SRA737 concentrations induced a cytotoxic response in drug-naïve cells, as identified by data points below T_0 (Figure 4-1B); notably, this effect was abrogated in both DTEP and released populations suggesting they are more tolerant of high doses of SRA737.

Therapeutic resistance can be conferred by genetic mutation of drug targets (Yun et al. 2008) and/or upregulation of drug efflux pumps (Bell et al. 1985), both of which would be expected to prevent downstream biomarker changes in response to drug treatment. To determine whether these mechanisms underlie changes in SRA737 sensitivity in DTEP or released populations, CHK1 activity was investigated by Western blotting. In response to genotoxic stress, CHK1 is

phosphorylated by ATR at serine-317 and serine-345, then autophosphorylated at serine-296 to complete activation (Zhao and Piwnica-Worms 2001; Okita et al. 2012). Accordingly, levels of phosphorylated serine-296 (pS296-CHK1) are a suitable proxy for CHK1 activity and were increased in drug-naïve controls, DTEP and drug-released populations upon exposure to the DNA damaging agent gemcitabine (200 nM, 24 h) (Figures 4-1C & 4-1D). This was inhibited in a dose-dependent manner by a one-hour pre-treatment with SRA737 in all populations, confirming drug engagement with the target and inhibition of CHK1 activity. These findings strongly argue against mutation of the CHK1 drug binding site as the driver of resistance. This result also suggests that increased drug efflux is unlikely to explain SRA737 tolerance in DTEP and released cells since CHK1 autophosphorylation at Ser-296 was inhibited by similar concentrations of SRA737 as drug-naïve cells.

High doses of SRA737, either alone or in combination with gemcitabine, reduced total CHK1 protein levels in drug-naïve and DTEP populations (Figure 4-1C), and in released cells to a lesser extent (Figure 4-1D). This observation is consistent with published results (Walton et al. 2016), though there is currently no evidence that SRA737 acts as a protein degrader as well as a small molecule inhibitor of CHK1.

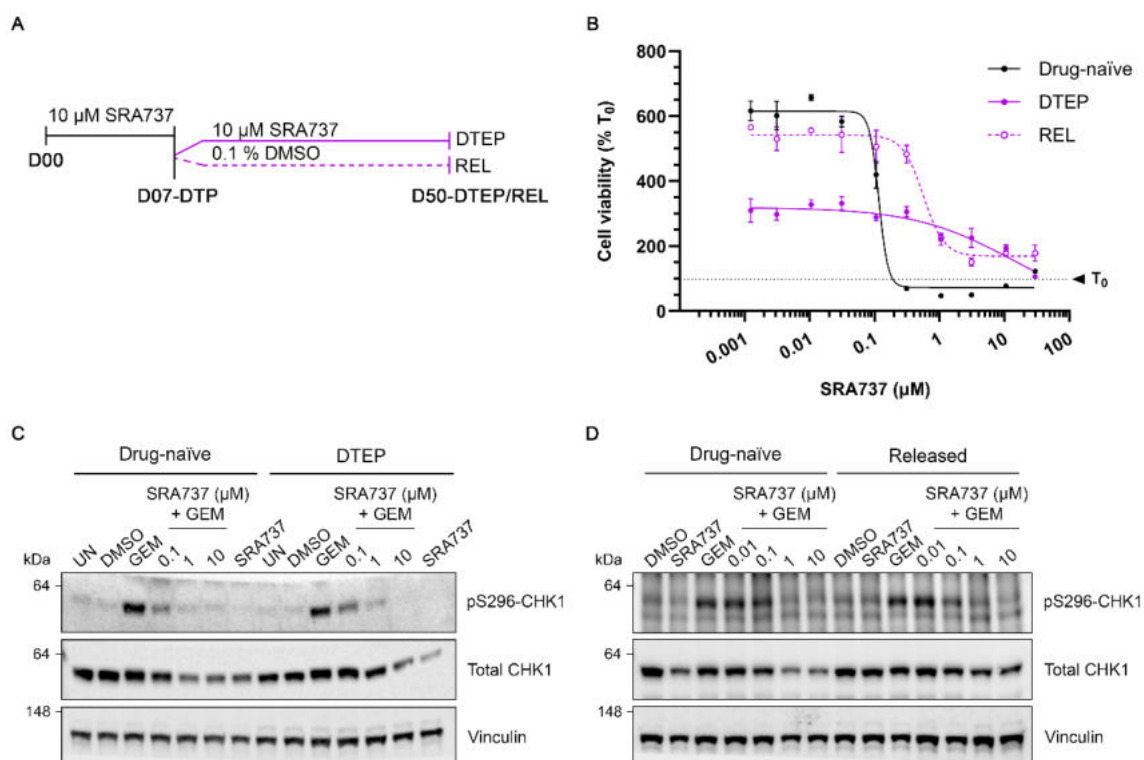


Figure 4-1: SK-N-AS DTEP and drug-released cells are insensitive to further pharmacological inhibition of CHK1.

(A) Schematic protocol for generation of persister-derived cell populations. **(B)** Non-linear regression analysis of SK-N-AS cell viability measured by CellTiter-Glo® 120h after SRA737 addition in indicated populations. **(C & D)** Western blot analysis of CHK1 activity in drug-naïve, **(C)** DTEP, and **(D)** drug-released (REL) populations after 24h exposure to 200 nM gemcitabine (GEM) \pm SRA737 at indicated concentrations, or 10 μ M SRA737 alone (SRA737). Graph shows mean \pm SD of two technical replicates and is representative of $n \geq 3$ experiments. Dotted line shows proportion of cells at T_0 .

4.2.2. SRA737-derived DTEP and released cells are cross-resistant to alternative small molecule inhibitors of CHK1 and CHK2

Glioblastoma persisters derived using the PDGFR inhibitor dasatinib are cross-resistant to alternative small molecule inhibitors against the same target (Liau et al. 2017). Additionally, NSCLC DTPs generated with targeted EGFR inhibitors (EGFRi) are less sensitive to the general cytotoxic agent cisplatin (Sharma et al. 2010). These reports suggest that persister populations induced with a single targeted agent can acquire cross-resistance to a variety of alternative drugs. In the present study, SRA737-derived DTEP and drug-released populations were tested for sensitivity to alternative CHK1 inhibitors (CHK1i) and a dual inhibitor also targeting CHK2 (CHK2i); a closely related protein that orchestrates the parallel ATM-CHK2 arm of the DNA damage response (DDR) signalling pathway (Ahn et al. 2000; Smith et al. 2010).

Similar to results obtained using SRA737, DTEP GI₅₀ values for the CHK1i LY2603618 and MK-8876 were reduced by 50- and 70-fold, respectively (Figure 4-2A, 4-2B & Table 4-1). DTEPs are 20X less sensitive to the dual CHK1/CHK2i AZD7762 (Figure 4-2C & Table 4-1), indicating that these populations are resistant to additional inhibitors of the DNA damage response (DDR) pathway. Drug-released cells (REL) are also less sensitive to these alternative CHK1/CHK2 inhibitors, to a lesser extent (Figure 4-2 & Table 4-1).

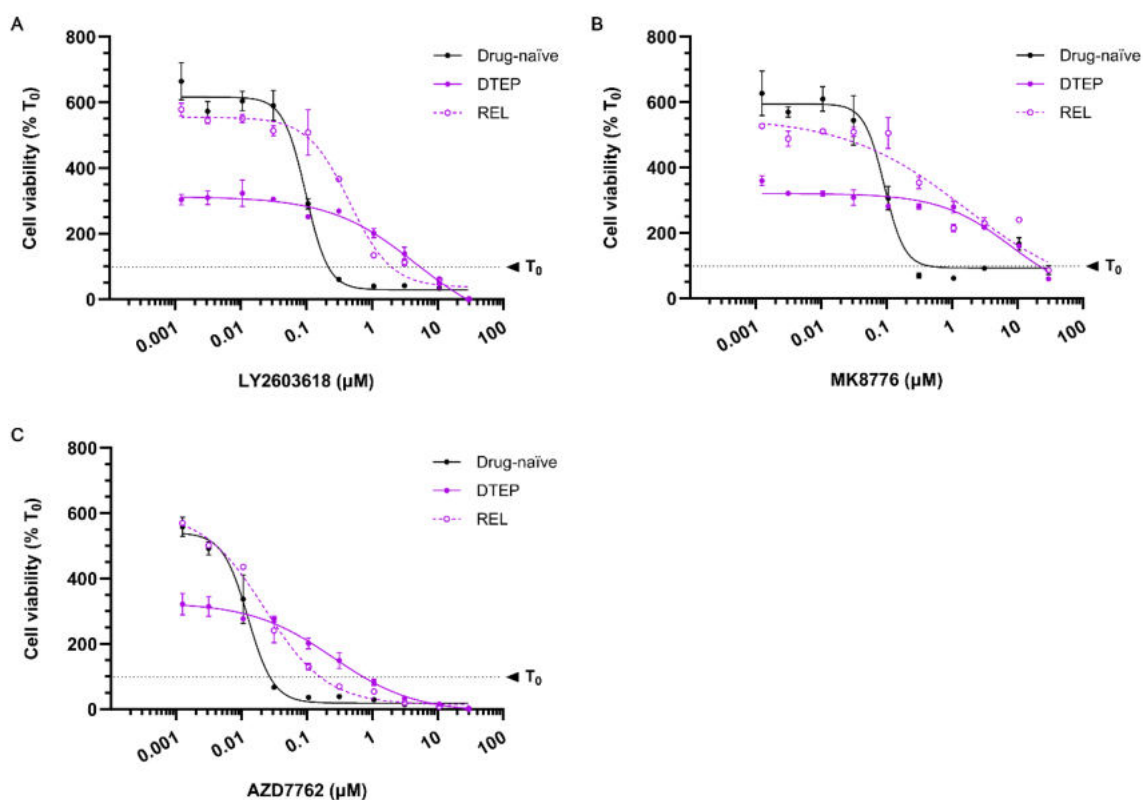


Figure 4-2: SK-N-AS DTEP and drug-released populations are cross-resistant to alternative small molecule inhibitors of CHK1 and CHK2.

(A – C) Non-linear regression analysis of SK-N-AS cell viability measured by CellTiter-Glo® 120h after addition of CHK1 inhibitors (A) LY2603618 and (B) MK8776, and (C) dual CHK1/2 inhibitor AZD7762 in indicated populations. Cells were seeded in the absence of SRA737 to avoid combination effects. Graphs show mean±SD of two technical replicates and is representative of $n \geq 2$ experiments. Dotted line shows proportion of cells at T₀.

Table 4-1: Summary of cellular potency values (GI₅₀) for indicated compounds in drug-naïve, DTEP, and drug-released populations at day 50.

GI₅₀ values are mean±SD. Cells are highlighted according to fold-increase in GI₅₀ value compared to drug-naïve control. Red ≥50-fold; orange ≥10-fold; yellow ≥2-fold.

Target	Compound	Population GI ₅₀ , μM (n)		
		Drug-naïve	DTEP	Released
ATM	AZD1390	6.83 ± 0.41 (4)	6.24 ± 0.60 (2)	7.38 ± 0.68 (3)
ATM	KU60019	3.99 ± 0.19 (4)	8.08 ± 1.22 (2)	6.70 ± 0.77 (3)
ATR	AZD6738	0.23 ± 0.04 (4)	0.55 ± 0.17 (2)	0.65 ± 0.23 (3)
ATR	VE822	0.08 ± 0.00 (4)	0.44 ± 0.12 (2)	0.31 ± 0.16 (3)
CHK1	LY2603618	0.08 ± 0.01 (4)	3.97 ± 0.92 (2)	0.53 ± 0.18 (3)
CHK1	MK8776	0.09 ± 0.01 (4)	6.47 ± 1.99 (2)	1.82 ± 0.61 (3)
CHK1	SRA737	0.12 ± 0.02 (5)	12.86 ± 2.52 (3)	0.55 ± 0.07 (4)
CHK1/2	AZD7762	0.01 ± 0.00 (4)	0.20 ± 0.07 (2)	0.05 ± 0.04 (3)
DNA	Gemcitabine	0.004 ± 0.001 (5)	0.008 ± 0.002 (3)	0.010 ± 0.002 (4)
WEE1	AZD1775	0.05 ± 0.001 (4)	0.04 ± 0.001 (2)	0.08 ± 0.02 (3)

4.2.3. DTEP and drug-released cells are cross-resistant to additional DDR inhibitors

To further investigate the scope of drug resistance, SRA737-derived DTEP and drug-released populations (REL) were tested for sensitivity to additional small molecule inhibitors of the DDR signalling pathway.

Compared to their drug-naïve counterparts DTEPs were less sensitive to the ATR inhibitors (ATRi) VE822 and AZD6738 by 2.4- and 5.5-fold, respectively (Figure 4-3 & Table 4-1). Additionally, potency of the DNA damaging agent gemcitabine was consistently reduced by 2-fold in DTEPs. Given that CHK1 is activated by ATR kinase in response to ssDNA damage and replication stress (Zhao and Piwnica-Worms 2001), and DTEP and drug-released cells are resistant to

multiple CHK1i (Figure 4-2), these results suggest that DDR signalling through the ATR-CHK1 axis is dysregulated in SRA737-derived DTEP populations.

The ATM-CHK2 signalling axis runs in parallel to the ATR-CHK1 pathway and is activated in response to dsDNA breaks (reviewed in (Ronco et al. 2017)). Cross-talk occurs between the two arms of the DDR pathway to exquisitely coordinate cellular responses to DNA damage (Cuadrado et al. 2006; Jazayeri et al. 2006; Shiotani and Zou 2009). Therefore, it is conceivable that DTEPs generated with a CHK1i could engage the ATM-CHK2 axis as a compensatory pathway for survival and, as such, be sensitive to ATM or CHK2 inhibition. The observation that SRA737-induced DTEPs are, in fact, less sensitive to the dual CHK1/2i AZD7762 (Figure 4-2C & Table 4-1) suggests this is not the case. This is further supported by relatively minimal changes in GI₅₀ values for the ATM inhibitors (ATMi) KU60019 and AZD1390 (Figure 4-3 & Table 4-1; reduced by 2-fold and unchanged, respectively).

Drug-released (REL) populations were also less sensitive to these agents, but not to the same magnitude as DTEPs (Figure 4-3 & Table 4-1). This difference could be explained by a gradual return to a drug sensitive control-like state following drug withdrawal. A notable difference between DTEP and drug-released cells was in their responses to challenge with the WEE1 inhibitor (WEE1i) AZD1775. While DTEPs showed no difference in AZD1775 sensitivity compared to drug-naïve controls, GI₅₀ potency was robustly reduced by approximately 2-fold in drug-released cells (Figure 4-3 & Table 4-1) suggesting that diverse drug resistance mechanisms may be employed by different persister-derived populations.

These results indicate that cell populations emerging from the persister cell bottleneck not only harbour selective resistance to the utilised drug, but also to a wider group of therapeutic agents targeting the same or closely related proteins. The observation that DTEPs are less sensitive to some but not all DDR inhibitors tested suggests that they harbour selective, rather than indiscriminate, cross-resistance. Importantly, observations from the drug-released population

demonstrate that an acute lethal drug exposure is sufficient for long-term drug-tolerance.

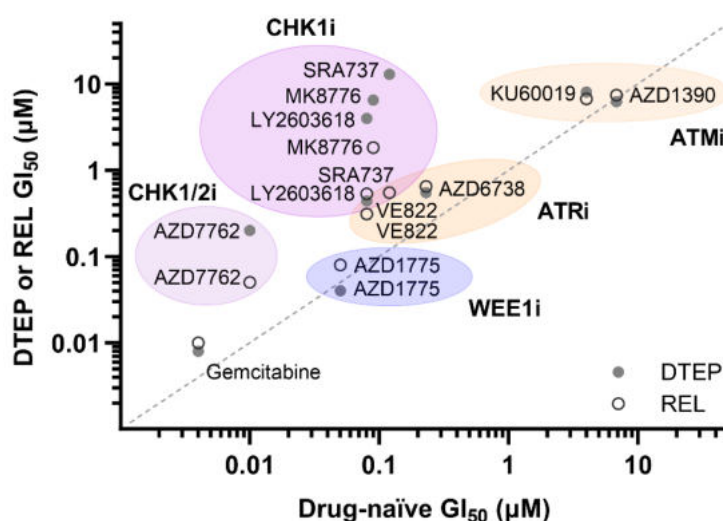


Figure 4-3: SK-N-AS DTEP and drug-released cells are similarly cross-resistant to additional DDR pathway inhibitors.

Potency of additional DDR pathway inhibitors in drug-naïve (x-axis) and DTEP or drug-released (REL) (y-axis) populations. Graph shows mean GI₅₀ value from n≥2 experiments. Dotted line represents line of identity.

4.3. Acute lethal SRA737 exposure has long-term effects following drug release

4.3.1. Drug-released populations show variation in recovering SRA737 sensitivity

Persister cells are characterised by reversible drug-tolerance, as evidenced by a return to sensitivity upon drug withdrawal (Sharma et al. 2010; Liao et al. 2017). PC9-DTPs generated using the EGFRi erlotinib quickly regained drug sensitivity within 9 population doublings in drug-free medium (Sharma et al. 2010). In the present study, released populations remained less sensitive to SRA737 43 days (~18 population doublings) after drug withdrawal (Figure 4-2, 4-3 & Table 4-1).

To investigate the kinetics of drug resensitisation, four independently generated DTP populations were released into drug-free medium (REL-1 to REL-4) and retested for SRA737 sensitivity at regular intervals over a period of approximately 40 weeks.

To monitor changes in SRA737 sensitivity over time, GI_{50} values were normalised to their corresponding time-matched drug-naïve control such that a value of 1 denotes equal drug potency, and <1 or >1 indicates increased or decreased sensitivity respectively. At day 50, all four released populations showed a similar reduction in sensitivity to SRA737 (Figure 4-4A & Table 4-1). This persisted through day 121, with REL-1 and REL-4 passing through a period of increased resistance before re-joining REL-2 and REL-3. Past this point, REL-4 diverged from the other replicates, on a course towards resensitisation to SRA737; cells became $\sim 2.6X$ more sensitive to SRA737 than drug-naïve controls at day 185 and then recovered to equal control GI_{50} values by day 274 (Figures 4-4A, 4-4C & Table 4-2). SRA737 potency fluctuated in REL-1, -2, and -3 up to day 220, with REL-3 regaining sensitivity to SRA737 by day 274 (Figure 4-4A & Table 4-2). Despite initially showing similar changes, REL-1 remained insensitive to SRA737 at day 274 (Figures 4-4A, 4-4B & Table 4-2). The differential responses observed in drug-released populations that have been generated in the same manner indicate that various routes can be taken to exit and recover from the DTP state.

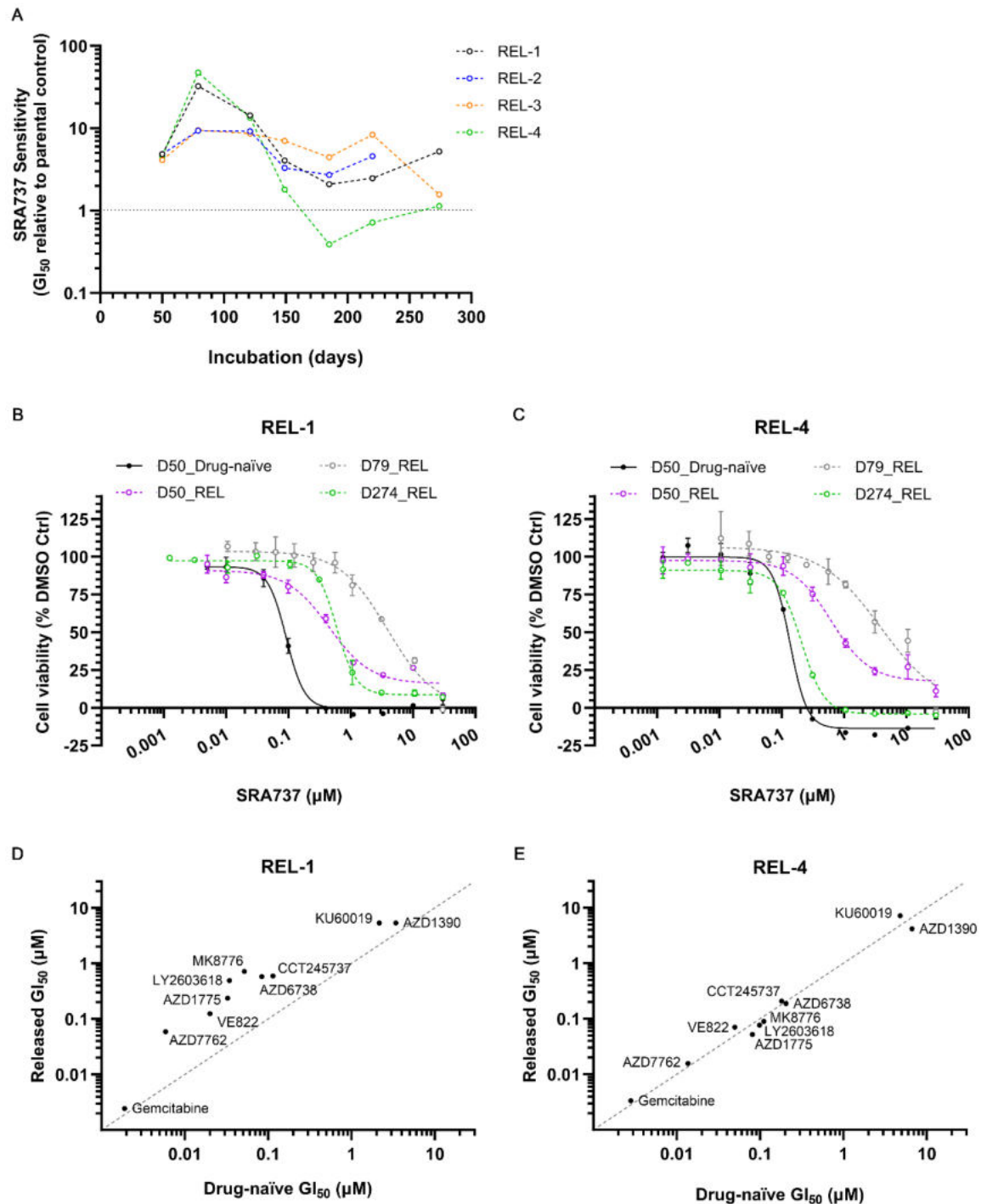


Figure 4-4: Drug-released populations regain SRA737 sensitivity via different routes.

(A) SRA737 GI_{50} potency over time in four independently generated drug-released populations (REL-1 to REL-4) relative to drug-naïve controls (dotted line). (B & C) Non-linear regression analysis of cell viability measured by CellTiter-Glo® 120h after addition of SRA737 in (B) SRA737-tolerant REL-1 and (C) SRA737 sensitive REL-4 at indicated time points. (D & E) GI_{50} potency of additional DDR pathway inhibitors in drug-naïve (x-axis) and (D) REL-1 or (E) REL-4 populations (y-axis). Dotted line represents line of identity. Graphs show (A, D & E) GI_{50} values from a single experiment, and (B & C) mean \pm SD of ≥ 2 technical replicates.

4.3.2. Resensitisation to SRA737 is accompanied by resensitisation to additional DDR inhibitors

To investigate if resensitisation to SRA737 translates to other agents, REL-1 to REL-4 were tested for sensitivity to the same panel of alternative DDRi and GI₅₀ values plotted against corresponding drug-naïve controls.

In the populations that remained resistant to SRA737, cross resistance to other agents was maintained. REL-1 was less sensitive to alternative CHK1i (LY2603618 and MK8876), and additional CHK1/2i (AZD7762), ATRi (AZD6738 and VE822), and WEE1i (AZD1775), as shown by ≥ 2 -fold increase in GI₅₀ values (Figure 4-4D & Table 4-2). A similar pattern was observed in REL-2 (Table 4-2), demonstrating continued DDRi cross-resistance in these SRA737-tolerant drug-released populations. For those populations that were resensitised to SRA737, sensitivity to other agents was also restored. REL-4 showed similar sensitivities to DDR inhibitors as drug-naïve controls, as indicated by GI₅₀ data points on the line of identity, with the exception of ATRi KU6009 that still had reduced potency (Figure 4-4E & Table 4-2). Comparable results were obtained from SRA737-sensitive population REL-3 (Table 4-2), demonstrating the reversal of cross-resistance that was observed in drug-released populations at day 50 (Figure 4-3 & Table 4-1).

Taken together, these results show that SRA737 and DDRi drug-tolerance can be reversed in persister cell populations following drug withdrawal. Interestingly, this data also illustrates variation in the fates of populations following exit from the DTP state, with some regaining drug sensitivity quickly and others taking longer to recover.

Table 4-2: Summary of cellular potency values (GI₅₀) for indicated compounds in drug-naïve cells and replicate drug-released populations at day 274.

GI₅₀ values are mean±SD. Cells are highlighted according to fold-increase in GI₅₀ value compared to drug-naïve control. Red ≥50-fold; orange ≥10-fold; yellow ≥2-fold.

Target	Compound	Population GI ₅₀ , μM (n)				
		Drug-naïve	REL-1	REL-2	REL-3	REL-4
ATM	AZD1390	4.69 ± 1.74 (3)	5.37	1.52	2.85	4.19
ATM	KU60019	3.54 ± 1.32 (3)	5.37	3.73	3.53	7.18
ATR	AZD6738	0.14 ± 0.06 (3)	0.58	0.07	0.11	0.19
ATR	VE822	0.04 ± 0.02 (3)	0.12	0.09	0.10	0.07
CHK1	CCT245737	0.14 ± 0.04 (3)	0.60	0.30	0.20	0.21
CHK1	LY2603618	0.06 ± 0.03 (3)	0.49	0.38	0.07	0.08
CHK1	MK8776	0.07 ± 0.04 (3)	0.72	0.37	0.10	0.09
CHK1/2	AZD7762	0.01 ± 0.00 (3)	0.06	0.04	0.01	0.02
DNA	Gemcitabine	0.003 ± 0.001 (3)	0.002	0.012	0.003	0.003
WEE1	AZD1775	0.05 ± 0.03 (3)	0.24	0.05	0.05	0.05

4.4. Gene expression profiles are altered in SK-N-AS persister cell populations

Reports from others have identified altered gene expression profiles in persister cells generated with TKi. Notably, expression of cell cycle and proliferation related genes are downregulated (Liau et al. 2017), while stem-like gene signatures are enriched (Liau et al. 2017; Rehman et al. 2021; Dhimolea et al. 2021). One unanswered question is whether persister cells generated with a differentially targeted therapeutic agent undergo similar transcriptional reprogramming. To investigate this, SRA737-derived DTPs, DTEPs, and drug-released populations were collected for RNA sequencing (RNAseq) and data subsequently interrogated by gene-set enrichment analysis (GSEA). A minimum of four 4

independently derived, pooled DTP, DTEP, or drug-released persister populations were generated for these studies.

4.4.1. Persister cell populations harbour distinct gene expression profiles

Multi-dimensional scaling (MDS) is a statistical technique used to summarise large, complex datasets with minimal loss of information. In the context of RNAseq data, gene expression profiles are reduced and plotted such that the distance between data points is proportional to their similarity (Hout, Papesh, and Goldinger 2013). This facilitates observation and identification of trends within complex, high-dimensional datasets.

In the present study, the top two dimensions identified by MDS explained 56% (dim-1) and 12% (dim-2) of the variance in the data. Day 0 (D00; pink open circles) and drug-naïve replicates (green circles, diamonds, triangles) clustered together upon MDS, revealing their close similarity, and indicating minimal gene expression changes during the 50-day experiment (Figure 4-5). Replicates from all other treatment conditions similarly clustered with each other, demonstrating robust transcriptional alterations in different persister cell populations that have been independently generated. Day 7 DTPs appeared most transcriptionally distinct compared to controls, as shown by differential clustering based on both dimensions (dim-1 and dim-2). Gene expression profiles from day 30 and day 50 DTEPs were comparable to day 7 DTPs according to dim-1 but showed similarity with drug-naïve controls by dim-2, suggesting both common and unique transcriptional changes between persister cell populations. Interestingly, drug-released (REL) populations shared transcriptional similarity with DTEPs at day 30 and then with controls at day 50. These results not only demonstrate durable changes in gene expression following acute lethal SRA737 exposure, but also gradual reversal upon subsequent drug withdrawal.

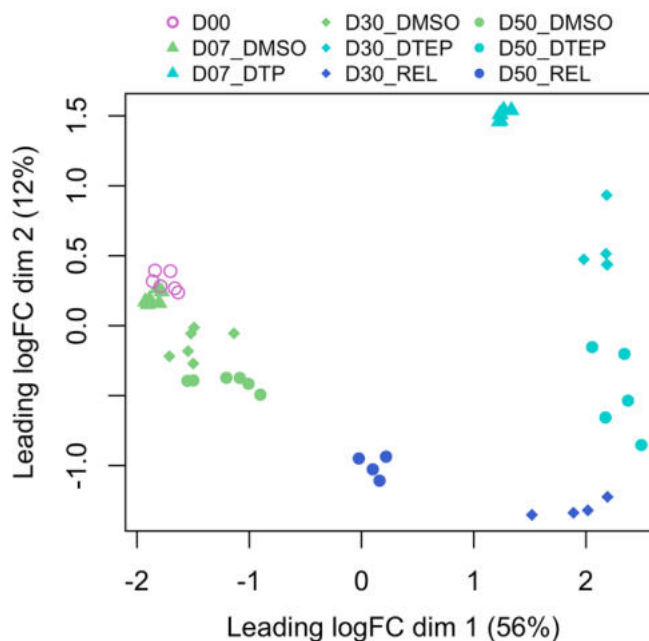


Figure 4-5: Transcriptional alterations in DTP and DTEPs are partially reversed after SRA737 withdrawal.

Multi-dimensional scaling (MDS) of RNAseq expression data from SRA737-induced DTPs, DTEPs, released (REL) and drug-naïve control (D00 & DMSO) populations.

To further explore transcriptional alterations, the distribution of differentially expressed genes was investigated for each persisting cell population, relative to D00 (absolute fold-change ≥ 2 , FDR $< 5\%$). A total of 5175 and 4983 genes were differentially expressed in day 7 DTPs and day 50 DTEPs, respectively (Figure 4-6A; left & middle panel). Given that SRA737-induced DTPs and DTEPs are enriched for repressive epigenetic modifications (Figure 3-5G), I predicted that the majority of transcripts would be downregulated. However, upregulated genes accounted for $>70\%$ of gene expression changes in DTP and DTEP populations (Figure 4-6A). *CHEK1* expression was significantly downregulated in DTPs but remained unchanged in DTEPs and REL cells. This is consistent with Western blot data showing comparable levels of total CHK1 protein expression between drug-naïve controls, DTEPs, and REL populations (Figure 1-1C & 1-1D). Upregulation also accounted for the majority of gene expression changes in REL

cells (76%) (Figure 4-6A; right panel). In comparison to DTPs and DTEPs, REL cells showed ~3X fewer gene expression changes overall, supporting the observation by MDS analysis that transcriptional alterations are partially reversed following SRA737 withdrawal (Figure 4-6A).

Hierarchical clustering of differentially expressed transcripts revealed four groups of genes with similar patterns of expression (Figure 4-6B). Group 1 is clustered by genes that have high mRNA abundance in DTP and DTEP populations relative to REL and drug-naïve control cells. These genes could represent those that are drug-induced since they are only increased in populations continuously exposed to SRA737. Group 2 is also defined by genes that are highly expressed in DTPs and DTEPs, but whose enrichment in REL populations at day 30 is almost completely reversed at day 50. These expression patterns are mirrored in group 4 by genes that are low in abundance in DTP and DTEP populations and return to control levels in REL cells by day 50. This data provides further evidence that gene expression changes induced in day 7 DTPs are gradually reversed with duration of SRA737 withdrawal, indicating that cells may be returning to a pre-treatment state.

A final group of genes were found to be affected by time (group 3), with their mRNA abundance gradually increasing in both drug-treated and time-matched drug-naïve controls. This finding is perhaps not surprising but provides measurable evidence that long-term 2D culture *in vitro* can induce gene expression changes in cells. These changes may account for the small divergence of the day 30 and day 50 drug-naïve control samples in the MDS plot (Figure 4-5); although it should be noted that these time-dependent changes are of a much smaller magnitude than those driven by compound treatment. Genes in this cluster (group 3) were excluded from all groups in subsequent GSEA analyses.

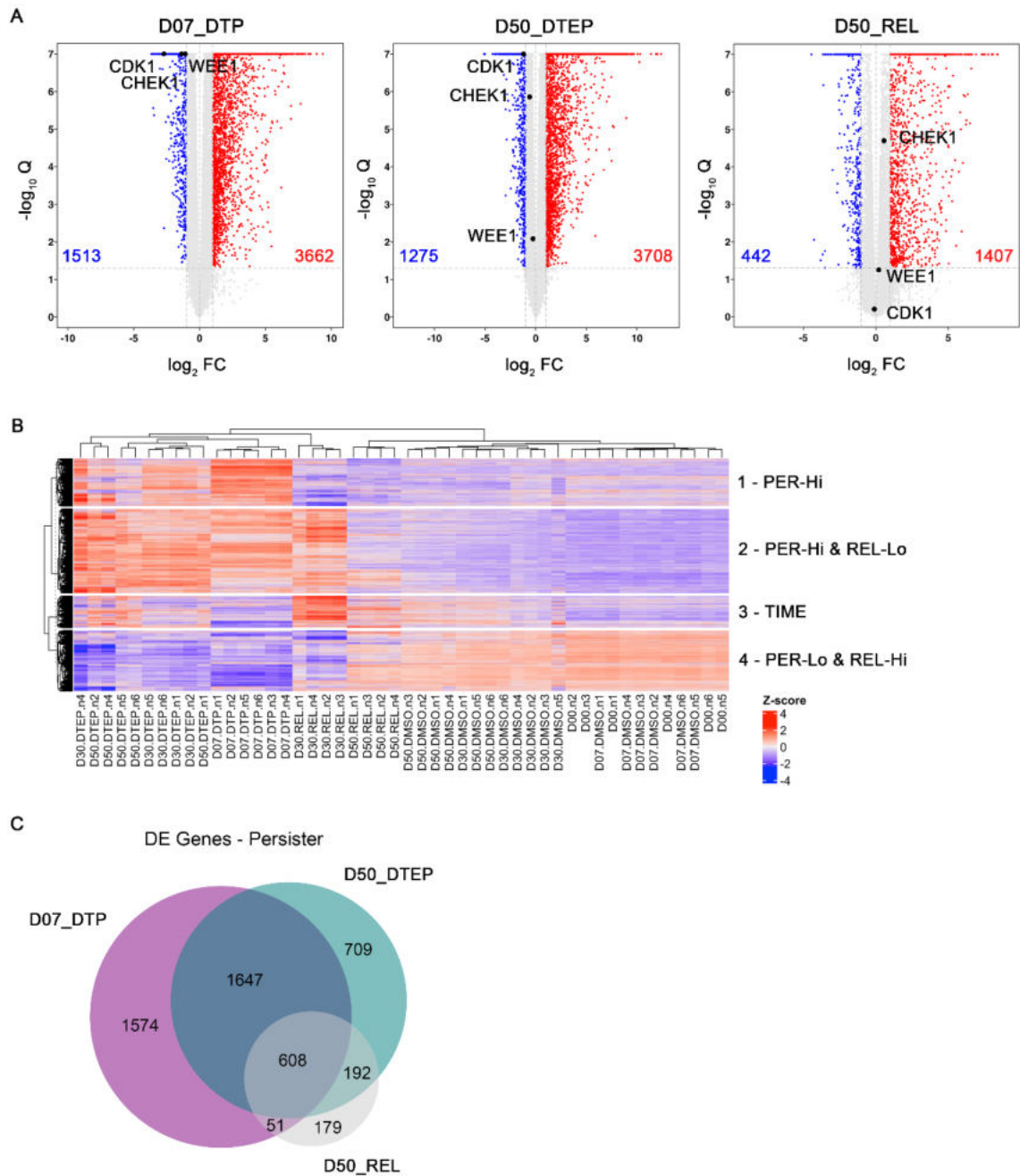


Figure 4-6: Persister cell populations adopt distinct gene expression profiles.

(A) Differentially expressed genes in day 7 DTPs (left), day 50 DTEPs (middle), and day 50 drug-released (REL; right) populations versus Day 0 control (AbsFC ≥ 2 , FDR $< 5\%$). Values correspond to number of downregulated (blue) or upregulated (red) genes. **(B)** Hierarchical clustering of differentially expressed genes in DTP, DTEP, REL and drug-naïve control (D00 & DMSO) populations. **(C)** Venn diagram of common and uniquely differentially expressed genes in DTP, DTEP, and REL populations.

4.4.2. GSEA reveals common transcriptional alterations in different persister cell populations

Comparison of differentially expressed genes from DTP, DTEP, and REL populations revealed both common and unique transcriptional alterations. DTPs and DTEPs shared >50% of gene expression changes (Figure 4-6C), indicating that a considerable proportion of gene expression changes occurring in day 7 DTPs are maintained in the DTEP state at day 50. This suggests that these genes may be required not only for DTP formation, but also subsequent survival and progression. Conversely, 40% and 23% of changes were unique to DTPs and DTEPs, respectively, suggesting that other transcriptional alterations also play a role. The majority of differentially expressed genes in REL cells were shared with either DTPs (64%), DTEPs (78%), or both (83%). The expression of 608 genes were commonly altered in all populations, accounting for 16%, 19%, and 83% of total changes in DTP, DTEP, and REL populations, respectively. This data reveals common and unique gene expression changes in DTP, DTEP, and REL populations that could represent potential persister cell mechanisms.

To further characterise the transcriptional changes underlying these cell states and discover potential persister cell mechanisms, GSEA was used to identify enriched and depleted MSigDB Hallmark gene sets that are common to DTP and DTEP populations. A total of 5 out of 50 hallmark gene sets were significantly downregulated, including E2F targets and cell cycle related genes (G2/M checkpoint control, Mitotic spindle, MYC targets) (Table 4-3). This is perhaps unsurprising given the reduced proliferation rate in DTPs (Figure 3-5C-E) and is consistent with others reporting similarly altered pathways in DTPs generated with alternative agents (Liau et al. 2017; Oren et al. 2021; Rehman et al. 2021), suggesting that downregulation of cell cycle related genes is a common persister cell characteristic. By contrast, 21 gene sets were significantly upregulated (Table 4-3) including genes related to apoptosis and EMT. This is consistent with the observed induction of apoptosis in SRA737-induced DTPs (Figure 3-6A) and provides molecular confirmation of morphological changes observed by microscopy during DTP-to-DTEP transition (Figure 3-4C). Notably, several gene

sets related to cytokine signalling, such as IL-2/STAT5 signalling and interferon gamma (IFN γ) response, were upregulated, suggesting that engagement of these pathways may be important for DTP formation and progression.

Together, GSEA has revealed common transcriptional alterations in persister cell populations arising in response to SRA737 exposure. While adding to persister cell characterisation within this novel therapeutic context, these alterations could also represent potentially targetable mechanisms to abrogate DTP formation and progression.

Table 4-3: Commonly enriched Hallmark gene sets from the MSigDB database in DTP and DTEP populations.

Terms are ordered by adjusted p-value.

Enriched Terms: MSigDB_HALLMARKS, Adjusted p-value <0.05 Common to D07_DTP & D50_DTEP	
Downregulated	Upregulated
E2F Targets	TNF-alpha Signaling via NF-kB
G2-M Checkpoint	Epithelial Mesenchymal Transition
Mitotic Spindle	KRAS Signaling Up
Myc Targets V1	Hypoxia
Estrogen Response Late	Inflammatory Response
	Coagulation
	Interferon Gamma Response
	Apoptosis
	IL-2/STAT5 Signaling
	Myogenesis
	UV Response Dn
	Complement
	p53 Pathway
	Estrogen Response Early
	IL-6/JAK/STAT3 Signaling
	Allograft Rejection
	Xenobiotic Metabolism
	Interferon Alpha Response
	Angiogenesis
	Apical Junction
	Estrogen Response Late

4.4.3. Persister cells express gene signatures related to senescence, diapause, and quiescence

As measured by increased β -galactosidase activity, a large proportion of SRA737-induced DTPs are senescent (Figure 3-6C). To investigate if this is also represented at the transcriptional level, RNAseq data from DTP, DTEP, and REL cells were evaluated for the expression of a universal senescence signature derived from multiple *in vitro* immortalisation and senescence models (Fridman and Tainsky 2008). This signature was significantly elevated in DTPs (Figure 4-7A), providing molecular confirmation of the observed senescence phenotype at day 7. Surprisingly, the signature was increased to a similar level in DTEPs. The senescence gene signature score was significantly reduced in REL cells compared to DTEPs, indicating a partial return to the drug-naïve state following SRA737 withdrawal (Figure 4-7A).

Previously characterised persister cells express genes related to embryonic diapause (Rehman et al. 2021; Dhimolea et al. 2021); a reversible state of arrested embryonic development that is triggered in response to unfavourable environmental conditions, such as nutrient deprivation (reviewed in (Fenelon, Banerjee, and Murphy 2014)). A gene signature derived from diapaused embryos (Boroviak et al. 2015; Rehman et al. 2021) was significantly elevated in DTPs, DTEPs, and, to a lesser extent, REL cells (Figure 4-7B), indicating that SRA737-induced DTPs also enter a diapause-like state. Surprisingly, the diapause signature score was also increased in day 50 drug-naïve control samples, perhaps suggesting that long-term culture contributes to the expression of these genes (time-effected genes were not excluded from this analysis) or mimics unfavourable environmental conditions.

The DTP state is often compared to dormancy, quiescence, and stemness. To determine if persister populations in the present study share similarities with these cellular phenotypes, RNAseq data was similarly assessed for expression of a quiescent neural stem cell signature (Llorens-Bobadilla et al. 2015). Gene signature scores were significantly increased in DTP and DTEP populations

(Figure 4-7C), suggesting that persister cells may also adopt a stem cell-like phenotype. Consistent with their transition to a more pre-treatment-like state, drug-released cells had a reduced gene signature score compared to DTEPs.

Together, this data demonstrates that persister populations are likely to engage multiple transcriptional programmes to adopt various cellular states associated with dormancy.

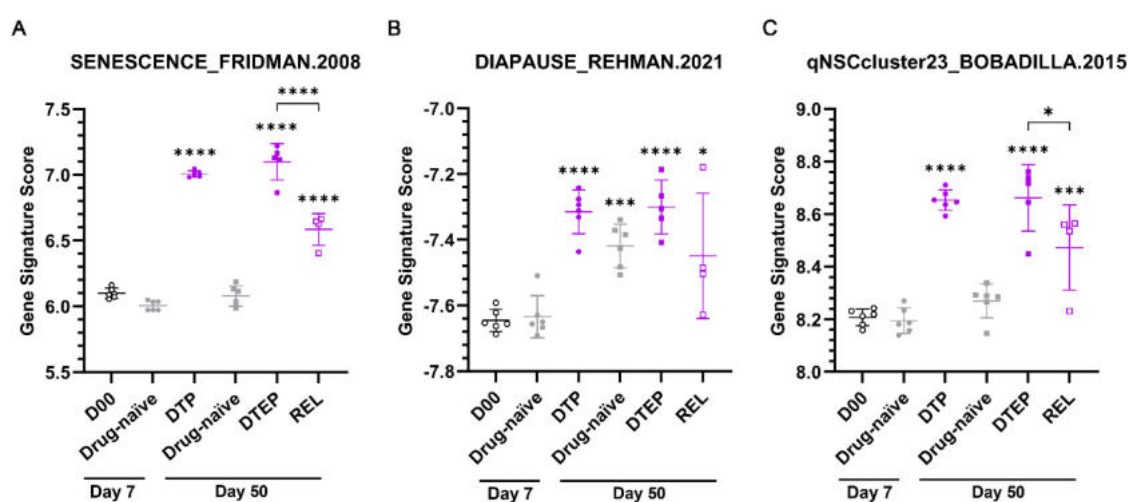


Figure 4-7: Persister cells express dormancy-related gene signatures.

(A) Senescence, (B) embryonic diapause, or (C) neural stem cell quiescence gene signature scores in SRA737-induced DTPs, DTEPs, drug-released (REL) and drug-naïve control (D00 & drug-naïve) populations. Graphs show mean \pm SD of $n \geq 4$ independently generated populations. Significance statements result from comparison of means versus D00, unless otherwise indicated, by ordinary one-way ANOVA with Šídák's correction. **** $p < 0.0001$; *** $p < 0.001$; * $p < 0.05$.

4.5. Characterising dose-escalated SRA737 resistant populations

Transition through the DTP bottleneck is one route by which cancer cells can acquire drug-resistance. Most drug resistance models are generated for *in vitro* studies by dose-escalation; wherein cells are gradually exposed to increasing drug concentration until proliferation is unconstrained at lethal doses. While several recent studies have used this approach to identify mechanisms of CHK1i resistance (Blosser et al. 2020; Nair et al. 2020; Zhao et al. 2021; Lee et al. 2020; Hunter et al. 2022), it is unclear whether the same strategies would emerge from a persister-derived drug-resistant population. CHK1 overexpression, for example, was not observed in DTEPs (Figure 4-1C) but has been reported in a dose-escalated model of resistance to the CHK1i prexasertib (Blosser et al. 2020). To identify additional differences, I generated a dose-escalated model of SRA737 resistance in SK-N-AS cells and compared them to DTEP populations. A minimum of three independently derived dose-escalated populations were generated for these studies.

4.5.1. Dose-escalated populations are insensitive to further challenge with SRA737

SRA737 dose-escalation in SK-N-AS cells was carried out over a period of three months. Cells were proliferating in 1 μM SRA737 by day 37 and routinely maintained in 10 μM by day 63 (Figure 4-8A & 4-8B). To evaluate acquisition of drug resistance, escalated populations were tested for SRA737 sensitivity by cell viability assay. Dose-escalated populations were less sensitive to SRA737 than drug-naïve controls, with GI_{50} values increased by ~5- and ~80-fold in those escalated to 1 μM or 10 μM , respectively. (Figure 4-8C & Table 4-4). In addition, the cytotoxic effects at high SRA737 concentration observed in drug-naïve controls were abrogated in escalated populations. These changes in SRA737 sensitivity are comparable to those observed in DTEP populations (Figure 4-1B & Table 4-1).

To date, no CHK1 'gatekeeper' mutations have been reported in resistant populations generated with the CHK1i prexasertib (Blosser et al. 2020; Nair et al. 2020; Zhao et al. 2021), arguing against mutation of the drug binding site as a primary mechanism of resistance. Consistent with this, gemcitabine-induced CHK1 autophosphorylation at Ser-296 continued to be inhibited by SRA737 in a dose-dependent manner in SRA737 dose-escalated cells (Figure 4-8D). In contrast to DTEPs, SRA737-mediated inhibition of pS296-CHK1 appeared to be less effective in escalated cells compared to drug-naïve controls. This was confirmed by quantitative analysis of pS296-CHK1 levels that revealed a ~4-fold drop-off in SRA737 IC₅₀ value (Figure 4-8E) and is consistent with the observation that escalated populations are less sensitive to SRA737 by proliferation assay (Figure 4-8B). A potential reason for this might be the upregulation of total CHK1 in this population (Figure 4-8D). Indeed, total CHK1 levels were unchanged in DTEP or released populations compared to drug-naïve controls (Figure 4-1C & 4-1D) suggesting different mechanisms may be employed by differentially generated SRA737 resistant populations. Nonetheless, as CHK1 phosphorylation continues to be dose-dependently inhibited by SRA737, and is maximally inhibited at 10 µM, resistance is unlikely to be accounted for by mutation of CHK1 drug binding site. Unlike for DTEPs, however, these investigations do not exclude upregulated drug efflux as a mechanism of SRA737 resistance.

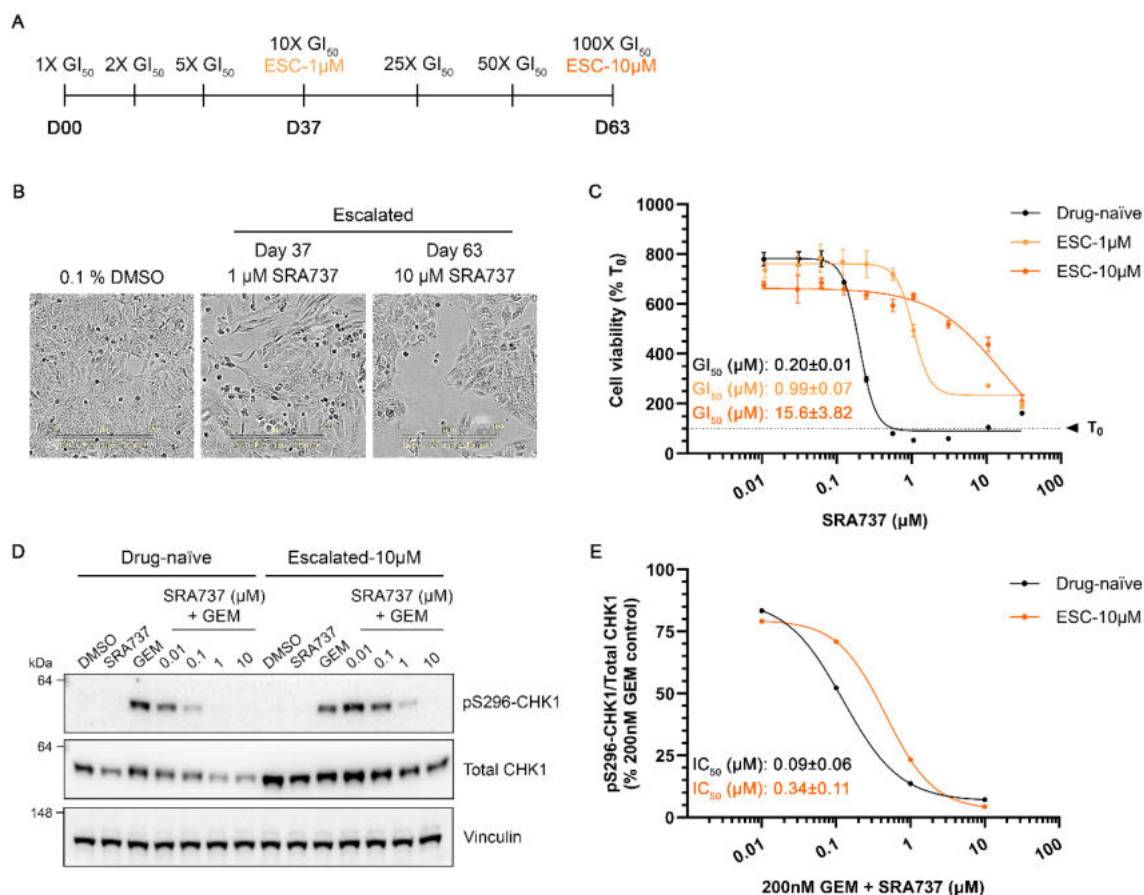


Figure 4-8: Dose-escalated SK-N-AS populations have a distinct resistance phenotype.

(A) Schematic protocol for generation of dose-escalated SRA737 resistant cell populations. **(B)** Phase contrast microscopy images of SK-N-AS cells after dose-escalation to 1 μM and 10 μM SRA737, or 0.1% DMSO as vehicle control. **(C)** Non-linear regression analysis of SK-N-AS cell viability measured by CellTiter-Glo® 120h after SRA737 addition in indicated populations. **(D)** Western blot analysis of CHK1 activity in drug-naïve and 10 μM SRA737 escalated (ESC-10 μM) cell populations after 24h exposure to 200 nM gemcitabine (GEM) \pm SRA737 at indicated concentrations, or 10 μM SRA737 alone (SRA737). **(E)** Non-linear regression analysis of pS296-CHK1 biomarker modulation measured by scanning densitometry in indicated populations treated as in (D). Images captured at 10X magnification, scale bar = 300 μm . Graphs show (C) mean \pm SD of three technical replicates and is representative of n=4 experiments, or (E) representative curves from n=3 experiments. GI₅₀ values are mean \pm SD of ≥ 3 independent experiments.

4.6. Dose-escalated cells are also cross-resistant to additional small molecule DDR inhibitors

Escalated populations were next tested for sensitivity to additional CHK1/CHK2 and DDR inhibitors to investigate differences in drug sensitivity profiles between persister-derived and dose-escalated cells.

Dose-escalated populations demonstrated considerable cross-resistance to the CHK1i LY2603618 and MK-8876, and the CHK1/2i AZD7762, as shown by ~40-fold reduction in GI₅₀ potency for all three agents (Figure 4-9 & Table 4-4). Similar results were reported in dose-escalated populations derived with the CHK1i prexasertib (Nair et al. 2020; Zhao et al. 2021), suggesting that SRA737 resistance may be acquired by the same mechanisms. Escalated cells were also less sensitive to gemcitabine and the ATRi VE822 and AZD6738, while there was minimal drop-off in GI₅₀ potency for the ATMi KU60019 and AZD1390. These results are similar to the findings in DTEPs (Figure 4-3 & Table 4-1), indicating a shared dysfunction in DDR signalling through the ATR-CHK1 axis, regardless of the route to therapeutic resistance. A notable exception is the differential response observed to the WEE1i. GI₅₀ value for AZD1775 was unchanged in DTEPs (Figure 4-3 & Table 4-1) but was reproducibly reduced by 2.3-fold in dose-escalated cells (Figure 4-9 & Table 4-4). A similar reduction in AZD1775 potency was observed in drug-released cells at day 50, and in SRA737-tolerant REL-1 at day 274 (Tables 4-1 & 4-2). Nonetheless, these data suggest that SRA737 resistance acquired through different routes can result in similar profiles of sensitivity to other compounds.

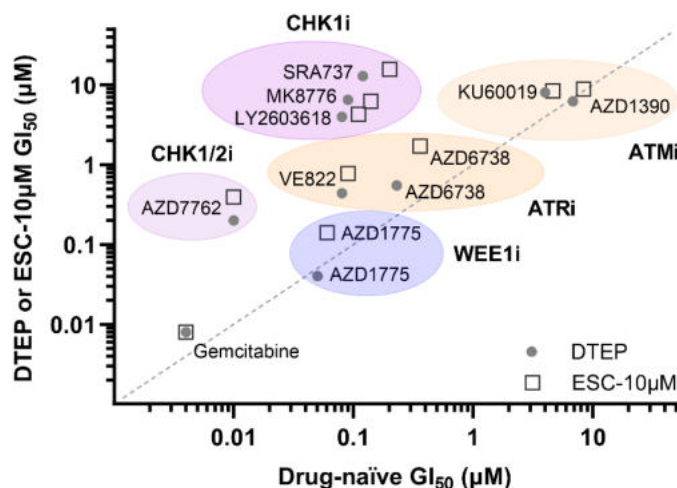


Figure 4-9: SRA737 resistant populations derived through the persister cell bottleneck or dose-escalation are similarly cross-resistant to additional DDR inhibitors.

Potency of additional DDR pathway inhibitors in drug-naïve (x-axis) and DTEP or escalated (ESC-10µM) (y-axis) populations. Graph shows mean GI_{50} value from $n \geq 2$ experiments. Dotted line represents line of identity.

Table 4-4: Summary of cellular potency values (GI_{50}) for indicated compounds in drug-naïve and 10 µM dose-escalated populations at day 71.

GI_{50} values are mean \pm SD. Cells are highlighted according to fold-increase in GI_{50} value compared to drug-naïve control. Red ≥ 50 -fold; orange ≥ 10 -fold; yellow ≥ 2 -fold.

Target	Compound	Population GI_{50} , µM (n)	
		Drug-naïve	Escalated-10µM
ATM	AZD1390	8.39 ± 1.36 (4)	8.92 ± 3.34 (4)
ATM	KU60019	4.63 ± 0.65 (4)	8.37 ± 3.10 (4)
ATR	AZD6738	0.36 ± 0.02 (4)	1.71 ± 0.47 (4)
ATR	VE822	0.09 ± 0.01 (4)	0.77 ± 0.31 (4)
CHK1	LY2603618	0.11 ± 0.01 (4)	4.30 ± 0.84 (4)
CHK1	MK8776	0.14 ± 0.01 (4)	6.24 ± 1.42 (4)
CHK1	SRA737	0.20 ± 0.01 (4)	15.57 ± 3.82 (4)
CHK1/2	AZD7762	<0.01 ± 0.00 (4)	0.39 ± 0.11 (4)
DNA	Gemcitabine	0.004 ± 0.000 (4)	0.008 ± 0.002 (4)
WEE1	AZD1775	0.06 ± 0.01 (4)	0.14 ± 0.04 (4)

4.7. Gene expression profiles are altered in dose-escalated SRA737-resistant populations

4.7.1. Dose-escalated SRA737-resistant cells harbour transcriptional changes

To further characterise dose-escalated resistant populations, cells escalated to 1 μM (ESC-1 μM) or 10 μM (ESC-10 μM) SRA737 were collected for RNAseq, and data subsequently interrogated using GSEA.

The top two dimensions identified by MDS explained 38% (dim-1) and 24% (dim-2) of the variance in the data (Figure 4-10). MDS plotting of gene expression data revealed differential clustering of ESC-1 μM (blue triangles) and ESC-10 μM (blue circles) resistant populations. These clusters were similarly altered according to dim-2 but showed a considerable difference in dim-1, suggesting both common and unique transcriptional changes in each of the dose-escalated populations. Furthermore, clusters were more spread out indicating differential gene expression changes among independently derived populations that were generated in the same manner. Of note, day 37 and day 63 drug-naïve controls (green triangles, circles) clustered distantly from day 0 samples (D00; pink open circles), indicating considerable transcriptional changes during the course of the experiment. Drug-naïve data points were also spread out, suggesting there was more variation between these independently generated replicate samples.

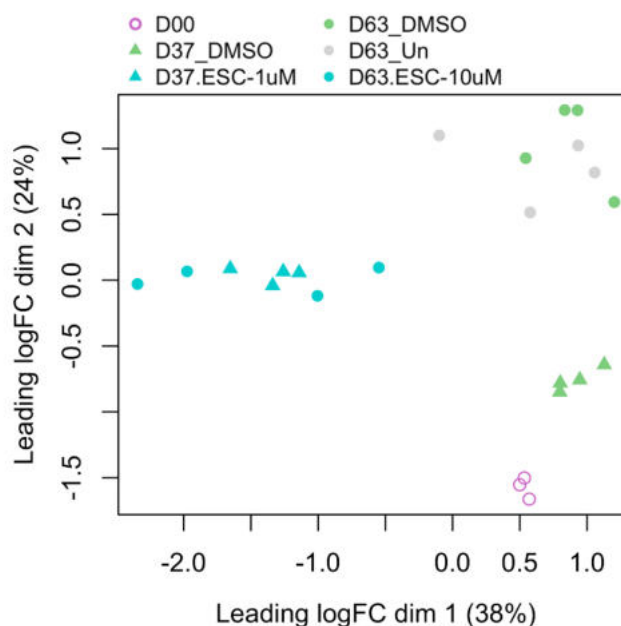


Figure 4-10: Transcriptional profiles are altered in dose-escalated SRA737-resistant populations.

Multi-dimensional scaling (MDS) of RNAseq expression data from dose-escalated populations (ESC-1 μ M & ESC-10 μ M) and drug-naïve control (D00, DMSO & Untreated (Un)) populations.

A total of 1298 and 1870 genes were differentially expressed (AbsFC \geq 2, FDR <5%) in ESC-1 μ M and ESC-10 μ M resistant cells, respectively (Figure 4-11A). The number of differentially expressed genes in DTP and DTEP populations was \sim 4X higher (Figure 4-6A), suggesting that SRA737 resistance achieved by dose-escalation requires fewer transcriptional changes. Over 85% of gene expression changes were accounted for by upregulation in ESC-1 μ M and ESC-10 μ M populations (Figure 4-11A). This is slightly higher than observed for persister cell populations, in which 70-76% of genes were upregulated (Figure 4-6A). Total CHK1 protein levels were increased in ESC-10 μ M cells (Figure 4-8D), however *CHEK1* mRNA expression was not significantly upregulated (Figure 4-11A; right panel).

As observed for persisters, hierarchical clustering of differentially expressed transcripts revealed four groups of genes with similar patterns of expression (Figure 4-11B). Group 2 is clustered by genes whose mRNA is higher in abundance in ESC-1 μ M and ESC-10 μ M populations compared to drug-naïve control cells. On the other hand, group 4 is defined by genes that are low in abundance in dose-escalated cells but high in control populations. These genes likely represent those that are altered by acquisition of drug resistance, since their expression is specifically modified only in samples treated with SRA737. In contrast to persister cells, this analysis revealed a much larger group of genes that were affected by time (groups 1 & 3), as shown by their progressively increased mRNA abundance in time-matched controls. These genes were excluded from all groups in subsequent GSEA analysis.

Comparison of differentially expressed genes from ESC-1 μ M and ESC-10 μ M cells revealed both common and unique transcriptional alterations. Approximately 50% of gene expression changes are shared between the two dose-escalated populations, with the remaining 50% being uniquely altered (Figure 4-11C).

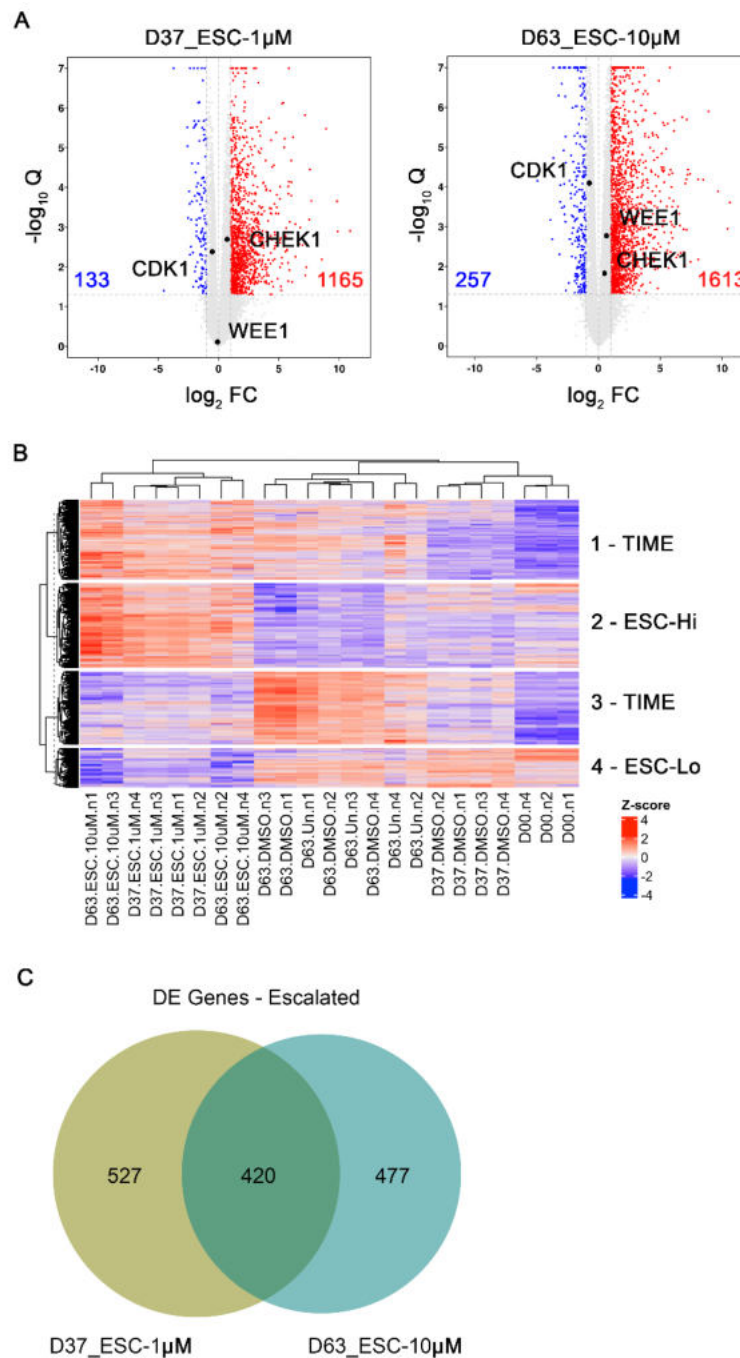


Figure 4-11: Dose-escalated SRA737-resistant populations have altered transcriptional profiles.

(A) Differentially expressed genes in day 37 ESC-1 μ M (left) and day 63 ESC-10 μ M (right) populations versus day 0 (D00) control (AbsFC \geq 2, FDR $<$ 5%). Values correspond to number of downregulated (blue) or upregulated (red) genes. **(B)** Hierarchical clustering of differentially expressed genes in ESC-1 μ M and ESC-10 μ M populations and drug-naïve controls (D00, UN & DMSO). **(C)** Venn diagram showing common and uniquely differentially expressed genes in ESC-1 μ M and ESC-10 μ M populations.

4.7.2. GSEA reveals common transcriptional alterations in dose-escalated populations

To further characterise the transcriptional changes underlying the dose-escalated drug-resistant state and identify mechanisms involved in the acquisition of SRA737 resistance, GSEA was used to identify enriched and depleted MSigDB Hallmark gene sets that are common to ESC-1 μ M and ESC-10 μ M.

No hallmark gene sets were commonly downregulated in ESC-1 μ M and ESC-10 μ M populations. This is likely a reflection of the minimal number of genes (<15%) found to be downregulated in either of these samples (Figure 4-11A). Of note, cell cycle related genes were significantly downregulated in DTP and DTEP populations (Table 4-3). The absence of these enrichments here indicate that dose-escalated cells do not adopt a slow-cycling state during acquisition of drug-resistance. This is supported by cell viability data in which ESC-1 μ M and ESC-10 μ M populations proliferated as much as drug-naïve controls during a 5-day proliferation assay (Figure 4-8C). In contrast, 12 out of 50 hallmark gene sets were significantly upregulated in both dose-escalated populations (Table 4-5), including genes related to apoptosis, EMT, and TNF α /NF κ B signalling. Interestingly, all of these gene sets were also significantly upregulated in DTP and DTEP populations. This suggests that dose-escalated and persister-derived SRA737-resistant populations share transcriptional alterations and potentially employ similar mechanisms on the journey to drug-resistance. A limitation of this analysis is that only the Hallmark gene set collection was interrogated, which consists of a relatively small number of gene sets. Further investigation using larger collections, such as gene ontology (containing 10,532 gene sets), will help to identify potential similarities or differences between differentially derived SRA737-resistant populations.

Table 4-5: Commonly enriched Hallmark gene sets from the MSigDB database in dose-escalated populations.

Terms are ordered by adjusted p-value.

Enriched Terms: MSigDB_HALLMARKS, Adjusted p-value <0.05 Common to D37_ESC-1 μ M & D63_ESC-10 μ M	
Downregulated	Upregulated
N/A	Epithelial Mesenchymal Transition TNF-alpha Signaling via NF-kB Coagulation Estrogen Response Early Complement Hypoxia KRAS Signaling Up Inflammatory Response Apoptosis UV Response Dn Estrogen Response Late Apical Junction

4.7.3. Gene signatures related to senescence and quiescence are elevated in dose-escalated populations

In light of the similarities in Hallmark gene set enrichments between dose-escalated and persister populations, I wondered if this extended to expression of the senescence, diapause, or quiescent gene signatures. Indeed, scores for the senescence and quiescent stem cell signatures were significantly increased to comparable levels in ESC-1 μ M and ESC-10 μ M populations (Figure 4-12A & 4-12C). While gene signature scores were not increased to quite the same magnitude as persisters (Figure 4-7A & 4-C), these results indicate that upregulation of these transcriptional programmes is a common response to drug challenge with SRA737. By contrast, expression of genes related to embryonic diapause were unaltered in ESC-1 μ M and ESC-10 μ M cells (Figure 4-12B), suggesting that this represents a persister-specific response. However, this conclusion is challenged by the observation that gene scores were significantly increased in drug-naïve controls versus D00.

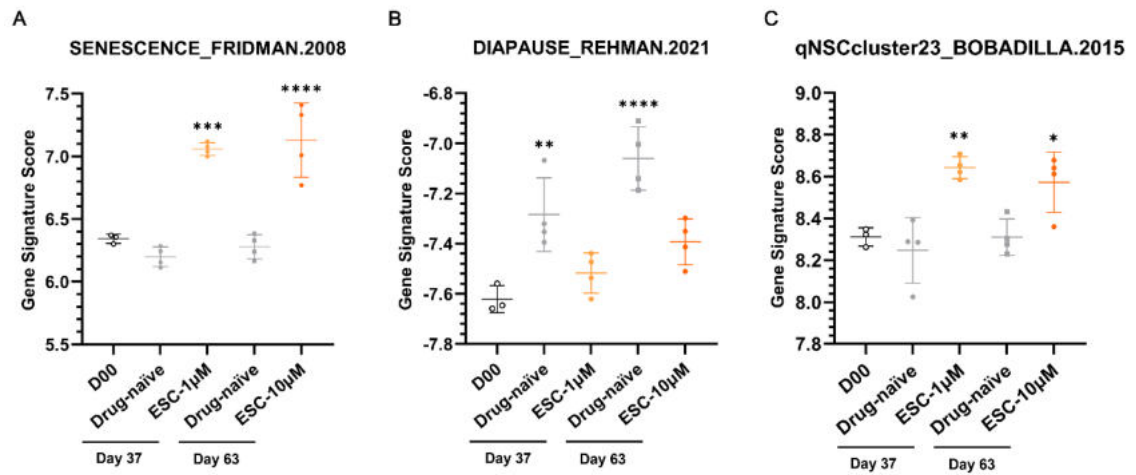


Figure 4-12: Dose-escalated SRA737-resistant cells express senescence and quiescence-related gene signatures.

(A) Senescence, (B) embryonic diapause, or (C) neural stem cell quiescence gene signature scores in SRA737-resistant ESC-1µM and ESC-10µM populations and drug-naïve controls (D00 & drug-naïve). Graphs show mean±SD of $n \geq 3$ independently generated populations. Significance statements result from comparison of means versus D00 by ordinary one-way ANOVA with Šídák's correction. **** $p < 0.0001$; *** $p < 0.001$; ** $p < 0.01$; * $p < 0.05$.

4.8. Comparison of persister and dose-escalated populations reveals persister-specific mechanisms of SRA737 drug-resistance

4.8.1. The ATR-CHK1 DDR signalling axis is differentially altered in persister-derived and dose-escalated SRA737 resistant populations

Drug sensitivity profiling indicated that dysregulation of DDR signalling could represent a common SRA737-resistance mechanism adopted by persister-derived and dose-escalated populations (Figure 4-9). To characterise this further, biomarker activity in the ATR-CHK1 signalling axis was investigated in response to genotoxic stress. DTEP, drug-released, and dose-escalated cells were pre-treated for 1 h with increasing doses of SRA737 prior to induction of DNA damage using 200 nM gemcitabine. Cells were collected 24 h later and biomarkers of ATR-CHK1 DDR signalling activity investigated by Western blotting.

CHK1 activation in response to DNA damage leads to downstream phosphorylation and inhibition of CDK1 at Tyr-15, resulting in cell cycle arrest and DNA repair (O'Connell et al. 1997). This is repressed in the context of CHK1 inhibition, promoting DNA instability and subsequent cell death (Walton et al. 2016). DNA damage can be measured experimentally as an increase in γ H2AX (Mah, El-Osta, and Karagiannis 2010). Indeed, CDK1 phosphorylation at Tyr-15 (pY15-CDK1) and γ H2AX were induced in drug-naïve cells treated with 200 nM gemcitabine (Figure 4-13A, 4-13B & 4-13C). Gemcitabine-induced pY15-CDK1 was abrogated by addition of SRA737 and was concomitant with increased γ H2AX levels, demonstrating robust induction of DNA damage. In DTEP, drug-released and dose-escalated cells, gemcitabine similarly induced CDK1 phosphorylation, which was inhibited by the addition of SRA737 (Figure 4-13A, 4-13B & 4-13C, respectively). However, in DTEP and dose-escalated populations this failed to translate into apoptotic cell death, indicated by a relative reduction in PARP cleavage compared to drug-naïve controls (Figure 4-13A & 4-13C). In drug-released cells, PARP cleavage was observed at the highest doses of SRA737 in combination with gemcitabine (Figure 4-13B), suggesting CHK1i-

induced cell death was only partially inhibited in these cells. Drug-induced increases in γ H2AX were attenuated in DTEPs and, to a lesser extent, in drug-released and dose-escalated cells, indicating that DNA damage does not accumulate in these populations despite effective CHK1 inhibition. These data confirm functional DDR signalling through the ATR-CHK1 axis in DTEP, drug-released, and dose-escalated cells that is inhibited by SRA737, suggesting that aberrant DDR responses do not account for SRA737 resistance in these populations.

WEE1 upregulation has been implicated in dose-escalated models of resistance using the CHK1i prexasertib (Zhao et al. 2021). In agreement with this, WEE1 protein levels were increased in SRA737 dose-escalated cells (Figure 4-13C); a finding that is consistent with decreased sensitivity of the escalated population to WEE1i. Total CHK1 levels were also increased in dose-escalated cells. Interestingly, no increase was observed in *WEE1* or *CHEK1* mRNA expression (Figure 4-11A; right panel), suggesting that post-translational mechanisms may be responsible for the upregulation of these proteins. These changes were not observed in DTEPs (Figure 4-13A), indicating that WEE1 and CHK1 upregulation may specifically represent dose-escalated SRA737 resistance mechanisms. Interestingly, both total CHK1 and WEE1 protein levels were upregulated in drug-released cells relative to drug-naïve controls (Figure 4-13B). This could be explained by a rebound increase in protein expression following SRA737 withdrawal and exit from the DTP state. As observed for dose-escalated cells, these increases were not due to upregulated expression of *CHEK1* or *WEE1* at the transcript level (Figure 4-6A; right panel). In contrast, total CDK1 protein and mRNA were reduced in DTEPs but remained unchanged in released and dose-escalated populations (Figures 4-13A-4-13 & 4-6; middle panel), highlighting a potential DTEP-specific SRA737 resistance mechanism.

Taken together, these results confirm that the ATR-CHK1 signalling axis is functionally intact and CHK1 continues to be inhibited by SRA737 in DTEP, drug-released, and dose-escalated populations. Resistance to SRA737 appears to be achieved, in part, by compensatory signalling and/or rewiring in the DDR

pathway; however the exact mechanisms employed differ depending on the route taken.

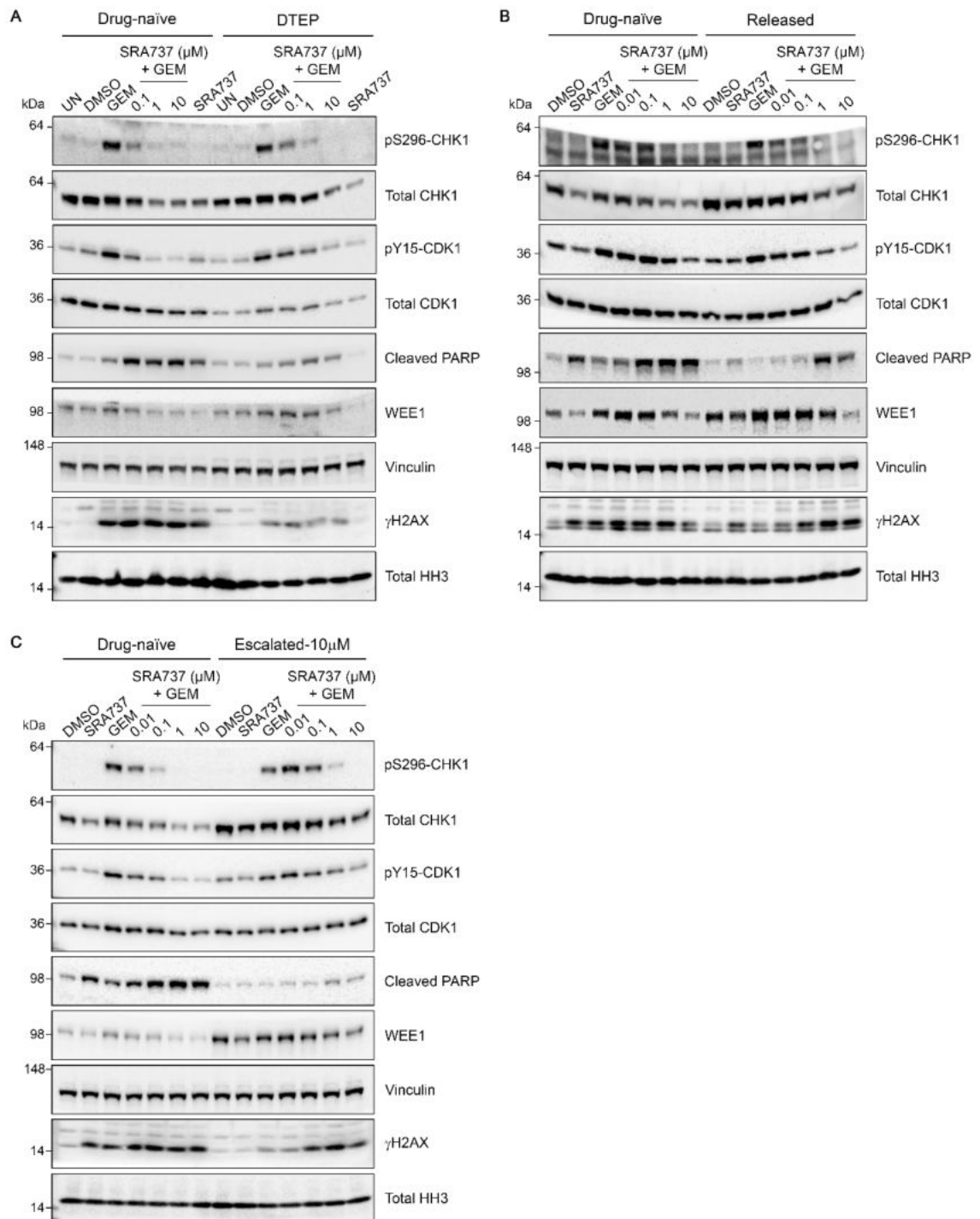


Figure 4-13: Persister-derived and dose-escalated SRA737 resistant populations harbour distinct alterations in the ATR-CHK1 DDR signalling axis.

(A - C) Western blot analysis of CHK1 activity biomarkers in (A) DTEP, (B) drug-released, and (C) 10 μM dose-escalated cells after 24h exposure to 200 nM gemcitabine (GEM) ± SRA737 at indicated concentrations, or 10 μM SRA737 alone (SRA737).

4.8.2. Dose-escalated cells are more sensitive to WEE1/CHK1 inhibitor combination treatment than DTEPs

CHK1i resistant cells generated by dose-escalation using the CHK1i prexasertib upregulate WEE1 expression and are resensitised to CHK1i by combination treatment with a WEE1 inhibitor (Zhao et al. 2021). Consistent with this, dose-escalated SRA737-resistant populations generated in the present study overexpress WEE1 protein (Figure 4-13C) and are less sensitive to further challenge with WEE1i AZD1775 (Figure 4-9 & Table 4-4). In contrast, WEE1 overexpression is not observed in SRA737-induced DTEPs (Figure 4-13A) and DTEPs show a minimal reduction in sensitivity to AZD1775 (Figure 4-3 & Table 4-1). To investigate to what extent this mechanism is shared between differentially derived SRA737-resistant populations, DTEPs and dose-escalated cells were pre-treated with 60 nM AZD1775, representing a non-toxic dose (Appendix Figure 2), for 24 h and then tested for SRA737 sensitivity.

SRA737 GI_{50} potency was increased 4.2-fold by the addition of AZD1775 in DTEPs (Figure 4-14A). However, the GI_{50} value for SRA737 under combination was still ~15X higher in DTEPs compared to SRA737 alone in drug-naïve controls. These results demonstrate that WEE1i combination partially resensitises DTEPs to SRA737. A greater effect was observed in dose-escalated cells. The SRA737 GI_{50} value was reduced by >10-fold upon AZD1775 addition (Figure 4-14B). Furthermore, SRA737 potency was restored to near control levels, illustrating that dose-escalated cells are more sensitive to WEE1i combination than DTEP populations.

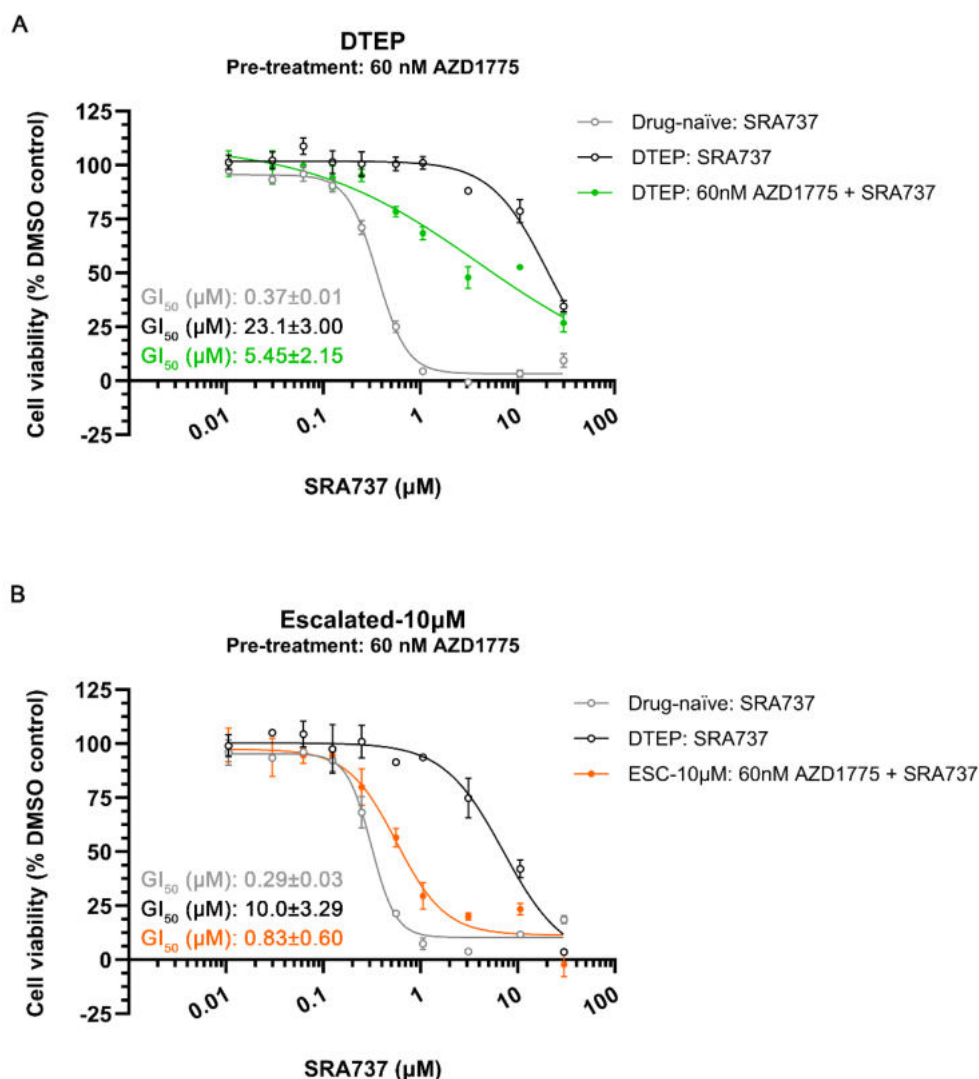


Figure 4-14: Dose-escalated cells are more sensitive to WEE1 and CHK1 inhibitor combination.

(A & B) Non-linear regression analysis of SK-N-AS cell viability measured by CellTiter-Glo® 120h after compound addition in (A) DTEP and (B) 10 μM dose-escalated populations, along with their respective drug-naïve controls. Dose-response curves generated following treatment with SRA737 alone, or SRA737 after 24h pre-treatment with 60 nM AZD1775 (WEE1i). Graphs show mean \pm SD of three technical replicates and are representative of n=3 experiments. GI_{50} values are mean \pm SD of three independent experiments.

4.8.3. Epigenetic alteration is a persister cell specific strategy

Following the observation of global changes to the epigenetic landscape in persister cells (Figure 3-5G), histone H3 modifications were investigated in dose-escalated populations to determine if epigenetic mechanisms are similarly involved in mediating resistance to SRA737. In contrast to DTPs and DTEPs, H3K27_{me3} levels were minimally altered in ESC-1 μ M and ESC-10 μ M populations (Figure 4-15A & 4-15B). Furthermore, there were no concomitant decreases in H3K27_{me1} or H3K27_{ac}, and all other modifications remained unchanged. Nonetheless, these results suggest that while epigenetic mechanisms are important for persister cell responses, they may not be necessary for acquisition of SRA737 resistance in dose-escalated cells.

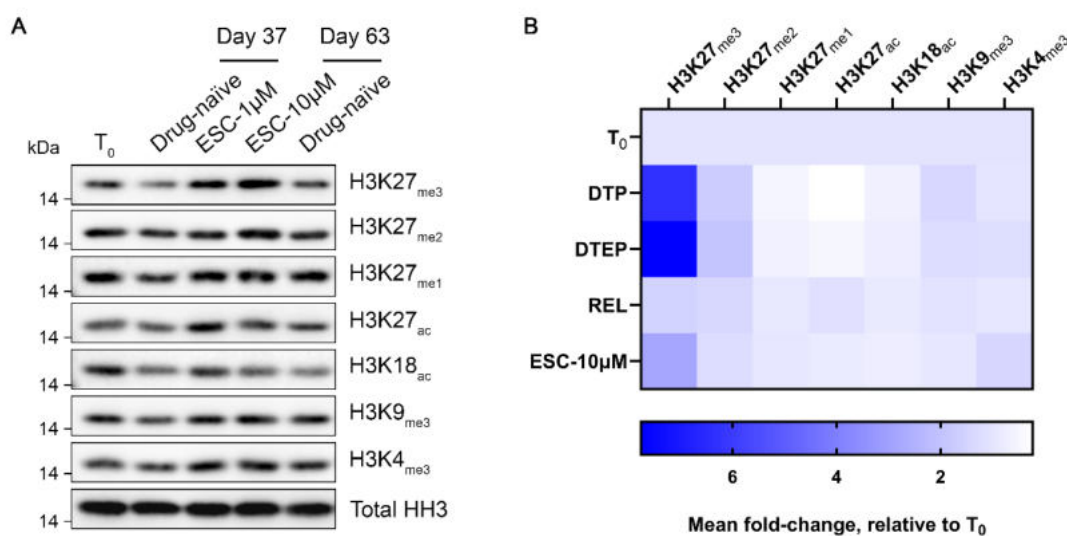


Figure 4-15: Epigenetic alterations are specific to persister-derived populations.

(A) Western blot analysis of histone H3 modifications in 1 μ M (ESC-1 μ M) and 10 μ M (ESC-10 μ M) SRA737 dose-escalated populations and respective controls. **(B)** Quantitative comparison of epigenetic changes in persister and dose-escalated cells relative to T₀. Heatmap shows mean fold-change in scanning densitometry signal from $n \geq 2$ experiments.

4.8.4. Identifying persister-specific mechanisms by comparison of RNAseq data

Analysis of RNAseq data from persister and dose-escalated populations revealed comparable alterations in their transcriptional profiles, indicating that they employ similar mechanisms en route to SRA737 resistance. However, the observation that considerably more genes are differentially expressed in DTP and DTEP populations (Figure 4-6A) suggests there may be unique transcriptional alterations that could represent potentially targetable persister-specific mechanisms. To identify these differences, gene expression data from persister and dose-escalated cells were compared.

Direct comparison of differentially expressed genes confirmed similar transcriptional alterations in DTEP and ESC-10 μ M populations, with 785 and 102 genes commonly up- or downregulated, respectively (Figure 4-16A). However the magnitude of change was stronger in DTEPs, as demonstrated by a higher proportion of datapoints below the line of identity. In addition, a number of genes were significantly upregulated in DTEPs but were undetected in ESC-10 μ M cells, confirming the presence of persister-specific transcriptional changes.

Differentially expressed genes from DTP, DTEP and ESC-10 μ M populations were interrogated by GSEA using the MSigDB Hallmarks, KEGG, Gene Ontology: Biological Process gene set collections, and transcription factor databases from ENCODE and CHEA. Result comparison identified 16 gene sets that were commonly enriched in DTP and DTEP populations, including those related to the IFN γ response and IL-2/STAT5 signalling (Figure 4-16B). As these genes are specifically enriched in persister populations, they could represent key biological pathways that are required for DTP formation, survival, and progression. This is supported by the unique enrichment of genes associated with IL-6/JAK/STAT3 signalling in DTPs. These results are consistent with reports from DTP models generated with TKi (Guler et al. 2017; Al Emran et al. 2018), indicating that these pathways represent common persister cell mechanisms. A total of 29 gene sets were commonly enriched in DTP, DTEP and ESC-10 μ M populations. Amongst these were genes associated with SUZ12

and EZH2 transcriptional activity (CHEA collection) which are both members of polycomb repressive complex 2 (PRC2). However, the observation that H3K27 methylation (H3K27_{me3}) is more prevalent in DTPs and DTEPs provides greater evidence for EZH2 activity as a persister-specific mechanism. This is further supported by the unique enrichment of EZH2-related genes from the ENCODE collection in DTPs.

Gene set expression data were subsequently interrogated to determine if these persister-specific pathways are up- or downregulated. For the IFN γ response gene set, the majority of genes were increased in DTP and DTEP populations (Figure 4-16C). These alterations were largely reversed in drug-released (REL) cells, although the expression of a subset of genes remained high at day 50. Similar patterns were observed for IL-2/STAT5 and IL-6/JAK/STAT3 signalling gene sets (Appendix Figure 3), suggesting engagement of cytokine signalling to support persister cell responses.

Similarly, the majority of differentially expressed genes in the EZH2 collection were increased in DTP and DTEP populations (Figure 4-16D), an effect that was partially reversed upon SRA737 withdrawal, with a subset of genes remaining highly expressed in REL cells. These results are surprising. If EZH2 activity is increased, as indicated by the enrichment of H3K27_{me3} in DTP and DTEP populations (Figure 3-5G), it should follow that the expression of target genes is repressed. Indeed, there are subsets of genes whose expression was reduced in DTP and DTEP cells versus Day 0 (D00), however this is not the predominant effect. This is perhaps consistent with the observation that most differentially expressed genes are upregulated (Figure 4-6A), despite a global increase in H3K27_{me3}, indicating that regulatory mechanisms to promote gene expression remain active. Furthermore, EZH2 has been reported to promote gene expression in some contexts by associating with activating transcriptional machinery through its transactivation domain (Jiao et al. 2020). Nonetheless, in combination with the observation that H3K27_{me3} is enriched in DTPs and DTEPs, these results indicate a role for EZH2 activity in persister cell formation and progression.

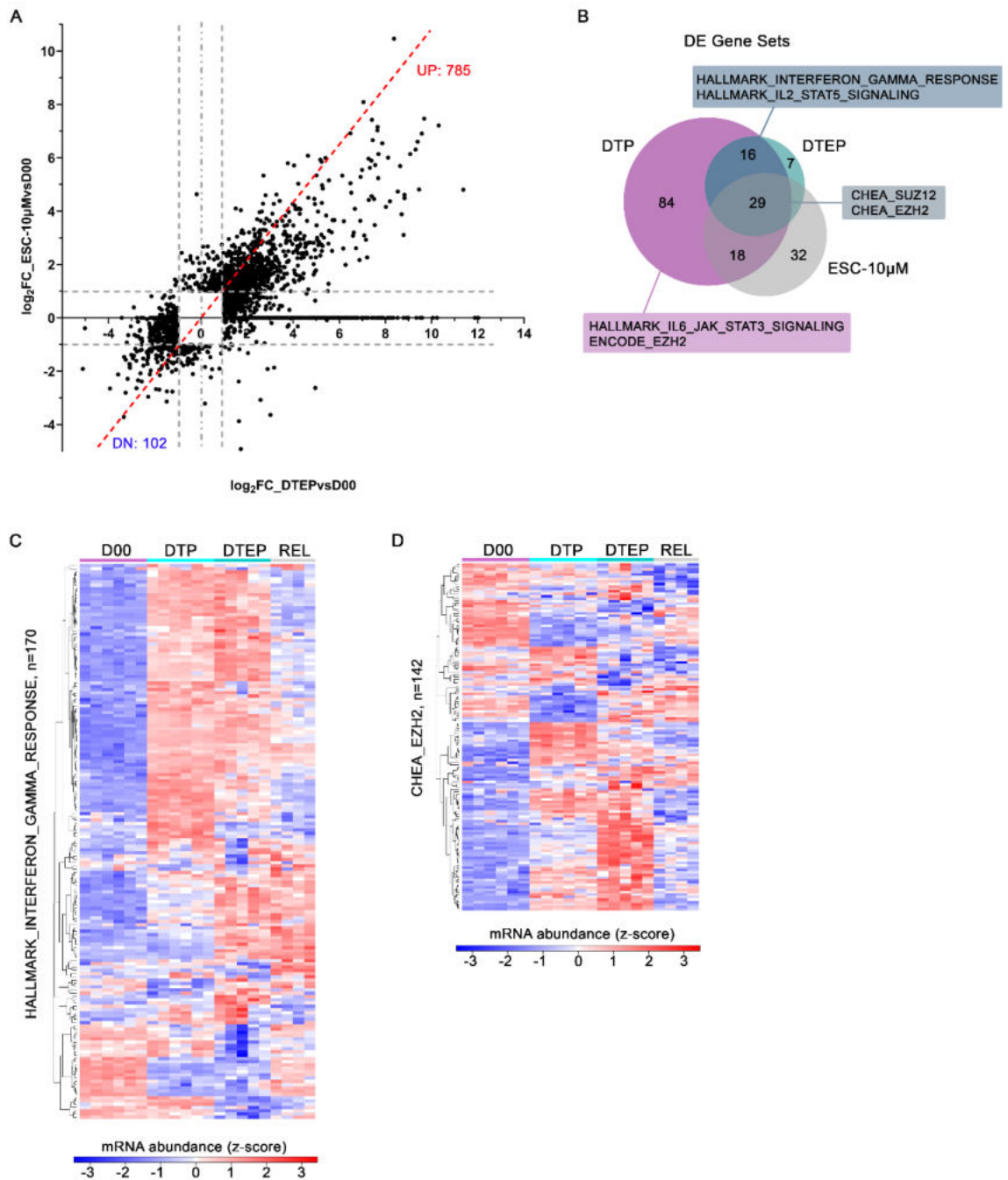


Figure 4-16: Persister populations harbour unique transcriptional alterations.

(A) Log₂ fold-change in differentially expressed genes (AbsFC ≥ 2, FDR < 5%) from day 50 DTEP (x-axis) and day 63 ESC-10µM (y-axis) populations. Values correspond to number of downregulated (blue) or upregulated (red) genes. Red line represents line of identity. **(B)** Venn diagram showing common and uniquely differentially expressed GSEA gene sets in DTP, DTEP, and ESC-10µM populations. Heatmaps showing log₂ normalised gene expression of differentially expressed genes within **(C)** interferon gamma response and **(D)** EZH2 gene sets in DTP, DTEP, drug-released (REL), and D00 control populations.

4.9. Discussion

DTEP populations that emerged during 50 days continuous lethal drug exposure were >100-fold less sensitive to SRA737 upon drug rechallenge. This was accompanied by cross-resistance to alternative small molecule CHK1i, and inhibitors of upstream ATR, demonstrating that persister populations generated using a specific agent can also acquire resistance to alternative agents targeting the same protein or pathway. DTEPs showed no collateral sensitivity to ATMi or CHK1/2i, suggesting that compensatory signalling through the parallel ATM-CHK2 DDR axis is not employed as a drug resistance strategy in SRA737-induced persisters. Similar alterations were observed in dose-escalated populations, indicating that SRA737 resistance acquired through different routes can result in similar behavioural outcomes. A notable exception to this was observed in response to the WEE1i AZD1775, in which dose-escalated cells, but not DTEPs, demonstrated a reproducible 2.3-fold decrease in drug sensitivity. Interrogation of the ATR-CHK1 signalling axis revealed specific upregulation of WEE1 protein expression in these cells, consistent with reports from other dose-escalated models of CHK1i resistance (Zhao et al. 2021). Accordingly, dose-escalated cells were resensitised to SRA737 when treated in combination with AZD1775, whereas GI₅₀ potency was only mildly increased in DTEPs. These results demonstrate that WEE1 upregulation is unlikely to be a driver of SRA737 resistance in persister populations and, as such, indicates drug resistance acquired through the DTP bottleneck is mediated by alternative mechanisms.

Although CHK1 activity continued to be inhibited and signalling through the ATR-CHK1 axis remained functional, induction of DNA damage (γ H2AX) and apoptosis (cleaved PARP) was attenuated in DTEP and dose-escalated cells following combination treatment with SRA737 and gemcitabine, suggesting that differentially generated SRA737 resistant populations undergo rewiring of the DDR signalling pathway to overcome genotoxic stress. While drug sensitivity data indicate that neither population relies on compensatory signalling, biomarkers of ATM-CHK2 activity were not investigated; this would be useful to confirm if SRA737 resistant populations engage alternative DNA repair pathways

to promote survival in the face of DNA damage. Despite these similarities, these investigations did reveal mechanistic differences between persister and dose-escalated populations. Total CDK1 protein levels were exclusively downregulated in DTEPs, while total CHK1 and WEE1 were specifically overexpressed in dose-escalated cells. Interestingly, neither *CHEK1* nor *WEE1* gene expression was increased in dose-escalated cells, suggesting that post-translational mechanisms may be responsible for the observed upregulation in these proteins. These results indicate that the exact mechanisms underlying DDR rewiring differ depending on the route to drug resistance. This conclusion is complicated by an added layer of complexity in light of differential results from biological replicates. For instance, total CHK1 levels were downregulated in one DTEP population but remained unchanged in another (Appendix Figure 4), and WEE1 overexpression was observed in three out of four individually generated dose-escalated populations (Appendix Figure 5). These observations demonstrate that drug resistant populations generated in the same way can adopt different mechanisms or alterations.

This phenomenon is further exemplified by observations from drug-released populations, which were initially exposed to a lethal dose SRA737 for 7 days to induce DTP formation and then cultured in drug-free medium for a further 43 days. As observed in DTEP and dose-escalated populations, SRA737 continued to inhibit CHK1 activity and ATR-CHK1 signalling remained intact in drug-released cells. In addition, high doses of SRA737 in combination with gemcitabine induced PARP cleavage (apoptosis), indicating a partial return of drug sensitivity following SRA737 withdrawal. In contrast to DTEPs, total CDK1 levels were unchanged and total CHK1 and WEE1 were overexpressed in this population, as they were in dose-escalated cells, and, similarly, was not due to increased *CHEK1* or *WEE1* gene expression. This could have been caused by a rebound effect following removal of extreme therapeutic stress or be indicative of an intermediate state between persister and dose-escalated phenotypes. These alterations were not observed in all biological replicates; in particular, total CHK1 levels were unchanged and WEE1 expression was reduced in REL-4 (Appendix Figure 6).

Persister cells are characterised by reversible drug-tolerance, as evidenced by a return to sensitivity upon drug withdrawal (Sharma et al. 2010; Liau et al. 2017). Sensitivity profiling revealed that drug-released cells were generally more sensitive to rechallenge with additional DDRi than DTEPs but had failed to completely regain SRA737 sensitivity after 43 days culture in drug-free medium, demonstrating the long-term effect of acute lethal SRA737 exposure. Further investigation into the kinetics of drug resensitisation revealed differential responses between independently generated drug-released populations (REL-1 to REL-4), with two out of four remaining SRA737-tolerant through day 274 (267 days after SRA737 withdrawal). It remains unknown whether these populations would eventually regain SRA737 sensitivity given more time. Of note, resensitisation to SRA737 tracked with resensitisation to additional DDRi, suggesting complete recovery from the DTP state. REL-4 was one of the drug-released populations that regained SRA737 sensitivity. This is interesting because total CHK1 and WEE1 overexpression was absent in this population (Appendix Figure 6); however, it is unclear if this is the cause of return to SRA737 sensitivity. Together, these results demonstrate that acute lethal SRA737 exposure has a durable effect, and drug-released populations generated in the same manner can take various routes to exit and recover from the DTP state.

RNA sequencing was performed to characterise the transcriptional profiles underlying the persister and dose-escalated SRA737-resistant states. Analysis of gene expression data revealed a large number of transcriptional alterations in DTP, DTEP, and drug-released populations. The majority of gene expression changes were accounted for by upregulation, which was surprising given the enrichment of repressive epigenetic modifications (globally increased H3K27_{me3} and depleted H3K27_{ac}) in DTPs and DTEPs. This could potentially be explained by localised enrichment of repressive histone modifications at regulatory genomic regions, such as enhancer or promotor sequences, to silence the expression of specific genes. Indeed, a subset of differentially expressed genes were downregulated in DTP, DTEP, and drug-released populations. While local epigenetic changes cannot be determined by Western blotting, molecular profiling using chromatin immunoprecipitation with sequencing (ChIPseq) or

Cleavage Under Targets and Tagmentation (CUT&Tag) techniques could be used to investigate this further.

Consistent with experimental observations of reduced proliferation rate in DTPs and DTEPs, downregulated Hallmark gene sets included those associated with cell cycle progression, such as E2F targets and G2/M transition. Upregulated gene sets included those related to apoptosis, EMT, and inflammatory signalling. The same pathways were upregulated in dose-escalated cells (ESC-10 μ M), suggesting common transcriptional reprogramming and engagement of similar mechanisms in differentially generated SRA737 resistant populations. This is further supported by the observation that expression of distinct gene signatures related to senescence, embryonic diapause, and stem cell quiescence are increased in persister and dose-escalated populations. However, as the diapause gene signature was also enriched in control samples it's unclear whether this mechanism reflects a drug resistant state, or a response to long-term culture or unfavourable environmental conditions.

To identify persister-specific mechanisms of drug-tolerance and -resistance, transcriptional profiles from DTP and DTEP populations were compared to those from dose-escalated cells. Direct comparison of differentially expressed genes revealed considerable similarity in gene expression changes between DTEP and ESC-10 μ M populations. Importantly, however, a number of genes were differentially expressed in DTEPs but were undetected in dose-escalated cells, suggesting the presence of unique transcriptional alterations that could represent persister-specific mechanisms. Further interrogation of RNAseq data using a wider range of gene set collections revealed a specific enrichment of genes associated with IFN γ responses, IL-2/STAT5, and IL-6/JAK/STAT3 signalling pathways. These pathways are upregulated in DTP and DTEP populations and partially reversed in drug-released cells, indicating a specific role for cytokine and inflammatory signalling in DTP formation, survival, and/or progression. Interestingly, interrogation of the ChIP Enrichment Analysis (CHEA) gene set, which infers transcription factor activity, showed common enrichment of EZH2 related genes in persister and dose-escalated populations. However, the

observation that global H3K27 hypermethylation (H3K27_{me3}) is more prevalent in DTPs and DTEPs than ESC-10 μ M cells provides greater evidence for EZH2 activity as a persister-specific mechanism. This is further supported by the unique enrichment of EZH2-related genes from an additional gene set collection (ENCODE) in DTPs.

The total number of differentially expressed genes was dramatically reduced in drug-released cells compared to DTP and DTEP populations, suggesting that gene expression changes are reversed following SRA737 withdrawal. This is further supported by MDS analysis, which showed that drug-released cells bear more similarity to drug-naïve controls than to DTPs or DTEPs. Additionally, upregulated genes in the IFN γ response and EZH2 gene sets in DTP and DTEP populations were largely reversed in drug-released cells. Together with drug sensitivity data, these findings demonstrate the transient and reversible nature of transcriptional alterations in SRA737-induced DTPs.

Overall, these data demonstrate that DTP and DTEP populations adopt distinct mechanisms to overcome lethal SRA737 exposure and have identified cytokine signalling pathways and EZH2 transcriptional activity as putative persister-specific mechanisms for further study.

Chapter 5

EZH2-mediated hypermethylation of histone H3 lysine 27 (H3K27) is required for persister cell progression

Chapter 5 **EZH2-mediated hypermethylation of histone H3 lysine 27 (H3K27) is required for persister cell progression**

5.1. Introduction

In the absence of genetic resistance, persister cells employ epigenetic mechanisms to adapt and overcome therapeutic challenge. Indeed, persisters are characterised by global changes to epigenetic histone modifications that alter DNA accessibility and gene expression profiles (Sharma et al. 2010; Al Emran et al. 2018). Such changes are believed to facilitate cellular reprogramming and promote survival in the face of overt drug toxicity (Liau et al. 2017; Guler et al. 2017; Rehman et al. 2021). The observation that multiple epigenetic enzymes are dysregulated at the transcriptional and protein level in persister populations (Vinogradova et al. 2016; Guler et al. 2017; Al Emran et al. 2018) makes them an attractive target for abrogating persister cell formation, progression, and survival. Consistent with this hypothesis, several studies have reported an anti-persister cell effect upon pharmacological and/or genetic inhibition of epigenetic enzyme activity. For example, small molecule inhibition of KDM5 histone demethylases reduces DTP formation in PC9 cells upon lethal exposure to EGFRi erlotinib (Vinogradova et al. 2016). In another study, shRNA-mediated knockdown of the mRNA/DNA m⁶A methyltransferase complex suppressed DTEP emergence in response to prolonged BRAFi and MEKi combination exposure (Shen et al. 2019), illustrating the wide range of epigenetic mechanisms exploited by persister cells and their therapeutic potential.

In the present study, global epigenetic changes have been observed in persister populations induced with SRA737; in particular, hypermethylation of H3K27 was increased in day 7 DTP and day 50 DTEP populations (Figure 3-5G), but not in dose-escalated models of SRA737 resistance (Figure 4-15). Furthermore, H3K27_{me3} enrichment in DTPs was reversed following SRA737 withdrawal (Figure 3-5G). These data suggest that gene expression changes that occur as

a result of H3K27_{me3} remodelling may contribute to the adaptive state/plasticity that promotes DTP formation, survival and/or progression.

H3K27 is methylated by the histone-lysine N-methyltransferase enhancer of zeste homolog 2 (EZH2) (Cao et al. 2002). Along with suppressor of zeste 12 protein homolog (SUZ12), EZH2 forms part of the core polycomb repressive *complex 2* (PRC2); an epigenetic complex that functions as a transcriptional repressor by methylating H3K27 residues (Cao and Zhang 2004; Pasini et al. 2004). Consistent with this, GSEA of RNA sequencing data revealed an enrichment of gene sets associated with EZH2 and SUZ12 transcriptional activity in SRA737-induced DTP and DTEP populations (Figure 4-16B & 4-16D), further supporting a role for EZH2 activity in SRA737-induced persister cells.

EZH2 activity has been implicated in the emergence and progression of many human cancers (Varambally et al. 2002; Kleer et al. 2003; Bachmann et al. 2006; Pawlyn et al. 2017), spurring the development of commercially available and clinically utilised small molecule EZH2 inhibitors, including tazemetostat (Knutson et al. 2013; Hoy 2020). To test the hypothesis that EZH2 activity is required for persister cell responses in the context of lethal SRA737 exposure, the effect of EZH2 inhibition on SRA737-induced DTP formation, progression, and survival was investigated using tazemetostat.

5.2. Investigating the requirement of EZH2 for persister cell formation and survival

5.2.1. SRA737-induced DTEPs are not sensitive to EZH2 inhibition

Persister cells are sensitive to pharmacological and genetic inhibition of epigenetic enzymes (Sharma et al. 2010; Guler et al. 2017; Liao et al. 2017). Given that gene signatures related to EZH2 transcriptional activity are enriched (Figure 4-16B & 4-16D) and H3K27_{me3} levels remain elevated in SRA737-induced DTEPs after passage through the DTP bottleneck (Figure 3-5G), I reasoned that DTEPs may now be dependent on EZH2 activity for survival and therefore more sensitive to EZH2 inhibition. To test this, drug-naïve, DTEP, and drug-released populations were tested for sensitivity to the EZH2 inhibitor tazemetostat in a 5-day proliferation assay. GI₅₀ potencies were >30 μ M in each population, indicating that DTEPs are not collaterally sensitive to tazemetostat (Figure 5-1A). However, previous reports demonstrate that ≥ 14 days treatment is required for tazemetostat to exert an anti-proliferative effect (Knutson et al. 2013; Knutson et al. 2014). As such, a colony forming assay was performed to test tazemetostat sensitivity in this longer context. Due to the reversible nature of epigenetic alterations following drug release (Figure 3-5G), DTEPs were maintained in medium containing 10 μ M SRA737 for the duration of this experiment. In this extended investigation, DTEPs showed no increased sensitivity to tazemetostat (Figure 5-1B). By contrast, a slight decrease in sensitivity was observed, perhaps reflecting the drug-tolerant/persistent nature of the DTEP population. In addition, maintenance of H3K27_{me3} was not necessary for DTEP survival. Despite increased H3K27 hypermethylation in DTEPs, tazemetostat effectively abrogated H3K27_{me3} levels without affecting cell survival (Figure 5-1C).

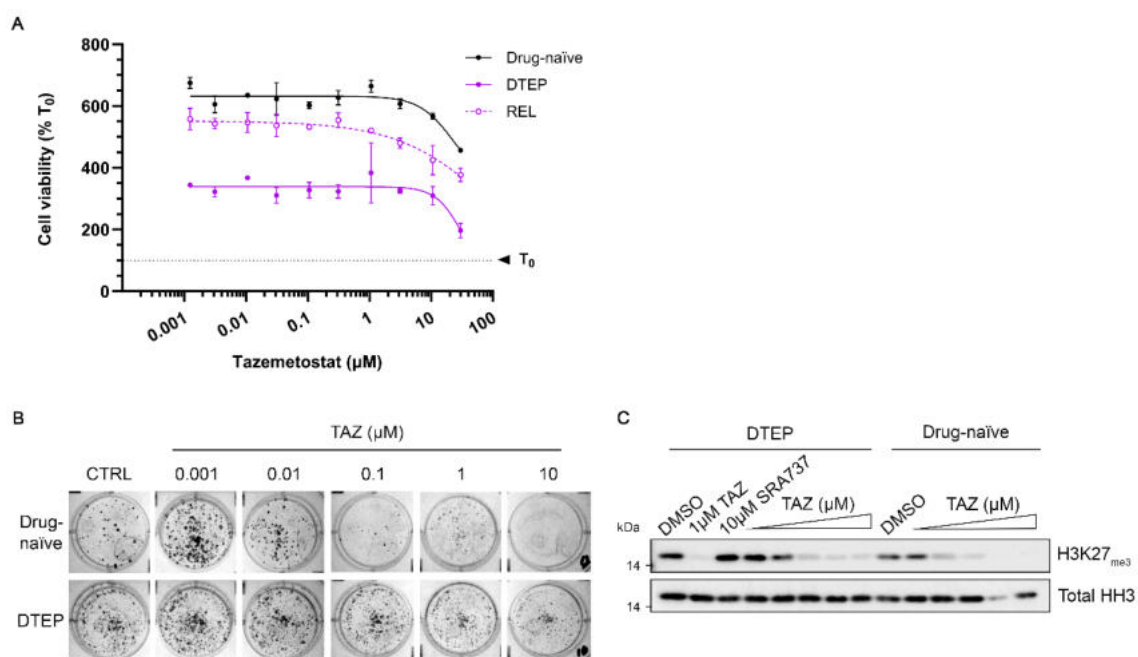


Figure 5-1: SRA737-induced DTEPs are not sensitive to EZH2 inhibition using tazemetostat.

(A) Non-linear regression analysis of cell viability measured by CellTiter-Glo® 120h after tazemetostat addition in drug-naïve, DTEP, and drug-released (REL) populations. **(B)** Images of SRB-stained colonies in drug-naïve and DTEP populations after 13 days exposure to tazemetostat (TAZ) at indicated concentrations. DTEPs were maintained in culture medium supplemented with 10 μM SRA737 for the duration of the experiment. **(C)** Western blot analysis of H3 lysine 27 tri-methylation (H3K27_{me3}) in samples corresponding to (B). Images shown in (B) & (C) are representative of two independent experiments. Graph shows mean±SD of two technical replicates and is representative of n≥2 experiments. Dotted line represents proportion of cells present at T₀.

5.2.2. EZH2 activity is not required for DTP formation

In addition to reducing persister cell survival, several studies also report that inhibition of epigenetic enzymes prevents DTP formation in response to lethal drug exposure (Sharma et al. 2010; Vinogradova et al. 2016; Al Emran et al. 2018; Shen et al. 2019). Following the observation of elevated H3K27_{me3} in SRA737-induced DTPs, I hypothesised that K27 hypermethylation was required for cells to adopt the DTP state and that inhibition of this process would abrogate DTP formation in response to lethal SRA737 exposure. As cells would require pre-treatment with tazemetostat to drive down H3K27 tri-methylation prior to DTP induction with SRA737, the dose and duration of tazemetostat treatment was first optimised in SK-N-AS cells. While tazemetostat reduced H3K27_{me3} levels in a dose-dependent manner after 24 h (Figure 5-2A, left panel), the effect was greater after 120 h incubation (Figure 5-2A, right panel) suggesting an optimal pre-treatment time of at least 5 days. Encouragingly, no anti-proliferative effect was observed at any of the doses tested (Figure 5-1A). In light of these results, SK-N-AS cells were pre-treated with 1 μ M tazemetostat for 7 days and then exposed to 10 μ M SRA737 alone or in combination with 1 μ M tazemetostat, and DTPs quantified at day 7 (Figure 5-2B).

Consistent with previous results, treatment with tazemetostat alone had no impact on cell number compared to DMSO treated control (Figure 5-2C), and H3K27 tri-methylation was effectively inhibited in all tazemetostat treated samples at T₀ and day 7 (Figure 5-2D). There was no significant decrease in the number of DTPs formed under tazemetostat combination treatment versus SRA737 alone (Figure 5-2C), indicating that EZH2-mediated H3K27 hypermethylation is not required for DTP formation in response to lethal drug exposure. SRA737-induced DTPs were previously shown to enter a slow-cycling state and originate from the starting cell population using a dilutive proliferation dye (Figure 3-5C). Similarly, DTPs generated with SRA737 alone or in combination with tazemetostat retained comparable levels of the ViaFluor® dye (Figure 5-1E), demonstrating that persister cell behaviour is not altered when H3K27 methylation is abrogated.

Taken together, these data show that H3K27 hypermethylation by EZH2 is not required for SK-N-AS cells to enter the DTP state in response to lethal SRA737 exposure, nor are DTEPs dependent on EZH2 activity for survival. An important implication of these findings is that we would not expect the use of tazemetostat to eradicate persister cell populations arising in the context of SRA737 treatment in the clinic. However, these results do not exclude the requirement for H3K27_{me3} and EZH2 activity in DTP-to-DTEP transition.

alters this composition, apoptosis, cytotoxicity, and senescence were measured in day 7 DTPs.

For apoptosis and cytotoxicity, an ApoTox-Glo® triplex assay was carried out. SK-N-AS cells treated with 1 μ M etoposide for 7 days were used as a positive assay control and, accordingly, significantly increased caspase 3/7 (apoptosis) and dead cell protease activity (cytotoxicity) in SK-N-AS cells (Figure 5-3A & 5-3B). There was no significant change in levels of apoptosis or cytotoxicity in DTPs generated with SRA737 and tazemetostat in combination, although these tended to be slightly reduced compared to SRA737 alone, suggesting a mild abrogation of cell death upon tazemetostat addition. A similar result was observed in cells treated with 1 μ M tazemetostat. Cell death was slightly reduced in SRA737-induced DTPs in this experiment compared to previous results (Figure 3-6A & 3-6B). Regardless, this data shows that the addition of tazemetostat does not alter levels of apoptosis or cytotoxicity in the day 7 DTP population.

Senescence is significantly induced in DTPs generated with SRA737 (Figure 3-6C). To investigate this under tazemetostat combination, senescence was assessed in day 7 DTPs using a FACS-based β -galactosidase (β -gal) activity assay and a threshold applied to classify cells as β -gal positive (senescent) or β -gal negative (non-senescent). SK-N-AS cells treated with 10 μ M palbociclib for 14 days were used as a positive assay control and, correspondingly, significantly increased the proportion of β -gal positive cells compared to DMSO treated control (Figure 5-3C). Surprisingly, treatment with SRA737 in combination with tazemetostat significantly increased the number of β -gal positive cells by 2.3-fold compared to SRA737 alone (42.6% and 18.3%, respectively), demonstrating a substantial increase in the proportion of senescent cells in the day 7 DTP population. The number of β -gal positive cells was also increased following treatment with 1 μ M tazemetostat alone, however this was not statistically significant versus DMSO control (Figure 5-3C). Together, these results demonstrate that the addition of tazemetostat alters the composition of SRA737-DTPs by promoting entry into senescence.

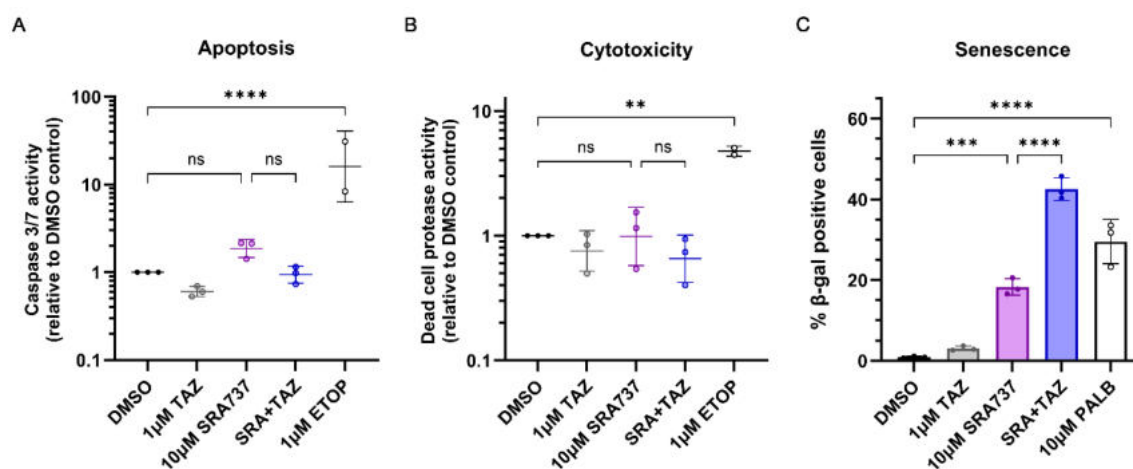


Figure 5-3: EZH2 inhibition induces β -galactosidase activity in SRA737-induced DTPs.

(A) Caspase 3/7 and (B) dead cell protease activity measured by ApoTox-Glo® in day 7 DTPs generated with SRA737 alone or in combination with tazemetostat (SRA+TAZ) relative to DMSO treated control. Cells treated with 1 μ M etoposide (ETOP) for 7 days served as a positive control. Graphs show mean \pm SD of log₁₀ transformed data from n \geq 2 independent experiments. (C) Proportion of β -galactosidase positive cells in day 7 vehicle treated controls or indicated DTP populations. Cells treated with 10 μ M palbociclib (PALB) for 14 days served as a positive control. Graph shows mean \pm SD from three independent experiments. Significance statements result from comparison of means by ordinary one-way ANOVA with Tukey's correction. **** p<0.0001; *** p<0.001; ** p<0.01; * p<0.05; ns = not significant.

5.3. Investigating the requirement of EZH2 activity for DTP progression

5.3.1. Tazemetostat abrogates DTP-to-DTEP transition under continued SRA737 exposure

The observation that tazemetostat failed to abrogate the formation or survival of SRA737-induced persister cells does not exclude the possibility that EZH2 activity is important for progression of DTPs to DTEPs. Indeed, Sharma and colleagues reported that inhibition of class I and II histone deacetylases (HDACs) virtually eliminated the emergence of DTEP clones in response to lethal EGFRi exposure (Sharma et al. 2010). The shift in DTP population dynamics under SRA737 and tazemetostat combination treatment away from death and towards senescence suggests an alteration in the long-term response of the cells and resultant DTEP population. To test this, I used a stable, nuclear-labelled mKate2-SK-N-AS cell line to monitor cell number during the course of long-term exposure to 10 μ M SRA737 alone or in combination with 1 μ M tazemetostat (Figure 5-4A).

In line with previous observations, tazemetostat alone had no significant effect on cell proliferation, and cells maintained in SRA737 alone gradually progressed as DTEPs after 14 days of treatment (Figure 5-4B, left panel). In contrast, cells maintained in a combination of SRA737 and tazemetostat did not progress and the number of cells declined throughout the time-course, resulting in a significant reduction in cell number at day 51 (Figure 5-4B, left panel & 5-4C). Consistent with this, the proliferation rate of cells maintained under combination treatment was significantly reduced compared to those treated with SRA737 alone (Figure 5-4D).

As cellular senescence is at least partly responsible for the inhibition of proliferation under SRA737 and tazemetostat combination, and senescence can be reversed (reviewed in (Saleh, Tyutyunyk-Massey, and Gewirtz 2019)), I tested whether cells treated with SRA737, tazemetostat, or both agents in combination, could recover following complete drug withdrawal. Drug-released populations

were generated by removing single-agent or combination treatment after 7 days and subsequently culturing cells in DMSO-supplemented medium. DTPs generated with SRA737, or with SRA737 and tazemetostat in combination resumed proliferation after drug withdrawal, but the recovery was slower for those treated with the combination (Figure 5-4B, left panel). Although proliferation rate had recovered to control levels (Figure 5-4D), there were significantly fewer cells following release from combination treatment at day 51 (Figure 5-4B, left panel & 5-4C). H3K27_{me3} levels agreed with previous observations. SRA737 exposure induced H3K27 tri-methylation across the time-course and this was inhibited by tazemetostat treatment (Figure 5-5). Removal of SRA737 and tazemetostat was accompanied by a return of H3K27 methylation back to control levels at day 51. These results demonstrate that combination treatment with tazemetostat inhibits the progression of DTEPs from the SRA737-induced DTP bottleneck, and that this effect is reversed following complete drug withdrawal.

These observations support a hypothesis that DTPs could require EZH2 activity to exit from the DTP state and become DTEPs, or to recover from drug withdrawal. To test this, DTPs generated under combination treatment were released into either 10 μ M SRA737 or 1 μ M tazemetostat alone at day 7 (Figure 5-4A; SRA+TAZ>SRA and SRA+TAZ>TAZ, respectively). Surprisingly, DTP progression remained suppressed in cells that were released into SRA737 alone, despite recovery of H3K27_{me3} levels following tazemetostat removal (Figure 5-4B, right panel, 5-4C & Figure 5-5). Furthermore, this anti-proliferative effect remained significant versus prolonged exposure to SRA737 alone (Figure 5-4B, right panel). In contrast, cells released into tazemetostat alone proliferated in line with combination-induced DTPs that had been recovered in DMSO, with no significant difference in the number of cells at day 51 (Figure 5-4B, right panel & Figure 5-4C). Moreover, these cells had recovered proliferation rate to control levels (Figure 5-4D). This was observed despite continued effective EZH2 inhibition (Figure 5-5). Together, these data demonstrate that DTPs generated with SRA737 and tazemetostat can resume proliferation if the therapeutic pressure imposed by SRA737 is removed but are unable to recover with continued SRA737 exposure, even after tazemetostat withdrawal.

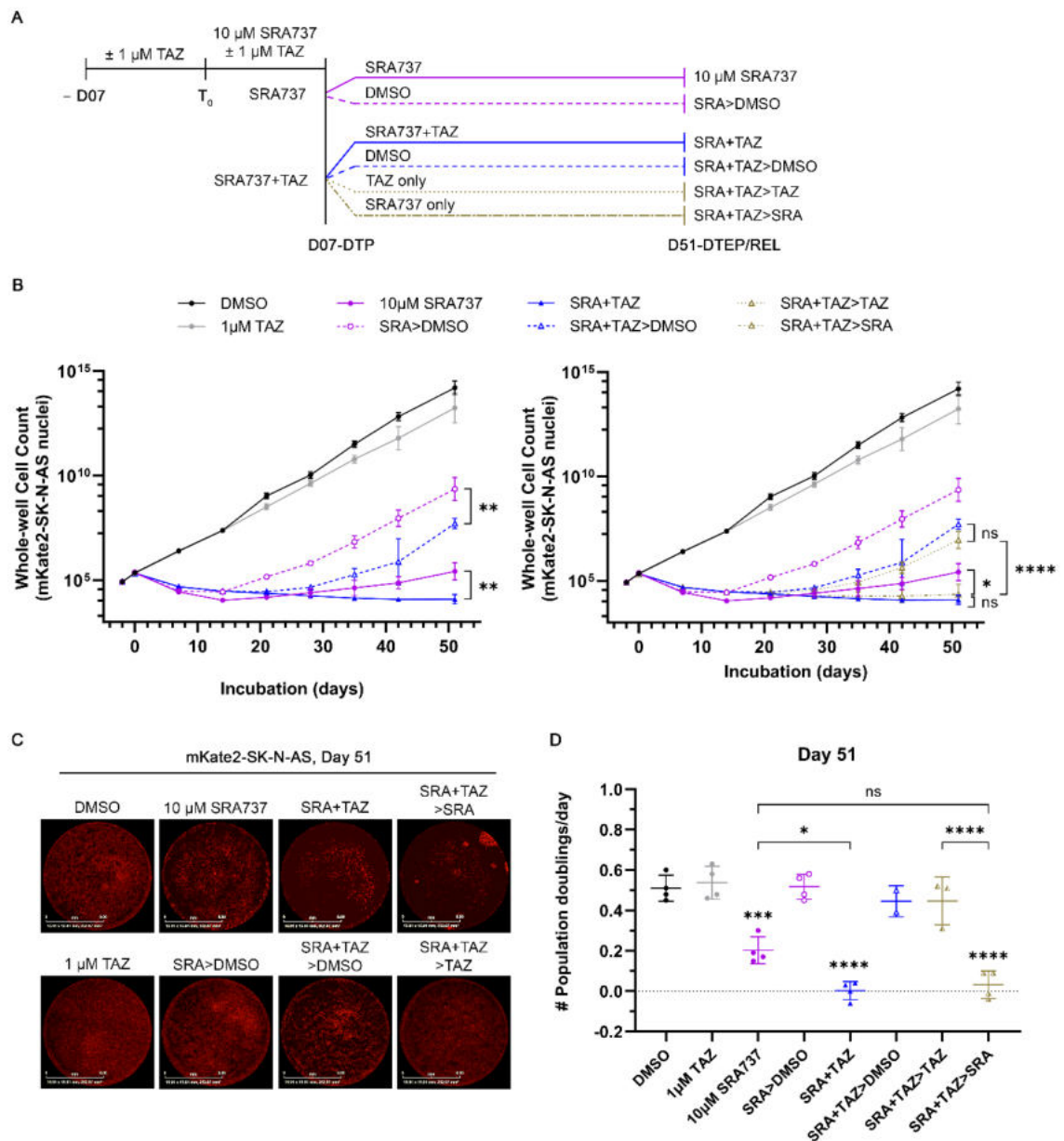


Figure 5-4: EZH2 activity is required for DTEP progression under continued SRA737 exposure.

(A) Schematic protocol for generation of indicated DTEP populations with SRA737 alone or in combination with TAZ. **(B)** Quantification of mKate2-labelled SK-N-AS cells treated as shown in (A) at indicated time points. **(C)** Whole-well fluorescence microscopy images of mKate2-SK-N-AS cells treated as in (A) at experimental end-point (day 51). **(D)** Proliferation rate measured by number of population doublings per day in day 51 control and persister-derived populations as indicated. Images captured at 4X magnification, scale bar = 8 μm. Graphs show mean±SD from $n \geq 2$ independent experiments. Significance statements in (B) result from analysis of log₁₀ transformed data by ordinary one-way ANOVA with Šidák's correction, and (D) from comparison of means by ordinary one-way ANOVA with Tukey's correction versus DMSO control, unless otherwise indicated. **** $p < 0.0001$; *** $p < 0.001$; ** $p < 0.01$; * $p < 0.05$; ns = not significant.

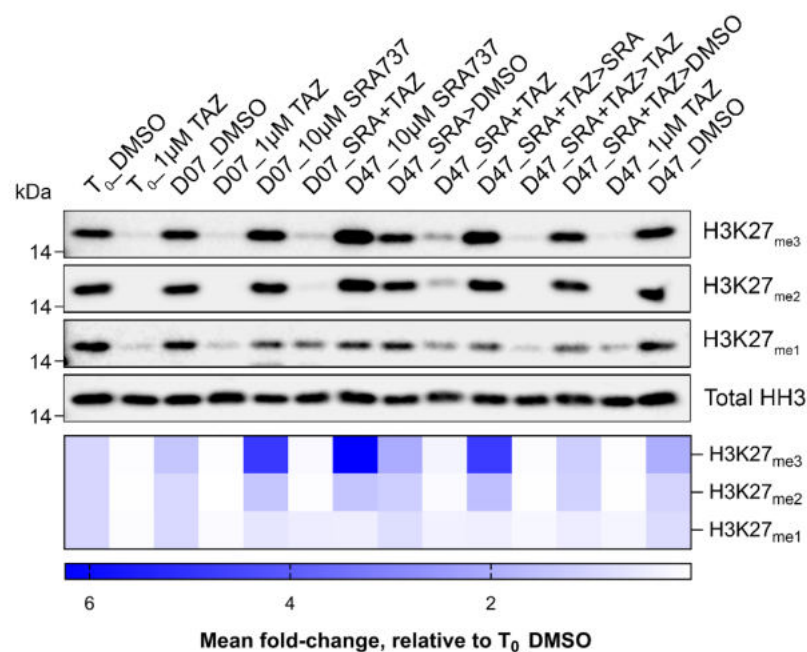


Figure 5-5: Biomarker modulation in SRA737 and tazemetostat combination studies.

Western blot analysis (upper panel) and quantification (lower panel) of H3K27 methylation in control and different persister cell populations at indicated time points. Heatmap shows mean fold-change in scanning densitometry signal of $n=4$ independent experiments.

5.3.2. Populations emerging from a combination-induced DTP bottleneck are more resistant to SRA737

Having generated persister populations with SRA737 and tazemetostat treatment, I wondered whether cells generated under drug combination responded differently to further challenge with SRA737.

To investigate this, DTEP and drug-released populations generated with SRA737 alone or in combination with tazemetostat were tested for SRA737 sensitivity. Dose-response curves and GI_{50} potency values were not obtained for cells under continuous SRA737 and tazemetostat combination treatment, or those released into SRA737 alone, as their proliferation rate was insufficient for robust measurement (Figure 5-4D). DMSO and tazemetostat controls were equally

sensitive to SRA737 and GI_{50} values were consistent with previous observations in SK-N-AS cells (Figure 5-6 & Table 5-1). In line with previous results, SRA737-induced DTEPs and SRA737 drug-released cells were $\sim 70X$ and $\sim 7X$ less sensitive to SRA737, respectively, compared to DMSO control (Figure 5-6 & Table 5-1; 10 μM SRA737 and SRA737>DMSO). The average GI_{50} values in populations released from combination treatment into DMSO (SRA737+TAZ>DMSO) or tazemetostat alone (SRA737+TAZ>TAZ) were 4.74 μM and 4.86 μM , respectively, representing a greater reduction in SRA737 potency compared to SRA737>DMSO populations (Figure 5-6 & Table 5-1). Furthermore, the maximal effect observed at 30 μM SRA737 was also reduced in these cells compared to both SRA737-induced DTEP and drug-released populations (Figure 5-6). Although the GI_{50} data shows a relatively high degree of variation amongst the biological replicates, these results suggest that populations emerging from a combination DTP bottleneck are even more resistant to SRA737 than those generated with SRA737 alone.

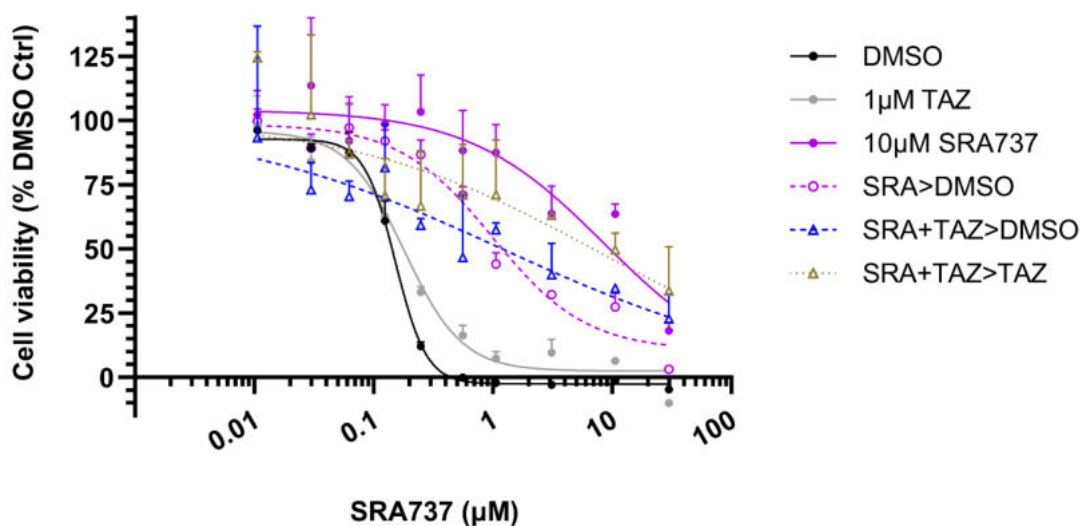


Figure 5-6: Persister-derived populations emerging from SRA737 and tazemetostat combination treatment appear to be more resistant to SRA737.

Non-linear regression analysis of cell viability measured by CellTiter-Glo® 120h after SRA737 addition in drug-naïve and indicated persister-derived populations. Graph shows mean \pm SD of two technical replicates and is representative of n=3 experiments.

Table 5-1: Summary of cellular potency values (GI_{50}) for SRA737 in indicated persister-derived and control populations.

GI_{50} values are mean \pm SD. Cells are highlighted according to fold-increase in GI_{50} value compared to drug-naïve (DMSO) control. Red \geq 50-fold; orange \geq 10-fold; yellow \geq 2-fold. N/A; not applicable, Un; undetermined.

Population	SRA737 GI_{50} , μ M (n)	Fold-change from DMSO
DMSO	0.18 \pm 0.02 (3)	N/A
1 μ M TAZ	0.18 \pm 0.02 (3)	0.98
10 μ M SRA737	12.20 \pm 7.76 (3)	67.81
SRA737>DMSO	1.33 \pm 0.94 (3)	7.36
SRA737+TAZ	Un	N/A
SRA737+TAZ>DMSO	4.74 \pm 2.43 (3)	26.36
SRA737+TAZ>SRA737	Un	N/A
SRA737+TAZ>TAZ	4.86 \pm 5.42 (3)	27.03

5.4. Discussion

Epigenetic alterations are frequently reported in persister cells generated using TKi, with several epigenetic enzymes shown to be important for their formation and progression (Sharma et al. 2010; Guler et al. 2017; Liao et al. 2017; Vinogradova et al. 2016; Shen et al. 2019). Profiling of specific histone H3 modifications revealed similar alterations in SRA737-induced persisters. In particular, there is a global enrichment of H3K27 tri-methylation in DTP and DTEP populations that was not present in dose-escalated SRA737-resistant cells. Furthermore, RNA sequencing revealed an enrichment of gene sets related to EZH2 transcriptional activity in DTPs and DTEPs that was partially reversed following SRA737 withdrawal, suggesting a role for the EZH2 methyltransferase in persister cell formation and survival. However, EZH2 inhibition using the small molecule inhibitor tazemetostat failed to abrogate DTP formation or DTEP viability, suggesting that K27 hypermethylation and EZH2 activity are not essential for adoption of the DTP state or DTEP survival in the context of SRA737 exposure. This observation could be explained by activity of other K27 methyltransferases, such as G9a (Wu et al. 2011), that remain functional while EZH2 is inhibited; however, this is unlikely since H3K27 methylation was effectively diminished in DTP and DTEP populations. Another possibility is the presence of additional epigenetic alterations that were not explored as part of initial characterisation, such as alternative histone modifications or DNA methylation. Moreover, as H3K27_{me3} enrichment was accompanied by a reduction in H3K27_{ac}, inhibition of histone deacetylases might also be required to mitigate DTP formation. Since H3K27_{ac} levels were not measured as part of these investigations, it is unclear whether histone deacetylase activity continues to maintain a repressive chromatin state while EZH2 is effectively inhibited.

While tazemetostat failed to inhibit DTP formation in response to lethal SRA737 exposure, further characterisation of the day 7 DTP population revealed a significant increase in the proportion of senescent cells compared to SRA737 alone. Subsequent culture under continuous combination treatment significantly hindered DTEP outgrowth, indicating a requirement for EZH2 activity during DTP-

to-DTEP transition under lethal SRA737 exposure. This is consistent with reports from other DTP models following inhibition of epigenetic enzymes (Sharma et al. 2010); however, it remains unknown if promotion of cellular senescence by tazemetostat is the mechanism of action underlying these findings. Interestingly, DTPs generated with combination treatment resumed proliferation following release into DMSO or tazemetostat but failed to recover when released into SRA737 alone, despite restoration of H3K27_{me3} levels. This inhibitory effect was equal to those maintained under combination for the duration of the experiment and was significantly reduced versus SRA737 exposure alone. Together, these data suggest that DTPs induced by combination treatment are different to those generated under SRA737 alone, perhaps in terms of adaptive capability, and inhibition of EZH2 leads to a DTP state that is more difficult to recover from. The mechanisms by which tazemetostat exerts this anti-persist effect could be investigated using additional ChIPseq analysis to identify regions of the genome and genes that are differentially regulated under combination treatment.

Crucially, SRA737 potency was reduced even further following transition through the SRA737 and tazemetostat combination DTP bottleneck. In comparison to SRA737 drug-released populations, combination DTPs released into DMSO or tazemetostat were ~3.5X less sensitive to SRA737. Although SRA737 sensitivity could not be measured in DTEPs generated by continuous exposure to SRA737 and tazemetostat, these data indicate that populations emerging from this combination bottleneck are even more resistant to SRA737 than those generated with SRA737 alone. As such, it will be important to assess the impact this may have on the evolution of drug-resistance.

Altogether, these studies have revealed a role for EZH2 activity in DTP-to-DTEP progression under lethal SRA737 exposure and exposed a potential drawback of abrogating DTP progression using tazemetostat.

Chapter 6

**IFN γ activation hinders DTEP
emergence under lethal SRA737
exposure**

Chapter 6 IFN γ activation hinders DTEP emergence under lethal SRA737 exposure

6.1. Introduction

Cytokines are the key signalling molecules of the immune system. They are secreted by immune and non-immune cells to activate and coordinate immune and inflammatory responses to a range of pathogens. Cytokine signalling is mediated by JAK-STAT pathways, wherein receptor binding activates janus kinases (JAKs) that subsequently phosphorylate and activate signal transducer and activator of transcription (STAT) transcription factors to promote expression of target genes. Multiple cytokine-JAK-STAT signalling pathways exist to elicit pleiotropic effects in target cells by promoting expression of genes that regulate proliferation, differentiation, and migration (Figure 6-1). Dysregulated JAK/STAT signalling is prevalent in many inflammatory and autoimmune diseases, such as rheumatoid arthritis and systemic lupus erythematosus, resulting in the development of targeted small molecule JAK inhibitors that are approved for clinical use or under clinical investigation (Table 6-1).

While the primary function of cytokine signalling is to coordinate appropriate immune responses, these pathways can be hijacked by cancer cells to promote survival and tumour progression (Figure 6-1). Upregulated IFN γ signalling is associated with metastatic and invasive disease (Lo et al. 2019; Chen et al. 2023), as well as impaired immune detection by cytotoxic T-cells (Lane et al. 2018). Constitutive STAT5 activation in head and neck, and prostate cancer cell lines promotes tumour survival and growth by inhibiting apoptosis and increasing proliferation and migration (Koppikar et al. 2008; Gu et al. 2010). Furthermore, IL-6-STAT3 signalling activity is upregulated and required for the development of vincristine-resistance in an *in vitro* model of medulloblastoma (Sreenivasan et al. 2020), demonstrating the role of cytokine signalling pathways in the acquisition of therapeutic resistance.

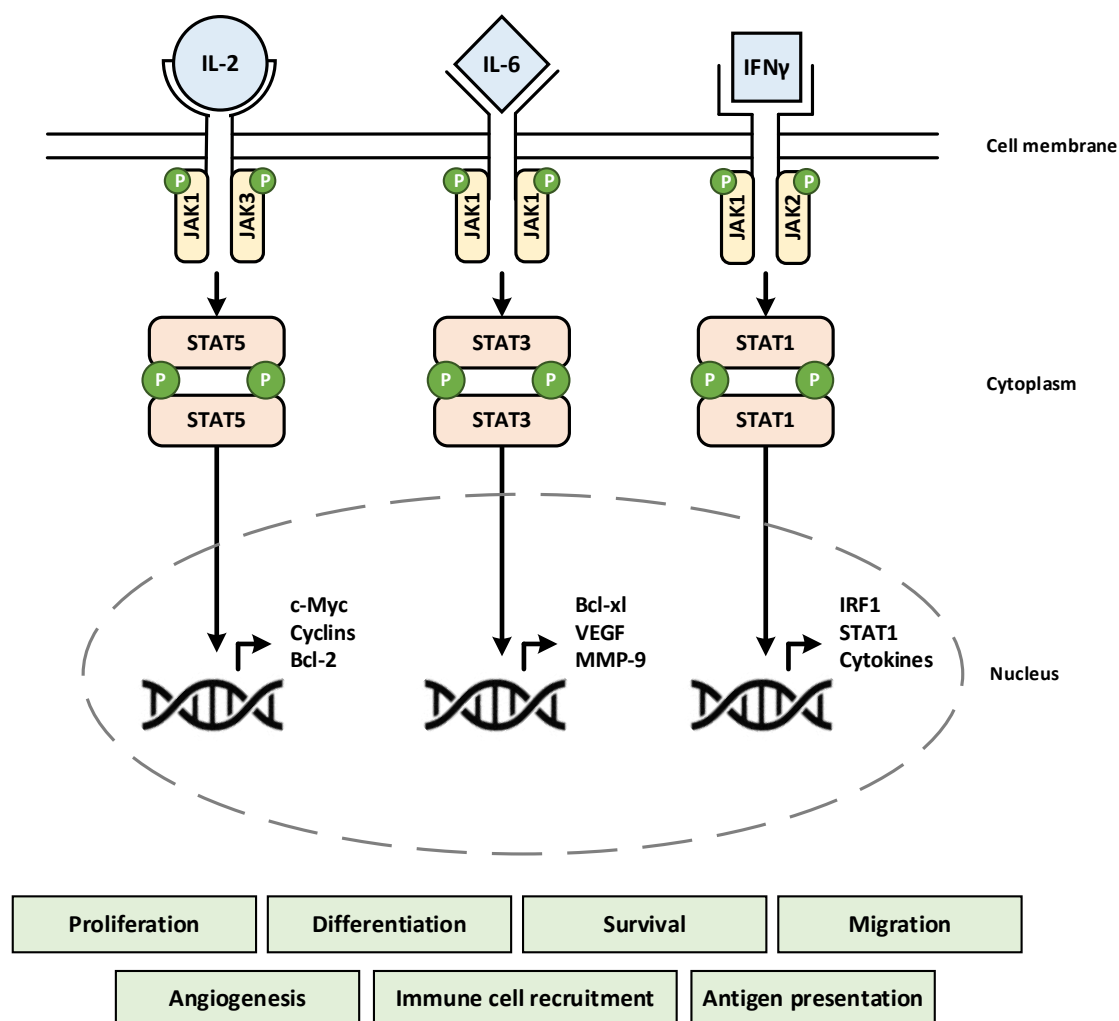


Figure 6-1: IL-2, IL-6, and IFN γ signalling through the JAK-STAT pathway.

Cytokine-receptor binding activates JAK kinases that phosphorylate STAT transcription factors. Activated STAT dimers translocate to the nucleus to induce transcription of target genes that promote pleiotropic effects in cells, including proliferation, differentiation, and migration.

In the present study, transcriptional profiling of SRA737-induced DTP and DTEP populations revealed an increase in the expression of genes involved in multiple cytokine signalling pathways, including IL-2, IL-6, and IFN γ (Figure 4-16B, 4-16C & Appendix Figure 3). Interestingly, these pathways were not enriched in dose-escalated SRA737-resistant cells, indicating that upregulated cytokine signalling is a persister-specific mechanism. Consistent with this hypothesis, dysregulated inflammatory signalling has been reported in other stress and drug-induced persister cell models (Guler et al. 2017; Al Emran et al. 2018; Kurppa et al. 2020).

However, there are limited studies investigating their contribution to DTP formation and progression.

The majority of IL-2, IL-6, and IFN γ related genes are increased in persister populations, suggesting that upregulation of these signalling pathways is required for DTP formation, survival, and progression. As such, I hypothesised that suppression of cytokine signalling using commercially available JAK inhibitors or STAT protein degraders (Table 6-1) would reduce DTP formation in response to lethal SRA737 exposure. Conversely, I reasoned that priming these pathways with exogenous cytokines would promote adoption of the persister cell state and increase the number of DTPs generated under SRA737.

Table 6-1: *In vitro* biochemical and cellular potency values of JAK or STAT inhibitors.

^[1] (Wan et al. 2015); ^[2] (Changelian et al. 2003); ^[3] (Quintás-Cardama et al. 2010); ^[4] (Zhou et al. 2019)

Compound	BMS-911543	Tofacitinib	Ruxolitinib	SD-36
Target	JAK2	JAK1/2/3	JAK1/2	STAT3
Clinical Phase	I/II	Approved	Approved	N/A
<i>In vitro</i> IC ₅₀ (nM)	^[1] JAK1: 360 JAK2: 1.1 JAK3: 75	^[2] JAK1: 112 JAK2: 20 JAK3: 1	^[3] JAK1: 3.3 JAK2: 2.8 JAK3: 428	^[4] STAT3 DC ₅₀ : 60
Cellular potency Cell line Measure IC ₅₀ (nM)	^[1] SET-2 Proliferation 60	^[2] HUO3 Proliferation 324	^[3] Ba/F3 Proliferation 126	^[4] Molm-16 Proliferation 13

6.2. Investigating the role of IFN γ -JAK1/2-STAT1 signalling in DTP formation in response to lethal SRA737 exposure

6.2.1. Cytokine secretion is upregulated in SRA737-induced DTPs

Cytokine secretion was measured in supernatants from SRA737-induced DTPs and drug-naïve controls using a cytokine array. Cytokines that were specifically upregulated in persisters were identified by a $\geq 2.5X$ increase in signal intensity versus drug-naïve controls (Figure 6-2) and represented 36.1% of all cytokines tested (13 out of 36). This considerable alteration in secretion profile suggests that modification of cytokine and/or immune signalling may be important for DTP formation. Included in this shortlist were IFN γ , IL-2, and IL-6 themselves, that are known to regulate the expression of other cytokines such IL-4 (Kovanen et al. 2005) and CCL5 (Liu, Guan, and Ma 2005). In agreement with this, IL-4 and CCL5 levels were increased in supernatants from SRA737-induced DTPs (Figure 6-2). Although from a single experiment, these results help validate the gene expression data at the protein level and provide further evidence implicating cytokine signalling in persister cell formation under lethal SRA737 exposure.

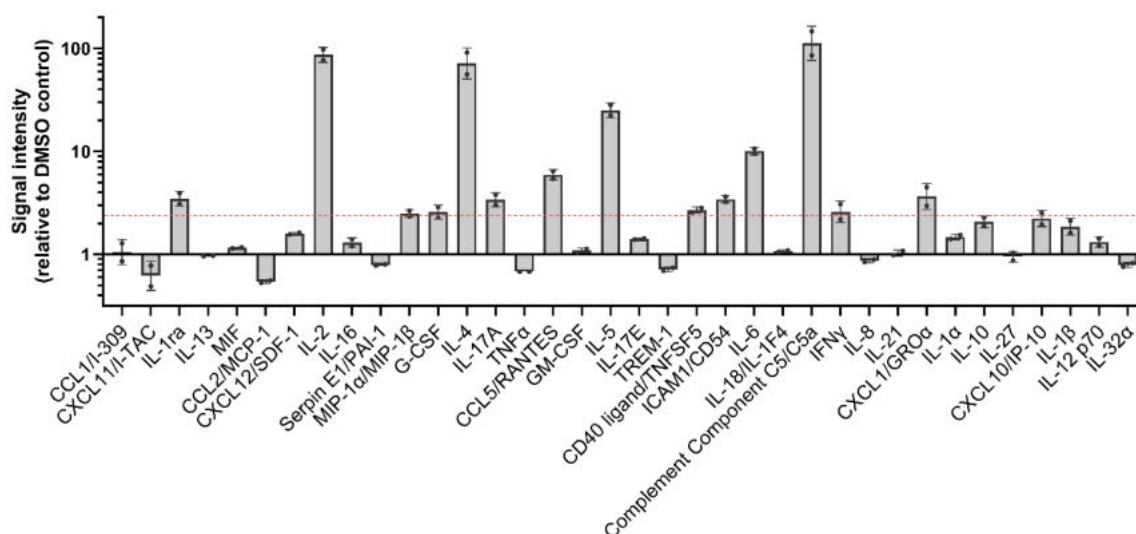


Figure 6-2: SRA737-induced DTPs upregulate cytokine secretion.

Measurement of 36 cytokines in day 7 DTP cell supernatants using the Proteome Profiler™ Human Cytokine Array. Signal intensities are expressed relative to a time-matched DMSO-treated control. Graph shows mean±SD of two technical replicates from a single experiment. Red dotted line represents a 2.5X increase in signal intensity versus DMSO control.

6.2.2. Optimising conditions for persistor cell studies using exogenous IFN γ and JAK/STAT inhibitors

Gene expression and cytokine array data show that SRA737-induced DTPs upregulate IL-2, IL-6, and IFN γ signalling. If these pathways are required for DTP formation, the number of DTPs generated in response to SRA737 could be reduced or increased by inhibiting or priming the signalling pathways, respectively.

Before investigating these hypotheses, I first examined the response of SK-N-AS cells to exogenous human recombinant IL-2, IL-6, and IFN γ . IL-2, IL-6, and IFN γ receptor binding activates intracellular JAK-STAT signalling pathways (Figure 6-1) whose activation can be measured by Western blotting for phosphorylated STAT proteins. IFN γ was the only cytokine to induce STAT phosphorylation in SK-N-AS cells, with increased pY701-STAT1 observed at even the lowest dose tested (Figure 6-3A & Appendix Figure 7A). Consistent with published values, IFN γ -mediated STAT1 activation was inhibited most effectively by the small

molecule JAK1/2 inhibitor ruxolitinib, with an IC_{50} of 0.02 μ M (Figure 6-3B, Tables 6-1 & 6-2 & Appendix Figure 7B & 7C). To test the hypothesis that inhibiting IFN γ signalling will abrogate DTP formation, SK-N-AS cells will need to be treated with ruxolitinib in combination with SRA737. As such, it is important to use a concentration that will suppress STAT1 activation without causing overt cytotoxicity. Encouragingly, ruxolitinib was only weakly anti-proliferative in SK-N-AS cells, with a GI_{50} value of 21.53 μ M (Table 6-2 & Appendix Figure 7E). Together, these results outline the optimal experimental conditions to investigate the role of IFN γ -mediated JAK1/2-STAT1 signalling in persister cell studies.

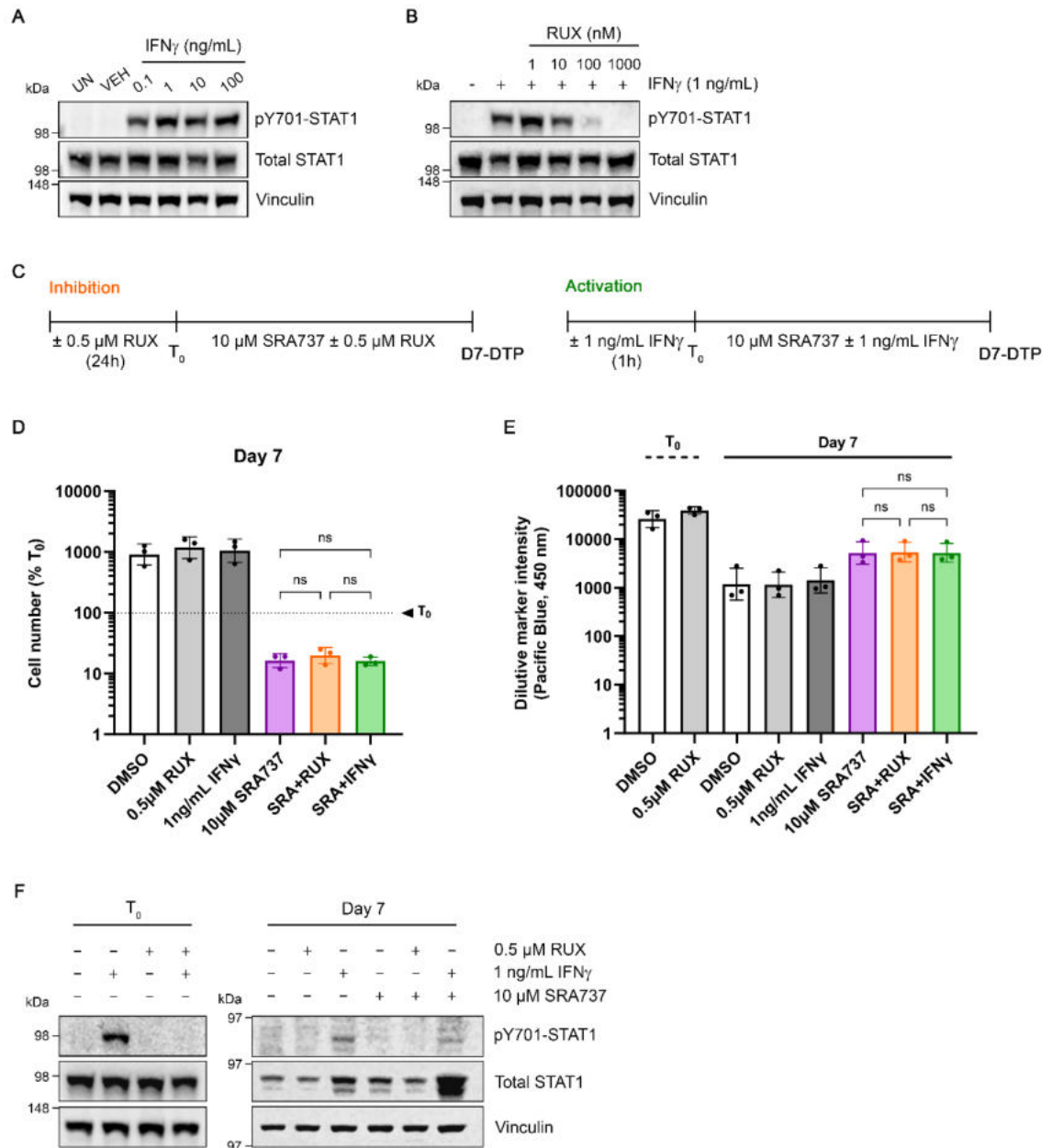


Figure 6-3: SRA737-induced DTP formation is unaffected by inhibition or activation of the IFN γ -JAK1/2-STAT1 pathway.

(A) Western blot analysis of activated pY701-STAT1 levels in SK-N-AS cells after treatment with indicated concentrations of IFN γ for 1h. (B) Western blot analysis of IFN γ -induced pY701-STAT1 activation after 24h pre-treatment with indicated concentrations of ruxolitinib. (C) Schematic protocol for generation of DTPs with SRA737 alone, or in combination with RUX (left panel) or IFN γ (right panel). (D) Number of DTPs at day 7 following treatment with RUX, IFN γ or SRA737 as single agents, or in combination (SRA+RUX or SRA+IFN γ). (E) Quantification of ViaFluor $\text{\textcircled{R}}$ proliferative dye in T_0 populations, day 7 controls, and indicated DTP populations. (F) Western blot analysis of pY701-STAT1 levels in T_0 and day 7 samples treated as in (C). Graphs show mean \pm SD of three independent experiments. Dotted line in (C) represents proportion of cells present at T_0 . Western blots shown are representative of three independent experiments. Significance statements in (D) result from comparison of means by ordinary one-way ANOVA with Šídák's correction, and (E) from comparison of means by ordinary one-way ANOVA with Tukey's correction. ns = not significant.

Table 6-2: Potency of JAK/STAT inhibitors in SK-N-AS cells as measured by pY701-STAT1 modulation (IC₅₀) and cell viability (GI₅₀).

GI₅₀ values represent a single experiment.

Target	Compound	pY701-STAT1 modulation IC ₅₀ , μ M	Cell Viability GI ₅₀ , μ M
JAK2	BMS-911543	0.28	24.74
JAK1/2/3	Tofacitinib	0.14	>30
JAK1/2	Ruxolitinib	0.02	21.53
STAT3	SD-36	0.96	>30

6.2.3. DTP formation is unaffected by inhibition or activation of IFN γ -JAK1/2-STAT1 signalling

To investigate the requirement for IFN γ -mediated JAK-STAT1 signalling in DTP formation, the pathway was inhibited or primed by pre-treating SK-N-AS cells with 0.5 μ M ruxolitinib for 24 h or 1 ng/mL IFN γ for 1 h, respectively, before DTP induction with 10 μ M SRA737 (Figure 6-3C). Cells were then maintained in SRA737 alone, or in combination with either ruxolitinib or IFN γ , and DTPs quantified at day 7. There was no difference in the number of DTPs generated under SRA737 exposure alone or in combination with either ruxolitinib or IFN γ (Figure 6-3D). Furthermore, there was no alteration in proliferative dye retention upon combination treatment with ruxolitinib or IFN γ (Figure 6-3E), despite effective pathway inhibition or activation at T₀ and day 7 (Figure 6-3F), indicating that these DTPs similarly originate from the starting cell population and adopt the same slow-cycling state as those induced with SRA737 alone. Consistent with published data describing STAT1 as an interferon-stimulated gene (Shuai et al. 1992), cells treated with 1 ng/mL IFN γ for 7 days showed an increase in total STAT1 protein level compared to DMSO or ruxolitinib treated controls (Figure 6-3F). A small increase in total STAT1 was also observed in SRA737-induced DTPs, consistent with the cytokine array finding that these cells secrete IFN γ ; however this was not accompanied by an increase in pY701-STAT1 levels. Strikingly, total STAT1 was upregulated to the greatest level in DTPs generated with SRA737 and IFN γ , indicating an additive effect of this combination treatment on IFN γ signalling. This could be explained by an increase in overall IFN γ

concentration as a result of upregulated cytokine secretion from DTPs (Figure 6-2) and exogenous treatment.

6.2.4. Inhibition or activation of IFN γ signalling does not alter composition of the SRA737-induced DTP population at day 7

The observation that neither inhibition nor activation of the IFN γ -JAK1/2-STAT1 signalling pathway impacted DTP formation in response to SRA737 does not exclude the possibility that ruxolitinib or IFN γ alter the day 7 persister cell population. Indeed, the same conclusion was made for tazemetostat (Figure 5-2C-D) and subsequent studies revealed that tazemetostat increased the proportion of senescent cells in SRA737-induced DTPs (Figure 5-3C).

To investigate potential changes to the day 7 population, DTPs generated under SRA737 alone, or in combination with ruxolitinib or IFN γ , were assayed for levels of apoptosis and cytotoxicity as previously described (see Section 5.2.3). In line with previous results, levels of apoptosis and cytotoxicity were higher in SRA737-induced DTPs versus DMSO-treated controls; but this increase was not significantly affected by the combination of SRA737 with ruxolitinib or IFN γ (Figure 6-4A & 6-4B).

Senescence was also quantified by β -galactosidase activity assay, as previously described (see Section 5.2.3). Consistent with previous results, the number of β -galactosidase positive cells was increased in SRA737-induced DTPs compared to DMSO control (Figure 6-4C). While this was unaffected by the addition of IFN γ , there was a small but significant decrease in the number of senescent cells under SRA737 and ruxolitinib combination treatment in comparison to SRA737 alone (Figure 6-4C; 10.9% vs. 18.3%, respectively). However, the observation that this was not significantly altered compared to the SRA737 and IFN γ combination and that the addition of IFN γ failed to inversely induce senescence, suggests this reduction may not be biologically important. As such, it would be interesting to see if this decrease has an effect on DTP progression. Nonetheless, these data

demonstrate that addition of ruxolitinib or IFN γ causes minimal compositional change to the SRA737-induced DTP population.

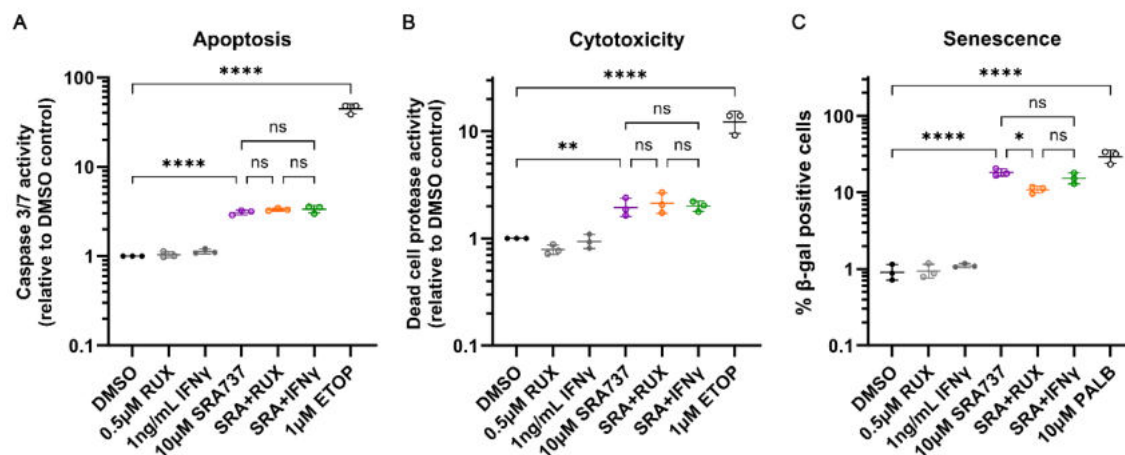


Figure 6-4: The SRA737-induced DTP population is unperturbed by combination treatment with ruxolitinib or exogenous IFN γ .

(A) Caspase 3/7 and (B) dead cell protease activity measured by ApoTox-Glo® in day 7 DTPs generated with SRA737 alone or in combination with ruxolitinib (SRA+RUX) or IFN γ (SRA+IFN γ), relative to DMSO treated control. Cells treated with 1 μ M etoposide (ETOP) for 7 days served as a positive control. Graphs show mean \pm SD of log₁₀ transformed data from three independent experiments. (C) Proportion of β -galactosidase positive cells in day 7 controls or indicated DTP populations. Cells treated with 10 μ M palbociclib (PALB) for 14 days served as a positive control. Graph shows mean \pm SD from three independent experiments. Significance statements result from comparison of means by ordinary one-way ANOVA with Tukey's correction. **** p<0.0001; ** p<0.01; * p<0.05; ns = not significant.

6.2.5. SRA737-induced DTPs have an IFN γ -like secretory cytokine profile

Although neither ruxolitinib nor IFN γ altered the cellular composition of SRA737-induced DTPs, I wondered whether there might be any changes to their secretory profiles instead. To investigate this, supernatants from combination-induced DTPs were similarly analysed by cytokine array as previously described (see Section 6.2.1). SK-N-AS cells treated for 7 days with 1 ng/mL IFN γ served as a positive control and, accordingly, showed upregulated secretion in 50% (18 out of 36) of all cytokines tested, including IL-2, IL-4, and IL-6 (Figure 6-5A). Conversely, cytokine secretion was effectively inhibited by exposure to 0.5 μ M ruxolitinib, with only IL-17A and complement component C5/C5a showing increased secretion.

There was remarkable similarity in the secretory profiles from DTPs generated with 10 μ M SRA737 and cells treated with IFN γ alone (Figure 6-5A & 6-5B). SRA737-DTPs shared 13 cytokine enrichments with IFN γ treated controls, including IL-1ra, G-CSF, and complement component C5/C5a (Figure 6-5A & 6-5B; purple). This suggests that SRA737-induced DTPs adopt a similar cellular state to cells that have been stimulated with IFN γ . DTPs generated with SRA737 and IFN γ in combination shared an almost identical profile with DTPs induced by SRA737 alone, sharing 91.7% of enrichments (Figure 6-5A & 6-5B; green). The observation that total STAT1 was highly overexpressed in DTPs generated under SRA737 and IFN γ combination (Figure 6-3F) suggested cumulative upregulation of IFN γ signalling in these cells. However, the addition of IFN γ did not appear to have a synergistic effect on cytokine secretion, as shown by similar alterations compared to DTPs generated with SRA737 alone (Figure 6-5A & 6-5B). Interestingly, cytokine secretion was not inhibited in DTPs generated under SRA737 and ruxolitinib combination treatment, indicating that JAK1/2 inhibition alone is insufficient to overcome this phenomenon in response to lethal SRA737 exposure.

An important caveat of these data is that this experiment was performed on a single occasion. Nonetheless, these results demonstrate a clear similarity

between SRA737-induced DTPs and IFN γ stimulation. While these alterations do not appear to be important for DTP formation, this work will now focus on whether there is a subsequent effect on DTP-to-DTEP transition.

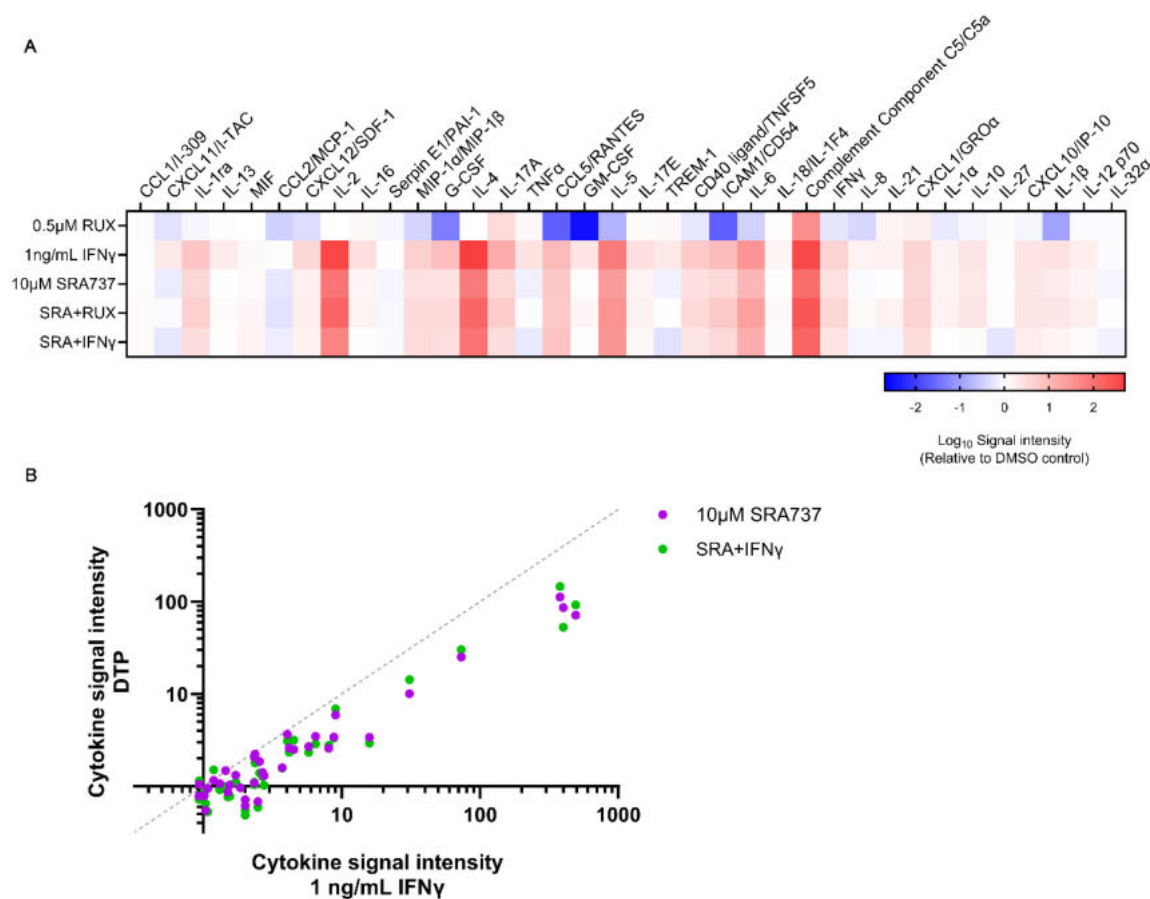


Figure 6-5: Cytokine secretion in SRA737-induced DTPs phenocopies direct IFN γ stimulation.

(A) Analysis of cytokine secretion in day 7 supernatants from control treated SK-N-AS cells (0.5 μ M RUX or 1 ng/mL IFN γ) and DTPs generated with SRA737 alone, or in combination with RUX (SRA+RUX) or IFN γ (SRA+IFN γ) using the Proteome ProfilerTM Human Cytokine Array. Signal intensity is expressed relative to a time-matched DMSO-treated control. **(B)** Comparison of cytokine secretion between IFN γ -treated control (x-axis) and DTPs generated with SRA737 alone or in combination with IFN γ (y-axis). Dotted line represents line of identity. Heat map and graph shows mean of two technical replicates from a single experiment.

6.3. Investigating the requirement of IFN γ -JAK1/2-STAT1 signalling for persister cell progression

6.3.1. Ruxolitinib fails to abrogate DTP-to-DTEP transition under SRA737 exposure

Although the IFN γ response was shown to be upregulated in day 7 DTPs (Figure 4-16C), pathway inhibition using the JAK1/2i ruxolitinib failed to reduce DTP formation under lethal SRA737 exposure (Figure 6-3D). Combined with the observation that genes associated with IFN γ responses are also upregulated in day 50 DTEPs (Figure 4-16C), I reasoned that JAK1/2-STAT1 signalling may instead be required for DTP progression. To test this, mKate2-SK-N-AS cells were used to monitor cell number during the course of long-term exposure to 10 μ M SRA737 alone or in combination with 0.5 μ M ruxolitinib (Figure 6-6A). mKate2-SK-N-AS cells treated with 0.11% DMSO or 0.5 μ M ruxolitinib alone were cultured in parallel as controls.

In line with previous observations, ruxolitinib had no significant effect on cell proliferation, and cells maintained in SRA737 gradually recovered as DTEPs after 13 days of treatment (Figure 6-6B, left panel). The addition of ruxolitinib failed to inhibit the progression of a DTEP population under continued SRA737 exposure (Figure 6-6B, left panel). In fact, responses were so similar that there was no significant difference in cell number at day 48 or proliferation rate between the two populations (Figure 6-6B, left panel, 6-6C & 6-6D). As such, these results suggest that JAK1/2 activity is not essential for DTP-to-DTEP transition under prolonged lethal SRA737 exposure.

To test if DTPs induced by SRA737 and ruxolitinib combination treatment were equally capable of recovery following complete drug withdrawal, drug-released populations were generated by removing single-agent or combination treatment after 7 days and subsequently culturing cells in DMSO-supplemented medium (Figure 6-6A). DTPs generated under SRA737 and ruxolitinib combination treatment showed no difference in proliferative recovery after drug withdrawal

(SRA+RUX>DMSO) in comparison to SRA737-released cells (SRA>DMSO), as demonstrated by no difference in day 48 cell number or proliferation rate between the two populations (Figure 6-6B, left panel, 6-6C & 6-6D). Furthermore, no differential responses were observed after release into SRA737 (SRA+RUX>SRA) or ruxolitinib (SRA+RUX>RUX) alone compared to their counterparts treated with SRA737 only (Figure 6-6B, right panel, 6-6C & 6-6D).

Together, these data demonstrate that long-term inhibition of JAK1/2 activity fails to abrogate DTP progression under continued lethal SRA737 exposure or delay recovery from the SRA737-induced DTP state.

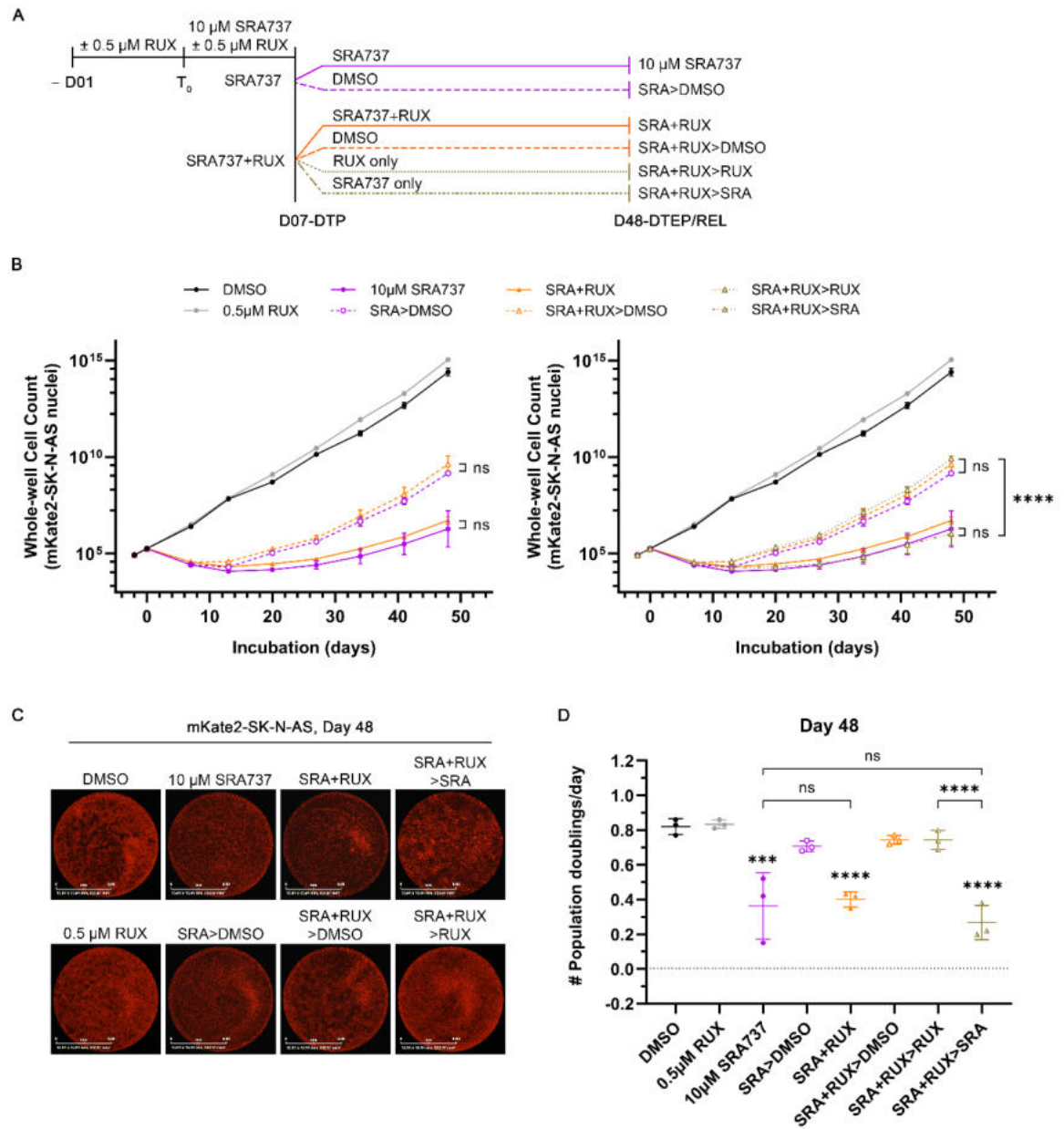


Figure 6-6: DTP-to-DTEP transition under lethal SRA737 exposure is unaffected by ruxolitinib-mediated inhibition of JAK1/2.

(A) Schematic protocol for generation of indicated DTEP populations with SRA737 alone or in combination with RUX. (B) Quantification of mKate2-labelled SK-N-AS cells treated as shown in (A) at indicated time points. (C) Whole-well fluorescence microscopy images of mKate2-SK-N-AS cells treated as in (A) at experimental end-point (day 48). (D) Proliferation rate measured by number of population doublings per day in day 48 control and persister-derived populations, as indicated. Images captured at 4X magnification, scale bar = 8 mm. Graphs show mean \pm SD from $n \geq 2$ independent experiments. Significance statements in (B) result from analysis of log₁₀ transformed data by ordinary one-way ANOVA with Šídák's correction, and (D) from comparison of means by ordinary one-way ANOVA with Tukey's correction versus DMSO control, unless otherwise indicated. **** $p < 0.0001$; *** $p < 0.001$; ns = not significant.

6.3.2. Exogenous IFN γ treatment hinders DTP-to-DTEP transition under continued SRA737 exposure

The expression of IFN γ response genes was upregulated in day 7 DTPs generated with SRA737 (Figure 4-16C), but further addition of IFN γ failed to promote DTP formation or alter the composition of the day 7 SRA737-induced DTP population (Figures 6-3 and 6-4, respectively). Since IFN γ response genes were also upregulated in day 50 DTEPs (Figure 4-16C), I hypothesised that IFN γ stimulation might instead promote quicker transition from the DTP to DTEP state with long-term SRA737 exposure. To test this, mKate2-SK-N-AS cells were used to measure long-term proliferation under SRA737 and IFN γ combination treatment (Figure 6-7A). mKate2-SK-N-AS cells treated with 0.11 % DMSO or 1 ng/mL IFN γ were cultured in parallel as controls.

In contrast to the hypothesis under test, cell numbers in DTPs generated with and continuously exposed to SRA737 and IFN γ (SRA+IFN γ) actually declined and remained suppressed through day 48 in comparison to single-agent SRA737 exposure, resulting in considerably fewer cells at day 48 (Figure 6-7B, left panel & Figure 6-7C). Consistent with this, there was a significant reduction in proliferation rate between combination-treated cells and those exposed to SRA737 alone (Figure 6-7D). These results demonstrate that the addition of IFN γ hinders DTEP emergence from the SRA737-induced DTP state.

Following this observation, I wondered if DTPs generated by SRA737 and IFN γ combination treatment were less capable of recovery following complete drug withdrawal. To test this, drug-released populations were generated as previously described (see Section 6.3.1) and proliferation monitored over time (Figure 6-7A). Combination and single-agent SRA737 DTPs recovered similarly after release into DMSO-supplemented medium at day 7, resulting in no significant difference in cell number at day 48 (Figure 6-7B, left panel & 6-7C). Furthermore, these cells (SRA+IFN γ >DMSO) recovered proliferation rate to control levels by day 48 (Figure 6-7D). These data demonstrate that DTPs generated by SRA737 and

IFN γ combination treatment are equally capable of revival following complete removal of therapeutic pressure.

These observations support a hypothesis that overstimulation of the IFN γ signalling pathway inhibits DTP progression under prolonged lethal SRA737 exposure. As such, if overactivation of IFN γ signalling is required for the observed anti-proliferative effect, cells should recover following removal of exogenous IFN γ . Conversely, continued IFN γ treatment should inhibit population recovery. To test these hypotheses, DTPs generated under combination treatment were released into either 10 μ M SRA737 or 1 ng/mL IFN γ alone at day 7 (Figure 6-7A; SRA+IFN γ >SRA and SRA+IFN γ >IFN γ , respectively). Surprisingly, cells that were released into SRA737 alone did not resume proliferation, and there was no difference in cell number at day 48 compared to those that were continuously exposed to combination treatment (Figure 6-7B, right panel & 6-7C). In contrast, cells released into IFN γ alone proliferated in line with combination-induced DTPs that had been recovered in DMSO, with no significant difference in the number of cells at day 48 (Figure 6-7B, right panel & Figure 6-7C). These cells also showed an almost complete recovery of proliferation rate to control levels (Figure 6-7D).

This additional data shows that DTPs generated by combination treatment with SRA737 and IFN γ can resume proliferation if the therapeutic pressure imposed by SRA737 is removed. However, they are unable to recover under continued lethal SRA737 exposure, even following removal of exogenous IFN γ . As observed for tazemetostat combination studies, these data suggest that DTPs induced by combination treatment are different to those generated under SRA737 alone, and overstimulation of IFN γ signalling leads to a DTP state that is more difficult to recover from.

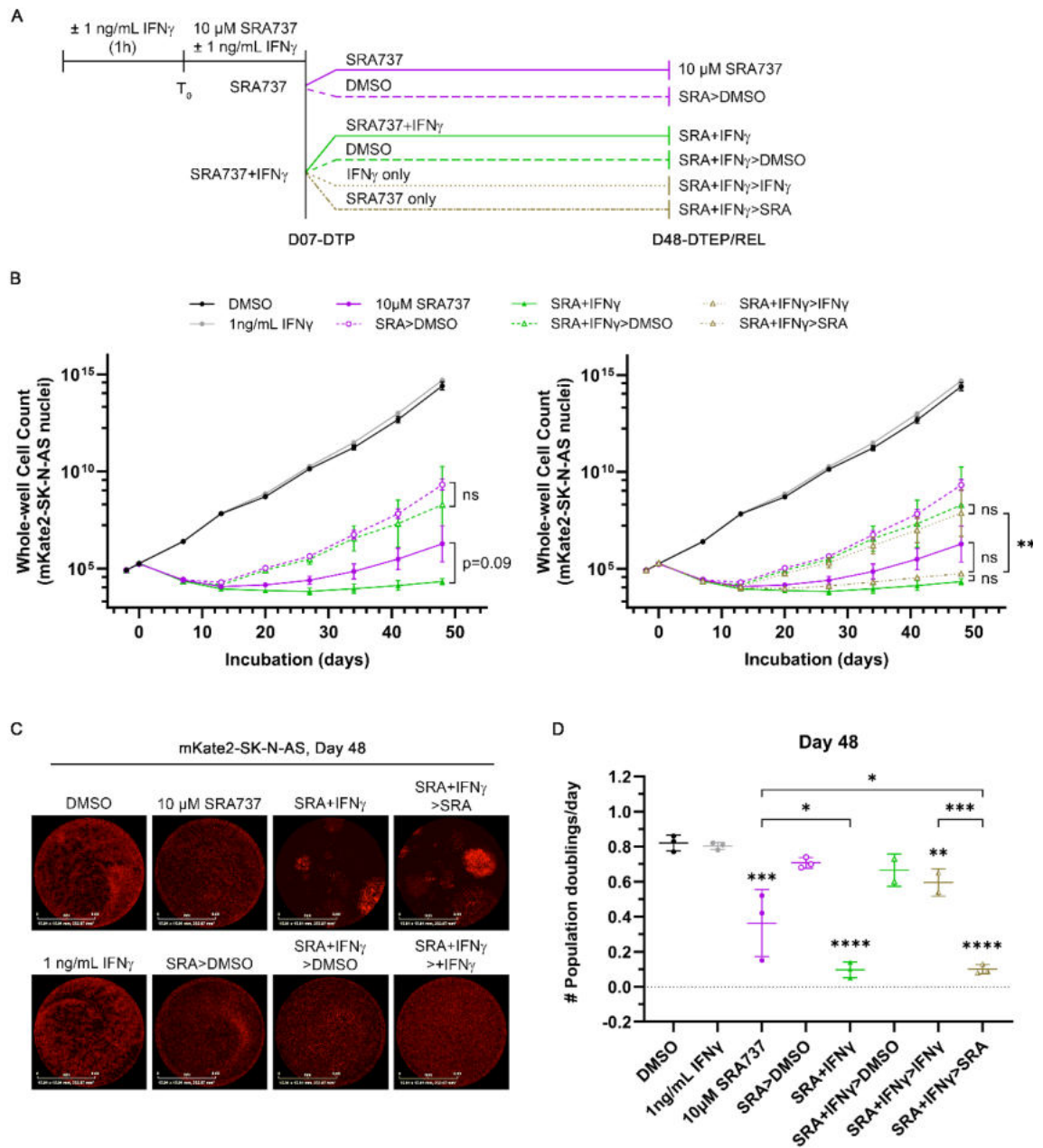


Figure 6-7: Exogenous IFN γ treatment abrogates DTP-to-DTEP transition under lethal SRA737 exposure.

(A) Schematic protocol for generation of indicated DTEP populations with SRA737 alone or in combination with IFN γ . (B) Quantification of mKate2-labelled SK-N-AS cells treated as shown in (A) at indicated time points. (C) Whole-well fluorescence microscopy images of mKate2-SK-N-AS cells treated as in (A) at experimental end-point (day 48). (D) Proliferation rate measured by number of population doublings per day in day 48 control and persister-derived populations as indicated. Images captured at 4X magnification, scale bar = 8 μ m. Graphs show mean \pm SD from three independent experiments. Significance statements in (B) result from analysis of log₁₀ transformed data by ordinary one-way ANOVA with Šidák's correction, and (D) from comparison of means by ordinary one-way ANOVA with Tukey's correction versus DMSO control, unless otherwise indicated. **** $p < 0.0001$; *** $p < 0.001$; ** $p < 0.01$; * $p < 0.05$.

6.4. Characterising populations emerging from a combination-induced DTP bottleneck

6.4.1. Populations emerging under SRA737 alone and in combination with ruxolitinib or IFN γ respond similarly to further challenge with SRA737

Having generated persister populations with SRA737 in combination with ruxolitinib or IFN γ , I wondered whether these cells behaved differently in response to further drug challenge. To investigate this, DTEP and drug-released populations were tested for SRA737 sensitivity.

Control cells exposed to DMSO, 0.5 μ M ruxolitinib, or 1 ng/mL IFN γ were equally sensitive to SRA737 and GI₅₀ values were consistent with previous observations in SK-N-AS cells (Figure 6-8A & 6-8B, left panels & Table 6-3). In comparison to previous results, SRA737-induced DTEPs were slightly more sensitive to SRA737 (~2X), with an average GI₅₀ of 6.56 μ M (Figure 6-8A, left panel, and Table 6-3). Conversely, drug-released populations were ~7X less sensitive, as shown by a SRA737 GI₅₀ of 4.05 μ M.

SRA737 GI₅₀ values were similar in DTEPs generated with SRA737 alone or in combination with ruxolitinib (Figure 6-8A, left panel & Table 6-3). SRA737 potency was also comparable in combination DTEPs maintained in SRA737 only (SRA+RUX>SRA). In comparison, combination DTEPs recovered into DMSO (SRA+RUX>DMSO) or ruxolitinib alone (SRA+RUX>RUX) were slightly more sensitive to SRA737 and GI₅₀ values were similar to SRA737 drug-released populations (SRA737>DMSO). These results are consistent with previous data showing partial resensitisation to SRA737 following drug withdrawal (Table 4-1 & 5-1). Interestingly, a very similar pattern of results was observed in populations generated from SRA737 and IFN γ combination studies (Figure 6-8B, left panel & Table 6-3). Together, these observations indicate that passage through an SRA737-induced bottleneck in combination with ruxolitinib or IFN γ does not alter responses of emerging DTEP or drug-released populations to further challenge with SRA737.

Populations were additionally tested for ruxolitinib sensitivity. Measuring population changes were more difficult in this case due to the relative low potency of ruxolitinib. Consistent with previous observations in parental SK-N-AS cells, control populations had GI₅₀ values ~20 μM (Figure 6-8A & 6-8B, right panels & Table 6-3). Small decreases in GI₅₀ potency and maximal effect at top dose (30 μM) were observed in some of the differentially derived populations, however this was limited by the assay dose range used for testing. As such, it is not presently possible to assess if populations emerging from the differential DTP states are altered in response to further challenge to ruxolitinib; however, they certainly don't show increased drug sensitivity. It would be necessary to repeat this experiment with a wider dose range to characterise this fully.

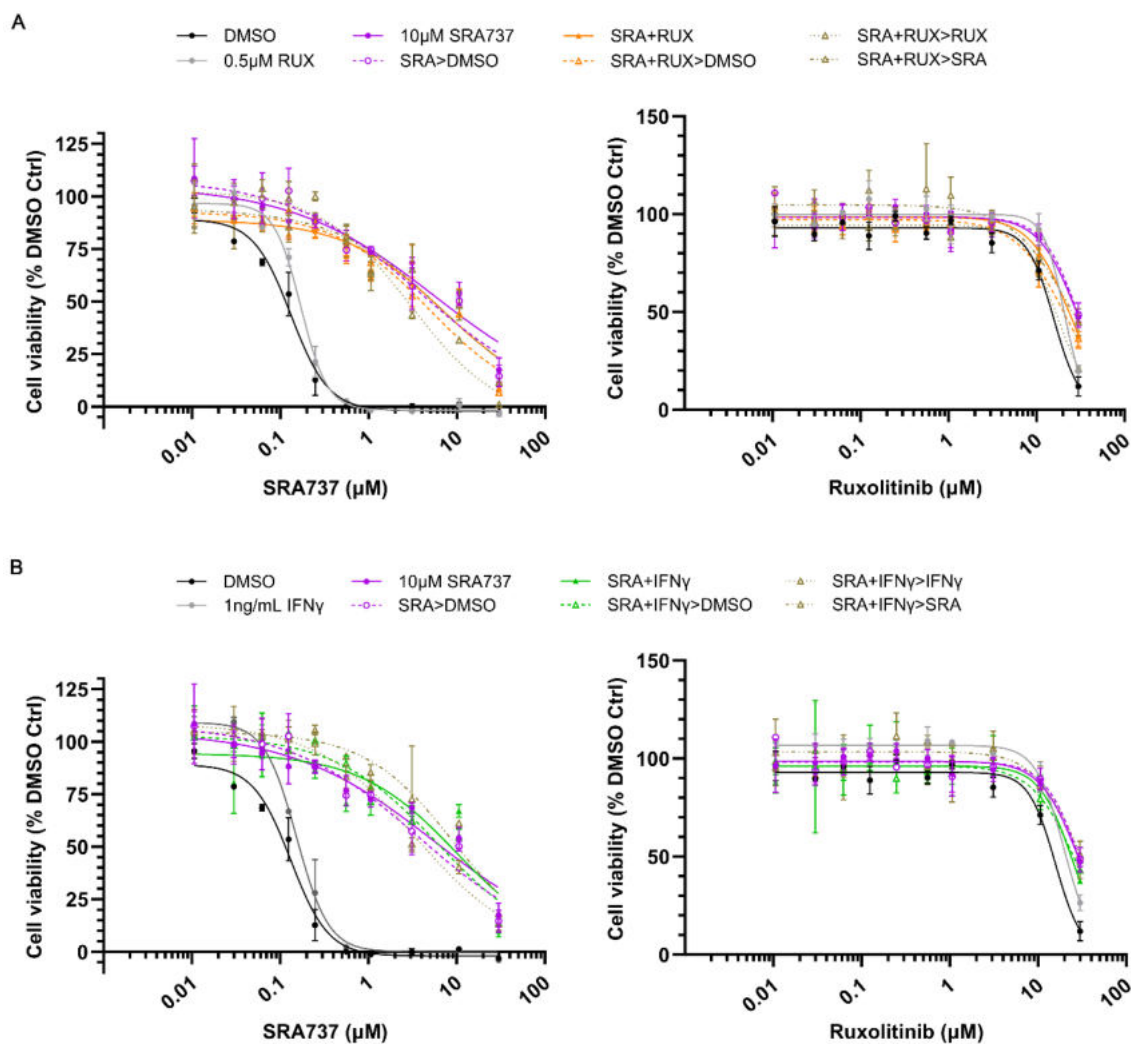


Figure 6-8: SRA737 potency is unchanged in populations emerging from the SRA737 and ruxolitinib or SRA737 and IFN γ combination DTP bottlenecks.

Non-linear regression analysis of cell viability measured by CellTiter-Glo® 120h after compound addition in populations from **(A)** SRA737 and ruxolitinib (SRA+RUX), or **(B)** SRA737 and IFN γ (SRA+IFN γ) combination studies. Graphs show mean \pm SD of two technical replicates and is representative of $n \geq 1$ independent experiments.

Table 6-3: Summary of cellular potency (GI_{50}) values for SRA737 or ruxolitinib in indicated persistor-derived and control populations.

GI_{50} values are mean \pm SD. Cells are highlighted according to fold-increase in GI_{50} value compared to drug-naïve (DMSO) control. Red \geq 50-fold; orange \geq 10-fold; yellow \geq 2-fold. N/A; not applicable, Un; undetermined.

Population	SRA737		Ruxolitinib	
	GI_{50} , μ M (n)	Fold-change from DMSO	GI_{50} , μ M (n)	Fold-change from DMSO
DMSO	0.14 \pm 0.02 (3)	N/A	20.6 \pm 3.6 (3)	N/A
0.5 μ M RUX	0.16 \pm 0.02 (3)	1.11	22.3 \pm 0.6 (3)	1.08
1 ng/mL IFN γ	0.16 \pm 0.01 (3)	1.10	22.1 \pm 0.9 (3)	1.07
10 μ M SRA737	6.56 \pm 3.74 (2)	46.16	>30 (2)	Un
SRA737>DMSO	4.05 \pm 3.04 (3)	28.51	28.8 (1)	1.40
SRA737+RUX	9.07 \pm 2.44 (3)	63.80	26.4 \pm 0.7 (2)	1.28
SRA737+RUX>DMSO	3.62 \pm 2.60 (3)	25.49	21.8 \pm 2.8 (2)	1.06
SRA737+RUX>RUX	2.09 \pm 0.79 (3)	14.71	18.9 \pm 0.3 (2)	0.91
SRA737+RUX>SRA737	8.38 \pm 2.41 (3)	58.93	25.3 \pm 1.1 (2)	1.22
SRA737+IFN γ	12.07 (1)	84.90	>30 (1)	Un
SRA737+IFN γ >DMSO	5.05 \pm 3.19 (3)	35.51	25.5 \pm 2.2 (2)	1.24
SRA737+IFN γ > IFN γ	4.04 \pm 2.40 (3)	28.43	24.4 \pm 3.7 (2)	1.18
SRA737+IFN γ >SRA737	8.95 \pm 3.95 (3)	62.94	>30 (3)	Un

6.5. Discussion

Transcriptional upregulation of inflammatory response genes are reported in persister cells generated with targeted TKi (Guler et al. 2017; Al Emran et al. 2018). Consistent with this, gene sets related to IL-2 and IL-6 signalling pathways and IFN γ responses are specifically upregulated in SRA737-induced DTP and DTEP populations, and are partially reversed after drug withdrawal, suggesting that engagement of these pathways represents a common persister cell response to diverse therapeutic challenges. This is further supported by the observation that cytokine secretion is increased in supernatants from day 7 SRA737-induced DTPs. Despite these common observations, studies investigating the requirement of cytokine signalling for DTP formation, survival, and progression are lacking.

Considering the vast majority of genes in the IFN γ response signature are upregulated, I hypothesised that SRA737-induced DTP formation could be abrogated by inhibiting the IFN γ signalling pathway using the small molecule JAK1/2 inhibitor ruxolitinib. However, there was no change in the number of DTPs generated by SRA737 alone or in combination with ruxolitinib. There were also no considerable alterations to the proportion of apoptotic, cytotoxic, or senescent cells in the day 7 DTP population. This occurred despite effective inhibition of IFN γ signalling, as measured by reduced phospho-STAT1 activation, indicating that DTP formation in response to lethal SRA737 exposure is not dependent on IFN γ -JAK1/2-STAT1 signalling.

A potential explanation for the absence of an anti-persister response upon JAK1/2 inhibition is that ruxolitinib failed to abrogate cytokine secretion in SRA737-induced DTPs, despite showing effective inhibition as a single-agent in control SK-N-AS cells. Although this experiment was performed on one occasion and would require repeating to confirm, this result indicates that inhibition of JAK1/2-STAT1 signalling is insufficient to overcome cytokine production and secretion in DTPs arising in response to SRA737. Moreover, ruxolitinib did not inhibit the emergence of a SRA737-resistant DTEP population and combination-

induced DTPs were equally capable of recovery following drug withdrawal. Together, this data indicates that alternative mechanisms of IFN γ pathway activation or compensatory signalling may contribute to cytokine production and/or signalling in SRA737-induced DTPs. Further investigation using biomarkers of IFN γ -JAK1/2-STAT1 pathway activity, such as IFN receptor activation or downstream target gene expression, or alternative cytokine-JAK-STAT signalling would help to characterise these mechanisms.

Alternatively, I hypothesised that priming the IFN γ pathway with exogenous cytokine would promote adoption of the persistor cell state and increase the number of DTPs generated under SRA737. However, as observed for ruxolitinib, there was no difference in the number of DTPs when IFN γ was included, nor were there any alterations to the day 7 DTP population in terms of apoptosis, cytotoxicity, or senescence. This was surprising given the observed overexpression of total STAT1 protein in DTPs generated with SRA737 and IFN γ combination treatment. Since STAT1 is an interferon stimulated gene, this suggested synergistic overstimulation of the IFN γ signalling pathway in combination-induced DTPs. However, this did not translate to a cumulative effect on cytokine secretion, since secretory profiles were comparably altered in DTPs induced with SRA737 alone. This could provide a potential explanation for the lack of synergy observed in this therapeutic combination. Cytokine profiling also revealed a striking similarity in secretory profiles from DTPs generated with SRA737 alone, or in combination with IFN γ , and control cells treated with 1 ng/mL IFN γ , including increased secretion of IFN γ itself. It would be important to confirm these results by repetition or using an alternative method, such as RT-qPCR, to ensure these results are not due to a limitation of the cytokine array used. Nonetheless, this data indicates that SRA737-induced DTPs may activate IFN γ response pathways, perhaps through autocrine IFN γ signalling, as a mechanism to promote their survival or maintain the DTP state.

Surprisingly, the emergence of a drug-resistant DTEP population was inhibited by combination treatment with SRA737 and IFN γ , especially since there were no alterations to the day 7 DTP population under combination treatment. This effect

was not dependent on the continued presence of IFN γ , as combination DTPs released into SRA737 alone could not progress to DTEPs. This anti-proliferative effect was equal to those maintained under combination treatment for the duration of the experiment and was substantially reduced versus SRA737 exposure alone. Conversely, combination DTPs released into IFN γ quickly resumed proliferation in line with those generated and released from single-agent SRA737 exposure. Together, these data suggest that day 7 DTPs generated by SRA737 in combination with IFN γ are different to those generated with SRA737 alone and are less capable of overcoming therapeutic challenge with SRA737.

While these data confirm that inhibition of JAK1/2 activity is insufficient to abrogate DTP formation or progression, results indicate that overactivation of the IFN γ response pathway hinders DTP-to-DTEP transition and emergence of a drug-resistant population under prolonged lethal SRA737 exposure.

Chapter 7

General Discussion

Chapter 7 General Discussion

7.1. Introduction

The emergence of drug-tolerant persister cells in response to targeted therapies has been identified as a non-mutational resistance mechanism in cancer that can precede acquired genetic resistance and serve as a reservoir for refractory disease (Sharma et al. 2010; Ramirez et al. 2016; Russo et al. 2019). Persister cells have been studied extensively in the context of tyrosine kinase inhibitors (TKi) and have recently been detected in response to alternative chemotherapies with different mechanisms of action, including anti-metabolites (Rehman et al. 2021), anti-microtubule agents (Dhimolea et al. 2021), DNA damaging agents (Dhimolea et al. 2021; Rehman et al. 2021), immunomodulatory drugs (Sehgal et al. 2021), and even radiotherapy (Zhao et al. 2023), indicating that they represent a common resistance strategy in response to drug challenge. To date, no studies have been conducted using small molecule inhibitors that interfere with DNA integrity, such as those targeting MPS1 or CHK1. With small molecule MPS1/CHK1 inhibitors currently under clinical investigation, the aims of this thesis were to identify and characterise persister cells arising in response to these novel agents, determine their contribution to the emergence of drug resistance, and identify potential therapeutic intervention points to abrogate their formation, survival, and/or progression.

7.2. DTPs mediate resistance to SRA737

Results presented in chapter three demonstrate the formation of putative persister cell populations in MDA-MB-231, SK-N-AS, and A549 cells after acute exposure to lethal concentrations (~100X GI₅₀) of targeted MPS1 or CHK1 inhibitors, and the general chemotherapeutics paclitaxel or gemcitabine. However, a *bona fide* persister response consistent with the hallmarks defined by Sharma and colleagues (2010) was achieved only in SK-N-AS cells exposed to the CHK1i SRA737.

A DTP response was excluded in MDA-MB-231 and A549 models within the remit of the characterisation work performed in these studies. Specifically, this was based on muted epigenetic changes and failure to progress or recover in the continued presence/absence of drug by day 50. However, these observations do not absolutely exclude the identity of surviving MDA-MB-231 or A549 cells as drug-tolerant persisters. As only a small number of histone modifications were measured, it is possible that putative DTPs harbour alternative or additional epigenetic alterations that play a role in DTP formation, survival, and progression under these differential contexts. The full epigenetic landscape of these cells could be defined using techniques such as CUT&Tag to investigate this further. Data presented in chapter three also indicate that DTP responses are context specific; depending on both the cellular model and therapeutic agent used. As such, it's possible that DTPs formed in response to MPS1i, paclitaxel, or gemcitabine may require longer treatment and/or recovery times to exit the persister cell state. Furthermore, DTP responses could be influenced by the genetic background or initial drug sensitivity of the cells; for example, a highly potent agent may induce a DTP state that is more difficult to overcome. Indeed, neither MDA-MB-231 nor A549 'DTPs' progressed under or recovered from lethal exposure to paclitaxel or gemcitabine, respectively, whose GI₅₀ values are both in the low nanomolar range. Additionally, while no persister cell response was observed in MDA-MB-231 cells following lethal exposure to paclitaxel, DTPs have been identified and isolated using this agent in MDA-MB-231 3D organoid models (Dhimolea et al. 2021). This highlights cell growth conditions as another

contextual difference that may influence persister cell responses to lethal drug exposure.

By contrast, a consistent subpopulation of drug-tolerant SK-N-AS cells survive 7 days treatment with a lethal dose of SRA737. These cells are slow-cycling and harbour global epigenetic alterations, including hypermethylation and deacetylation at H3K27 residues. Drug withdrawal reverses these changes and restores SRA737 sensitivity to parental levels. Conversely, prolonged drug exposure leads to the emergence of a proliferating population that are $\geq 100X$ less sensitive to SRA737. These results satisfy the persister cell hallmarks defined by Sharma and colleagues who first characterised a transiently slow-cycling, reversibly drug-tolerant DTP population in PC9 cells following lethal exposure to small molecule EGFR inhibitors (Sharma et al. 2010). Furthermore, these observations are consistent with reports from others that have identified DTP and DTEP populations using additional TKi (Liau et al. 2017; Hangauer et al. 2017; Al Emran et al. 2018; Shen et al. 2019), providing confirmation of a persister cell response under the novel therapeutic context of CHK1 inhibition.

SK-N-AS DTPs give rise to an expanded persister (DTEP) population with prolonged SRA737 exposure or resume growth after drug withdrawal (drug-released). In addition to being $\geq 100X$ less sensitive to SRA737, DTEPs are also cross-resistant to alternative CHK1i, such as LY2603618 (rabusertib), as well as DDR inhibitors targeting upstream ATR. In addition, DTEPs show no collateral sensitivity to ATMi or CHK2i, indicating that compensatory engagement of the parallel ATM-CHK2 DDR signalling axis is not a mechanism employed by persister cells to withstand SRA737 exposure; however, this was not confirmed by Western blotting for biomarkers of ATM-CHK2 activity. These results indicate that populations emerging from a DTP bottleneck are resistant to the utilised drug and a wider group of therapeutic agents targeting the same protein or pathway. These observations are in line with reports from others detailing cross-resistance in TKi-induced persister populations (Ravindran Menon et al. 2015; Liau et al. 2017; Hangauer et al. 2017), suggesting that therapeutic cross-resistance is a common persister cell characteristic, perhaps reflecting their drug-tolerant nature.

This has potential implications for treating persister-derived drug-resistant tumours in the clinic that may also demonstrate similar cross-resistance profiles. As such, it is imperative to identify and exploit therapeutic vulnerabilities that target persisters and populations emerging from the DTP state.

A caveat to this work is that only one CHK1i was used in a single cancer cell line. Expansion into alternative CHK1i, additional small molecule inhibitors of the DDR signalling pathway, such as ATRi, and other models of neuroblastoma would provide further support for DTP responses as a survival strategy to these agents.

7.3. DTPs are more prevalent in response to SRA737 exposure

SK-N-AS DTPs surviving 7 days lethal SRA737 exposure account for almost 25% of the starting population (T_0) and, furthermore, originate from the T_0 cells. By contrast, previous studies have concluded that DTPs are rare within bulk tumour populations, accounting for $\leq 5\%$ of the cell population under therapeutic challenge (Sharma et al. 2010). A potential explanation for this differential result is that DTP responses are context specific. It's reasonable to assume that different cancer types may harbour different persister cell capacities, or that DTP responses are related to the mechanism of therapeutic assault. For instance, a CHK1 inhibitor may require several rounds of cell division to accumulate irrecoverable levels of DNA damage, giving more cells a window of opportunity to survive by adopting the DTP state. This theory is supported by results from chapter three, where the number of cells surviving acute lethal drug exposure differed between cancer cell lines and type of therapeutic assault. For instance, a higher proportion of A549 cells survive gemcitabine treatment in comparison to SK-N-AS cells, despite exposure to equipotent lethal doses ($100\times GI_{50}$). These observations are in line with Sharma et al. (2010) who isolated a different number of DTPs from melanoma (1.71%) or colorectal (4.31%) cancer cell lines exposed to the RAF kinase inhibitor AZ628. Nevertheless, this result indicates that, in the context of CHK1i, a considerable proportion of cells can adopt the DTP state to survive drug challenge; a finding that contrasts with the current understanding in

the field and highlights the importance of characterising persister cell responses using a broader range of targeted therapeutics.

An important implication of this result is that this increases the pool of viable cells available for acquisition of *de novo* resistance mutations. Recent reports have shown that DTPs transiently employ adaptive mutability in response to therapeutic stress. This mechanism is utilised by bacterial persisters to boost genetic diversity and promote survival under unfavourable environmental conditions (McKenzie et al. 2001; Ponder, Fonville, and Rosenberg 2005; Rodriguez et al. 2012; Gutierrez et al. 2013). Colorectal cancer DTPs generated with cetuximab (EGFR targeted monoclonal antibody) alone, or in combination with dabrafenib (BRAF^{V600E} inhibitor), downregulated the expression of mismatch repair (MMR) and homologous recombination (HR) genes, including MLH1 and BRCA1 (Russo et al. 2019). As MMR and HR are high-fidelity DNA repair mechanisms, these results suggest that faithful restoration of DNA damage lesions may be inhibited in drug-tolerant cells. Furthermore, the expression of error-prone DNA polymerases, such as POL κ , POL λ , and POL μ , were increased while high-fidelity enzymes, such as POL ϵ and REV1, were decreased, indicating a potential switch to haphazard DNA replication. Importantly, these alterations were reversed upon drug withdrawal and were also not observed in genetically resistant populations, confirming their specific induction in the transient DTP state. Interestingly, pharmacological inhibition of REV1 activity delayed outgrowth of a persister-derived drug resistant population in response to prolonged cetuximab exposure (Russo et al. 2022), suggesting that these mechanisms represent viable therapeutic targets to abrogate DTP progression. These results suggest a general reduction in the efficacy of DNA repair and replication processes that may contribute to adaptive mutability in drug-tolerant populations. Indeed, mathematical modelling and experimental studies utilising a modified version of the Lurai-Debrück fluctuation test revealed a 7- to 50-fold increase in the mutation rate of persister populations compared to drug-sensitive cells (Russo et al. 2022), demonstrating the link between suppression of DNA integrity and increased mutational rate in DTPs, and providing evidence for the

contribution of adaptive mutability to the emergence of spontaneous resistance mutations in drug-tolerant cancer cell populations.

A more recent study has unveiled a novel source of mutability in drug-tolerant persisters. EGFR^{T790M}-resistant NSCLC clones emerging from a gefitinib-induced persister cell bottleneck showed enrichment of apolipoprotein B messenger RNA editing catalytic polypeptide-like (APOBEC) mutational signatures (Isozaki et al. 2023). APOBEC proteins are cytidine deaminases that catalyse the deamination of cytidine to uridine in DNA and RNA, causing C>T or C>G mutations in the event of ineffective repair (Butler and Banday 2023). Their activity has been implicated in promoting tumour development, with APOBEC mutational signatures identified in various cancer types (Alexandrov et al. 2013; Jakobsdottir et al. 2022). Consistent with an enrichment of APOBEC mutational signatures, APOBEC3A (A3A) mRNA and activity was increased in PC9 DTPs after 14 days exposure to gefitinib or osimertinib (Isozaki et al. 2023). As observed for mechanisms of adaptive mutability, this was reversed by drug withdrawal. While overexpression of doxycycline-inducible, catalytically active wild-type A3A (A3A^{WT}) failed to increase the number of DTP colonies, CRISPR-mediated A3A knockout delayed the emergence of drug resistant PC9 populations under prolonged osimertinib exposure. This was accompanied by a reduction in APOBEC mutational signatures in DTPs generated with lorlatinib; a small molecule inhibitor of anaplastic lymphoma kinase (ALK). Importantly, this phenotype was rescued by re-expression of exogenous A3A^{WT}, although an enzymatically inactive control was not used to verify that this was due to A3A's deaminase activity. Together, this data demonstrates the role of APOBEC enzymes in facilitating adaptive mutability in drug-tolerant cancer cell populations and highlights the value in targeting these enzymes to abrogate the emergence of resistant disease. However, the authors do address some key caveats to this work. Firstly, clinically relevant mutations that arise in EGFRi-refractory disease, such as EGFR^{T790M}, cannot be attributed to APOBEC-driven mutagenesis since the base substitutions involved are not APOBEC substrates. Secondly, the APOBEC mutations observed in persister populations are not predicted to alter protein sequence. As such, while this is certainly promising work, it is clear that

the biological significance of APOBEC induction in drug-tolerant cancer cells requires further investigation.

Considering these mutational processes are engaged in persister cells, the large DTP population observed under SRA737 exposure could further promote the evolution of drug resistance by increasing the reservoir of viable cells. Additional interrogation of RNAseq data would reveal if the expression of MMR/HR-related genes are downregulated, or any APOBEC family members are upregulated in SRA737-induced persister populations. Furthermore, comparison to dose-escalated cells would help to determine if these processes are persister-specific or represent common drug-resistance mechanisms. Indeed, work from our group (unpublished; Dr Michael Walton and Dr Fiona Want) and others (Kanu et al. 2016; Periyasamy et al. 2021) have shown that APOBEC3A/B expression and activity is upregulated in response to treatment with various chemotherapeutic agents *in vitro*, including those that induce replication stress. As CHK1 is a key mediator of the replication stress (RS) response, CHK1 inhibitors could similarly induce APOBEC activity. Moreover, given that CHK1i reduces cellular capacity to recover from RS or DNA damage by inhibiting the DDR, DTPs surviving lethal CHK1i exposure could be primed for the acquisition of genetic resistance and have increased mutational rates. These mechanisms could work in concert to drive adaptive mutability in DTPs generated with CHK1i. DNA sequencing would reveal if the frequency of genetic mutation is increased in SRA737-induced persister populations to help answer this interesting question.

7.4. Persistence and dormancy are interlinked

Further investigation of the day 7 DTP population revealed that ~20% of SRA737-induced DTPs are positive for β -galactosidase activity, a marker of cellular senescence. In addition, conditioned medium is enriched for secretory factors that form part of the senescence-associated secretory phenotype (SASP), including IL-6, GM-CSF, GRO α , and ICAM-1 (Coppé et al. 2008). Finally, expression of a universal senescence-associated gene signature (Fridman and Tainsky 2008) is upregulated in DTP and DTEP populations and is partially

reversed by drug withdrawal. It was surprising to find that this signature is still enriched in DTEPs, considering they have exited the DTP state and resumed proliferation. Perhaps this reflects a long-term consequence of becoming a DTP or is symptomatic of incomplete recovery of proliferation rate to control levels. It would be interesting to re-investigate expression of the senescence signature at a later time-point when DTEPs have completely restored proliferation. Nonetheless, these data strongly implicate cellular senescence in SRA737-induced persister cell responses. Similar observations were recently reported in dormant persister-like cells induced by combination EGFRi/MEKi treatment (Kurppa et al. 2020). Molecular profiling using Assay for Transposase-Accessible Chromatin sequencing (ATACseq) revealed an enrichment of TEA domain (Smith et al.) transcription factor motifs, suggesting that TEAD activity is important for this dormant drug-tolerant state. Indeed, both pharmacological inhibition and genetic knockout of the TEAD coactivator yes-associated protein (YAP) reduced the number of drug-induced dormant cells and abrogated regrowth following drug withdrawal. Similar results were observed in primary human acute myeloid leukemic (AML) cells after treatment with the antimetabolite chemotherapy arabinosylcytosine (Ara-C) (Duy et al. 2021). While these studies were not DTP focussed, the dormant populations generated after drug exposure harboured persister cell characteristics including drug-tolerance, epigenetic alterations, resumed proliferation with prolonged drug exposure, and recovery after drug withdrawal. As such, these data implicate senescence in DTP formation and reveal key similarities between chemotherapy induced dormancy and persistence.

This data also raises further interesting questions. Drug-induced senescence is a recognised cellular response to therapeutic stress and several studies indicate that it is reversible (Kurppa et al. 2020; Duy et al. 2021; Saleh, Tyutyunyk-Massey, and Gewirtz 2019). As such, it's possible that these cells could eventually exit the senescent state and re-enter the cell cycle following drug withdrawal or contribute to the emergence of drug-resistance in an analogous mechanism to DTEPs. Senescence could even form part of an overall persister cell response. It is likely that persistence and senescence are interlinked, and

understanding the nuances of these intertwined mechanisms could be key to addressing drug resistance arising from them. Combined with the observation that some SRA737-induced DTPs are apoptotic or necrotic, this data is particularly fascinating as it implies that not all persisters have the same fate upon lethal drug exposure. Some will adopt the DTP state, while others will enter senescence or commit apoptosis. Some may even become persisters and then perish. It would be interesting to investigate this further to identify regulatory mechanisms that could be targeted to eradicate persister cell emergence or alter cell fate, for example by promoting commitment to apoptosis over persistence. Indeed, combination studies using SRA737 and the EZH2i tazemetostat revealed a >2-fold increase in the number of senescent cells in the day 7 DTP population. This was accompanied by a small abrogation of apoptotic and cytotoxic responses, indicating that tazemetostat directs cells away from death and towards senescence, potentially allowing more cells to survive lethal SRA737 exposure. However, long-term combination treatment delayed the progression of DTEPs from an SRA737-induced DTP bottleneck, suggesting that tazemetostat-mediated inhibition of epigenetic plasticity impedes exit from the DTP state. Still, it remains unclear if tazemetostat hinders DTP-to-DTEP transition by promoting senescence in DTPs. Techniques such as lineage tracing using lentiviral barcodes could be used to determine the fate of these senescent cells. For example, the observed inhibitory effect of tazemetostat could be explained if all senescent cells eventually commit apoptosis.

More recently, induction of stress responses has been reported in persisters. Persisters generated with irinotecan in a patient-derived xenograft (PDX) model of colorectal cancer were enriched for a gene signature derived from *in vitro* diapaused mammalian embryos (Rehman et al. 2021). Embryonic diapause is a reversible state of arrested embryonic development that is triggered in response to unfavourable environmental conditions, such as nutrient deprivation (reviewed in (Fenelon, Banerjee, and Murphy 2014)). Interestingly, the diapause signature was not upregulated in tumours that had regrown following removal of chemotherapy (Rehman et al. 2021), demonstrating transient and reversible engagement of this mechanism in DTPs. Interrogation of RNA sequencing data

from additional PDX studies revealed that this signature was upregulated in patient minimal residual disease (MRD) samples compared to matched pre-treatment tumours. Furthermore, Kaplan-Meier analysis of TCGA data for patients with colorectal cancer showed that high signature expression was associated with reduced survival probability. Together, these data provide evidence for DTP formation *in vivo* and highlight the potential clinical implications of persister cell responses for prognosis and survival.

Similar results were obtained using a 3D organoid PDX model of triple negative breast cancer (TNBC) (Dhimolea et al. 2021). In this case, treatment persistent tumours were characterised by an embryonic diapause-like state in which MYC Proto-Oncogene, BHLH transcription factor (Grossmann et al.) activity was suppressed. Transcriptional profiling of persisters generated *in vitro* revealed that this was accompanied by a downregulation of metabolic processes, including DNA synthesis, RNA translation, and oxidative phosphorylation. Mechanistic investigations showed that overexpression of doxycycline-inducible Myc reduced the number of persistent cells arising in response to drug exposure, whereas CRISPR-mediated Myc knockout promoted chemotherapeutic resistance. These data reveal a key role for Myc in regulating biosynthetic dormancy as part of the persister/diapause-like cell state.

In agreement with these studies, the diapause signature defined by Rehman et al. (2021) is enriched in SRA737-induced DTP and DTEP populations and is partially reversed after drug withdrawal. Furthermore, the MSigDB Hallmark 'Myc Targets' gene set is downregulated in DTP and DTEPs, but not in drug-released populations. Altogether, this suggests that persister cells adopt a diapause-like state as a common stress response strategy to promote their survival under therapeutic challenge. A caveat to this is that the diapause signature is also enriched in control populations, perhaps suggesting that long-term culture contributes to the expression of these genes or mimics unfavourable environmental conditions. As such, characterisation of these mechanisms in SRA737-induced persisters warrants further investigation to determine if they

represent a therapeutic target to specifically abrogate DTP formation, survival, and/or progression.

In further support of the link between persistence and dormancy, the expression of a gene signature derived from quiescent neural stem cells is also enriched in SRA737-induced DTP and DTEP populations, and is partially recovered following drug withdrawal. There is much discussion in the field about whether drug-tolerant persisters are in fact cancer stem cells (CSCs). Indeed, increased expression of classic CSC markers, including CD133 (Sharma et al. 2010) and ALDH (Raha et al. 2014), is reported in some DTP models. However, this is not consistent across all DTP studies. Furthermore, several reports have demonstrated that cancer cells can stochastically enter and exit the DTP state (Rehman et al. 2021; Dhimolea et al. 2021; Oren et al. 2021; Duy et al. 2021), while CSCs follow hierarchal proliferation and are capable of self-renewal. In addition, DTPs do not show increased tumour initiating potential (Rehman et al. 2021; Echeverria et al. 2019), which is a key CSC characteristic. As such, the consensus is that DTPs share stem-like properties but are not CSCs themselves.

The enrichment of three distinct signatures that define separate cellular states suggests that DTPs are a highly heterogeneous population. However, it remains unclear whether these results are due to the simultaneous expression of different signatures within a cell, or the presence of different populations. These questions could be addressed using single-cell RNAseq or using a clonal population to reduce population heterogeneity.

7.5. Distinct drug-resistance mechanisms emerge from the DTP bottleneck

Transition through the DTP bottleneck is one route by which cancer cells can acquire drug resistance. Experimentally, most drug resistance mechanisms are studied using dose-escalated models with several reports using this approach to identify mechanisms of resistance to CHK1 inhibitors. To date, no studies have made a direct comparison between dose-escalated and persister-derived CHK1i

resistant models to investigate if the same strategies emerge via the DTP bottleneck.

Results presented in chapter four address this question. DTEP and dose-escalated populations are similarly altered in sensitivity to SRA737, alternative CHK1 inhibitors, additional DDRi targeting CHK2 and ATR, and gemcitabine. No CHK1 “gatekeeper” mutations have been reported in dose-escalated models of CHK1i-resistance using prexasertib (Blosser et al. 2020; Nair et al. 2020; Zhao et al. 2021). Consistent with this, SRA737 continues to inhibit CHK1 activation in DTEPs and dose-escalated cells, although *CHEK1* mutational status was not confirmed by DNA sequencing. Furthermore, ATR-CHK1 signalling remains functionally active in response to gemcitabine exposure and continues to be inhibited by SRA737. In both populations, however, on-target SRA737 activity fails to induce DNA damage or apoptosis, as shown by abrogation of γ H2AX and cleaved PARP accumulation, indicating that persister and dose-escalated populations are equally able to cope with genotoxic stress. These results agree with reports from dose-escalated models of prexasertib resistance (Blosser et al. 2020; Nair et al. 2020; Zhao et al. 2021), suggesting that this represents a common strategy to overcome CHK1i. This could be conferred by engagement of other DNA repair or biosynthetic pathways. Indeed, prexasertib resistant OVCAR5 cell lines are enriched for genes associated with DNA mismatch and base excision repair (Nair et al. 2020). Further interrogation of RNAseq data would reveal if alternative DNA repair pathways are employed in SRA737-induced persister or SRA737-resistant dose-escalated populations, and to what extent this represents a common mechanism of CHK1i resistance. Regardless, these results suggest that SRA737 resistance acquired through different routes results in similar drug sensitivity profiles and common dysregulation of the DDR signalling pathway. One speculation is that each transition through a DTP bottleneck would be unique, resulting in different cellular outcomes. However, RNA sequencing and drug sensitivity profiling revealed remarkable similarity in transcriptional and behavioural profiles between independently generated DTP, DTEP, or drug-released persister populations, suggesting that populations generated in the same manner can arrive at similar destinations.

However, further interrogation of the ATR-CHK1 signalling axis revealed key differences between the two SRA737-resistant populations. In line with previous reports from dose-escalated models of CHK1i resistance using prexasertib, SRA737 dose-escalated cells upregulate WEE1 protein expression (Zhao et al. 2021). Increased WEE1 levels could explain the selective reduction in potency of the WEE1i AZD1775 in dose-escalated cells. WEE1 protein levels are unaltered in DTEPs, indicating that this is not a drug-resistance mechanism employed by persister cells to overcome SRA737. Accordingly, combination treatment with AZD1775 resensitises dose-escalated cells to SRA737 more effectively than in DTEPs. Dose-escalated cells also upregulate CHK1; a mechanism that has also been reported in prexasertib resistant cells (Blosser et al. 2020). While this was not observed in persisters, one independently generated DTEP population did show a reduction in CHK1 protein levels. Interestingly, this was reported in CHK1i-resistant U2OS cells generated with CCT244747 (Hunter et al. 2022), a pre-clinical compound related to SRA737 (Walton et al. 2012), suggesting that different resistance mechanisms can arise using alternative inhibitors of the same therapeutic target. This effect arose from the concomitant downregulation of USP1, resulting in CHK1 protein destabilisation and promotion of its proteasomal degradation (Hunter et al. 2022). It would be interesting to investigate if this same mechanism was employed by SRA737-induced DTEPs.

By contrast, CDK1 protein and gene expression is specifically downregulated in SRA737-induced DTEPs. Reduced cyclin B1 expression and CDK1 activity is reported to promote prexasertib resistance in a dose-escalated model of *BRCA*^{WT} ovarian cancer by inducing a sustained G2 cell cycle delay (Nair et al. 2020), suggesting that the same drug-resistance mechanisms can emerge in dose-escalated and persister-derived drug-resistant populations. However, no changes to CDK1 expression are present in SRA737 dose-escalated cells, indicating that, in this context, downregulation of CDK1 could represent a persister-specific drug-resistance mechanism.

Profiling of specific histone H3 modifications revealed epigenetic alterations in SRA737-derived persisters that are reversed after drug withdrawal. In particular, H3K27 hypermethylation is globally enriched alongside depletion of H3K27 acetylation in DTP and DTEP populations; modifications associated with heterochromatic, genetically silent regions of the genome (Wang et al. 2008; Heintzman et al. 2009; Pasini et al. 2010; Wiles and Selker 2017). These same alterations were reported in PC9 DTPs generated with erlotinib (Guler et al. 2017), indicating that SRA737- and TKi-induced DTPs are commonly regulated by epigenetic mechanisms that alter gene expression. Furthermore, there were minimal changes to global epigenetic profiles in dose-escalated cells, suggesting that epigenetic mechanisms are specifically required for DTP formation, survival, or progression. Indeed, epigenetic alterations are consistently reported in persister cells generated using TKi (Sharma et al. 2010; Guler et al. 2017; Liao et al. 2017; Al Emran et al. 2018), confirming the importance of epigenetic mechanisms in persister cell biology. An important consideration for this data is that measurement of histone modifications by Western blotting can only provide information about changes to the global epigenetic landscape, neglecting the contextual importance of epigenetic alterations at regulatory genomic loci, such as enhancer or promoter regions. As such, while no substantial changes were observed in dose-escalated populations using this method, this does not exclude the presence of localised epigenetic alterations that can alter gene expression. Techniques such as ChIPseq or CUT&Tag could be used to define these changes and their transcriptional consequences in SRA737-induced DTP populations, as well as reveal alterations to a wider range of epigenetic modifications that were unexplored in this work.

Interrogation of RNAseq data from dose-escalated cells and DTP and DTEP populations revealed common and unique transcriptional changes. Several gene sets were commonly upregulated in persister and dose-escalated cells, including those related to apoptosis and EMT. These have been similarly reported in dose-escalated models of prexasertib resistance (Blosser et al. 2020), suggesting that these represent common CHK1i resistance mechanisms. Consistent with other DTP models generated with TKi (Liao et al. 2017; Shen et al. 2019),

topoisomerase inhibitors (Rehman et al. 2021), and anti-microtubule agents (Dhimolea et al. 2021), cell cycle and proliferation related genes are downregulated in SRA737-induced persisters, but not in dose-escalated populations. This could be representative of the slow cycling DTP state or reflect induction of persister-related dormancy (see Section 7.4). Regardless, downregulation of proliferative activity is a common persister cell strategy.

The expression of gene signatures related to senescence, quiescence, and embryonic diapause have been reported in other DTP models (Liau et al. 2017; Kurppa et al. 2020; Duy et al. 2021; Rehman et al. 2021; Dhimolea et al. 2021) and are upregulated in SRA737-induced DTP and DTEPs. Their expression was partially recovered after SRA737 withdrawal, indicating that these represented persister-specific mechanisms. However, this is challenged by the observation that senescence and quiescence signatures were also increased in dose-escalated cells, suggesting that these may actually be common drug resistance mechanisms. Further investigation using cellular markers could be used to determine whether these gene expression changes translate to a senescent or quiescent phenotype, as observed for persister populations (see Section 7.4).

Interestingly, a number of pathways related to inflammatory responses and cytokine signalling are upregulated in SRA737-derived persister populations. These include IL-2/STAT5, IL-6/JAK/STAT3, and IFN γ response genes that have similarly been reported in other DTP models (Guler et al. 2017; Al Emran et al. 2018; Isozaki et al. 2023). Given that these gene sets were not enriched in dose-escalated SRA737-resistant populations, these results indicate that they represent genuine persister-specific mechanisms.

Together, these results demonstrate that distinct SRA737-resistance mechanisms can arise through the DTP bottleneck, contributing to the growing body of evidence that DTPs are a potential source of alternative or additional drug-resistance mechanisms. As such, persister-derived populations represent a different entity that require selective targeting to eradicate.

7.6. Entry into the DTP state has long-term consequences

Persister cells are characterised by reversible drug-tolerance, as evidenced by a return to sensitivity upon drug withdrawal (Sharma et al. 2010; Liau et al. 2017). PC9-DTPs generated using the EGFRi erlotinib regain drug sensitivity within 9 population doublings in drug-free medium (Sharma et al. 2010), and glioblastoma DTPs resensitise to dasatinib as quickly as two weeks after drug withdrawal (Liau et al. 2017). By comparison, CHK1i-induced DTPs remain less sensitive to SRA737 43 days after drug release (equivalent to ~18 population doublings). This is quite remarkable considering SK-N-AS DTPs are induced by only 7 days treatment with lethal SRA737 concentrations. A potential reason for this disparity is that a DTP state induced by a CHK1 inhibitor may be more difficult to recover from than TKi exposure, especially given the function of CHK1 in coordinating DNA damage responses and maintaining genome integrity (Walworth, Davey, and Beach 1993; Sanchez et al. 1997; Gupta et al. 2018). This also highlights the importance of characterising persister cells using a diverse range of therapeutic agents in different cancer types, since not all persister responses may be the same.

Drug-released cells recover proliferation rate, reverse epigenetic changes, and re-express CDK1 after 43 days culture in SRA737-free medium, suggesting a return to a control-like state. While RNA sequencing revealed a relatively smaller number of differentially expressed genes in drug-released cells compared to DTPs and DTEPs, gene sets that were upregulated in DTP and DTEP populations are only partially restored after SRA737 withdrawal, indicating that drug-released cells had not yet fully recovered from the DTP state. Indeed, DDRi profiling revealed incomplete drug resensitisation in these cells, as shown by GI_{50} values remaining elevated; but not to the same magnitude as DTEPs. This is further supported by the partial induction of apoptosis (cleaved PARP) in drug-released populations upon treatment with SRA737 in combination with gemcitabine that is absent in SRA737-resistant DTEPs. Together, these data demonstrate that while adoption of the DTP state is transient and reversible, there are long-term consequences to becoming a persister cell.

These observations are in line with those from a recent report using drug-released persisters (DRPs) generated by 6 weeks drug withdrawal after initial DTP induction with the EGFRi gefitinib (Jacob Berger et al. 2021). Despite regaining drug sensitivity, PC9 DRP populations generated 4.2X more DTPs upon drug re-challenge compared to drug-naïve control. This was maintained ≥ 10 weeks after DTP induction, suggesting that entry into the persister cell state leaves an imprint long after cells have recovered. This effect was mathematically quantified as “chance to persist” (CTP), which was calculated to be higher in DRP populations and accounted for by selective enrichment of cells with a greater CTP probability. Furthermore, CTP increased with duration of initial drug exposure and multiple cycles of drug treatment suggesting that drug-tolerance is, to some degree, a heritable trait. It would be interesting to investigate whether SRA737-released persisters show the same response to rechallenge with lethal drug concentrations. Considering the large proportion of DTPs generated in response to SRA737 exposure and the chance of adopting the DTP state accumulating with treatment time and cycles, this could provide an even greater reservoir for the emergence of treatment refractory disease.

Further long-term studies using four independently generated SRA737-released populations showed that, despite being similarly less sensitive to SRA737 at day 50 (43 days after drug withdrawal), only two populations (REL-3 and REL-4) resensitised to SRA737 by day 274 (~40 weeks). Furthermore, each of these two populations took different routes to SRA737 resensitisation, with REL-4 regaining sensitivity ~12 weeks earlier than REL-3. SRA737 resensitisation is accompanied by restored sensitivity to additional DDRi inhibitors while, conversely, populations remaining resistant to SRA737 are also cross-resistant to these agents. These results indicate that not all DTPs are created equal; some can fully recover drug sensitivity while others maintain a drug-resistant state long after alleviation of therapeutic pressure.

A potential explanation for these differential results are the alterations observed in the ATR-CHK1 signalling axis between REL-1 to REL-4. For example, REL-4 regained SRA737 sensitivity the quickest and was the only population without

overexpression of CHK1 or WEE1 at day 50. By contrast, REL-1 remained insensitive to SRA737 and overexpressed both these proteins. However, these cannot be the sole determinants since CHK1 and WEE1 were similarly overexpressed in REL-3, that eventually resensitised to SRA737 after ~40 weeks in drug-free medium. Therefore, there must be additional mechanisms involved in regulating recovery from the DTP state. Given these differential results in populations generated in the same manner, it would be interesting to determine what these mechanisms are. As it stands, these data reveal the long-term consequences of adopting the DTP state in response to SRA737. This could have potential clinical implications as it suggests that use of a “drug-holiday” may not be an effective therapeutic strategy when treating patients with DDR inhibitors.

7.7. EZH2 activity is required for DTEP emergence from the DTP bottleneck

H3K27 is methylated by the histone methyltransferase EZH2 that works in concert with SUZ12 as part of PRC2 protein complex; an epigenetic complex that functions as a transcriptional repressor by methylating H3K27 residues (Cao et al. 2002; Cao and Zhang 2004; Pasini et al. 2004). Global enrichment of H3K27_{me3} in DTP and DTEP populations suggests a requirement for EZH2 activity and gene suppression in SRA737-induced DTP formation, survival, or progression. This is supported by concomitant global depletion of H3K27 acetylation in these cells, a mark associated with active gene expression (Wang et al. 2008; Pasini et al. 2010). Consistent with this hypothesis, genes associated with EZH2 and SUZ12 transcriptional activity are enriched in DTPs and DTEPs, with these changes partially reversed after SRA737 withdrawal. Moreover, an increased H3K27_{me3}/H3K27_{ac} ratio is observed in PC9-DTPs generated with erlotinib (Guler et al. 2017) and proteomic analysis of lapatinib-induced SKBR3 persisters revealed an increase in EZH2 methyltransferase activity (Pham et al. 2020), suggesting that engagement of EZH2 activity is a common persister mechanism that could be targeted to abrogate DTP formation. Combined with the observation that minimal global epigenetic changes are observed in dose-

escalated SRA737-resistant cells, these data indicate that engagement of EZH2 activity is predominantly a persister-specific strategy.

EZH2 inhibition using the small molecule inhibitor tazemetostat failed to abrogate DTP formation in response to lethal SRA737 exposure, or inhibit DTEP survival, despite effective depletion of H3K27_{me3} levels. This contradicts observations from PC9 persisters in which tazemetostat-mediated EZH2 inhibition reduced the number of DTPs generated in response to erlotinib exposure (Guler et al. 2017). Emergence of a DTEP population from an SRA737-induced bottleneck was inhibited by tazemetostat in long-term studies, demonstrating that EZH2 activity is required for DTP-to-DTEP transition. The observation that this effect is not dependent on the continued presence of tazemetostat after day 7 indicates that combination induced DTPs are fundamentally different to those generated under SRA737 alone, and EZH2 inhibition leads to a DTP state with reduced capacity to overcome therapeutic pressure imposed by SRA737. As such, these data support a therapeutic rationale for the combinatorial use of tazemetostat with SRA737 to prevent further growth and expansion of DTPs to a *bona fide* drug resistant population.

Further mechanistic investigations will be required to decipher the observed effects of tazemetostat on SRA737-induced persister cell progression. Evidence indicates that tazemetostat exerts its inhibitory effect at the early DTP stage. Therefore, molecular profiling of combination DTPs using H3K27_{me3}-directed ChIPseq could be used to identify genes that are specifically regulated by EZH2 and reveal potential mechanisms underlying this altered DTP state. Additionally, it would be interesting to determine if EZH2 enzymatic activity alone or its function as part of the larger PRC2 complex is important for the observed anti-persister effect. This could be achieved using pharmacological or genetic tools to inhibit individual PRC2 components, including SUZ12 and embryonic ectoderm development (EED) proteins that are both essential for PRC2 function (Pasini et al. 2004; Cao et al. 2014). The effect of EZH2 overexpression on DTP formation, population composition, and progression could also be investigated as part of complementary studies.

Notably, while tazemetostat combination delays DTP progression under prolonged SRA737 exposure, it does not eradicate these cells, at least *in vitro*. It is unclear if this inhibitory effect alone would be efficacious enough to mitigate the emergence of drug-resistance in the clinic. It is possible that these remaining DTPs eventually die or are cleared by the immune system. Certainly, SRA737-induced DTPs increase secretion of a number of cytokines that are reported to promote immune cell infiltration into solid tumours, including CCL5 and CXCL10 (Zumwalt et al. 2015; Dangaj et al. 2019; Mowat et al. 2021). As the majority of persistence cell studies are conducted *in vitro*, or using immunodeficient/immunocompromised animal models, it remains unclear how DTPs interact with the microenvironment and the immune system. As such, the development of alternative *in vitro* or *in vivo* models may be required to answer these key questions.

Alternatively, the remaining DTPs could eventually overcome drug challenge and resume proliferation given more time. The characteristics of the resulting population are unknown, however drug sensitivity testing in combination DTPs that were recovered into drug-free medium suggests that these cells could be even more resistant to SRA737. While this requires confirmation and further characterisation, these results have potential implications for the use of tazemetostat in combination with SRA737 in the clinic. A way of addressing this could be to assess emerging populations for further therapeutic vulnerabilities using pharmacological and/or genetic screens.

7.8. IFN γ signalling – master regulator of DTP cell fate?

IL-2/STAT5, IL-6/JAK/STAT3, and IFN γ response genes are specifically upregulated in SRA737-induced DTP and DTEP populations, suggesting a role for inflammatory signalling in DTP formation, survival, and/or progression. Consistent with this, conditioned medium from day 7 DTPs was enriched for pro-inflammatory cytokines and chemokines that are known to be regulated by these signalling pathways, such as IL-4 (Kovanen et al. 2005), CCL5 (Liu, Guan, and Ma 2005), and CXCL10 (Ren, Kennedy, and Colletti 2002), as well as IL-2, IL-6,

and IFN γ themselves. Upregulation of genes associated with inflammatory signalling has been similarly reported in TKi-induced DTPs (Guler et al. 2017; Al Emran et al. 2018), indicating that persister cells engage these mechanisms as a common response to drug challenge.

This raises questions about the function of inflammatory signalling and cytokine secretion in DTP biology. Molecular profiling of persister-like cells emerging in response to EGFRi revealed an enrichment of IFN γ , TNF α , and IL-6/JAK/STAT signalling pathways that was accompanied by increased senescence markers, including β -galactosidase activity and p27^{Kip} induction (Kurppa et al. 2020), suggesting a key role for immune and inflammatory signalling pathways in mediating or regulating cellular senescence. This is interesting given that a large proportion of SRA737-induced DTPs are senescent, as shown by ~20% staining positive for β -galactosidase activity, and also express a senescence-associated gene signature. Day 7 DTPs also secrete high levels of IL-6; a prominent soluble SASP factor (Coppé et al. 2008). As such, activation of inflammatory signalling and resultant cytokine secretions could promote entry into and maintenance of a senescent state as part of a persister response to SRA737 exposure.

Another potential function of cytokine signalling in DTPs is to promote adaptive mutability. ATACseq analysis of PC9 DTPs with increased A3A activity and mRNA expression revealed an increase in chromatin accessibility upstream of the transcription start site of the *APOBEC3A* gene (Isozaki et al. 2023). This was enriched for NF κ B and STAT2/3 transcription factor motifs. RNAi-mediated NF κ B knockdown abrogated *APOBEC3A* gene expression in response to osimertinib exposure. Combined with the observation that IFN γ can activate NF κ B (Lin, Jamison, and Lin 2012; Mitchell et al. 2019), and IFN γ secretion and pathway gene expression are increased in SRA737-DTPs, this suggests that IFN γ signalling could promote DTP survival by driving adaptive mutability.

As key mediators of immune responses that regulate cell proliferation, differentiation, and migration, persister cells could potentially exploit cytokine/JAK/STAT signalling pathways to promote their survival under

therapeutic assault. Indeed, medulloblastoma cells exposed to IL-6 supplemented medium were less sensitive to the alkaloid chemotherapy agent vincristine (Sreenivasan et al. 2020). This was found to be due to autocrine IL-6 signalling that activated STAT3 transcriptional activity and expression of IL-6 target genes. In addition, IL-2 signalling activates the JAK1/3/STAT5 pathway to induce expression of the anti-apoptotic *BCL-2* gene (Akbar et al. 1996). IFN γ /JAK/STAT1 signalling can also induce PD-L1 expression to promote immune evasion in cancer (Moon et al. 2017; Garcia-Diaz et al. 2017). Since these cytokines are increased in SRA737-DTP supernatants, it's possible they function in a similar autocrine/paracrine manner to promote DTP survival. This theory is supported by the observation that STAT1 protein expression is increased in day 7 DTPs. As an IFN γ stimulated gene, its upregulated expression could be the result of increased IFN γ secretion in the DTP microenvironment, leading to the hypothesis that inhibiting this pathway using a small molecule JAK inhibitor would abrogate DTP formation, survival, or progression. Against the hypothesis under test, inhibition of IFN γ -JAK1/2-STAT1 signalling using the JAK1/2 inhibitor ruxolitinib failed to abrogate DTP formation or delay the emergence of a DTEP population in response to SRA737 exposure. Perhaps this is unsurprising given that JAK inhibition also failed to inhibit the emergence of drug-tolerant PC9 clones under prolonged erlotinib exposure (Sharma et al. 2010). A potential reason for this result could be the engagement of compensatory JAK/STAT or alternative signalling pathways that promote or regulate IFN γ signalling. Certainly, ruxolitinib combination treatment did not suppress cytokine secretion in SRA737-DTPs.

By contrast, combination treatment with exogenous IFN γ inhibited DTP-to-DTEP transition and the emergence of a DTEP population under prolonged SRA737 exposure. This result was surprising given that I expected priming the IFN γ pathway to promote DTP progression and no alterations in levels of apoptosis, cytotoxicity, or necrosis were observed in the day 7 DTP population to indicate an anti-persist effect. The only differential result was a substantial overexpression of STAT1 protein in combination-induced DTPs, indicating hyperactivation of the IFN γ signalling pathway in these cells. However, this was

not reflected by a cumulative increase in cytokine secretion. Perhaps signalling hyperactivation crosses a threshold that is no longer compatible with persister cell adaptability or survival. The exact nature of the remaining cells after ~50 days combination treatment was not investigated; it would be interesting to find out whether they have entered a prolonged dormant state. However, the observation that these cells could be tested for drug sensitivity in a proliferation assay that was conducted in the absence of continued drug exposure suggests this is not the case. This combination effect was not dependent on the continued presence of IFN γ as cell numbers remained suppressed after release into SRA737 alone. As such, this indicates that IFN γ alters the early DTP state in a way that renders them less capable of recovery with continued therapeutic challenge with SRA737. Further profiling using RNA sequencing could help to reveal the molecular mechanisms underlying this effect.

There is considerable similarity in DTP responses to combination treatment with exogenous IFN γ and the EZH2 inhibitor tazemetostat. The addition of neither agent had an impact on SRA737-induced DTP formation or population composition, and yet they both inhibited DTP progression under prolonged SRA737 exposure. This is conferred by alterations to the early DTP state, since cells were unable to progress with continued SRA737 exposure following removal of tazemetostat or IFN γ . It's very interesting that this short-term combination treatment dictated long-term cellular responses, and perhaps reflects reduced cellular plasticity in the day 7 DTP population. Further investigation and comparison of these populations will help determine if these effects are regulated by common mechanisms.

7.9. Concluding remarks

This study is the first to identify and characterise the emergence of a drug-tolerant persister cell population using a small molecule CHK1 inhibitor, adding to the body of work investigating the emergence of this problematic population and expanding the persister cell response into a novel therapeutic context. Furthermore, I have identified EZH2 as a target to abrogate DTP progression, consolidating the requirement of epigenetic modifications to support cellular plasticity as a common persister cell mechanism. Moreover, I have uncovered additional evidence to support the engagement of inflammatory signalling pathways as a shared tactic in persister cell populations and characterised an anti-persister effect using exogenous IFN γ . In light of SRA737 being under clinical investigation, this expands our knowledge of the persister cell response into a new, therapeutically relevant context. This is particularly poignant since other agents targeting DNA repair mechanisms are similarly in clinical trial or approved for use, such as the PARP inhibitor olaparib. Therefore, identification of a DTP response within this class of anti-cancer agents could inform clinical practice.

To date, the persister cell phenomenon has been identified in additional cancer cell types (AML, breast and colorectal cancer, melanoma, glioblastoma) in response to a growing number of diverse chemotherapeutic agents, including targeted small molecules, anti-metabolites, immunomodulatory drugs, and even radiotherapy, demonstrating the extent of the persister cell problem. It is becoming increasingly evident that persister cells represent a common response to drug challenge, and it is imperative that further studies are conducted to identify therapeutic interventions to undermine and/or abrogate the drug-tolerant state for the successful treatment of cancer.

References

- Abrieu, A., L. Magnaghi-Jaulin, J. A. Kahana, M. Peter, A. Castro, S. Vigneron, T. Lorca, D. W. Cleveland, and J. C. Labbé. 2001. 'Mps1 is a kinetochore-associated kinase essential for the vertebrate mitotic checkpoint', *Cell*, 106: 83-93.
- Ahn, Joon-Young, Julie K. Schwarz, Helen Piwnica-Worms, and Christine E. Canman. 2000. 'Threonine 68 Phosphorylation by Ataxia Telangiectasia Mutated Is Required for Efficient Activation of Chk2 in Response to Ionizing Radiation1', *Cancer Research*, 60: 5934-36.
- Akbar, A. N., N. J. Borthwick, R. G. Wickremasinghe, P. Panayoitidis, D. Pilling, M. Bofill, S. Krajewski, J. C. Reed, and M. Salmon. 1996. 'Interleukin-2 receptor common gamma-chain signaling cytokines regulate activated T cell apoptosis in response to growth factor withdrawal: selective induction of anti-apoptotic (bcl-2, bcl-xL) but not pro-apoptotic (bax, bcl-xS) gene expression', *Eur J Immunol*, 26: 294-9.
- Al Emran, A., D. M. Marzese, D. R. Menon, M. S. Stark, J. Torrano, H. Hammerlindl, G. Zhang, P. Brafford, M. P. Salomon, N. Nelson, S. Hammerlindl, D. Gupta, G. B. Mills, Y. Lu, R. A. Sturm, K. Flaherty, D. S. B. Hoon, B. Gabrielli, M. Herlyn, and H. Schaidler. 2018. 'Distinct histone modifications denote early stress-induced drug tolerance in cancer', *Oncotarget*, 9: 8206-22.
- Alexandrov, Ludmil B., Serena Nik-Zainal, David C. Wedge, Samuel A. J. R. Aparicio, Sam Behjati, Andrew V. Biankin, Graham R. Bignell, Niccolò Bolli, Ake Borg, Anne-Lise Børresen-Dale, Sandrine Boyault, Birgit Burkhardt, Adam P. Butler, Carlos Caldas, Helen R. Davies, Christine Desmedt, Roland Eils, Jörunn Erla Eyfjörd, John A. Foekens, Mel Greaves, Fumie Hosoda, Barbara Hutter, Tomislav Ilcic, Sandrine Imbeaud, Marcin Imielinski, Natalie Jäger, David T. W. Jones, David Jones, Stian Knappskog, Marcel Kool, Sunil R. Lakhani, Carlos López-Otín, Sancha Martin, Nikhil C. Munshi, Hiromi Nakamura, Paul A. Northcott, Marina Pajic, Elli Papaemmanuil, Angelo Paradiso, John V. Pearson, Xose S. Puente, Keiran Raine, Manasa Ramakrishna, Andrea L. Richardson, Julia Richter, Philip Rosenstiel, Matthias Schlesner, Ton N. Schumacher, Paul N. Span, Jon W. Teague, Yasushi Totoki, Andrew N. J. Tutt, Rafael Valdés-Mas, Marit M. van Buuren, Laura van 't Veer, Anne Vincent-Salomon, Nicola Waddell, Lucy R. Yates, Jessica Zucman-Rossi, P. Andrew Futreal, Ultan McDermott, Peter Lichter, Matthew Meyerson, Sean M. Grimmond, Reiner Siebert, Elías Campo, Tatsuhiro Shibata, Stefan M. Pfister, Peter J. Campbell, Michael R. Stratton, Initiative Australian Pancreatic Cancer Genome, ICGC Breast Cancer Consortium, ICGC MML-Seq Consortium, and ICGC PedBrain. 2013. 'Signatures of mutational processes in human cancer', *Nature*, 500: 415-21.
- Anderhub, S. J., G. W. Mak, M. D. Gurden, A. Faisal, K. Drosopoulos, K. Walsh, H. L. Woodward, P. Innocenti, I. M. Westwood, S. Naud, A. Hayes, E. Theofani, S. Filosto, H. Saville, R. Burke, R. L. M. van Montfort, F. I. Raynaud, J. Blagg, S. Hoelder, S. A. Eccles, and S. Linardopoulos. 2019. 'High Proliferation Rate and a Compromised Spindle Assembly Checkpoint Confers Sensitivity to the MPS1 Inhibitor BOS172722 in Triple-Negative Breast Cancers', *Mol Cancer Ther*, 18: 1696-707.
- Arora, S., K. M. Bisanz, L. A. Peralta, G. D. Basu, A. Choudhary, R. Tibes, and D. O. Azorsa. 2010. 'RNAi screening of the kinome identifies modulators of cisplatin response in ovarian cancer cells', *Gynecol Oncol*, 118: 220-7.
- Baba, A., F. Ohtake, Y. Okuno, K. Yokota, M. Okada, Y. Imai, M. Ni, C. A. Meyer, K. Igarashi, J. Kanno, M. Brown, and S. Kato. 2011. 'PKA-dependent regulation of the histone lysine demethylase complex PHF2-ARID5B', *Nat Cell Biol*, 13: 668-75.
- Bachmann, I. M., O. J. Halvorsen, K. Collett, I. M. Stefansson, O. Straume, S. A. Haukaas, H. B. Salvesen, A. P. Otte, and L. A. Akslen. 2006. 'EZH2 expression is associated with high proliferation rate and aggressive tumor subgroups in cutaneous melanoma and cancers of the endometrium, prostate, and breast', *J Clin Oncol*, 24: 268-73.
- Balaban, Nathalie Q., Jack Merrin, Remy Chait, Lukasz Kowalik, and Stanislas Leibler. 2004. 'Bacterial Persistence as a Phenotypic Switch', *Science*, 305: 1622-25.
- Barnard, Darlene, H. Bruce Diaz, Teresa Burke, Gregory Donoho, Richard Beckmann, Bonita Jones, David Barda, Constance King, and Mark Marshall. 2016. 'LY2603618, a selective CHK1 inhibitor, enhances the anti-tumor effect of gemcitabine in xenograft tumor models', *Invest New Drugs*, 34: 49-60.

- Baskin, F., R. N. Rosenberg, and V. Dev. 1981. 'Correlation of double-minute chromosomes with unstable multidrug cross-resistance in uptake mutants of neuroblastoma cells', *Proc Natl Acad Sci U S A*, 78: 3654-8.
- Bean, James, Cameron Brennan, Jin-Yuan Shih, Gregory Riely, Agnes Viale, Lu Wang, Dhananjay Chitale, Noriko Motoi, Janos Szoke, Stephen Broderick, Marissa Balak, Wen-Cheng Chang, Chong-Jen Yu, Adi Gazdar, Harvey Pass, Valerie Rusch, William Gerald, Shiu-Feng Huang, Pan-Chyr Yang, Vincent Miller, Marc Ladanyi, Chih-Hsin Yang, and William Pao. 2007. '<i>MET</i> amplification occurs with or without <i>T790M</i> mutations in <i>EGFR</i> mutant lung tumors with acquired resistance to gefitinib or erlotinib', *Proceedings of the National Academy of Sciences*, 104: 20932-37.
- Bell, Charles C., and Omer Gilan. 2020. 'Principles and mechanisms of non-genetic resistance in cancer', *British Journal of Cancer*, 122: 465-72.
- Bell, D. R., J. H. Gerlach, N. Kartner, R. N. Buick, and V. Ling. 1985. 'Detection of P-glycoprotein in ovarian cancer: a molecular marker associated with multidrug resistance', *J Clin Oncol*, 3: 311-5.
- Berger, M. S., G. W. Locher, S. Saurer, W. J. Gullick, M. D. Waterfield, B. Groner, and N. E. Hynes. 1988. 'Correlation of c-erbB-2 gene amplification and protein expression in human breast carcinoma with nodal status and nuclear grading', *Cancer Res*, 48: 1238-43.
- Bertoni, F., A. M. Codegoni, D. Furlan, M. G. Tibiletti, C. Capella, and M. Broggin. 1999. 'CHK1 frameshift mutations in genetically unstable colorectal and endometrial cancers', *Genes Chromosomes Cancer*, 26: 176-80.
- Bigger, Joseph W. 1944a. 'The bactericidal action of penicillin on Staphylococcus pyogenes', *Irish Journal of Medical Science (1926-1967)*, 19: 553-68.
- Bigger, Joseph W. 1944b. 'TREATMENT OF STAPHYLOCOCCAL INFECTIONS WITH PENICILLIN BY INTERMITTENT STERILISATION', *The Lancet*, 244: 497-500.
- Blosser, W. D., J. A. Dempsey, A. M. McNulty, X. Rao, P. J. Ebert, C. D. Lowery, P. W. Iversen, Y. W. Webster, G. P. Donoho, X. Gong, F. F. Merzoug, S. Buchanan, K. Boehnke, C. Yu, X. T. You, R. P. Beckmann, W. Wu, S. C. McNeely, A. B. Lin, and R. Martinez. 2020. 'A pan-cancer transcriptome analysis identifies replication fork and innate immunity genes as modifiers of response to the CHK1 inhibitor prexasertib', *Oncotarget*, 11: 216-36.
- Boroviak, T., R. Loos, P. Lombard, J. Okahara, R. Behr, E. Sasaki, J. Nichols, A. Smith, and P. Bertone. 2015. 'Lineage-Specific Profiling Delineates the Emergence and Progression of Naive Pluripotency in Mammalian Embryogenesis', *Dev Cell*, 35: 366-82.
- Boyerinas, B., C. Jochems, M. Fantini, C. R. Heery, J. L. Gulley, K. Y. Tsang, and J. Schlom. 2015. 'Antibody-Dependent Cellular Cytotoxicity Activity of a Novel Anti-PD-L1 Antibody Avelumab (MSB0010718C) on Human Tumor Cells', *Cancer Immunol Res*, 3: 1148-57.
- Butler, Kelly, and A. Rouf Banday. 2023. 'APOBEC3-mediated mutagenesis in cancer: causes, clinical significance and therapeutic potential', *Journal of Hematology & Oncology*, 16: 31.
- Cabanos, H. F., and A. N. Hata. 2021. 'Emerging Insights into Targeted Therapy-Tolerant Persister Cells in Cancer', *Cancers (Basel)*, 13.
- Cao, Q., X. Wang, M. Zhao, R. Yang, R. Malik, Y. Qiao, A. Poliakov, A. K. Yocum, Y. Li, W. Chen, X. Cao, X. Jiang, A. Dahiya, C. Harris, F. Y. Feng, S. Kalantry, Z. S. Qin, S. M. Dhanasekaran, and A. M. Chinnaiyan. 2014. 'The central role of EED in the orchestration of polycomb group complexes', *Nat Commun*, 5: 3127.
- Cao, R., and Y. Zhang. 2004. 'SUZ12 is required for both the histone methyltransferase activity and the silencing function of the EED-EZH2 complex', *Mol Cell*, 15: 57-67.
- Cao, Ru, Liangjun Wang, Hengbin Wang, Li Xia, Hediye Erdjument-Bromage, Paul Tempst, Richard S. Jones, and Yi Zhang. 2002. 'Role of Histone H3 Lysine 27 Methylation in Polycomb-Group Silencing', *Science*, 298: 1039-43.
- Cara, S., and I. F. Tannock. 2001. 'Retreatment of patients with the same chemotherapy: implications for clinical mechanisms of drug resistance', *Ann Oncol*, 12: 23-7.
- Chaft, J. E., M. E. Arcila, P. K. Paik, C. Lau, G. J. Riely, M. C. Pietanza, M. F. Zakowski, V. Rusch, C. S. Sima, M. Ladanyi, and M. G. Kris. 2012. 'Coexistence of PIK3CA and other oncogene mutations in lung adenocarcinoma-rationale for comprehensive mutation profiling', *Mol Cancer Ther*, 11: 485-91.
- Changelian, Paul S., Mark E. Flanagan, Douglas J. Ball, Craig R. Kent, Kelly S. Magnuson, William H. Martin, Bonnie J. Rizzuti, Perry S. Sawyer, Bret D. Perry, William H. Brissette, Sandra P. McCurdy, Elizabeth M. Kudlacz, Maryrose J. Conklyn, Eileen A. Elliott, Erika

- R. Koslov, Michael B. Fisher, Timothy J. Strelvitz, Kwansik Yoon, David A. Whipple, Jianmin Sun, Michael J. Munchhof, John L. Doty, Jeffrey M. Casavant, Todd A. Blumenkopf, Michael Hines, Matthew F. Brown, Brett M. Lillie, Chakrapani Subramanyam, Chang Shang-Poa, Anthony J. Milici, Gretchen E. Beckius, James D. Moyer, Chunyan Su, Thasia G. Woodworth, Anderson S. Gaweco, Chan R. Beals, Bruce H. Littman, Douglas A. Fisher, James F. Smith, Panayiotis Zagouras, Holly A. Magna, Mary J. Saltarelli, Kimberly S. Johnson, Linda F. Nelms, Shelley G. Des Etages, Lisa S. Hayes, Thomas T. Kawabata, Deborah Finco-Kent, Deanna L. Baker, Michael Larson, Ming-Sing Si, Ricardo Paniagua, John Higgins, Bari Holm, Bruce Reitz, Yong-Jie Zhou, Randall E. Morris, John J. O'Shea, and Dominic C. Borie. 2003. 'Prevention of Organ Allograft Rejection by a Specific Janus Kinase 3 Inhibitor', *Science*, 302: 875-78.
- Chen, Edward Y., Christopher M. Tan, Yan Kou, Qiaonan Duan, Zichen Wang, Gabriela Vaz Meirelles, Neil R. Clark, and Avi Ma'ayan. 2013. 'Enrichr: interactive and collaborative HTML5 gene list enrichment analysis tool', *BMC Bioinformatics*, 14: 128.
- Chen, Y., H. Xu, P. Yu, Q. Wang, S. Li, F. Ji, C. Wu, and Q. Lan. 2023. 'Interferon- γ inducible protein 30 promotes the epithelial-mesenchymal transition-like phenotype and chemoresistance by activating EGFR/AKT/GSK3 β / β -catenin pathway in glioma', *CNS Neurosci Ther*.
- Chihara, D., M. A. Fanale, R. N. Miranda, M. Noorani, J. R. Westin, L. J. Nastoupil, F. B. Hagemeister, L. E. Fayad, J. E. Romaguera, F. Samaniego, F. Turturro, H. J. Lee, S. S. Neelapu, M. A. Rodriguez, M. Wang, N. H. Fowler, R. E. Davis, L. J. Medeiros, C. Hosing, Y. L. Nieto, and Y. Oki. 2017. 'The survival outcome of patients with relapsed/refractory peripheral T-cell lymphoma-not otherwise specified and angioimmunoblastic T-cell lymphoma', *Br J Haematol*, 176: 750-58.
- Christensen, J., K. Agger, P. A. Cloos, D. Pasini, S. Rose, L. Sennels, J. Rappsilber, K. H. Hansen, A. E. Salcini, and K. Helin. 2007. 'RBP2 belongs to a family of demethylases, specific for tri- and dimethylated lysine 4 on histone 3', *Cell*, 128: 1063-76.
- Cobleigh, M. A., C. L. Vogel, D. Tripathy, N. J. Robert, S. Scholl, L. Fehrenbacher, J. M. Wolter, V. Paton, S. Shak, G. Lieberman, and D. J. Slamon. 1999. 'Multinational study of the efficacy and safety of humanized anti-HER2 monoclonal antibody in women who have HER2-overexpressing metastatic breast cancer that has progressed after chemotherapy for metastatic disease', *J Clin Oncol*, 17: 2639-48.
- Coldren, Christopher D., Barbara A. Helfrich, Samir E. Witta, Michio Sugita, Razvan Lapadat, Chan Zeng, Anna Barón, Wilbur A. Franklin, Fred R. Hirsch, Mark W. Geraci, and Paul A. Bunn, Jr. 2006. 'Baseline Gene Expression Predicts Sensitivity to Gefitinib in Non-Small Cell Lung Cancer Cell Lines', *Molecular Cancer Research*, 4: 521-28.
- Cole, K. A., J. Huggins, M. Laquaglia, C. E. Hulderman, M. R. Russell, K. Bosse, S. J. Diskin, E. F. Attiyeh, R. Sennett, G. Norris, M. Laudenslager, A. C. Wood, P. A. Mayes, J. Jagannathan, C. Winter, Y. P. Mosse, and J. M. Maris. 2011. 'RNAi screen of the protein kinome identifies checkpoint kinase 1 (CHK1) as a therapeutic target in neuroblastoma', *Proc Natl Acad Sci U S A*, 108: 3336-41.
- Coppé, J. P., C. K. Patil, F. Rodier, Y. Sun, D. P. Muñoz, J. Goldstein, P. S. Nelson, P. Y. Desprez, and J. Campisi. 2008. 'Senescence-associated secretory phenotypes reveal cell-nonautonomous functions of oncogenic RAS and the p53 tumor suppressor', *PLoS Biol*, 6: 2853-68.
- Corrado, Giacomo, Vanda Salutari, Eleonora Palluzzi, Maria Grazia Distefano, Giovanni Scambia, and Gabriella Ferrandina. 2017. 'Optimizing treatment in recurrent epithelial ovarian cancer', *Expert Review of Anticancer Therapy*, 17: 1147-58.
- Crump, M., S. S. Neelapu, U. Farooq, E. Van Den Neste, J. Kuruvilla, J. Westin, B. K. Link, A. Hay, J. R. Cerhan, L. Zhu, S. Boussetta, L. Feng, M. J. Maurer, L. Navale, J. Wieszorek, W. Y. Go, and C. Gisselbrecht. 2017. 'Outcomes in refractory diffuse large B-cell lymphoma: results from the international SCHOLAR-1 study', *Blood*, 130: 1800-08.
- Cuadrado, M., B. Martinez-Pastor, M. Murga, L. I. Toledo, P. Gutierrez-Martinez, E. Lopez, and O. Fernandez-Capetillo. 2006. 'ATM regulates ATR chromatin loading in response to DNA double-strand breaks', *J Exp Med*, 203: 297-303.
- Dangaj, D., M. Bruand, A. J. Grimm, C. Ronet, D. Barras, P. A. Duttagupta, E. Lanitis, J. Duraiswamy, J. L. Tanyi, F. Benencia, J. Conejo-Garcia, H. R. Ramay, K. T. Montone, D. J. Powell, Jr., P. A. Gimotty, A. Facciabene, D. G. Jackson, J. S. Weber, S. J. Rodig, S. F. Hodi, L. E. Kandalaft, M. Irving, L. Zhang, P. Foukas, S. Rusakiewicz, M. Delorenzi,

- and G. Coukos. 2019. 'Cooperation between Constitutive and Inducible Chemokines Enables T Cell Engraftment and Immune Attack in Solid Tumors', *Cancer Cell*, 35: 885-900.e10.
- Davies, H., G. R. Bignell, C. Cox, P. Stephens, S. Edkins, S. Clegg, J. Teague, H. Woffendin, M. J. Garnett, W. Bottomley, N. Davis, E. Dicks, R. Ewing, Y. Floyd, K. Gray, S. Hall, R. Hawes, J. Hughes, V. Kosmidou, A. Menzies, C. Mould, A. Parker, C. Stevens, S. Watt, S. Hooper, R. Wilson, H. Jayatilake, B. A. Gusterson, C. Cooper, J. Shipley, D. Hargrave, K. Pritchard-Jones, N. Maitland, G. Chenevix-Trench, G. J. Riggins, D. D. Bigner, G. Palmieri, A. Cossu, A. Flanagan, A. Nicholson, J. W. Ho, S. Y. Leung, S. T. Yuen, B. L. Weber, H. F. Seigler, T. L. Darrow, H. Paterson, R. Marais, C. J. Marshall, R. Wooster, M. R. Stratton, and P. A. Futreal. 2002. 'Mutations of the BRAF gene in human cancer', *Nature*, 417: 949-54.
- Dhimolea, Eugen, Ricardo de Matos Simoes, Dhvanir Kansara, Aziz Al'Khafaji, Juliette Bouyssou, Xiang Weng, Shruti Sharma, Joseline Raja, Pallavi Awate, Ryosuke Shirasaki, Huihui Tang, Brian J. Glassner, Zhiyi Liu, Dong Gao, Jordan Bryan, Samantha Bender, Jennifer Roth, Michal Scheffer, Rinath Jeselsohn, Nathanael S. Gray, Irene Georgakoudi, Francisca Vazquez, Aviad Tsherniak, Yu Chen, Alana Welm, Cihangir Duy, Ari Melnick, Boris Bartholdy, Myles Brown, Aedin C. Culhane, and Constantine S. Mitsiades. 2021. 'An Embryonic Diapause-like Adaptation with Suppressed Myc Activity Enables Tumor Treatment Persistence', *Cancer Cell*, 39: 240-56.e11.
- Dobin, A., C. A. Davis, F. Schlesinger, J. Drenkow, C. Zaleski, S. Jha, P. Batut, M. Chaisson, and T. R. Gingeras. 2013. 'STAR: ultrafast universal RNA-seq aligner', *Bioinformatics*, 29: 15-21.
- Dou, Zhen, Xing Liu, Wenwen Wang, Tongge Zhu, Xinghui Wang, Leilei Xu, Ariane Abrieu, Chuanhai Fu, Donald L. Hill, and Xuebiao Yao. 2015. 'Dynamic localization of Mps1 kinase to kinetochores is essential for accurate spindle microtubule attachment', *Proceedings of the National Academy of Sciences*, 112: E4546-E55.
- Duy, Cihangir, Meng Li, Matt Teater, Cem Meydan, Francine E. Garrett-Bakelman, Tak C. Lee, Christopher R. Chin, Ceyda Durmaz, Kimihito C. Kawabata, Eugen Dhimolea, Constantine S. Mitsiades, Hartmut Doehner, Richard J. D'Andrea, Michael W. Becker, Elisabeth M. Paietta, Christopher E. Mason, Martin Carroll, and Ari M. Melnick. 2021. 'Chemotherapy Induces Senescence-Like Resilient Cells Capable of Initiating AML Recurrence', *Cancer Discovery*, 11: 1542-61.
- Echeverria, Gloria V., Zhongqi Ge, Sahil Seth, Xiaomei Zhang, Sabrina Jeter-Jones, Xinhui Zhou, Shirong Cai, Yizheng Tu, Aaron McCoy, Michael Peoples, Yuting Sun, Huan Qiu, Qing Chang, Christopher Bristow, Alessandro Carugo, Jiansu Shao, Xiaoyan Ma, Angela Harris, Prabhjot Mundi, Rosanna Lau, Vandhana Ramamoorthy, Yun Wu, Mariano J. Alvarez, Andrea Califano, Stacy L. Moulder, William F. Symmans, Joseph R. Marszalek, Timothy P. Heffernan, Jeffrey T. Chang, and Helen Piwnicka-Worms. 2019. 'Resistance to neoadjuvant chemotherapy in triple-negative breast cancer mediated by a reversible drug-tolerant state', *Science Translational Medicine*, 11: eaav0936.
- ENCODE. 2012. 'An integrated encyclopedia of DNA elements in the human genome', *Nature*, 489: 57-74.
- Engelman, J. A., K. Zejnullahu, T. Mitsudomi, Y. Song, C. Hyland, J. O. Park, N. Lindeman, C. M. Gale, X. Zhao, J. Christensen, T. Kosaka, A. J. Holmes, A. M. Rogers, F. Cappuzzo, T. Mok, C. Lee, B. E. Johnson, L. C. Cantley, and P. A. Jänne. 2007. 'MET amplification leads to gefitinib resistance in lung cancer by activating ERBB3 signaling', *Science*, 316: 1039-43.
- Fehrenbacher, L., R. S. Cecchini, C. E. Geyer, Jr., P. Rastogi, J. P. Costantino, J. N. Atkins, J. P. Crown, J. Polikoff, J. F. Boileau, L. Provencher, C. Stokoe, T. D. Moore, A. Robidoux, P. J. Flynn, V. F. Borges, K. S. Albain, S. M. Swain, S. Paik, E. P. Mamounas, and N. Wolmark. 2020. 'NSABP B-47/NRG Oncology Phase III Randomized Trial Comparing Adjuvant Chemotherapy With or Without Trastuzumab in High-Risk Invasive Breast Cancer Negative for HER2 by FISH and With IHC 1+ or 2', *J Clin Oncol*, 38: 444-53.
- Fenelon, JaneC, Arnab Banerjee, and BruceD Murphy. 2014. 'Embryonic diapause: development on hold', *The International Journal of Developmental Biology*, 58: 163-74.
- Franza, M., J. Albanesi, B. Mancini, R. Pennisi, S. Leone, F. Acconcia, F. Bianchi, and A. di Masi. 2023. 'The clinically relevant CHK1 inhibitor MK-8776 induces the degradation of the

- oncogenic protein PML-RAR α and overcomes ATRA resistance in acute promyelocytic leukemia cells', *Biochem Pharmacol*, 214: 115675.
- Freeman, G. J., A. J. Long, Y. Iwai, K. Bourque, T. Chernova, H. Nishimura, L. J. Fitz, N. Malenkovich, T. Okazaki, M. C. Byrne, H. F. Horton, L. Fouser, L. Carter, V. Ling, M. R. Bowman, B. M. Carreno, M. Collins, C. R. Wood, and T. Honjo. 2000. 'Engagement of the PD-1 immunoinhibitory receptor by a novel B7 family member leads to negative regulation of lymphocyte activation', *J Exp Med*, 192: 1027-34.
- Fridman, A. L., and M. A. Tainsky. 2008. 'Critical pathways in cellular senescence and immortalization revealed by gene expression profiling', *Oncogene*, 27: 5975-87.
- Gao, Q., N. Patani, A. K. Dunbier, Z. Ghazoui, M. Zvelebil, L. A. Martin, and M. Dowsett. 2014. 'Effect of aromatase inhibition on functional gene modules in estrogen receptor-positive breast cancer and their relationship with antiproliferative response', *Clin Cancer Res*, 20: 2485-94.
- Garcia-Diaz, A., D. S. Shin, B. H. Moreno, J. Saco, H. Escuin-Ordinas, G. A. Rodriguez, J. M. Zaretsky, L. Sun, W. Hugo, X. Wang, G. Parisi, C. P. Saus, D. Y. Torrejon, T. G. Graeber, B. Comin-Anduix, S. Hu-Lieskovan, R. Damoiseaux, R. S. Lo, and A. Ribas. 2017. 'Interferon Receptor Signaling Pathways Regulating PD-L1 and PD-L2 Expression', *Cell Rep*, 19: 1189-201.
- Gebhart, E. 2005. 'Double minutes, cytogenetic equivalents of gene amplification, in human neoplasia - a review', *Clin Transl Oncol*, 7: 477-85.
- Gerber, D. E. 2008. 'EGFR Inhibition in the Treatment of Non-Small Cell Lung Cancer', *Drug Dev Res*, 69: 359-72.
- Ghuwalewala, Sangeeta, Dishari Ghatak, Pijush Das, Sanjib Dey, Shreya Sarkar, Neyaz Alam, Chinmay K. Panda, and Susanta Roychoudhury. 2016. 'CD44^{high}CD24^{low} molecular signature determines the Cancer Stem Cell and EMT phenotype in Oral Squamous Cell Carcinoma', *Stem Cell Research*, 16: 405-17.
- Grossmann, Liron D., Yasin Uzun, Jarrett Lindsay, Chia-Hui Chen, Catherine Wingrove, Peng Gao, Anusha Thadi, Quinlen Marshall, Nathan M. Kendsersky, Lea Surrey, Daniel Martinez, Emily Mycek, Colleen Casey, Kateryna Krytska, Matthew Tsang, Adam Wolpaw, David N. Groff, Erin Runbeck, Jayne McDevitt, Dinh Diep, Tasleema Patel, Kathrin M. Bernt, Chi Dang, Kun Zhang, Yael P. Mosse, Kai Tan, and John M. Maris. 2022. 'Abstract 699: NF- κ B is a master regulator of resistance to therapy in high-risk neuroblastoma', *Cancer Research*, 82: 699-99.
- Gu, Lei, Paraskevi Vogiatzi, Martin Pühr, Ayush Dagvadorj, Jacqueline Lutz, Amy Ryder, Sankar Addya, Paolo Fortina, Carlton Cooper, Benjamin Leiby, Abhijit Dasgupta, Terry Hyslop, Lukas Bubendorf, Kalle Alanen, Tuomas Mirtti, and Marja T Nevalainen. 2010. 'Stat5 promotes metastatic behavior of human prostate cancer cells in vitro and in vivo', *Endocrine-Related Cancer*, 17: 481-93.
- Guervilly, Jean-Hugues, Emilie Renaud, Minoru Takata, and Filippo Rosselli. 2011. 'USP1 deubiquitinase maintains phosphorylated CHK1 by limiting its DDB1-dependent degradation', *Human Molecular Genetics*, 20: 2171-81.
- Guler, G. D., C. A. Tindell, R. Pitti, C. Wilson, K. Nichols, T. KaiWai Cheung, H. J. Kim, M. Wongchenko, Y. Yan, B. Haley, T. Cuellar, J. Webster, N. Alag, G. Hegde, E. Jackson, T. L. Nance, P. G. Giresi, K. B. Chen, J. Liu, S. Jhunjhunwala, J. Settleman, J. P. Stephan, D. Arnott, and M. Classon. 2017. 'Repression of Stress-Induced LINE-1 Expression Protects Cancer Cell Subpopulations from Lethal Drug Exposure', *Cancer Cell*, 32: 221-37 e13.
- Gupta, Dipika, Bo Lin, Ann Cowan, and Christopher D. Heinen. 2018. 'ATR-Chk1 activation mitigates replication stress caused by mismatch repair-dependent processing of DNA damage', *Proceedings of the National Academy of Sciences*, 115: 1523-28.
- Gupta, R., A. M. Dastane, F. Forozan, A. Riley-Portuguez, F. Chung, J. Lopategui, and A. M. Marchevsky. 2009. 'Evaluation of EGFR abnormalities in patients with pulmonary adenocarcinoma: the need to test neoplasms with more than one method', *Mod Pathol*, 22: 128-33.
- Gutierrez, A., L. Laureti, S. Crussard, H. Abida, A. Rodríguez-Rojas, J. Blázquez, Z. Baharoglu, D. Mazel, F. Darfeuille, J. Vogel, and I. Matic. 2013. ' β -lactam antibiotics promote bacterial mutagenesis via an RpoS-mediated reduction in replication fidelity', *Nature Communications*, 4: 1610.

- Guzi, Timothy J., Kamil Paruch, Michael P. Dwyer, Marc Labroli, Frances Shanahan, Nicole Davis, Lorena Taricani, Derek Wiswell, Wolfgang Seghezzi, Ervin Penafior, Bhagyashree Bhagwat, Wei Wang, Danling Gu, Yunsheng Hsieh, Suining Lee, Ming Liu, and David Parry. 2011. 'Targeting the Replication Checkpoint Using SCH 900776, a Potent and Functionally Selective CHK1 Inhibitor Identified via High Content Screening', *Molecular Cancer Therapeutics*, 10: 591-602.
- Hangauer, M. J., V. S. Viswanathan, M. J. Ryan, D. Bole, J. K. Eaton, A. Matov, J. Galeas, H. D. Dhruv, M. E. Berens, S. L. Schreiber, F. McCormick, and M. T. McManus. 2017. 'Drug-tolerant persister cancer cells are vulnerable to GPX4 inhibition', *Nature*, 551: 247-50.
- Hata, Aaron N., Matthew J. Niederst, Hannah L. Archibald, Maria Gomez-Caraballo, Faria M. Siddiqui, Hillary E. Mulvey, Yosef E. Maruvka, Fei Ji, Hyo-eun C. Bhang, Viveksagar Krishnamurthy Radhakrishna, Giulia Siravegna, Haichuan Hu, Sana Raoof, Elizabeth Lockerman, Anuj Kalsy, Dana Lee, Celina L. Keating, David A. Ruddy, Leah J. Damon, Adam S. Crystal, Carlotta Costa, Zofia Piotrowska, Alberto Bardelli, Anthony J. Iafrate, Ruslan I. Sadreyev, Frank Stegmeier, Gad Getz, Lecia V. Sequist, Anthony C. Faber, and Jeffrey A. Engelman. 2016. 'Tumor cells can follow distinct evolutionary paths to become resistant to epidermal growth factor receptor inhibition', *Nat Med*, 22: 262-69.
- Heintzman, Nathaniel D., Gary C. Hon, R. David Hawkins, Pouya Kheradpour, Alexander Stark, Lindsey F. Harp, Zhen Ye, Leonard K. Lee, Rhona K. Stuart, Christina W. Ching, Keith A. Ching, Jessica E. Antosiewicz-Bourget, Hui Liu, Xinmin Zhang, Roland D. Green, Victor V. Lobanenkov, Ron Stewart, James A. Thomson, Gregory E. Crawford, Manolis Kellis, and Bing Ren. 2009. 'Histone modifications at human enhancers reflect global cell-type-specific gene expression', *Nature*, 459: 108-12.
- Hirsch, F. R., M. Varella-Garcia, P. A. Bunn, Jr., M. V. Di Maria, R. Veve, R. M. Bremmes, A. E. Barón, C. Zeng, and W. A. Franklin. 2003. 'Epidermal growth factor receptor in non-small-cell lung carcinomas: correlation between gene copy number and protein expression and impact on prognosis', *J Clin Oncol*, 21: 3798-807.
- Hout, M. C., M. H. Papesh, and S. D. Goldinger. 2013. 'Multidimensional scaling', *Wiley Interdiscip Rev Cogn Sci*, 4: 93-103.
- Hoy, Sheridan M. 2020. 'Tazemetostat: First Approval', *Drugs*, 80: 513-21.
- Hudziak, R. M., G. D. Lewis, M. Winget, B. M. Fendly, H. M. Shepard, and A. Ullrich. 1989. 'p185HER2 monoclonal antibody has antiproliferative effects in vitro and sensitizes human breast tumor cells to tumor necrosis factor', *Mol Cell Biol*, 9: 1165-72.
- Huemer, M., S. Mairpady Shambat, S. D. Brugger, and A. S. Zinkernagel. 2020. 'Antibiotic resistance and persistence-Implications for human health and treatment perspectives', *EMBO Rep*, 21: e51034.
- Hulsen, T., J. de Vlieg, and W. Alkema. 2008. 'BioVenn - a web application for the comparison and visualization of biological lists using area-proportional Venn diagrams', *BMC Genomics*, 9: 488.
- Hunter, J. E., A. E. Campbell, N. L. Hannaway, S. Kerridge, S. Luli, J. A. Butterworth, H. Sellier, R. Mukherjee, N. Dhillon, P. D. Sudhindar, R. Shukla, P. J. Brownridge, H. L. Bell, J. Coxhead, L. Taylor, P. Leary, M. S. R. Hasoon, I. Collins, M. D. Garrett, C. E. Evers, and N. D. Perkins. 2022. 'Regulation of CHK1 inhibitor resistance by a c-Rel and USP1 dependent pathway', *Biochem J*, 479: 2063-86.
- Hurt, E. M., B. T. Kawasaki, G. J. Klarmann, S. B. Thomas, and W. L. Farrar. 2008. 'CD44+CD24- prostate cells are early cancer progenitor/stem cells that provide a model for patients with poor prognosis', *British Journal of Cancer*, 98: 756-65.
- Inman, B. A., T. J. Sebo, X. Frigola, H. Dong, E. J. Bergstralh, I. Frank, Y. Fradet, L. Lacombe, and E. D. Kwon. 2007. 'PD-L1 (B7-H1) expression by urothelial carcinoma of the bladder and BCG-induced granulomata: associations with localized stage progression', *Cancer*, 109: 1499-505.
- Isozaki, Hideko, Ramin Sakhtemani, Ammal Abbasi, Naveed Nikpour, Marcello Stanzione, Sunwoo Oh, Adam Langenbacher, Susanna Monroe, Wenjia Su, Heidie Frisco Cabanos, Faria M. Siddiqui, Nicole Phan, Pégah Jalili, Daria Timonina, Samantha Bilton, Maria Gomez-Caraballo, Hannah L. Archibald, Varuna Nangia, Kristin Dionne, Amanda Riley, Matthew Lawlor, Mandeep Kaur Banwait, Rosemary G. Cobb, Lee Zou, Nicholas J. Dyson, Christopher J. Ott, Cyril Benes, Gad Getz, Chang S. Chan, Alice T. Shaw, Justin F. Gainor, Jessica J. Lin, Lecia V. Sequist, Zofia Piotrowska, Beow Y. Yeap, Jeffrey A. Engelman, Jake June-Koo Lee, Yosef E. Maruvka, Rémi Buisson, Michael S. Lawrence,

- and Aaron N. Hata. 2023. 'Therapy-induced APOBEC3A drives evolution of persistent cancer cells', *Nature*.
- Iwai, Y., M. Ishida, Y. Tanaka, T. Okazaki, T. Honjo, and N. Minato. 2002. 'Involvement of PD-L1 on tumor cells in the escape from host immune system and tumor immunotherapy by PD-L1 blockade', *Proc Natl Acad Sci U S A*, 99: 12293-7.
- Jacob Berger, Adi, Elinor Gigi, Lana Kupersmidt, Zohar Meir, Nancy Gavert, Yaara Zwang, Amir Prior, Shlomit Gilad, Uzi Harush, Izhak Haviv, Salomon M. Stemmer, Galia Blum, Emmanuelle Merquiol, Mariya Mardamshina, Sivan Kaminski Strauss, Gilgi Friedlander, Jair Bar, Iris Kamer, Yitzhak Reizel, Tamar Geiger, Yitzhak Pilpel, Yishai Levin, Amos Tanay, Baruch Barzel, Hadas Reuveni, and Ravid Straussman. 2021. 'IRS1 phosphorylation underlies the non-stochastic probability of cancer cells to persist during EGFR inhibition therapy', *Nature Cancer*, 2: 1055-70.
- Jakobsdottir, G. Maria, Daniel S. Brewer, Colin Cooper, Catherine Green, and David C. Wedge. 2022. 'APOBEC3 mutational signatures are associated with extensive and diverse genomic instability across multiple tumour types', *BMC Biology*, 20: 117.
- Jazayeri, A., J. Falck, C. Lukas, J. Bartek, G. C. Smith, J. Lukas, and S. P. Jackson. 2006. 'ATM- and cell cycle-dependent regulation of ATR in response to DNA double-strand breaks', *Nat Cell Biol*, 8: 37-45.
- Jiao, L., M. Shubbar, X. Yang, Q. Zhang, S. Chen, Q. Wu, Z. Chen, J. Rizo, and X. Liu. 2020. 'A partially disordered region connects gene repression and activation functions of EZH2', *Proc Natl Acad Sci U S A*, 117: 16992-7002.
- Jones, Robert, Ruth Plummer, Victor Moreno, Louise Carter, Desamparados Roda, Elena Garralda, Rebecca Kristeleit, Debashis Sarker, Tobias Arkenau, Patricia Roxburgh, Harriet S. Walter, Sarah Blagden, Alan Anthoney, Barbara J. Klencke, Mark M. Kowalski, and Udai Banerji. 2023. 'A Phase I/II Trial of Oral SRA737 (a Chk1 Inhibitor) Given in Combination with Low-Dose Gemcitabine in Patients with Advanced Cancer', *Clinical Cancer Research*, 29: 331-40.
- Kanu, N., M. A. Cerone, G. Goh, L. P. Zalmas, J. Bartkova, M. Dietzen, N. McGranahan, R. Rogers, E. K. Law, I. Gromova, M. Kschischo, M. I. Walton, O. W. Rossanese, J. Bartek, R. S. Harris, S. Venkatesan, and C. Swanton. 2016. 'DNA replication stress mediates APOBEC3 family mutagenesis in breast cancer', *Genome Biol*, 17: 185.
- Kaufman, H. L., J. Russell, O. Hamid, S. Bhatia, P. Terheyden, S. P. D'Angelo, K. C. Shih, C. Lebbé, G. P. Linette, M. Milella, I. Brownell, K. D. Lewis, J. H. Lorch, K. Chin, L. Mahnke, A. von Heydebreck, J. M. Cuillerot, and P. Nghiem. 2016. 'Avelumab in patients with chemotherapy-refractory metastatic Merkel cell carcinoma: a multicentre, single-group, open-label, phase 2 trial', *Lancet Oncol*, 17: 1374-85.
- Keren, Iris, Niilo Kaldalu, Amy Spoering, Yipeng Wang, and Kim Lewis. 2004. 'Persister cells and tolerance to antimicrobials', *FEMS Microbiology Letters*, 230: 13-18.
- King, C., H. Diaz, D. Barnard, D. Barda, D. Clawson, W. Blosser, K. Cox, S. Guo, and M. Marshall. 2014. 'Characterization and preclinical development of LY2603618: a selective and potent Chk1 inhibitor', *Invest New Drugs*, 32: 213-26.
- King, Constance, H. Bruce Diaz, Samuel McNeely, Darlene Barnard, Jack Dempsey, Wayne Blosser, Richard Beckmann, David Barda, and Mark S. Marshall. 2015. 'LY2606368 Causes Replication Catastrophe and Antitumor Effects through CHK1-Dependent Mechanisms', *Molecular Cancer Therapeutics*, 14: 2004-13.
- Kleer, Celina G., Qi Cao, Sooryanarayana Varambally, Ronglai Shen, Ichiro Ota, Scott A. Tomlins, Debashis Ghosh, Richard G. A. B. Sewalt, Arie P. Otte, Daniel F. Hayes, Michael S. Sabel, Donna Livant, Stephen J. Weiss, Mark A. Rubin, and Arul M. Chinnaiyan. 2003. 'EZH2 is a marker of aggressive breast cancer and promotes neoplastic transformation of breast epithelial cells', *Proceedings of the National Academy of Sciences*, 100: 11606-11.
- Knutson, S. K., S. Kawano, Y. Minoshima, N. M. Warholic, K. C. Huang, Y. Xiao, T. Kadowaki, M. Uesugi, G. Kuznetsov, N. Kumar, T. J. Wagle, C. R. Klaus, C. J. Allain, A. Raimondi, N. J. Waters, J. J. Smith, M. Porter-Scott, R. Chesworth, M. P. Moyer, R. A. Copeland, V. M. Richon, T. Uenaka, R. M. Pollock, K. W. Kuntz, A. Yokoi, and H. Keilhack. 2014. 'Selective inhibition of EZH2 by EPZ-6438 leads to potent antitumor activity in EZH2-mutant non-Hodgkin lymphoma', *Mol Cancer Ther*, 13: 842-54.
- Knutson, Sarah K., Natalie M. Warholic, Tim J. Wagle, Christine R. Klaus, Christina J. Allain, Alejandra Raimondi, Margaret Porter Scott, Richard Chesworth, Mikel P. Moyer, Robert

- A. Copeland, Victoria M. Richon, Roy M. Pollock, Kevin W. Kuntz, and Heike Keilhack. 2013. 'Durable tumor regression in genetically altered malignant rhabdoid tumors by inhibition of methyltransferase EZH2', *Proceedings of the National Academy of Sciences*, 110: 7922-27.
- Koppikar, P., V. W. Lui, D. Man, S. Xi, R. L. Chai, E. Nelson, A. B. Tobey, and J. R. Grandis. 2008. 'Constitutive activation of signal transducer and activator of transcription 5 contributes to tumor growth, epithelial-mesenchymal transition, and resistance to epidermal growth factor receptor targeting', *Clin Cancer Res*, 14: 7682-90.
- Kovanen, Panu E., Lynn Young, Amin Al-Shami, Valentina Rovella, Cynthia A. Pise-Masison, Michael F. Radonovich, John Powell, Jacqueline Fu, John N. Brady, Peter J. Munson, and Warren J. Leonard. 2005. 'Global analysis of IL-2 target genes: identification of chromosomal clusters of expressed genes', *International Immunology*, 17: 1009-21.
- Kuleshov, M. V., M. R. Jones, A. D. Rouillard, N. F. Fernandez, Q. Duan, Z. Wang, S. Koplev, S. L. Jenkins, K. M. Jagodnik, A. Lachmann, M. G. McDermott, C. D. Monteiro, G. W. Gundersen, and A. Ma'ayan. 2016. 'Enrichr: a comprehensive gene set enrichment analysis web server 2016 update', *Nucleic acids research*, 44: W90-7.
- Kurata, T., K. Tamura, H. Kaneda, T. Nogami, H. Uejima, G. Asai, K. Nakagawa, and M. Fukuoka. 2004. 'Effect of re-treatment with gefitinib ('Iressa', ZD1839) after acquisition of resistance', *Annals of Oncology*, 15: 173-74.
- Kurppa, K. J., Y. Liu, C. To, T. Zhang, M. Fan, A. Vajdi, E. H. Knelson, Y. Xie, K. Lim, P. Cejas, A. Portell, P. H. Lizotte, S. B. Ficarro, S. Li, T. Chen, H. M. Haikala, H. Wang, M. Bahcall, Y. Gao, S. Shalhout, S. Boettcher, B. H. Shin, T. Thai, M. K. Wilkens, M. L. Tillgren, M. Mushajiang, M. Xu, J. Choi, A. A. Bertram, B. L. Ebert, R. Beroukhim, P. Bandopadhyay, M. M. Awad, P. C. Gokhale, P. T. Kirschmeier, J. A. Marto, F. D. Camargo, R. Haq, C. P. Paweletz, K. K. Wong, D. A. Barbie, H. W. Long, N. S. Gray, and P. A. Jänne. 2020. 'Treatment-Induced Tumor Dormancy through YAP-Mediated Transcriptional Reprogramming of the Apoptotic Pathway', *Cancer Cell*, 37: 104-22.e12.
- Kussell, E., R. Kishony, N. Q. Balaban, and S. Leibler. 2005. 'Bacterial persistence: a model of survival in changing environments', *Genetics*, 169: 1807-14.
- Lachmann, A., H. Xu, J. Krishnan, S. I. Berger, A. R. Mazloom, and A. Ma'ayan. 2010. 'ChEA: transcription factor regulation inferred from integrating genome-wide ChIP-X experiments', *Bioinformatics*, 26: 2438-44.
- Lane, R. S., J. Femel, A. P. Breazeale, C. P. Loo, G. Thibault, A. Kaempf, M. Mori, T. Tsujikawa, Y. H. Chang, and A. W. Lund. 2018. 'IFN γ -activated dermal lymphatic vessels inhibit cytotoxic T cells in melanoma and inflamed skin', *J Exp Med*, 215: 3057-74.
- Lechner, Sabrina, Kim Lewis, and Ralph Bertram. 2012. 'Staphylococcus aureus Persists Tolerant to Bactericidal Antibiotics', *Microbial Physiology*, 22: 235-44.
- Lee, Kevin J., Griffin Wright, Hannah Bryant, Leigh Ann Wiggins, Michele Schuler, and Natalie R. Gassman. 2020. 'EGFR signaling promotes resistance to CHK1 inhibitor prexasertib in triple negative breast cancer', *Cancer Drug Resistance*, 3: 980-91.
- Leonetti, A., S. Sharma, R. Minari, P. Perego, E. Giovannetti, and M. Tiseo. 2019. 'Resistance mechanisms to osimertinib in EGFR-mutated non-small cell lung cancer', *Br J Cancer*, 121: 725-37.
- Liau, B. B., C. Sievers, L. K. Donohue, S. M. Gillespie, W. A. Flavahan, T. E. Miller, A. S. Venteicher, C. H. Hebert, C. D. Carey, S. J. Rodig, S. J. Shareef, F. J. Najm, P. van Galen, H. Wakimoto, D. P. Cahill, J. N. Rich, J. C. Aster, M. L. Suva, A. P. Patel, and B. E. Bernstein. 2017. 'Adaptive Chromatin Remodeling Drives Glioblastoma Stem Cell Plasticity and Drug Tolerance', *Cell Stem Cell*, 20: 233-46 e7.
- Liberzon, A., C. Birger, H. Thorvaldsdóttir, M. Ghandi, J. P. Mesirov, and P. Tamayo. 2015. 'The Molecular Signatures Database (MSigDB) hallmark gene set collection', *Cell Syst*, 1: 417-25.
- Lin, Y., S. Jamison, and W. Lin. 2012. 'Interferon- γ activates nuclear factor- κ B in oligodendrocytes through a process mediated by the unfolded protein response', *PLoS One*, 7: e36408.
- Liu, Jianguo, Xiuqin Guan, and Xiaojing Ma. 2005. 'Interferon Regulatory Factor 1 Is an Essential and Direct Transcriptional Activator for Interferon γ -induced RANTES/CC15 Expression in Macrophages*', *Journal of Biological Chemistry*, 280: 24347-55.

- Llorens-Bobadilla, E., S. Zhao, A. Baser, G. Saiz-Castro, K. Zwadlo, and A. Martin-Villalba. 2015. 'Single-Cell Transcriptomics Reveals a Population of Dormant Neural Stem Cells that Become Activated upon Brain Injury', *Cell Stem Cell*, 17: 329-40.
- Lo, U. G., J. Bao, J. Cen, H. C. Yeh, J. Luo, W. Tan, and J. T. Hsieh. 2019. 'Interferon-induced IFIT5 promotes epithelial-to-mesenchymal transition leading to renal cancer invasion', *Am J Clin Exp Urol*, 7: 31-45.
- López-Contreras, A. J., P. Gutierrez-Martinez, J. Specks, S. Rodrigo-Perez, and O. Fernandez-Capetillo. 2012. 'An extra allele of Chk1 limits oncogene-induced replicative stress and promotes transformation', *J Exp Med*, 209: 455-61.
- Maciejowski, J., K. A. George, M. E. Terret, C. Zhang, K. M. Shokat, and P. V. Jallepalli. 2010. 'Mps1 directs the assembly of Cdc20 inhibitory complexes during interphase and mitosis to control M phase timing and spindle checkpoint signaling', *J Cell Biol*, 190: 89-100.
- Madoz-Gúrpide, J., M. Cañamero, L. Sanchez, J. Solano, P. Alfonso, and J. I. Casal. 2007. 'A proteomics analysis of cell signaling alterations in colorectal cancer', *Mol Cell Proteomics*, 6: 2150-64.
- Mah, L. J., A. El-Osta, and T. C. Karagiannis. 2010. 'γH2AX: a sensitive molecular marker of DNA damage and repair', *Leukemia*, 24: 679-86.
- Maia, A. R., J. de Man, U. Boon, A. Janssen, J. Y. Song, M. Omerzu, J. G. Sterrenburg, M. B. Prinsen, N. Willemsen-Seegers, J. A. de Roos, A. M. van Doornmalen, J. C. Uitdehaag, G. J. Kops, J. Jonkers, R. C. Buijsman, G. J. Zaman, and R. H. Medema. 2015. 'Inhibition of the spindle assembly checkpoint kinase TTK enhances the efficacy of docetaxel in a triple-negative breast cancer model', *Ann Oncol*, 26: 2180-92.
- Marcoux, N., S. N. Gettinger, G. O'Kane, K. C. Arbour, J. W. Neal, H. Husain, T. L. Evans, J. R. Brahmer, A. Muzikansky, P. D. Bonomi, S. Del Prete, A. Wurtz, A. F. Farago, D. Dias-Santagata, M. Mino-Kenudson, K. L. Reckamp, H. A. Yu, H. A. Wakelee, F. A. Shepherd, Z. Piotrowska, and L. V. Sequist. 2019. 'EGFR-Mutant Adenocarcinomas That Transform to Small-Cell Lung Cancer and Other Neuroendocrine Carcinomas: Clinical Outcomes', *J Clin Oncol*, 37: 278-85.
- McKenzie, G. J., P. L. Lee, M. J. Lombardo, P. J. Hastings, and S. M. Rosenberg. 2001. 'SOS mutator DNA polymerase IV functions in adaptive mutation and not adaptive amplification', *Mol Cell*, 7: 571-79.
- Michael, M., and M.M. Doherty. 2005. 'Tumoral Drug Metabolism: Overview and Its Implications for Cancer Therapy', *Journal of Clinical Oncology*, 23: 205-29.
- Minati, R., C. Perreault, and P. Thibault. 2020. 'A Roadmap Toward the Definition of Actionable Tumor-Specific Antigens', *Front Immunol*, 11: 583287.
- Mitchell, S., E. L. Mercado, A. Adelaja, J. Q. Ho, Q. J. Cheng, G. Ghosh, and A. Hoffmann. 2019. 'An NFκB Activity Calculator to Delineate Signaling Crosstalk: Type I and II Interferons Enhance NFκB via Distinct Mechanisms', *Front Immunol*, 10: 1425.
- Moasser, M. M. 2007. 'The oncogene HER2: its signaling and transforming functions and its role in human cancer pathogenesis', *Oncogene*, 26: 6469-87.
- Montano, Ryan, Injae Chung, Kristen M. Garner, David Parry, and Alan Eastman. 2012. 'Preclinical Development of the Novel Chk1 Inhibitor SCH900776 in Combination with DNA-Damaging Agents and Antimetabolites', *Molecular Cancer Therapeutics*, 11: 427-38.
- Moon, J. W., S. K. Kong, B. S. Kim, H. J. Kim, H. Lim, K. Noh, Y. Kim, J. W. Choi, J. H. Lee, and Y. S. Kim. 2017. 'IFNγ induces PD-L1 overexpression by JAK2/STAT1/IRF-1 signaling in EBV-positive gastric carcinoma', *Sci Rep*, 7: 17810.
- Morris, V., M. J. Overman, Z. Q. Jiang, C. Garrett, S. Agarwal, C. Eng, B. Kee, D. Fogelman, A. Dasari, R. Wolff, D. Maru, and S. Kopetz. 2014. 'Progression-free survival remains poor over sequential lines of systemic therapy in patients with BRAF-mutated colorectal cancer', *Clin Colorectal Cancer*, 13: 164-71.
- Mowat, C., S. R. Mosley, A. Namdar, D. Schiller, and K. Baker. 2021. 'Anti-tumor immunity in mismatch repair-deficient colorectal cancers requires type I IFN-driven CCL5 and CXCL10', *J Exp Med*, 218.
- Nair, Jayakumar, Tzu-Ting Huang, Junko Murai, Brittany Haynes, Patricia S. Steeg, Yves Pommier, and Jung-Min Lee. 2020. 'Resistance to the CHK1 inhibitor prexasertib involves functionally distinct CHK1 activities in BRCA wild-type ovarian cancer', *Oncogene*, 39: 5520-35.

- Nakanishi, J., Y. Wada, K. Matsumoto, M. Azuma, K. Kikuchi, and S. Ueda. 2007. 'Overexpression of B7-H1 (PD-L1) significantly associates with tumor grade and postoperative prognosis in human urothelial cancers', *Cancer Immunol Immunother*, 56: 1173-82.
- NCI. 2023. 'List of Targeted Therapy Drugs Approved for Specific Types of Cancer', Accessed 06/09/2023. <https://www.cancer.gov/about-cancer/treatment/types/targeted-therapies/approved-drug-list>.
- NCT01164995. 'Phase II Pharmacological Study With Wee-1 Inhibitor MK-1775 Combined With Carboplatin in Patients With p53 Mutated Epithelial Ovarian Cancer and Early Relapse (< 3 Months) or Progression During Standard First Line Treatment', National Institutes of Health: U.S. National Library of Medicine, Accessed 16th December 2022. <https://clinicaltrials.gov/ct2/show/NCT01164995?term=Wee1&cond=Cancer&phase=014&draw=2&rank=1>.
- NCT02797964. 'A Phase 1/2 Trial of SRA737 in Subjects With Advanced Cancer'. <https://ClinicalTrials.gov/show/NCT02797964>.
- NCT02797977. 'A Phase 1/2 Trial of SRA737 in Combination With Gemcitabine Plus Cisplatin or Gemcitabine Alone in Subjects With Advanced Cancer'. <https://ClinicalTrials.gov/show/NCT02797977>.
- NCT03328494. 'Study of Paclitaxel in Combination With BOS172722 in Patients With Advanced Nonhaematologic Malignancies'. <https://ClinicalTrials.gov/show/NCT03328494>.
- O'Connell, Matthew J., Jeanette M. Raleigh, Heather M. Verkade, and Paul Nurse. 1997. 'Chk1 is a wee1 kinase in the G2 DNA damage checkpoint inhibiting cdc2 by Y15 phosphorylation', *The EMBO Journal*, 16: 545-54.
- Ohashi, K., L. V. Sequist, M. E. Arcila, T. Moran, J. Chmielecki, Y. L. Lin, Y. Pan, L. Wang, E. de Stanchina, K. Shien, K. Aoe, S. Toyooka, K. Kiura, L. Fernandez-Cuesta, P. Fidias, J. C. Yang, V. A. Miller, G. J. Riely, M. G. Kris, J. A. Engelman, C. L. Vnencak-Jones, D. Dias-Santagata, M. Ladanyi, and W. Pao. 2012. 'Lung cancers with acquired resistance to EGFR inhibitors occasionally harbor BRAF gene mutations but lack mutations in KRAS, NRAS, or MEK1', *Proc Natl Acad Sci U S A*, 109: E2127-33.
- Ohigashi, Y., M. Sho, Y. Yamada, Y. Tsurui, K. Hamada, N. Ikeda, T. Mizuno, R. Yoriki, H. Kashizuka, K. Yane, F. Tsushima, N. Otsuki, H. Yagita, M. Azuma, and Y. Nakajima. 2005. 'Clinical significance of programmed death-1 ligand-1 and programmed death-1 ligand-2 expression in human esophageal cancer', *Clin Cancer Res*, 11: 2947-53.
- Okita, Naoyuki, Shota Minato, Eri Ohmi, Sei-ichi Tanuma, and Yoshikazu Higami. 2012. 'DNA damage-induced CHK1 autophosphorylation at Ser296 is regulated by an intramolecular mechanism', *FEBS Letters*, 586: 3974-79.
- Oren, Y., M. Tsabar, M. S. Cuoco, L. Amir-Zilberstein, H. F. Cabanos, J. C. Hütter, B. Hu, P. I. Thakore, M. Tabaka, C. P. Fulco, W. Colgan, B. M. Cuevas, S. A. Hurvitz, D. J. Slamon, A. Deik, K. A. Pierce, C. Clish, A. N. Hata, E. Zaganjor, G. Lahav, K. Politi, J. S. Brugge, and A. Regev. 2021. 'Cycling cancer persister cells arise from lineages with distinct programs', *Nature*, 596: 576-82.
- Osborne, James D., Thomas P. Matthews, Tatiana McHardy, Nicolas Proisy, Kwai-Ming J. Cheung, Michael Lainchbury, Nathan Brown, Michael I. Walton, Paul D. Eve, Katherine J. Boxall, Angela Hayes, Alan T. Henley, Melanie R. Valenti, Alexis K. De Haven Brandon, Gary Box, Yann Jamin, Simon P. Robinson, Isaac M. Westwood, Rob L. M. van Montfort, Philip M. Leonard, Marieke B. A. C. Lamers, John C. Reader, G. Wynne Aherne, Florence I. Raynaud, Suzanne A. Eccles, Michelle D. Garrett, and Ian Collins. 2016. 'Multiparameter Lead Optimization to Give an Oral Checkpoint Kinase 1 (CHK1) Inhibitor Clinical Candidate: (R)-5-((4-((Morpholin-2-ylmethyl)amino)-5-(trifluoromethyl)pyridin-2-yl)amino)pyrazine-2-carbonitrile (CCT245737)', *Journal of Medicinal Chemistry*, 59: 5221-37.
- Ou, Y. H., P. H. Chung, T. P. Sun, and S. Y. Shieh. 2005. 'p53 C-terminal phosphorylation by CHK1 and CHK2 participates in the regulation of DNA-damage-induced C-terminal acetylation', *Mol Biol Cell*, 16: 1684-95.
- Pao, W., V. A. Miller, K. A. Politi, G. J. Riely, R. Somwar, M. F. Zakowski, M. G. Kris, and H. Varmus. 2005. 'Acquired resistance of lung adenocarcinomas to gefitinib or erlotinib is associated with a second mutation in the EGFR kinase domain', *PLoS Med*, 2: e73.

- Pasini, D., A. P. Bracken, M. R. Jensen, E. Lazzerini Denchi, and K. Helin. 2004. 'Suz12 is essential for mouse development and for EZH2 histone methyltransferase activity', *Embo j*, 23: 4061-71.
- Pasini, Diego, Martina Malatesta, Hye Ryung Jung, Julian Walfridsson, Anton Willer, Linda Olsson, Julie Skotte, Anton Wutz, Bo Porse, Ole Nørregaard Jensen, and Kristian Helin. 2010. 'Characterization of an antagonistic switch between histone H3 lysine 27 methylation and acetylation in the transcriptional regulation of Polycomb group target genes', *Nucleic acids research*, 38: 4958-69.
- Pawlyn, C., M. D. Bright, A. F. Buros, C. K. Stein, Z. Walters, L. I. Aronson, F. Mirabella, J. R. Jones, M. F. Kaiser, B. A. Walker, G. H. Jackson, P. A. Clarke, P. L. Bergsagel, P. Workman, M. Chesi, G. J. Morgan, and F. E. Davies. 2017. 'Overexpression of EZH2 in multiple myeloma is associated with poor prognosis and dysregulation of cell cycle control', *Blood Cancer J*, 7: e549.
- Perez, M., S. Muñoz-Galván, M. P. Jiménez-García, J. J. Marín, and A. Carnero. 2015. 'Efficacy of CDK4 inhibition against sarcomas depends on their levels of CDK4 and p16ink4 mRNA', *Oncotarget*, 6: 40557-74.
- Periyasamy, M., A. K. Singh, C. Gemma, R. Farzan, R. C. Allsopp, J. A. Shaw, S. Charmsaz, L. S. Young, P. Cunnea, R. C. Coombes, B. Györfy, L. Buluwela, and S. Ali. 2021. 'Induction of APOBEC3B expression by chemotherapy drugs is mediated by DNA-PK-directed activation of NF-κB', *Oncogene*, 40: 1077-90.
- Pham, Victoria, Robert Pitti, Charles A. Tindell, Tommy K. Cheung, Alexandre Masselot, Jean-Phillipe Stephan, Gulfer D. Guler, Catherine Wilson, Jennie Lill, David Arnott, and Marie Classon. 2020. 'Proteomic Analyses Identify a Novel Role for EZH2 in the Initiation of Cancer Cell Drug Tolerance', *Journal of Proteome Research*, 19: 1533-47.
- Pond, K. W., C. de Renty, M. K. Yagle, and N. A. Ellis. 2019. 'Rescue of collapsed replication forks is dependent on NSMCE2 to prevent mitotic DNA damage', *PLoS Genet*, 15: e1007942.
- Ponder, R. G., N. C. Fonville, and S. M. Rosenberg. 2005. 'A switch from high-fidelity to error-prone DNA double-strand break repair underlies stress-induced mutation', *Mol Cell*, 19: 791-804.
- Quintás-Cardama, Alfonso, Kris Vaddi, Phillip Liu, Taghi Manshour, Jun Li, Peggy A. Scherle, Eian Caulder, Xiaoming Wen, Yanlong Li, Paul Waeltz, Mark Rugar, Timothy Burn, Yvonne Lo, Jennifer Kelley, Maryanne Covington, Stacey Shepard, James D. Rodgers, Patrick Haley, Hagop Kantarjian, Jordan S. Fridman, and Srdan Verstovsek. 2010. 'Preclinical characterization of the selective JAK1/2 inhibitor INCB018424: therapeutic implications for the treatment of myeloproliferative neoplasms', *Blood*, 115: 3109-17.
- Raha, D., T. R. Wilson, J. Peng, D. Peterson, P. Yue, M. Evangelista, C. Wilson, M. Merchant, and J. Settleman. 2014. 'The cancer stem cell marker aldehyde dehydrogenase is required to maintain a drug-tolerant tumor cell subpopulation', *Cancer Res*, 74: 3579-90.
- Ramirez, M., S. Rajaram, R. J. Steininger, D. Osipchuk, M. A. Roth, L. S. Morinishi, L. Evans, W. Ji, C. H. Hsu, K. Thurley, S. Wei, A. Zhou, P. R. Koduru, B. A. Posner, L. F. Wu, and S. J. Altschuler. 2016. 'Diverse drug-resistance mechanisms can emerge from drug-tolerant cancer persister cells', *Nat Commun*, 7: 10690.
- Ravindran Menon, D., S. Das, C. Krepler, A. Vultur, B. Rinner, S. Schauer, K. Kashofer, K. Wagner, G. Zhang, E. Bonyadi Rad, N. K. Haass, H. P. Soyer, B. Gabrielli, R. Somasundaram, G. Hoefler, M. Herlyn, and H. Schaidt. 2015. 'A stress-induced early innate response causes multidrug tolerance in melanoma', *Oncogene*, 34: 4448-59.
- Rehman, Sumaiyah K., Jennifer Haynes, Evelyne Collignon, Kevin R. Brown, Yadong Wang, Allison M. L. Nixon, Jeffrey P. Bruce, Jeffrey A. Wintersinger, Arvind Singh Mer, Edwyn B. L. Lo, Cherry Leung, Evelyne Lima-Fernandes, Nicholas M. Pedley, Fraser Soares, Sophie McGibbon, Housheng Hansen He, Aaron Pollet, Trevor J. Pugh, Benjamin Haibe-Kains, Quaid Morris, Miguel Ramalho-Santos, Sidhartha Goyal, Jason Moffat, and Catherine A. O'Brien. 2021. 'Colorectal Cancer Cells Enter a Diapause-like DTP State to Survive Chemotherapy', *Cell*, 184: 226-42.e21.
- Ren, X., A. Kennedy, and L. M. Colletti. 2002. 'CXC chemokine expression after stimulation with interferon-gamma in primary rat hepatocytes in culture', *Shock*, 17: 513-20.
- Riber, L., and L. H. Hansen. 2021. 'Epigenetic Memories: The Hidden Drivers of Bacterial Persistence?', *Trends Microbiol*, 29: 190-94.

-
- Robinson, M. D., D. J. McCarthy, and G. K. Smyth. 2010. 'edgeR: a Bioconductor package for differential expression analysis of digital gene expression data', *Bioinformatics*, 26: 139-40.
- Robinson, M. D., and A. Oshlack. 2010. 'A scaling normalization method for differential expression analysis of RNA-seq data', *Genome Biol*, 11: R25.
- Rodriguez, G. P., N. V. Romanova, G. Bao, N. C. Rouf, Y. W. Kow, and G. F. Crouse. 2012. 'Mismatch repair-dependent mutagenesis in nondividing cells', *Proc Natl Acad Sci U S A*, 109: 6153-8.
- Roesch, Alexander, Mizuho Fukunaga-Kalabis, Elizabeth C. Schmidt, Susan E. Zabierowski, Patricia A. Brafford, Adina Vultur, Devraj Basu, Phyllis Gimotty, Thomas Vogt, and Meenhard Herlyn. 2010. 'A Temporarily Distinct Subpopulation of Slow-Cycling Melanoma Cells Is Required for Continuous Tumor Growth', *Cell*, 141: 583-94.
- Ronco, Cyril, Anthony R. Martin, Luc Demange, and Rachid Benhida. 2017. 'ATM, ATR, CHK1, CHK2 and WEE1 inhibitors in cancer and cancer stem cells', *MedChemComm*, 8: 295-319.
- Russo, Mariangela, Giovanni Crisafulli, Alberto Sogari, Nicole M. Reilly, Sabrina Arena, Simona Lamba, Alice Bartolini, Vito Amodio, Alessandro Magri, Luca Novara, Ivana Sarotto, Zachary D. Nagel, Cortt G. Pielt, Alessio Amatu, Andrea Sartore-Bianchi, Salvatore Siena, Andrea Bertotti, Livio Trusolino, Mattia Corigliano, Marco Gherardi, Marco Cosentino Lagomarsino, Federica Di Nicolantonio, and Alberto Bardelli. 2019. 'Adaptive mutability of colorectal cancers in response to targeted therapies', *Science*, 366: 1473-80.
- Russo, Mariangela, Simone Pompei, Alberto Sogari, Mattia Corigliano, Giovanni Crisafulli, Alberto Puliafito, Simona Lamba, Jessica Erriquez, Andrea Bertotti, Marco Gherardi, Federica Di Nicolantonio, Alberto Bardelli, and Marco Cosentino Lagomarsino. 2022. 'A modified fluctuation-test framework characterizes the population dynamics and mutation rate of colorectal cancer persister cells', *Nature Genetics*, 54: 976-84.
- Saleh, T., L. Tyutyunyk-Massey, and D. A. Gewirtz. 2019. 'Tumor Cell Escape from Therapy-Induced Senescence as a Model of Disease Recurrence after Dormancy', *Cancer Res*, 79: 1044-46.
- Salgia, R., and P. Kulkarni. 2018. 'The Genetic/Non-genetic Duality of Drug 'Resistance' in Cancer', *Trends Cancer*, 4: 110-18.
- Sanchez, Yolanda, Calvin Wong, Richard S. Thoma, Ron Richman, Zhiqi Wu, Helen Piwnicka-Worms, and Stephen J. Elledge. 1997. 'Conservation of the Chk1 Checkpoint Pathway in Mammals: Linkage of DNA Damage to Cdk Regulation Through Cdc25', *Science*, 277: 1497-501.
- Sarmiento, L. M., V. Póvoa, R. Nascimento, G. Real, I. Antunes, L. R. Martins, C. Moita, P. M. Alves, M. Abecasis, L. F. Moita, R. M. E. Parkhouse, J. P. P. Meijerink, and J. T. Barata. 2015. 'CHK1 overexpression in T-cell acute lymphoblastic leukemia is essential for proliferation and survival by preventing excessive replication stress', *Oncogene*, 34: 2978-90.
- Segal, N. H., D. W. Parsons, K. S. Peggs, V. Velculescu, K. W. Kinzler, B. Vogelstein, and J. P. Allison. 2008. 'Epitope landscape in breast and colorectal cancer', *Cancer Res*, 68: 889-92.
- Sehgal, K., A. Portell, E. V. Ivanova, P. H. Lizotte, N. R. Mahadevan, J. R. Greene, A. Vajdi, C. Gurjao, T. Teceno, L. J. Taus, T. C. Thai, S. Kitajima, D. Liu, T. Tani, M. Nouredine, C. J. Lau, P. T. Kirschmeier, D. Liu, M. Giannakis, R. W. Jenkins, P. C. Gokhale, S. Goldoni, M. Pinzon-Ortiz, W. D. Hastings, P. S. Hammerman, J. J. Miret, C. P. Paweletz, and D. A. Barbie. 2021. 'Dynamic single-cell RNA sequencing identifies immunotherapy persister cells following PD-1 blockade', *J Clin Invest*, 131.
- Sen, T., C. M. Della Corte, S. Milutinovic, R. J. Cardnell, L. Diao, K. Ramkumar, C. M. Gay, C. A. Stewart, Y. Fan, L. Shen, R. J. Hansen, B. Strouse, M. P. Hedrick, C. A. Hassig, J. V. Heymach, J. Wang, and L. A. Byers. 2019. 'Combination Treatment of the Oral CHK1 Inhibitor, SRA737, and Low-Dose Gemcitabine Enhances the Effect of Programmed Death Ligand 1 Blockade by Modulating the Immune Microenvironment in SCLC', *J Thorac Oncol*, 14: 2152-63.
- Sequist, L. V., B. A. Waltman, D. Dias-Santagata, S. Digumarthy, A. B. Turke, P. Fidias, K. Bergethon, A. T. Shaw, S. Gettinger, A. K. Cospers, S. Akhavanfard, R. S. Heist, J. Temel, J. G. Christensen, J. C. Wain, T. J. Lynch, K. Vernovsky, E. J. Mark, M. Lanuti, A. J.
-

- lafrate, M. Mino-Kenudson, and J. A. Engelman. 2011. 'Genotypic and histological evolution of lung cancers acquiring resistance to EGFR inhibitors', *Sci Transl Med*, 3: 75ra26.
- Serra, V., M. Scaltriti, L. Prudkin, P. J. Eichhorn, Y. H. Ibrahim, S. Chandralapaty, B. Markman, O. Rodriguez, M. Guzman, S. Rodriguez, M. Gili, M. Russillo, J. L. Parra, S. Singh, J. Arribas, N. Rosen, and J. Baselga. 2011. 'PI3K inhibition results in enhanced HER signaling and acquired ERK dependency in HER2-overexpressing breast cancer', *Oncogene*, 30: 2547-57.
- Sharma, S. V., D. Y. Lee, B. Li, M. P. Quinlan, F. Takahashi, S. Maheswaran, U. McDermott, N. Azizian, L. Zou, M. A. Fischbach, K. K. Wong, K. Brandstetter, B. Wittner, S. Ramaswamy, M. Classon, and J. Settleman. 2010. 'A chromatin-mediated reversible drug-tolerant state in cancer cell subpopulations', *Cell*, 141: 69-80.
- Shen, S., S. Faouzi, A. Bastide, S. Martineau, H. Malka-Mahieu, Y. Fu, X. Sun, C. Mateus, E. Routier, S. Roy, L. Desaubry, F. Andre, A. Eggermont, A. David, J. Y. Scoazec, S. Vagner, and C. Robert. 2019. 'An epitranscriptomic mechanism underlies selective mRNA translation remodelling in melanoma persister cells', *Nat Commun*, 10: 5713.
- Shieh, S. Y., J. Ahn, K. Tamai, Y. Taya, and C. Prives. 2000. 'The human homologs of checkpoint kinases Chk1 and Cds1 (Chk2) phosphorylate p53 at multiple DNA damage-inducible sites', *Genes Dev*, 14: 289-300.
- Shiotani, B., and L. Zou. 2009. 'Single-stranded DNA orchestrates an ATM-to-ATR switch at DNA breaks', *Mol Cell*, 33: 547-58.
- Shuai, K., C. Schindler, V. R. Prezioso, and J. E. Darnell, Jr. 1992. 'Activation of transcription by IFN-gamma: tyrosine phosphorylation of a 91-kD DNA binding protein', *Science*, 258: 1808-12.
- Siegel, J. 1998. 'Herceptin FDA approval letter', *Rockville MD*.
- Singh, Sheila K., Cynthia Hawkins, Ian D. Clarke, Jeremy A. Squire, Jane Bayani, Takuichiro Hide, R. Mark Henkelman, Michael D. Cusimano, and Peter B. Dirks. 2004. 'Identification of human brain tumour initiating cells', *Nature*, 432: 396-401.
- Slamon, D. J., G. M. Clark, S. G. Wong, W. J. Levin, A. Ullrich, and W. L. McGuire. 1987. 'Human breast cancer: correlation of relapse and survival with amplification of the HER-2/neu oncogene', *Science*, 235: 177-82.
- Slamon, D. J., B. Leyland-Jones, S. Shak, H. Fuchs, V. Paton, A. Bajamonde, T. Fleming, W. Eiermann, J. Wolter, M. Pegram, J. Baselga, and L. Norton. 2001. 'Use of chemotherapy plus a monoclonal antibody against HER2 for metastatic breast cancer that overexpresses HER2', *N Engl J Med*, 344: 783-92.
- Smith, Christof C., Sara R. Selitsky, Shengjie Chai, Paul M. Armistead, Benjamin G. Vincent, and Jonathan S. Serody. 2019. 'Alternative tumour-specific antigens', *Nature Reviews Cancer*, 19: 465-78.
- Smith, J., L. M. Tho, N. Xu, and D. A. Gillespie. 2010. 'The ATM-Chk2 and ATR-Chk1 pathways in DNA damage signaling and cancer', *Adv Cancer Res*, 108: 73-112.
- Son, Myung Jin, Kevin Woolard, Do-Hyun Nam, Jeongwu Lee, and Howard A. Fine. 2009. 'SSEA-1 Is an Enrichment Marker for Tumor-Initiating Cells in Human Glioblastoma', *Cell Stem Cell*, 4: 440-52.
- Sørensen, C. S., L. T. Hansen, J. Dziegielewski, R. G. Syljuåsen, C. Lundin, J. Bartek, and T. Helleday. 2005. 'The cell-cycle checkpoint kinase Chk1 is required for mammalian homologous recombination repair', *Nat Cell Biol*, 7: 195-201.
- Sreenivasan, Lakshana, Hui Wang, Shyong Quin Yap, Pascal Leclair, Anthony Tam, and Chinten James Lim. 2020. 'Autocrine IL-6/STAT3 signaling aids development of acquired drug resistance in Group 3 medulloblastoma', *Cell Death & Disease*, 11: 1035.
- Sriuranpong, V., A. Mutirangura, J. W. Gillespie, V. Patel, P. Amornphimoltham, A. A. Molinolo, V. Kerekhanjanarong, S. Supanakorn, P. Supiyaphun, S. Rangaeng, N. Voravud, and J. S. Gutkind. 2004. 'Global gene expression profile of nasopharyngeal carcinoma by laser capture microdissection and complementary DNA microarrays', *Clin Cancer Res*, 10: 4944-58.
- Su, Y., W. Wei, L. Robert, M. Xue, J. Tsoi, A. Garcia-Diaz, B. Homet Moreno, J. Kim, R. H. Ng, J. W. Lee, R. C. Koya, B. Comin-Anduix, T. G. Graeber, A. Ribas, and J. R. Heath. 2017. 'Single-cell analysis resolves the cell state transition and signaling dynamics associated with melanoma drug-induced resistance', *Proc Natl Acad Sci U S A*, 114: 13679-84.

- Subramanian, A., P. Tamayo, V. K. Mootha, S. Mukherjee, B. L. Ebert, M. A. Gillette, A. Paulovich, S. L. Pomeroy, T. R. Golub, E. S. Lander, and J. P. Mesirov. 2005. 'Gene set enrichment analysis: a knowledge-based approach for interpreting genome-wide expression profiles', *Proc Natl Acad Sci U S A*, 102: 15545-50.
- Tannous, Bakhos A., Mariam Kerami, Petra M. Van der Stoop, Nicholas Kwiatkowski, Jinhua Wang, Wenjun Zhou, Almuth F. Kessler, Grant Lewandrowski, Lotte Hiddingh, Nik Sol, Tonny Lagerweij, Laurine Wedekind, Johanna M. Niers, Marco Barazas, R. Jonas A. Nilsson, Dirk Geerts, Philip C. De Witt Hamer, Carsten Hagemann, W. Peter Vandertop, Olaf Van Tellingen, David P. Noske, Nathanael S. Gray, and Thomas Würdinger. 2013. 'Effects of the Selective MPS1 Inhibitor MPS1-IN-3 on Glioblastoma Sensitivity to Antimitotic Drugs', *JNCI: Journal of the National Cancer Institute*, 105: 1322-31.
- TCGA. "The Cancer Genome Atlas." In: USA: National Cancer Institute, Center for Cancer Genomics.
- Terai, H., S. Kitajima, D. S. Potter, Y. Matsui, L. G. Quiceno, T. Chen, T. J. Kim, M. Rusan, T. C. Thai, F. Piccioni, K. A. Donovan, N. Kwiatkowski, K. Hinohara, G. Wei, N. S. Gray, E. S. Fischer, K. K. Wong, T. Shimamura, A. Letai, P. S. Hammerman, and D. A. Barbie. 2018. 'ER Stress Signaling Promotes the Survival of Cancer "Persister Cells" Tolerant to EGFR Tyrosine Kinase Inhibitors', *Cancer Res*, 78: 1044-57.
- Tho, L. M., S. Libertini, R. Rampling, O. Sansom, and D. A. Gillespie. 2012. 'Chk1 is essential for chemical carcinogen-induced mouse skin tumorigenesis', *Oncogene*, 31: 1366-75.
- Thompson, R. H., and E. D. Kwon. 2006. 'Significance of B7-H1 overexpression in kidney cancer', *Clin Genitourin Cancer*, 5: 206-11.
- Townsend, A. R. M., J. Rothbard, F. M. Gotch, G. Bahadur, D. Wraith, and A. J. McMichael. 1986. 'The epitopes of influenza nucleoprotein recognized by cytotoxic T lymphocytes can be defined with short synthetic peptides', *Cell*, 44: 959-68.
- Varambally, Sooryanarayana, Saravana M. Dhanasekaran, Ming Zhou, Terrence R. Barrette, Chandan Kumar-Sinha, Martin G. Sanda, Debashis Ghosh, Kenneth J. Pienta, Richard G. A. B. Sewalt, Arie P. Otte, Mark A. Rubin, and Arul M. Chinnaiyan. 2002. 'The polycomb group protein EZH2 is involved in progression of prostate cancer', *Nature*, 419: 624-29.
- Verlinden, L., I. Vanden Bempt, G. Eelen, M. Drijkoningen, I. Verlinden, K. Marchal, C. De Wolf-Peeters, M. R. Christiaens, L. Michiels, R. Bouillon, and A. Verstuyf. 2007. 'The E2F-regulated gene Chk1 is highly expressed in triple-negative estrogen receptor /progesterone receptor /HER-2 breast carcinomas', *Cancer Res*, 67: 6574-81.
- Villanueva, J., A. Vultur, J. T. Lee, R. Somasundaram, M. Fukunaga-Kalabis, A. K. Cipolla, B. Wubbenhorst, X. Xu, P. A. Gimotty, D. Kee, A. E. Santiago-Walker, R. Letrero, K. D'Andrea, A. Pushparajan, J. E. Hayden, K. D. Brown, S. Laquerre, G. A. McArthur, J. A. Sosman, K. L. Nathanson, and M. Herlyn. 2010. 'Acquired resistance to BRAF inhibitors mediated by a RAF kinase switch in melanoma can be overcome by cotargeting MEK and IGF-1R/PI3K', *Cancer Cell*, 18: 683-95.
- Vinogradova, Maia, Victor S. Gehling, Amy Gustafson, Shilpi Arora, Charles A. Tindell, Catherine Wilson, Kaylyn E. Williamson, Gulfer D. Guler, Pranoti Gangurde, Wanda Manieri, Jennifer Busby, E. Megan Flynn, Fei Lan, Hyo-jin Kim, Shobu Odate, Andrea G. Cochran, Yichin Liu, Matthew Wongchenko, Yibin Yang, Tommy K. Cheung, Tobias M. Maile, Ted Lau, Michael Costa, Ganapati V. Hegde, Erica Jackson, Robert Pitti, David Arnott, Christopher Bailey, Steve Bellon, Richard T. Cummings, Brian K. Albrecht, Jean-Christophe Harmange, James R. Kiefer, Patrick Trojer, and Marie Classon. 2016. 'An inhibitor of KDM5 demethylases reduces survival of drug-tolerant cancer cells', *Nature Chemical Biology*, 12: 531-38.
- Vogel, C. L., M. A. Cobleigh, D. Tripathy, J. C. Gutheil, L. N. Harris, L. Fehrenbacher, D. J. Slamon, M. Murphy, W. F. Novotny, M. Burchmore, S. Shak, S. J. Stewart, and M. Press. 2002. 'Efficacy and safety of trastuzumab as a single agent in first-line treatment of HER2-overexpressing metastatic breast cancer', *J Clin Oncol*, 20: 719-26.
- Walton, M. I., P. D. Eve, A. Hayes, A. T. Henley, M. R. Valenti, A. K. De Haven Brandon, G. Box, K. J. Boxall, M. Tall, K. Swales, T. P. Matthews, T. McHardy, M. Lainchbury, J. Osborne, J. E. Hunter, N. D. Perkins, G. W. Aherne, J. C. Reader, F. I. Raynaud, S. A. Eccles, I. Collins, and M. D. Garrett. 2016. 'The clinical development candidate CCT245737 is an orally active CHK1 inhibitor with preclinical activity in RAS mutant NSCLC and Eμ-MYC driven B-cell lymphoma', *Oncotarget*, 7: 2329-42.

- Walton, M. I., P. D. Eve, A. Hayes, M. R. Valenti, A. K. De Haven Brandon, G. Box, A. Hallsworth, E. L. Smith, K. J. Boxall, M. Lainchbury, T. P. Matthews, Y. Jamin, S. P. Robinson, G. W. Aherne, J. C. Reader, L. Chesler, F. I. Raynaud, S. A. Eccles, I. Collins, and M. D. Garrett. 2012. 'CCT244747 is a novel potent and selective CHK1 inhibitor with oral efficacy alone and in combination with genotoxic anticancer drugs', *Clin Cancer Res*, 18: 5650-61.
- Walworth, N., S. Davey, and D. Beach. 1993. 'Fission yeast chk1 protein kinase links the rad checkpoint pathway to cdc2', *Nature*, 363: 368-71.
- Wan, Honghe, Gretchen M. Schroeder, Amy C. Hart, Jennifer Inghrim, James Grebinski, John S. Tokarski, Matthew V. Lorenzi, Dan You, Theresa McDevitt, Becky Penhallow, Ragini Vuppugalla, Yueping Zhang, Xiaomei Gu, Ramaswamy Iyer, Louis J. Lombardo, George L. Trainor, Stefan Ruepp, Jonathan Lippy, Yuval Blat, John S. Sack, Javed A. Khan, Kevin Stefanski, Bogdan Slecicka, Arvind Mathur, Jung-Hui Sun, Michael K. Wong, Dauh-Rung Wu, Peng Li, Anuradha Gupta, P. N. Arunachalam, Bala Pragalathan, Sankara Narayanan, Nanjundaswamy K.C, Prakasam Kuppasamy, and Ashok V. Purandare. 2015. 'Discovery of a Highly Selective JAK2 Inhibitor, BMS-911543, for the Treatment of Myeloproliferative Neoplasms', *ACS Medicinal Chemistry Letters*, 6: 850-55.
- Wang, Zhibin, Chongzhi Zang, Jeffrey A. Rosenfeld, Dustin E. Schones, Artem Barski, Suresh Cuddapah, Kairong Cui, Tae-Young Roh, Weiqun Peng, Michael Q. Zhang, and Keji Zhao. 2008. 'Combinatorial patterns of histone acetylations and methylations in the human genome', *Nature Genetics*, 40: 897-903.
- Wiles, E. T., and E. U. Selker. 2017. 'H3K27 methylation: a promiscuous repressive chromatin mark', *Curr Opin Genet Dev*, 43: 31-37.
- Windels, Ethel Martha, Joran Elie Michiels, Maarten Fauvart, Tom Wenseleers, Bram Van den Bergh, and Jan Michiels. 2019. 'Bacterial persistence promotes the evolution of antibiotic resistance by increasing survival and mutation rates', *The ISME Journal*, 13: 1239-51.
- Wolchok, J. D., H. Kluger, M. K. Callahan, M. A. Postow, N. A. Rizvi, A. M. Lesokhin, N. H. Segal, C. E. Ariyan, R. A. Gordon, K. Reed, M. M. Burke, A. Caldwell, S. A. Kronenberg, B. U. Agunwamba, X. Zhang, I. Lowy, H. D. Inzunza, W. Feely, C. E. Horak, Q. Hong, A. J. Korman, J. M. Wigginton, A. Gupta, and M. Sznol. 2013. 'Nivolumab plus ipilimumab in advanced melanoma', *N Engl J Med*, 369: 122-33.
- Woodward, Hannah L., Paolo Innocenti, Kwai-Ming J. Cheung, Angela Hayes, Jennie Roberts, Alan T. Henley, Amir Faisal, Grace Wing-Yan Mak, Gary Box, Isaac M. Westwood, Nora Cronin, Michael Carter, Melanie Valenti, Alexis De Haven Brandon, Lisa O'Fee, Harry Saville, Jessica Schmitt, Rosemary Burke, Fabio Broccatelli, Rob L. M. van Montfort, Florence I. Raynaud, Suzanne A. Eccles, Spiros Linardopoulos, Julian Blagg, and Swen Hoelder. 2018. 'Introduction of a Methyl Group Curbs Metabolism of Pyrido[3,4-d]pyrimidine Monopolar Spindle 1 (MPS1) Inhibitors and Enables the Discovery of the Phase 1 Clinical Candidate N2-(2-Ethoxy-4-(4-methyl-4H-1,2,4-triazol-3-yl)phenyl)-6-methyl-N8-neopentylpyrido[3,4-d]pyrimidine-2,8-diamine (BOS172722)', *Journal of Medicinal Chemistry*, 61: 8226-40.
- Wu, Hui, Xiuzhen Chen, Jun Xiong, Yingfeng Li, Hong Li, Xiaojun Ding, Sheng Liu, She Chen, Shaorong Gao, and Bing Zhu. 2011. 'Histone methyltransferase G9a contributes to H3K27 methylation in vivo', *Cell Research*, 21: 365-67.
- Xie, Z., A. Bailey, M. V. Kuleshov, D. J. B. Clarke, J. E. Evangelista, S. L. Jenkins, A. Lachmann, M. L. Wojciechowicz, E. Kropiwnicki, K. M. Jagodnik, M. Jeon, and A. Ma'ayan. 2021. 'Gene Set Knowledge Discovery with Enrichr', *Curr Protoc*, 1: e90.
- Yang, W., P. W. Chen, H. Li, H. Alizadeh, and J. Y. Niederkorn. 2008. 'PD-L1: PD-1 interaction contributes to the functional suppression of T-cell responses to human uveal melanoma cells in vitro', *Invest Ophthalmol Vis Sci*, 49: 2518-25.
- Yu, H. A., M. E. Arcila, N. Rekhtman, C. S. Sima, M. F. Zakowski, W. Pao, M. G. Kris, V. A. Miller, M. Ladanyi, and G. J. Riely. 2013. 'Analysis of tumor specimens at the time of acquired resistance to EGFR-TKI therapy in 155 patients with EGFR-mutant lung cancers', *Clin Cancer Res*, 19: 2240-7.
- Yun, C. H., K. E. Mengwasser, A. V. Toms, M. S. Woo, H. Greulich, K. K. Wong, M. Meyerson, and M. J. Eck. 2008. 'The T790M mutation in EGFR kinase causes drug resistance by increasing the affinity for ATP', *Proc Natl Acad Sci U S A*, 105: 2070-5.
- Zannini, Laura, Domenico Delia, and Giacomo Buscemi. 2014. 'CHK2 kinase in the DNA damage response and beyond', *Journal of Molecular Cell Biology*, 6: 442-57.

-
- Zhang, Y., and T. Hunter. 2014. 'Roles of Chk1 in cell biology and cancer therapy', *Int J Cancer*, 134: 1013-23.
- Zhao, Hui, and Helen Piwnica-Worms. 2001. 'ATR-Mediated Checkpoint Pathways Regulate Phosphorylation and Activation of Human Chk1', *Molecular and Cellular Biology*, 21: 4129-39.
- Zhao, X., I. K. Kim, B. Kallakury, J. J. Chahine, E. Iwama, M. Pierobon, E. Petricoin, J. N. McCutcheon, Y. W. Zhang, S. Umemura, V. Chen, C. Wang, and G. Giaccone. 2021. 'Acquired small cell lung cancer resistance to Chk1 inhibitors involves Wee1 up-regulation', *Mol Oncol*, 15: 1130-45.
- Zhao, Y., T. Lu, Y. Song, Y. Wen, Z. Deng, J. Fan, M. Zhao, R. Zhao, Y. Luo, J. Xie, B. Hu, H. Sun, Y. Wang, S. He, Y. Gong, J. Cheng, X. Liu, L. Yu, J. Li, C. Li, Y. Shi, and Q. Huang. 2023. 'Cancer Cells Enter an Adaptive Persistence to Survive Radiotherapy and Repopulate Tumor', *Adv Sci (Weinh)*, 10: e2204177.
- Zhou, Haibin, Longchuan Bai, Renqi Xu, Yujun Zhao, Jianyong Chen, Donna McEachern, Krishnapriya Chinnaswamy, Bo Wen, Lipeng Dai, Praveen Kumar, Chao-Yie Yang, Zhaomin Liu, Mi Wang, Liu Liu, Jennifer L. Meagher, Han Yi, Duxin Sun, Jeanne A. Stuckey, and Shaomeng Wang. 2019. 'Structure-Based Discovery of SD-36 as a Potent, Selective, and Efficacious PROTAC Degradator of STAT3 Protein', *Journal of Medicinal Chemistry*, 62: 11280-300.
- Zou, L., and S. J. Elledge. 2003. 'Sensing DNA damage through ATRIP recognition of RPA-ssDNA complexes', *Science*, 300: 1542-8.
- Zumwalt, T. J., M. Arnold, A. Goel, and C. R. Boland. 2015. 'Active secretion of CXCL10 and CCL5 from colorectal cancer microenvironments associates with GranzymeB+ CD8+ T-cell infiltration', *Oncotarget*, 6: 2981-91.

Appendix

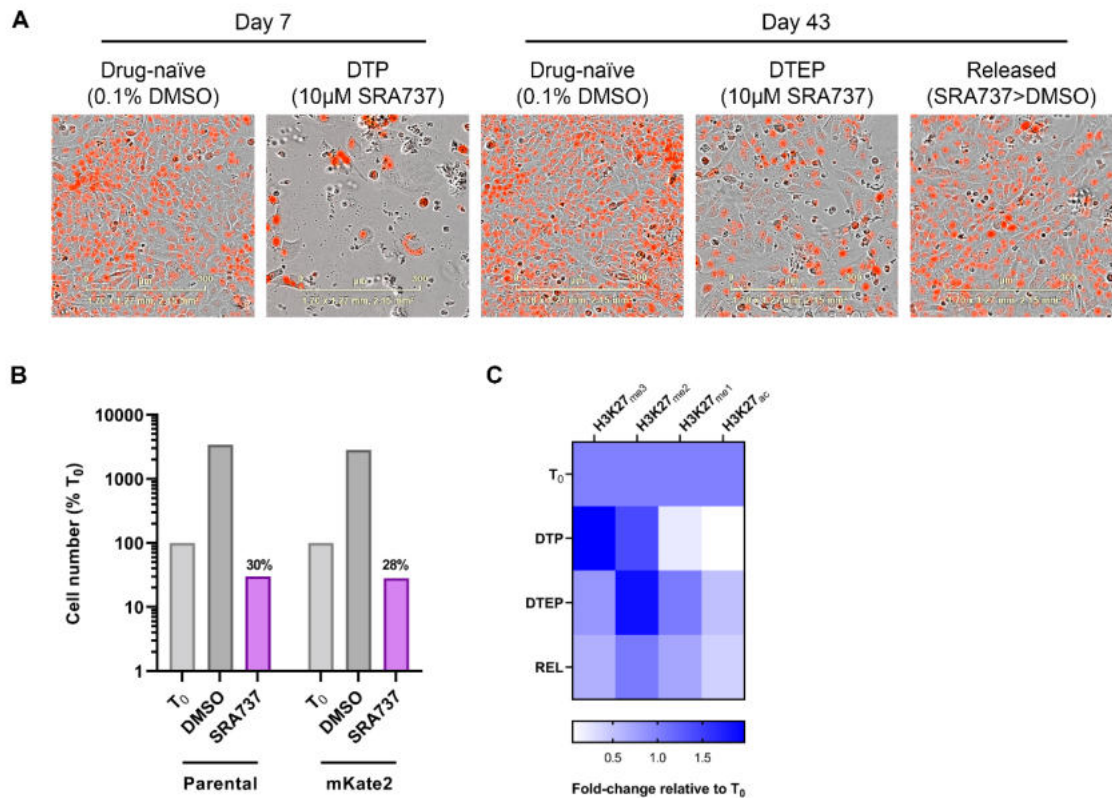
Appendix Table 1: *In vitro* biochemical kinase screen for SRA737.

Screen was performed against 124 kinases at 10 μ M SRA737 by MRC Dundee. Values are % remaining activity. Adapted from Walton et al. (2016).

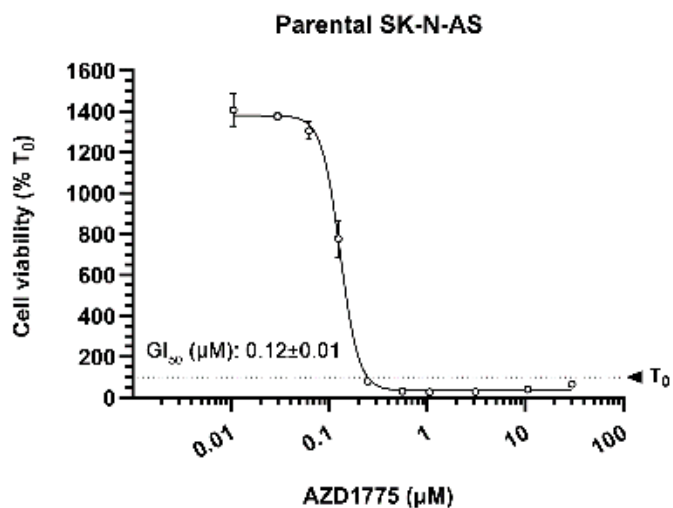
Kinase	%	Kinase	%	Kinase	%	Kinase	%
CHK1	4	LKB1	44	Aurora A	75	MAPKAP-K2	94
ERK8	4	MST4	44	MLK1	75	p38g MAPK	95
NUAK1	6	MINK1	44	PDK1	76	ROCK2	95
CLK1	6	GSK3b	47	EPH-A2	76	NEK2a	96
RSK	7	DAPK1	48	HIPK1	77	PAK2	96
BRSK1	12	MST2	48	PAK6	77	ERK2	98
MARK3	13	TAK1	48	MEKK1	77	EF2K	98
VEG-FR	13	PAK4	49	Lck 78	78	PKBb	100
PHK	15	S6K1	52	ASK1	80	TESK1	101
CHK2	15	TSSK1	53	CK2	81	RIPK2	101
PKD1	17	p38d MAPK	54	EPH-B4	81	IKKe	102
RSK2	19	TAO1	54	PKCa	82	EPH-B2	102
MARK2	21	PIM1	56	SRPK1	82	IR	102
CDK2-Cyc A	23	TLK1	59	TTBK1	82	PLK1	103
MLK3	23	MKK2	61	CSK	82	MKK6	104
DYRK3	24	DYRK2	61	SmMLCK	84	JNK1	104
Aurora B	26	MNK1	62	SYK	84	TIE2	104
MSK1	30	GCK	64	CK1	85	IGF-1R	104
TrkA	31	YES1	65	SGK1	87	EIF2AK3	105
AMPK	32	PRK2	67	PKC γ	87	JNK3	106
FGF-R1	33	MKK1	68	PIM2	88	JNK2	107
BRSK2	35	CAMK1	69	p38b MAPK	90	BRK	108
PIM3	36	PAK5	70	IKKb	91	NEK6	109
TTK	36	PRAK	71	PCKz	92	IRR	109
MELK	37	TBK1	71	HIPK2	92	OSR1	109
JAK2	37	EPH-A4	71	PKBa	93	HER4	110
IRAK1	38	BTK	72	PKA	93	EPH-B1	111
STK33	39	CAMKKb	73	ABL	93	MAPKAP-K3	114
MARK4	39	IRAK4	73	ZAP70	93	p38a MAPK	120
DYRK1A	41	ERK1	75	EPH-B3	93	MSK1	122
MARK1	43	MNK2	75	Src	93	HIPK3	124

Appendix Table 2: *In vitro* biochemical selectivity of SRA737 against selected kinases.
Adapted from Walton et al (2016).

Kinase	% Inh. @ 10 μ M (MRC Dundee)	Biochemical IC ₅₀ (nM)	Fold-selectivity
CHK1	96	1.4	-
ERK8	96	130	93
PKD1	83	298	213
RSK2	81	361	258
RSK1	93	362	258
FLT3	-	582	416
MARK3	87	698	499
NUAK1	94	711	507
CLK2	94	1370	978
BRSK1	88	1660	1190
CHK2	85	1260	1320
VEG-FR	87	15800	1500
AMPK	68	2970	2120
PHK	85	3470	2480
CDK2-Cyclin A	77	3850	2750
CDK1-Cyclin B	-	9030	6450

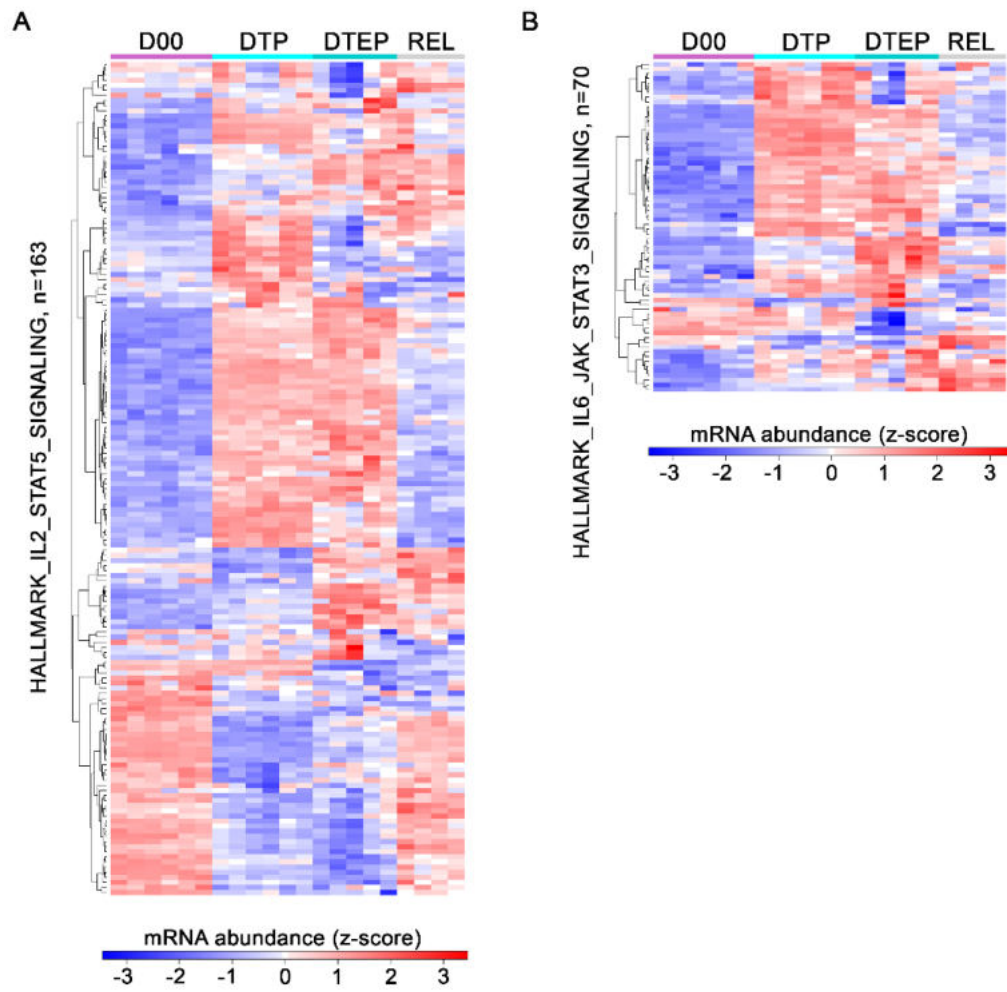


Appendix Figure 1: mKate2-SK-N-AS cells are a suitable model for persister cell studies. **(A)** Merged phase-contrast and red-fluorescence microscopy images of mKate2-SK-N-AS cells treated with vehicle (Drug-naïve), SRA737 (DTEP), or SRA737 for 7 days followed by vehicle (Released) at indicated time points. **(B)** Number of day 7 DTPs in parental and mKate2-SK-N-AS cells, relative to the starting population (T_0). **(C)** Quantification of epigenetic post-translational modifications on histone H3 lysine 27 (H3K27) in mKate2-SK-N-AS DTP, DTEP, and Released (REL) populations, relative to T_0 . Images captured at 10X magnification, scale bar = 300 μ m. Data shown are from a single experiment.

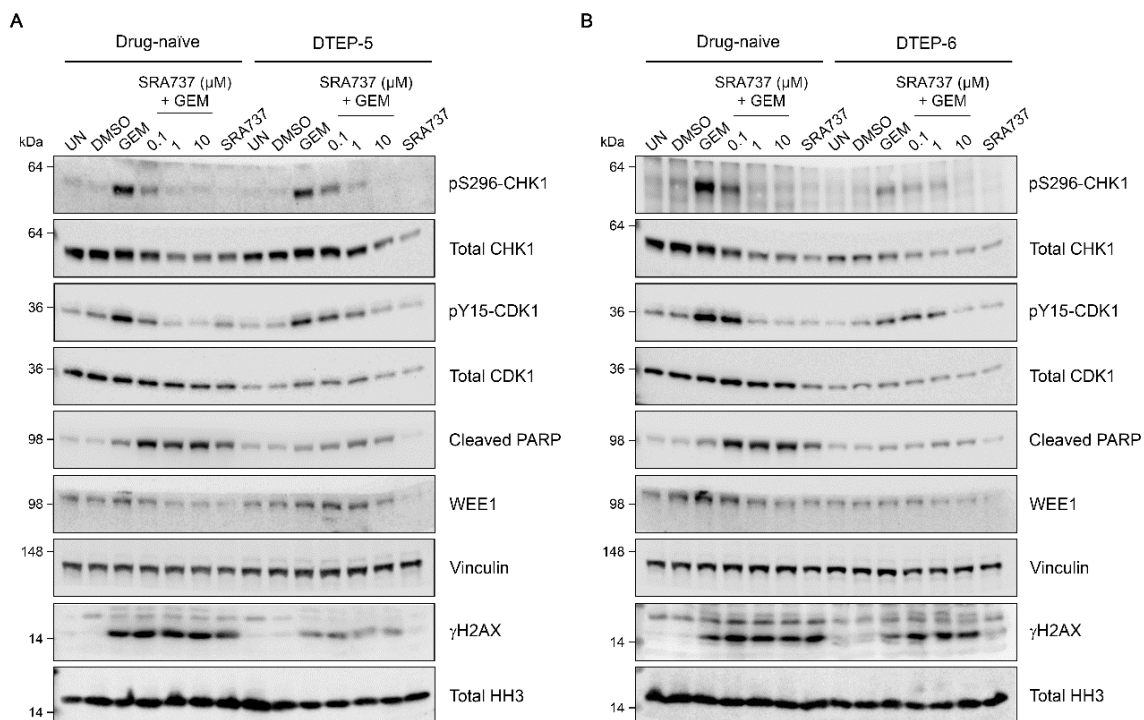


Appendix Figure 2: Potency of WEE1i AZD1775 in parental SK-N-AS cells.

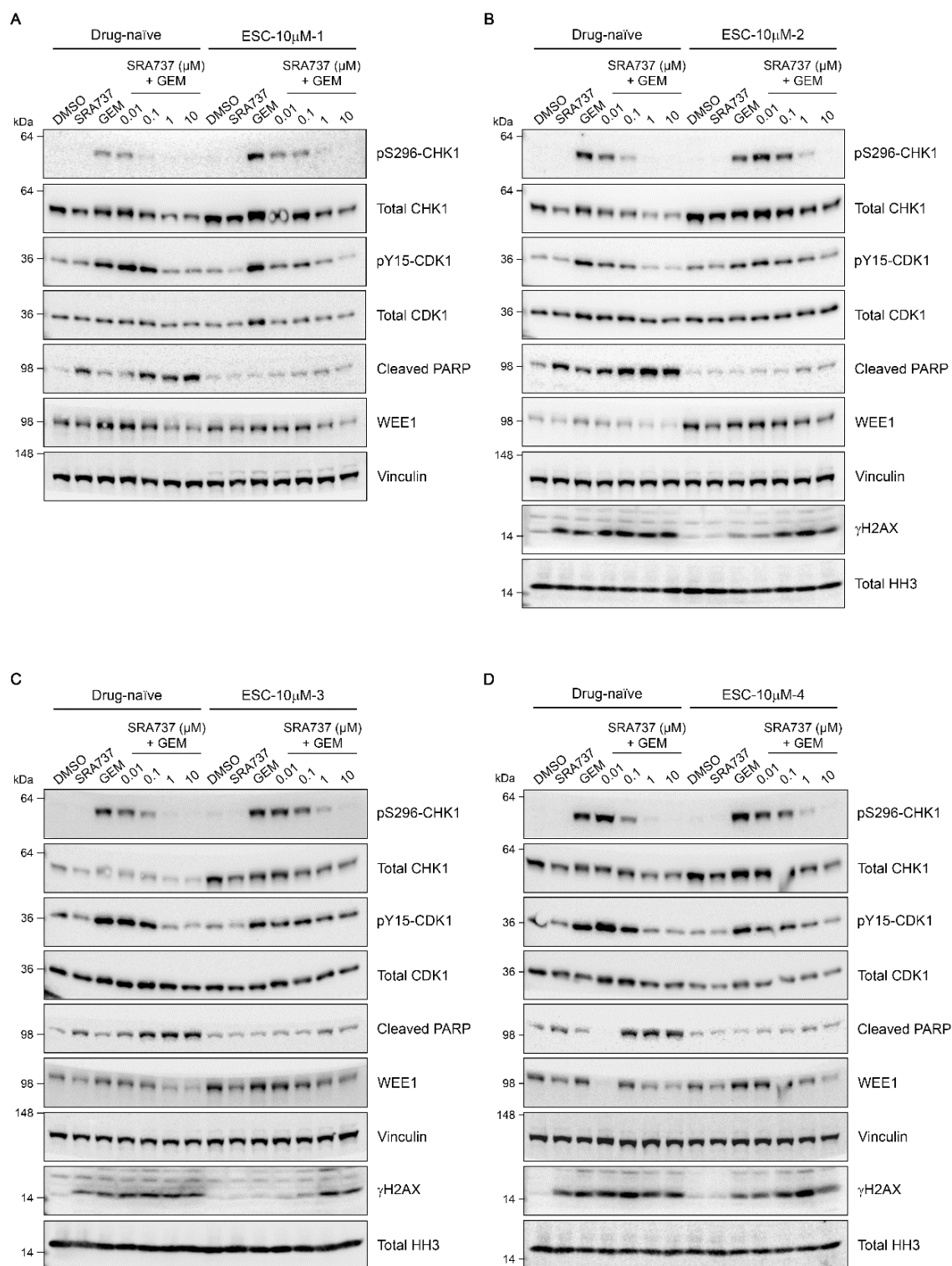
Non-linear regression analysis of cell viability measured by CellTiter-Glo® 120h after compound addition in parental SK-N-AS cells. Graph shows mean±SD of three technical replicates and is representative of n=3 experiments. GI₅₀ value is mean±SD of three independent experiments.



Appendix Figure 3: Gene expression changes in additional cytokine signalling pathways. Heatmaps showing \log_2 normalised gene expression of differentially expressed genes within (A) IL-2/STAT5 and (B) IL-6/JAK/STAT3 gene sets in DTP, DTEP, drug-released (REL), and D00 control populations.

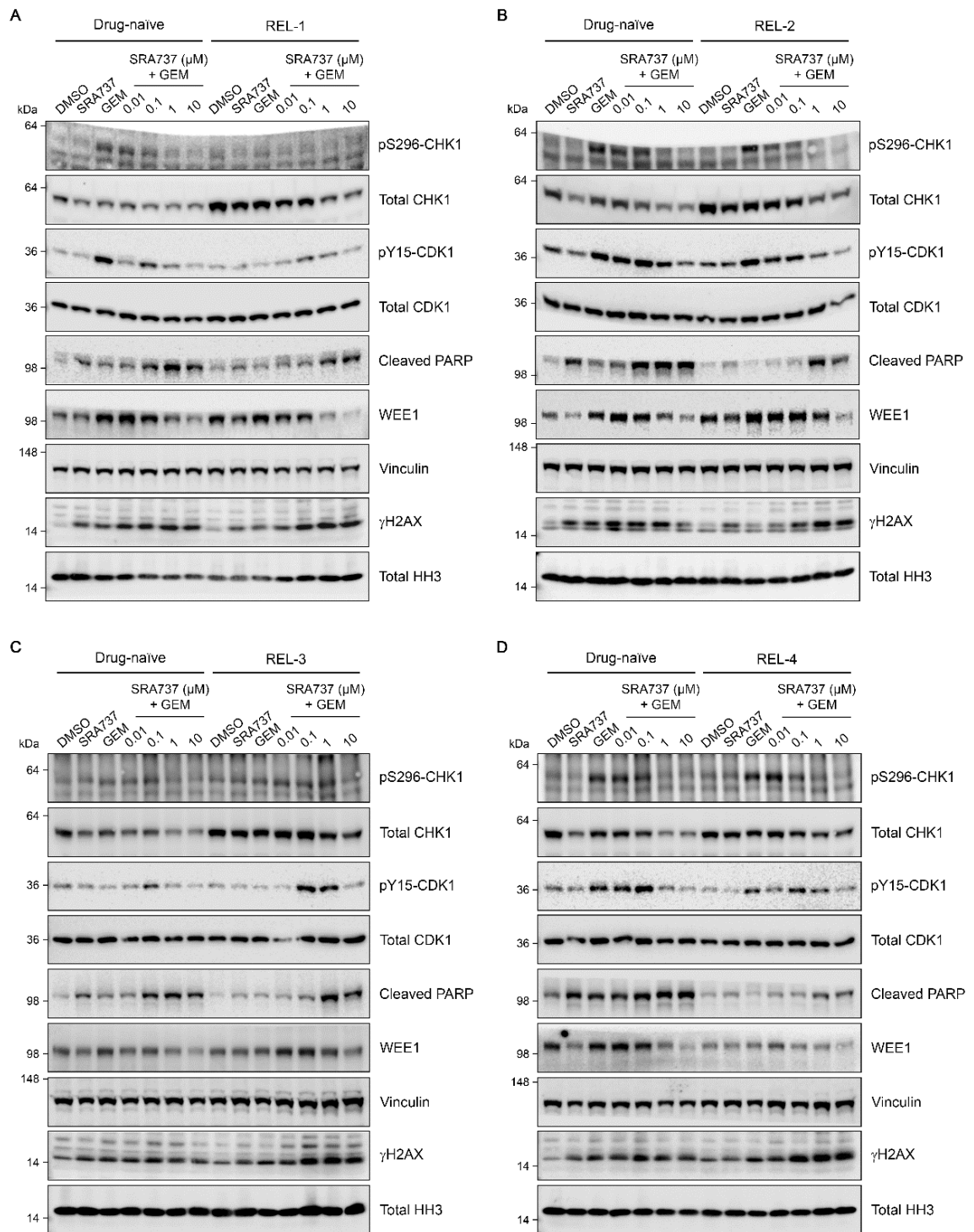


Appendix Figure 4: ATR-CHK1 signalling in independently generated DTEP populations.
(A & B) Western blot analysis of CHK1 activity biomarkers in replicate DTEP populations following 24h exposure to 200 nM gemcitabine (GEM) ± SRA737 at indicated concentrations, or 10 μM SRA737 alone (SRA737).



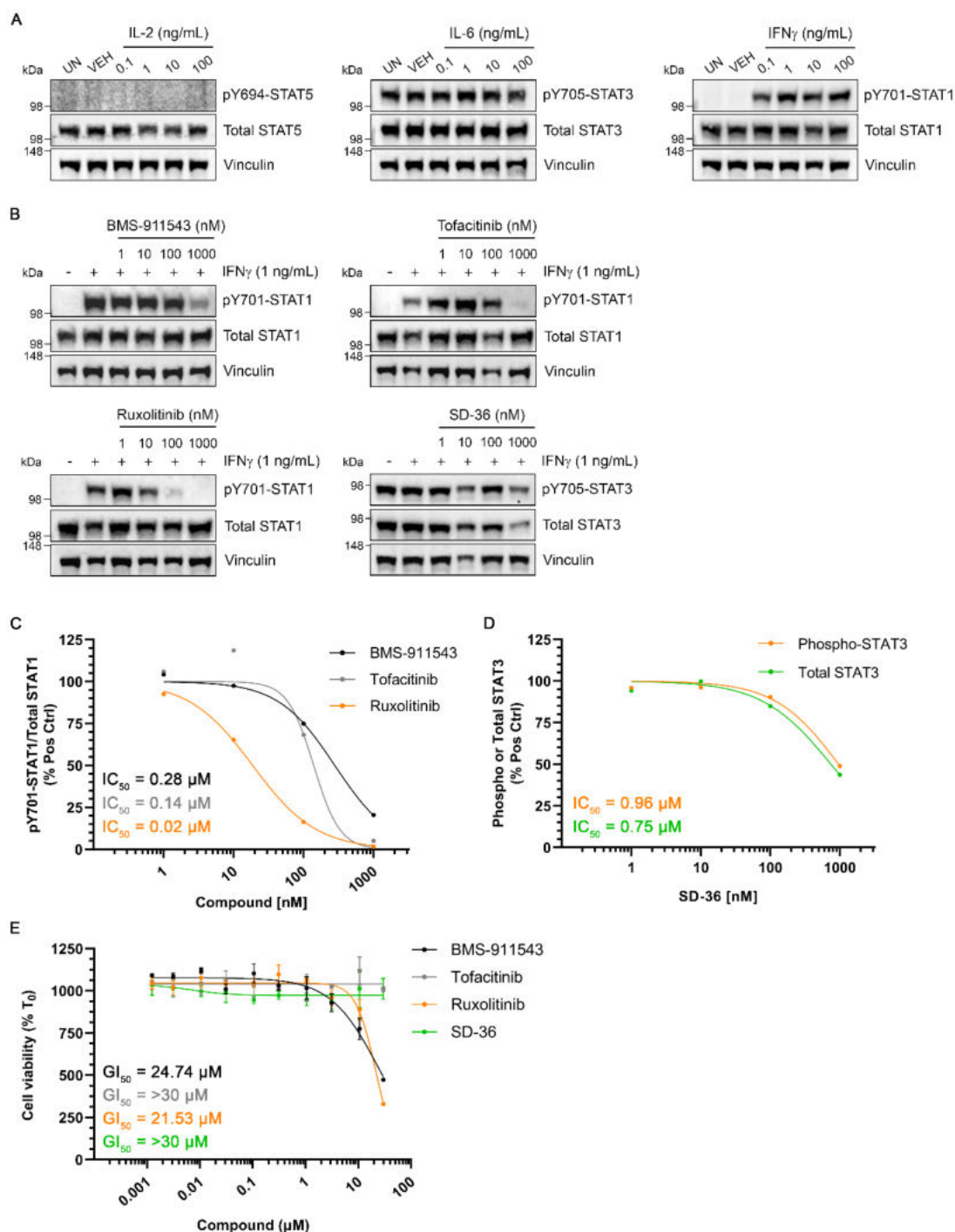
Appendix Figure 5: ATR-CHK1 signalling in independently generated dose-escalated populations.

(A - D) Western blot analysis of CHK1 activity biomarkers in replicate ESC-10 μ M populations following 24h exposure to 200 nM gemcitabine (GEM) \pm SRA737 at indicated concentrations, or 10 μ M SRA737 alone (SRA737).



Appendix Figure 6: ATR-CHK1 signalling in independently generated drug-released populations.

(A - D) Western blot analysis of CHK1 activity biomarkers in replicate drug-released (REL) populations following 24h exposure to 200 nM gemcitabine (GEM) ± SRA737 at indicated concentrations, or 10 μM SRA737 alone (SRA737).



Appendix Figure 7: Optimising recombinant human cytokine and small molecule JAK inhibitor doses for use in persister cell studies.

(A) Western blot analysis of activated STAT proteins in SK-N-AS cells after treatment with indicated concentrations of IL-2 (right), IL-6 (middle) or IFN γ (right) for 1h. (B) Western blot analysis of IFN γ -induced pY701-STAT1 activation after 24h pre-treatment with indicated concentrations of JAKi BMS-911543, tofacitinib, ruxolitinib, or STAT3 PROTAC SD-36. (C & D) Non-linear regression analysis of scanning densitometry data from Western blots shown in (B). (E) Non-linear regression analysis of cell viability measured by CellTiter-Glo® 120h after compound addition in SK-N-AS cells. Western blots and biomarker modulation IC₅₀ values are from a single experiment. Graph in (E) shows mean \pm SD of three technical replicates and GI₅₀ values from a single experiment.